LEWAN, MICHAEL DONALD

GEOCHEMISTRY OF VANADIUM AND NICKEL IN ORGANIC MATTER OF SEDIMENTARY ROCKS

University of Cincinnati PH.D. 1980

GEOCHEMISTRY OF VANADIUM AND NICKEL IN ORGANIC MATTER OF SEDIMENTARY ROCKS

A dissertation submitted to the

Division of Graduate Studies
of the University of Cincinnati

in partial fulfillment of the
requirements for the degree of

DOCTOR OF PHILOSOPHY

in the Department of Geology
of the Graduate School of Arts and Sciences

1980

BY

Michael Donald Lewan

B.S. Northern Illinois University, 1971
M.S. Michigan Technological University, 1972

UNIVERSITY OF CINCINNATI

April 7, 19 30

I hereby recommend that the thesis prepared under my supervision by Michael D. Lewan

entitled GEOCHEMISTRY OF VANADIUM AND NICKEL IN ORGANIC MATTER OF SEDIMENTARY ROCKS

be accepted as fulfilling this part of the requirements for the degree of DOCTOR OF PHILOSOPHY

Approved by:

J. Barry Maynard

John E. Grover

William A. Fuyat

ACKNOWLEDGMENTS

Acknowledgment is made to the Donors of the Petroleum Research Fund, administered by the American Chemical Society, for the support of this research (PRF #947-AC2). I am also grateful to the Amoco Production Company Research Center for making their facilities available to me for many of the analyses performed in this research.

My advisors J. B. Maynard, W. A. Pryor, and J. Grover at The University of Cincinnati have been instrumental in preparing me for this research. J. Grover's assistance in mineralogical considerations, W. A. Pryor's assistance in sedimentological aspects, and J. B. Maynard's assistance in geochemical considerations have been important in the development of this research. In the fields of biochemistry and microbiology, discussions with R. E. Kallio at The University of Illinois in Urbana were most helpful.

Support and encouragement from R. R. Thompson and J. C. Winters at the Amoco Production Company Research Center has been greatly appreciated. I would also like to extend my thanks to H. B. Bailey and M. J. Sutton for assistance in the drafting of figures and H. M. Chism for typing this manuscript.

I especially want to thank my wife, Jeannie, for her patience, encouragement, and understanding during the development and writing of this dissertation.

ABSTRACT

Enriched concentrations of vanadium and nickel have been noted in a variety of naturally occurring organic substances including crude oils, asphalts, and organic matter in some sedimentary rocks. The objectives of this study are to understand the preference, source and proportionality of these two metals in the organic matter of sedimentary rocks, as well as evaluate the usefulness of their proportionality in oil-to-source rock correlations.

The samples collected for this study include a wide range of depositional environments (lacustrine to open marine), types of organic matter (algal, higher plant, and sporopollenin), and geological age (Precambrian to Recent). Bitumen was extracted from these samples in a Sohxlet apparatus with a benzene-methanol mixture, and then analyzed for vanadium and nickel by neutron activation analysis. Additional analyses conducted on the samples may be categorized into two types; 1) organic analyses and 2) bulk rock analyses. The former includes bitumen content and kerogen evaluation by visual analysis, elemental analysis, and stable carbon isotopes. The bulk rock analyses include organic carbon content, semi-quantitative mineralogy, and petrographic studies. In order to employ field observations and published basin studies, the stratigraphic and basinal positions of the samples were noted.

The preferential concentration of vanadium and nickel appears to be dependent on the concentration of tetrapyrrole complexes in an organic

substance. A tetrapyrrole complex will preferentially bond with these two metals because of their small atomic radii, favorable electron configurations, and availability as bivalent cations. Thus, organic accumulations containing tetrapyrrole complexes have the potential of being enriched in vanadium and nickel, while those deficient in tetrapyrrole complexes do not have the potential of being enriched in the two metals. The amount of tetrapyrrole complexes within an organic accumulation is dependent on the amount of chlorophyll in the source of the organic matter and the preservation of chlorophyll derivatives in the environment of deposition. Chlorophyll concentrations are high in algae and higher plants, but the subaerial habitat of the latter makes the preservation of its chlorophyll or derivatives less likely. Appreciable quantities of chlorophyll are not likely in sporopollenin derived from spores or pollen, but minor quantities are likely in sporopollenin derived from the ultrastructure of some algae.

Although some vanadium and nickel in an organic accumulation may be endemic to its living organic sources, the source of enriched vanadium and nickel concentrations appears to be the aqueous metal cations in the interstitial waters of a sediment. This source of metals is dependent on diffusion of metal cations from the overlying water body, and is only effective as long as the sediment system remains open.

The proportionality of enriched vanadium and nickel in an organic accumulation is dependent on the hydrogen ion activity, redox potential, and biogenic sulfide activity of a sediment system. Hydrogen ion activity

and redox potential determine whether or not the proper metal species will be available for bonding, while biogenic sulfide activity tents to reduce the bonding potential of available nickelous cations. Deciphering the effects of these variables on the metal proportionality of a particular rock unit is best accomplished with the use of Eh-pH diagrams in conjunction with geochemical and geological data.

The ability of the vanadium-nickel fractions of a bitumen and an expelled crude oil to withstand alteration during thermal maturation, expulsion, migration, and entrapment, makes the vanadium-nickel fraction a good parameter for oil-to-source rock correlations, as well as for oil-to-oil and oil-to-asphalt correlations. Proper use of this parameter for oil-to-source rock correlations requires a thorough sampling of source rocks in a basin in order to develop an understanding of the stratigraphic and regional variations of the vanadium-nickel fractions.

TABLE OF CONTENTS

	Page
ACKNOWLEDGMENTS	i
ABSTRACT	ii
LIST OF FIGURES	vi
LIST OF TABLES	xx
CHAPTER 1 INTRODUCTION	1
1.1 Preference, Source, and Proportionality	2
1.2 Oil-to-Source Rock Correlation	3
CHAPTER 2 TYPES OF ANALYSES AND THEIR GEOCHEMICAL IMPLICATIONS	7
2.1 Amount of Organic Matter	7
2.2 Type of Organic Matter	10
2.3 Vanadium and Nickel Analyses	33
2.4 Evaluation of Depositional Environments	44
CHAPTER 3 SAMPLING TECHNIQUES AND THE EFFECTS OF WEATHERING	47
3.1 Surface Weathering	47
3.2 Pedogenic Weathering	55
3.3 Discussion	63
CHAPTER 4 NATURALLY OCCURRING VANADIUM- AND NICKEL-ORGANIC COMPLEXES	68
4.1 Tetrapyrrole Complexes	68
4.1.1 Stage I: From Water Column to Sediment Surface	72
4.1.2 Stage II: From Sediment Surface to Sediment Lithification	79
4.1.3 Stage III: From Sediment Lithification to Metamorphism	98
4.1.3 Summary	107
4.2 Mixed Ligand Tetradentates	109
4.3 Humate Complexes	109
4.4 Discussion	116
CHAPTER 5 SOURCES OF VANADIUM AND NICKEL IN NATURALLY OCCURRING ORGANIC SUBSTANCES	119
5.1 Living Matter	119
5.1.1 Higher Plants	120
5.1.2 Plankton	126
5.1.3 Sporopollenin	130
5.1.4 Summary	134
5.1 Interstitial Water	134
5.2.1 Closed Sediment System	136
5.2.2 Open Sediment System	140
5.2.3 Open-to-Closed Sediment System	140
5.2.4 Summary	143
5.3 Discussion	144

CHAPTER 6 FACTORS CONTROLLING THE PROPORTIONALITY OF VANADIUM AND NICKEL 150
6.1 Considerations in the Construction and Natural Limits of Eh-pH Diagrams 150
6.2 Significance of the Stability Fields for VO^{+2} and Ni^{+2} 156
6.2.1 Stability Field for VO^{+2} 156
6.2.2 Stability Field for Ni^{+2} 160
6.3 Discussion 169
6.4 Green River Formation. 172
6.4.1 Lake Gosiute 175
6.4.2 Lake Uinta 186
6.5 Mowry Shale. 197
6.6 Monterey Shale 213
6.7 Kreyenhagen Shale. 228
6.8 Devonian-Mississippian Black Shales. 237
CHAPTER 7 VANADIUM-NICKEL FRACTION IN OIL-TO-SOURCE ROCK CORRELATIONS. 254
7.1 Alteration Effects During Entrapment 255
7.2 Alteration Effects During Migration. 259
7.3 Alteration Effects During Expulsion. 263
7.4 Discussion 266
CHAPTER 8 SUMMARY OF CONCLUSIONS 271
8.1 Preference 271
8.2 Source 272
8.3 Proportionality. 272
8.4 Oil-to-Source Rock Correlations. 273
REFERENCES CITED. 274
APPENDICES
I: Locality Descriptions for Rock Samples. 307
II: Inventory of Collected Samples. 311
III: Locality Descriptions for Petroleum Samples 317
IV: Organic Carbon and Bitumen Analyses 319
V: Kerogen Analyses. 323
VI: Vanadium and Nickel Concentrations in Bitumens. 330
VII: Mineralogy of Rock Samples (Wt. %). 332
VIII: Physical, Isotopic, and Compositional Data on Petroleum Samples 337
IX: Gibbs Free Energies at 298°K and ATM for the Formation of Phases Considered in Text. 339
X: Reactions Considered in the Construction of the Eh-pH Diagrams Used in Chapter 6. 342

LIST OF FIGURES

Page

Figure 1.1: Map showing sampling localities for samples used in this study. 4

Figure 2.1: Types of analyses performed on the rock and sediment samples used in this study 8

Figure 2.2: Histogram showing the distribution of organic carbon contents in the rock samples used in this study 11

Figure 2.3: Plot modified after Tissot and others (1974) showing the chemical evolution of the three kerogen types with increasing thermal maturation 19

Figure 2.4: Atomic H/C to O/C plot of kerogens from rock samples collected for this study. The actual values from which these ratios were calculated are given in Appendix IV . . 22

Figure 2.5: Atomic H/C to O/C plot showing the suggested chemical trends for kerogen oxidation. Curve A represents early oxidation of kerogen precursors, curve B represents oxidation of kerogen in sediments (pre-lithification), and curve C represents oxidation of kerogen in sedimentary rocks 23

Figure 2.6: δC^{13} values of liptinitic and ligninic kerogens through the geological record, and their precursors. Plankton values from Degens and others (1968b), and Fontugene and Duplessy (1978); plant, leaves, and wood values from Craig (1953); Miocene values from Monterey samples (this study); Eocene values from Craig (1953), Cozy Dell samples (this study), and Kreyenhagen samples (this study); Paleocene-Cretaceous values from Ferris samples (this study); Cretaceous values from Craig (1953) and Frontier samples (this study); Permian values from Compston (1960) and Phosphoria samples (this study); Pennsylvanian values from Craig (1953), Breathitt samlples (this study), Pocahontas sample (this study), Carbondale sample (this study), and Manning Canyon sample (this study); Devonian values from Maynard (1979), Chattanooga samples (this study), New Albany samples (this study), and Woodruff samlples (this study); Ordovician values from Maquoketa samples (this study); Keweenawan values from Nonesuch samples (this study); and Huronian values from Barghoorn and others (1977) 25

Page

Figure 2.7: Carbon isotope values of major organic constituents comprising plankton (Degens et al., 1968b) and their proposed relationship with liptinitic kerogens 29

Figure 2.8: Histogram showing carbon isotope values of β-sporopolleninic leninic kerogen from the Green River Formation (GR-1 thru GR-39) 32

Figure 2.9: (a) Graph showing weight loss of bitumen sample in sealed polyethylene vials with increasing exposure time to atmospheric conditions. (b) Graph showing constant weight of bitumen sample in polyethylene vial with exposure time after heating at 84°C for 24 hours 41

Figure 3.1: Conceptional cross-sectional view of surface weathering zones 48

Figure 3.2: H/C versus O/C plot of kerogen alteration resulting from surface weathering 52

Figure 3.3: Plot showing alteration of the total organic carbon and the extractability factor (bitumen/total organic carbon) of a rock as a result of surface weathering 53

Figure 3.4: Conceptual cross-sectional view of pedogenic weathering horizons 56

Figure 3.5: H/C versus O/C plot of kerogen alteration resulting from pedogenic weathering 60

Figure 3.6: Plot showing the alteration of the total organic carbon and the extractability factor (bitumen/total organic carbon) of a rock as a result of pedogenic weathering 61

Figure 3.7: Graphs showing types of alteration and their occurrence through surface weathering zones (a) and pedogenic weathering horizons (b) 64

Figure 3.8: Conceptual drawing of the superimposition of surface weathering on pedogenic weathering of the Kreyenhagen shale at the Skunk Hollow Outcrop (Local No. 59) 67

Figure 4.1: Basic framework of tetrapyrrole complex and modifications resulting from the addition of peripheral functional groups 69

Page

Figure 4.2: Types of conjugated configurations in tetrapyrrole complexes 71

Figure 4.3: Formation of pheophytin as a result of the demetallation of chlorophyll 74

Figure 4.4: Plots showing organic variables in the offshore southern California water column. Data from (a) Jannasch and Jones (1959), (b) and (c) Holm-Hansen (1969). Shaded area represents zone of phytoplankton concentration (Sleggs, 1927) 76

Figure 4.5: Plots showing the preferred decomposition of tetrapyrrole pigments relative to total organic carbon in (a) a marine water column (Holm-Hansen, 1969) and (b) a lake sediment (Koyama et al., 1968) 78

Figure 4.6: Concentration of pheophytin in organic matter from surface sediments of offshore southern California versus height of water column above sediment. The sediments plotted have median grain diameters equal to or less than 10 microns. Data from Orr and others (1958) 80

Figure 4.7: Formation of purpurin and chlorin as a result of the allomerization of pheophytin 83

Figure 4.8: a) Reduction of phytol double bond, and b) dealkenylation of phytol side chain 84

Figure 4.9: Comparison of the amounts of deestrified tetrapyrroles in surface sediments with those in lithified sediments. Data from Baker and Hodgson (1968) and Shiobara and Taguchi (1975) 85

Figure 4.10: Three reactions involving the reduction of the 2-vinyl double bond to an ethyl side chain, reduction of the 9-keto group to methylene, and the aromitization of the pheophorbide structure to a porphyrin 87

Figure 4.11: Assimilation of pheophorbide into the kerogen structure. Kerogen linkages designated as K_1, K_2, and K_3 . . . 88

Figure 4.12: a) Plan view of metallation site in tetrapyrroles for a bivalent metal (M^{+2}); b) perspective view of nickelous (Ni^{+2}) metallation site; and c) perspective view of vanadyl (VO^{+2}) metallation site 89

Page

Figure 4.13: Variations in the amount of metallated tetrapyrroles through a lithified sedimentary section on the Boso Peninsula, Japan (Shiobara and Taguchi, 1975) 92

Figure 4.14: Eh-pH diagrams showing approximated stability field for tetrapyrrole preservation (stippled area) and stability field for bivalent cations of the first transition-series of elements (hatched area). Average sea water concentrations were used for the total dissolved metal concentrations (Goldberg, 1961) 94

Figure 4.15: The coordination of a bivalent cation in a tetrapyrrole may be considered octahedral (a and b) or square planar (c) 99

Figure 4.16: Energy level diagrams showing the ligand field splitting patterns for d orbitals of cations in octahedral and square planar coordination. Values are from Krishnamurthy and Schaap (1969) 100

Figure 4.17: Modifications to tetrapyrroles during low levels of thermal maturation; a) dealkylation and b) decarboxylation 103

Figure 4.18: Ring scission of the isocyclic pentane ring at moderate levels of thermal maturation 104

Figure 4.19: Examples of tetrapyrroles that may occur at moderate to high levels of thermal maturation; a) insular porphyrin, b) highly aromatic insular tetrapyrrole, and c) highly aromatic tetrapyrrole condensed within a kerogen (K) 106

Figure 4.20: Proposed reaction sequence for conversion of tetrapyrrole pigments to insular and assimilated tetrapyrroles in crude oils, bitumens, and kerogens 108

Figure 4.21: Several examples of mixed ligand tetradentate complexes (M = metal cation) 109

Figure 4.22: Examples of types and reactions of humate complexes (M = metal cation) 113

Figure 4.23: Plot showing the amount of iron and aluminum in humic substances relative to their vanadium and nickel content; circles represent humic acid fractions, triangles represent fulvic acid fractions, and squares represent total humic substances 115

Page

Figure 5.1: Vanadium concentrations in bitumen from rocks and sediments bearing ligninic kerogen, and precursory organic substances (Ref. 1, Bertrand, 1950; Ref. 2, Boyle, 1977; Ref. 3, Cannon, 1952, Table 7). Number of samples given in parentheses 122

Figure 5.2: Nickel concentrations in bitumens from rocks and sediments bearing ligninic kerogen, and precursory organic substances (Ref. 1, Boyle, 1977; Ref. 2, Kovdi et al., 1959; Ref. 3, Cannon, 1960, whole plant values were calculated by assuming ash values between 5.4 and 23.4 percent by weight). Number of samples given in parentheses . . .123

Figure 5.3: Vanadium concentrations in higher plants, peats, and coals (Ref. 1, Cameron and Wright, 1977; Ref. 2, Kochenov and Kreshtapova, 1967; Ref. 3, Ruch et al., 1974; Ref. 4, Zubovic et al., 1960a; Ref. 5, Abernethy et al., 1969; Ref. 6, Zubovic et al., 1960b.; Ref. 7, Szilagyi, 1971; Ref. 8, Swaine, 1975; Ref. 9, Yudovich et al., 1972). Number of samples given in parentheses 124

Figure 5.4: Nickel concentrations in higher plants, peats, and coals (Ref. 1, Cameron and Wright, 1977; Ref. 2, Casagrande and Erchull, 1977; Ref. 3, Kochenov and Kreshtapova, 1967; Ref. 4, Ruch et al., 1974; Ref. 5, Zubovic et al., 1960a.; Ref. 6, Abernethy et al., 1969; Ref. 7, Zubovic et al., 1960b.; Ref. 8, Swaine, 1975; Yudovich et al., 1972). Number of samples given in parentheses 125

Figure 5.5: Nickel concentrations in bitumens from rocks and sediments bearing liptinitic kerogen, extracts from brown and green algae, and precursory organisms (Ref. 1, Martin and Knauer, 1973; Ref. 2, Fowler, 1977; Ref. 3, Young and Langille, 1958; Ref. 4, Bollingberg, 1975; Ref. 5, Vinogradov, 1953, p. 121) 128

Figure 5.6: Vanadium concentrations in bitumens from rocks and sediment bearing liptinitic kerogen,extracts from brown and green algae, and precursory organisms (Ref. 1, Ostroumov and Silina, 1952; Ref. 2, Nicholls et al., 1959; Ref. 3, Martin and Knauer, 1973) 129

Figure 5.7: Vanadium concentrations in plankton, aquatic animals (Ref. 1, Bertrand, 1950; Ref. 2, Blotcky et al., 1979; Ref. 3, Nicholls et al., 1959; Ref. 4, Vinogradov, 1953, p. 425) and bitumens from rocks bearing liptinitic kerogens. The data on tunicata from Ref. 3 and Ref. 4 were classified according to Berrill (1950). Number of samples given in parentheses 131

Page

Figure 5.8: Comparison of vanadium and nickel concentrations in bitumens and kerogen of the Green River Formation with their endemic concentrations in higher plants and plankton 133

Figure 5.9: Vanadium concentrations in fresh surface waters (solid dots and bars; Ref. 1, Livingstone, 1963; Ref. 2, Konovalov, 1973), sea water (cross hatched dots and bars; Ref. 3, Riley, 1965; Ref. 4, Goldberg, 1965; Ref. 5, Angino, 1964; Ref. 6, Black and Mitchell, 1952), and subsurface waters (hatched bars; Ref. 7, Denson and Gill, 1965; Ref. 8, Sugawara, Naito, and Yamada, 1956). Number of samples given in parentheses 137

Figure 5.10: Nickel concentrations in fresh surface waters (solid dots and bars; Ref. 1, Livingston, 1963, Table 90; Ref. 2, Andelman, 1973; Ref. 3, Konovalov, 1973), sea water (cross hatched dots and bars; Ref. 4, Sclater et al., 1976; Ref. 5, Brewer and Spencer, 1974; Ref. 6, Goldberg, 1965; Ref. 7, Black and Mitchell, 1952), and subsurface waters (hatched dots and bars; Ref. 8, Denson and Gill, 1965; Ref. 9, Naboko et al., 1973). Number of samples given in parentheses 138

Figure 5.11: Graphs showing the maximum metal concentration that may occur in the organic matter of a sediment in a closed system. Calculations are based on 1 m^3 of sediment, and the parameters considered are percent water by volume, concentration of metal in interstitial water, and grams of organic matter in sediment. The dried sediment is assumed to have a density of 2.5 grams/cm^3. Graph A shows the dependence of grams of dissolved metal per cubic meter of sediment on percent water by volume in the sediment and concentration of metal in the water. Graph B shows the dependence of maximum metal concentration possible in the organic matter of a sediment on grams of dissolved metals per cubic meter of sediment and grams of organic matter per cubic meter of sediment. Numbers in parentheses represent the weight percent of organic matter on a dry weight basis for 1 cubic meter of sediment with 25, 50, and 75 percent water by volume, respectively 139

Figure 5.12: Graphs showing approximately the enriched metal concentrations that may be obtained by organic matter from interstitial waters in an open sediment system. Calculations are based on a sediment slab that has a surface area of 1cm^2 and a depth of 1 mm. The densities of the organic and inorganic fraction of the sediment slab are

Page

assumed to be 1.5 and 2.5 g/cm^3, respectively. Graph A shows approximately the minimal amount of metal required to pass through a sediment slab in order to obtain a specified enriched metal concentration in the organic matter of the sediment slab. The lines labeled OM represent sediment slabs with different amounts of organic matter, which are expressed in weight percent of the whole sediment slab. Graph B shows approximately the amount of time the sediment system must be open in order to obtain a specified enriched metal concentration in the organic matter. The lines labeled J represent different metal flux values, which are expressed in μmoles/cm^{2}sec. Graph C shows the burial depth of a sediment slab after a specified time. The lines labeled ω represent different sedimentation rates, which are expressed in cm/1000 years. The red lines labeled a, a_1, a_2, b, b_1, and b_2 are construction lines which are referred to in the text 142

Figure 5.13: Plot comparing the atomic N/C ratio of the three kerogen types with the vanadium plus nickel concentrations in their bitumens. The samples used include I-1, F-1, F-2, and H-1 for ligninic kerogen bearing rocks, MR-5 thru MR-10, MR-12, MR-13, and K-1 thru K-5 for liptinitic kerogen bearing rocks, and GR-1, GR-3 thru GR-7, GR-10 thru GR-13, GR-15 thru GR-21, GR-25 thru GR-27, GR-29, GR-30, GR-32, GR-34, and GR-37 thru GR-39 for sporopolleninic kerogen bearing rocks 147

Figure 6.1: Eh-pH diagrams showing the difference between the stability fields for a total dissolved vanadium concentration of $10^{-6.13}$ moles/liter (dashed lines) and those for a total dissolved vanadium concentration of $10^{-7.48}$ moles/liter 152

Figure 6.2: Natural stability fields for water (solid lines; Krauskopf, 1967, pp. 245-246), marine sediments (dotted-solid line; Baas Becking, et al., 1960), marginal marine sediments (dashed line; Baas Becking, et al., 1960), and organic sediments (shaded area; Krumbein and Garrels, 1952) 155

Figure 6.3: Eh-pH diagram for vanadium at sea water concentrations under surface and mild diagenetic conditions ($\Sigma S = 10^{-2.63}$ mol/liter and $\Sigma CO_2 = 10^{-2.63}$ mol/liter. Hatched area represents the stability field for vanadyl species. Explanation of stippled area and broken lines is given in Figure 6.2 158

Page

Figure 6.4: Eh-pH diagram for nickel at sea water concentrations under surface and mild diagenetic conditions ($\Sigma S = 10^{-1.56}$ mol/liters and $\Sigma CO_2 = 10^{-2.63}$ mol/liters). Hatched area represents the stability field for the nickelous cation (Ni^{+2}). Explanation of stippled area and broken lines is given in Figure 6.2 161

Figure 6.5: Conceptual view of relationships between height of aerobic water column, rate of sedimentation, oxygen content of encountered aerobic conditions, and probability of carbohydrate preservation. Oxygen levels are classified in accordance with Rhoads and Morse (1971, Figure 5; aerobic $\geq$ 1.0 ml O_2/liter, dysaerobic = 0.1 to 1.0 ml O_2/liter, and anaerobic < 0.1 ml O_2/liter) 168

Figure 6.6: Eh-pH diagram resulting from the superimposition of vanadium and nickel Eh-pH diagrams in Figures 6.3 and 6.4, respectively. Roman numerals designate major Eh-pH fields under which organic sediments may accumulate . . .170

Figure 6.7: Tertiary basins in which Green River Formation occurs (modified from Van West, 1972) 174

Figure 6.8: Geological map and stratigraphic section of the Green River Formation in the Green River Basin of Wyoming (map modified after Van West, 1972). Sampling locality numbers correspond with those given in Appendix I . .176

Figure 6.9: Organic carbon content of samples used in this study, and classification of their organic richness. Samples are from the Green River Formation in the Green River Basin 178

Figure 6.10: Atomic H/C ratio versus atomic O/C ratio plot of kerogens from the Green River Formation in the Green River Basin. Thermal maturation pathways for the three kerogen types are the same as those presented in Figure 2.3 . .179

Figure 6.11: Ternary diagrams showing mineralogy of the Tipton Member and Wilkins Peak Member of the Green River Formation. Plots are based on data given in Appendix VII . . .181

Figure 6.12: Interpreted trend of the playa-lake facies sequence of the Wilkins Peak Member on the Eh-pH diagram presented in Figure 6.6. Numbers on shaded trend correspond to the facies given in Table 6.8 185

Page

Figure 6.13: Geological map and stratigraphic section of the Green River Formation in the Uinta Basin of Utah (modified after Van West, 1972; and Cashion, 1967, Figure 8). Sampling locality numbers correspond to those given in Appendix I 188

Figure 6.14: Histogram showing organic carbon content of smaples used in this study, and classification of their organic richness. Samples are from the Green River Formation in the Uinta Basin 190

Figure 6.15: Atomic H/C ratios versus atomic O/C ratio plot of kerogens from the Green River Formation in the Uinta Basin. Thermal maturation pathways for the three kerogen types are the same as those presented in Figure 2.3 . .191

Figure 6.16: Ternary diagrams showing mineralogy of the Mahogany zone and Parachute Creek Member of the Green River Formation. Plots are based on data given in Appendix VII . . .192

Figure 6.17: Interpreted trend of the lacustrine facies sequence of the Parachute Creek Member on the Eh-pH diagram from Figure 6.6. Numbers on shaded trend correspond to facies given in Table 6.11 196

Figure 6.18: Map showing extent of Mowry Sea in the western interior of the United States, and the locations of successor basins around which the Mowry Shale is exposed and the outcrop near Steinaker Reservoir (modified after Figure 17 from Cobban, 1972). Insert map shows regional extent of Mowry Sea over North America and its relation to the Cretaceous Gulf of Mexico and boreal sea (modified after Figure 4 from Stelck, 1975) 198

Figure 6.19: Map showing sampling localities, structure, and organic-rich portions of the Mowry Shale in the Powder River Basin of Wyoming. Sampling locality numbers correspond to those given in Appendix I. Structure contours are relative to sea level and are modified after Figure 6 from McGregor (1972). The high organic carbon area is modified after Figure 13 from Nixon (1973). General stratigraphic section of Mowry Shale is modified after Figure 1 from Davis (1970) 200

Figure 6.20: Ternary diagram showing mineralogy and rock types of the Mowry Shale samples. Plots are based on data given in Apendix VII 201

Page

Figure 6.21: Ternary diagrams showing variations in the clay mineralogy and sample depth of the collected Mowry Shale samples. Plots are based on data given in Appendix VII 202

Figure 6.22: Histogram showing organic carbon content of samples used in this study and classification of their organic richness. Samples are from the Mowry Shale in the Powder River Basin and Steinaker reservoir outcrop 204

Figure 6.23: Characterization of kerogens from the Mowry Shale samples by a) visual analysis and b) carbon isotope values 206

Figure 6.24: Atomic H/C ratio versus atomic O/C ratio plot of kerogens from the Mowry Shale samples. Thermal maturation pathways for the three kerogen types are the same as those presented in Figure 2.3 207

Figure 6.25: Histogram showing bitumen contents and limits of acceptability for vanadium and nickel analyses of bitumens from the Mowry Shale samples 209

Figure 6.26: Interpreted trend of the Mowry Shale facies sequence on the Eh-pH diagram from Figure 6.6 Numbers on shaded trend correspond to facies given in Table 6.13 211

Figure 6.27: Map of southern California showing the limit of the Pacific Ocean during Late Miocene time and the major submarine basins. Map is based on work by Reed (1933), Reed and Hollister (1936), and Simonson (1958) 214

Figure 6.28: Geological map showing sampling localities of the Monterey Shale and the marine sedimentary rocks of Middle and Late Miocene age in southern California (modified from Jenkins, 1938). Localities referenced for future studies include Shell Beach (A, Sec. 4, T.32S., R.12E., San Luis Obispo Co.), Point Dume (B, Sec. 8, T.2S., R.18W., Los Angeles Co.), and Newport Bay (C, Sec. 26, T.6S., R.10W., Orange Co.). Insert showing types of rock sequences in the Monterey Shale is based on work by Pisciotto (1978) and a personal communique with Surdam (1979) 216

Figure 6.29: Ternary diagrams showing mineralogy of rock types collected from the Monterey Shale for this study. Plots based on data given in Appendix VII 218

Page

Figure 6.30: Histogram showing distribution of organic carbon in different rock sequences of the Monterey Shale, and classification of their organic richness 219

Figure 6.31: Histogram showing the distribution of kerogen δC^{13} values of Monterey Shale samples and their relationship to visual kerogen analyses 221

Figure 6.32: Atomic H/C ratios versus atomic O/C ratio plot of kerogens from the Monterey Shale samples. Thermal maturation pathways for the different kerogen types are the same as those presented in Figure 2.3 222

Figure 6.33: Histogram showing bitumen contents and limits of acceptability for vanadium and nickel analyses of bitumens from the Monterey Shale samples 223

Figure 6.34: Interpreted trends for the proposed facies of the Monterey Shale samples on the Eh-pH diagram from Figure 6.6. Numbers on shaded trends correspond to facies given in Table 6.14 224

Figure 6.35: Map of central California showing the Late Eocene and Early Oligocene inland sea, in which the Kreyenhagen Shale was deposited. Map is based on work by Reed (1933) and Reed and Hollister (1936) 229

Figure 6.36: Geological map showing sampling localities of the Kreyenhagen Shale and the Late Eocene and Early Oligocene sedimentary rocks in central California (modified from Jenkins, 1938). Unsampled localities include Woo Ranch Canyon (A, Secs. 1 and 12, T.12S., R.10E., Merced Co.), Arroyo Ciervo (B, Secs. 22, and 23, T.16S, R.13E., Fresno Co.), Oil Canyon (C, Sec. 20, T.19S., R.15E., Fresno Co.), and Devils Den (D, T.25S, R.18E., Kern Co.). Insert showing type of rock sequences in the Kreyenhagen Shale is base of field work by the author and described sections by von Etorff (1930), Woodring and others (1940), Cushman and Siegfus (1942), Kidson (1965), and Watkins (1974) 230

Figure 6.37: Ternary diagrams showing mineralogy and organic carbon content of rock types collected from the Kreyenhagen Shale. Plots based on data given in Appendix VII 233

Figure 6.38: Atomic H/C ratio versus atomic O/C ratio plot of kerogens from the Kreyenhagen Shale samples. Kerogen carbon isotope values are relative to PDB and given in per

Page

mil units. Thermal maturation pathways for the different kerogen types are the same as those presented in Figure 2.3 . .234

Figure 6.39: Interpretation of proposed Kreyenhagen Shale facies on the Eh-pH diagram presented in Figure 6.6. Circled numbers correspond to facies given in Table 6.15 236

Figure 6.40: Map showing extent of Devonian-Mississippian sea in the eastern half of the United States and basins around which outcrops of the Devonian-Mississippian black shales occur (modified after Conant and Swanson, 1961) 238

Figure 6.41: Geological map showing Devonian and Lower Mississippian rocks of the central lowland states (modified from King and Beikman, 1974), and localities where Devonian-Mississippian black shales were sampled for this study 240

Figure 6.42: Generalized stratigraphic sections showing the occurrence and distribution of greenish and light gray fine grained rocks in the Devonian-Mississippian black shales 241

Figure 6.43: Ternary diagram showing mineralogy of rock types collected from the Devonian-Mississippian black shales. Plots based on data given in Appendix VII 242

Figure 6.44: Histogram showing the distribution of organic carbon in different rock types collected from the Devonian-Mississippian black shales, and classification of their organic richness 247

Figure 6.45: Kerogen types in Devonian-Mississippian black shales as indicated by a) kerogen carbon isotopes and b) visual analysis 249

Figure 6.46: Atomic H/C ratio versus atomic O/C ratio plot of kerogens from the Devonian-Mississippian black shales. Thermal maturation pathways for the different kerogen types are the same as those presented in Figure 2.3 250

Figure 6.47: Interpretation of proposed Devonian-Mississippian black shale facies on the Eh-pH diagram presented in Figure 6.6. Circled numbers correspond to facies given in Table 6.18 253

Figure 7.1: Cross-section showing vertical migration of crude oil from the lower reservoir into the upper reservoir

Page

along a structural fracture system in the Ain Zalah Field of Iraqi (modified after Dunnington, 1958, Figure 15). The vanadium and nickel analyses of the crude oils from this field are presented in the insert and where determined by Al-Shahristani and Al-Atyia (1972) 265

Figure 7.2: Atomic H/C ratio versus atomic O/C ratio of samples that did not satisfy the minimum bitumen requirement for vanadium and nickel analyses 270

LIST OF TABLES

Page

Table 1.1: Formations sampled for this study, and their geological age and sample numbers 5

Table 2.1: Organic constituents of plankton in dry weight percent 30

Table 2.2: Vanadium and nickel concentrations in bitumens and kerogens 36

Table 2.3: Vanadium and nickel analyses of kerogen and the effect of pyrite contamination 37

Table 2.4: Elemental analyses of kerogens before and after being treated with 25 percent solution of nitric acid for 5 hours 38

Table 2.5: Vanadium and nickel analyses of kerogens before and after being treated with a 25 percent solution of nitric acid for 5 hours 39

Table 2.6: Vanadium and nickel analyses of bitumens extracted by different solvents from the New Albany Shale Standard No. 1 41

Table 2.7: Vanadium and nickel analyses showing the effect of heating bitumen at 96°C for 24 hours. Vales are means of 3 aliquots of Standard No. 1 43

Table 2.8: Vanadium and nickel concentrations in inorganic contaminants 45

Table 3.1: Mineralogy of surface weathered shales and their unweathered equivalents. Values are given in weight percent 50

Table 3.2: Carbon isotope values of kerogens from surface weathered rocks and their unweathered equivalents 52

Table 3.3: Mineralogy of pedogenic weathered shales and their unweathered equivalents. Values given in weight percent 58

Table 3.4: Carbon isotope values of kerogens from pedogenic weathered rocks and their unweathered equivalents 61

Page

Table 3.5: Data on the effect of weathering on the concentration and proportionality of vanadium and nickel in bitumen 64

Table 4.1: Distance between opposite nitrogen atoms in tetrapyrroles 96

Table 4.2: Ionic radii of metals (6 fold coordination) in bivalent cations of the first transition series 97

Table 4.3: Electron distribution and ligand field stabilization energies for high spin state, bivalent cations of the first transition series of elements in octahedral and square planar coordination 101

Table 4.4: Ligand field stabilization energies for high spin, bivalent cations of the first transition series of elements 111

Table 4.5: Vanadium and nickel concentrations in bitumens from the New Albany Shale Standard No. 1, which have been subjected to 18.5N and 37N solutions of sulfuric acid at 150°C for 7 hours 117

Table 5.1: A summary of the nature of vanadium and nickel in bitumens from rocks bearing different types of kerogen 135

Table 5.2: Concentrations of tetrapyrrole pigments in phytoplankton and higher plants 145

Table 5.3: Primary factors determining the amount of vanadium and nickel concentrated in organic matter and their controlling variables 149

Table 6.1: Gibbs free energies of formation for iron and nickel sulfides at 298°K and 1 ATM. Values were obtained from references cited in Appendix IX 154

Table 6.2: Parameters reflecting stability of vanadyl and nickelous cations in tetrapyrrole complexes 157

Table 6.3: Reactions between iron- and nickel-sulfides and their Gibbs free energy of reaction (ΔGr). Values based on Gibbs free energies of formation given in Appendix IX 163

Table 6.4: Sulfate concentrations in natural waters 165

Page

Table 6.5: Effect of type and amount of metabolite on rate of bacterial sulfate reduction 166

Table 6.6: Summary of the vanadium and nickel species that are available and unavailable for bonding with tetrapyrrole complexes under different conditions as categorized in Figure 6.6 173

Table 6.7: Classification of rock types in the Wilkins Peak and Tipton members of the Green River Formation 182

Table 6.8: Description of playa-lake facies sequence in the Wilkins Peak Member and the corresponding carbon isotope values of their kerogens and vanadium-nickel fractions of their bitumens 183

Table 6.9: Description of playa-lake facies sequence in the Tipton Member and the corresponding carbon isotope values of their kerogens and vanadium-nickel fractions of their bitumens 187

Table 6.10: Classification of rock types in the Mahogany Zone and Parachute Creek Member of the Green River Formation 193

Table 6.11: Description of lacustrine facies sequence in the Parachute Creek Member and corresponding carbon isotope values of their kerogens and vanadium-nickel fractions of their bitumens 194

Table 6.12: Basic petrologic data on Mowry Shale samples used in this study 203

Table 6.13: Description of Mowry Shale facies, based on vanadium-nickel fractions of their bitumen (V/(Ni+V)) 210

Table 6.14: Description of Monterey Shale facies and the vanadium-nickel fractions of their bitumens (V/(Ni+V)) 225

Table 6.15: Descriptions of Kreyenhagen Shale facies and the vanadium-nickel fractions of their bitumens (V/(Ni+V)) 235

Table 6.16: Some petrographic observations made on the Devonian-Mississippian black shales collected for this study 243

Table 6.16 (Cont'd): Some petrographic observations made on the Devonian-Mississippian black shales collected for this study 244

Page

Table 6.17: Comparison of iron sulfide concentrations in Devonian-Mississippian black shales with those in the other formations discussed. Iron sulfides include pyrite and marcasite 246

Table 6.18: Facies of the Devonian-Mississippian black shales, based on vanadium-nickel fraction of their bitumen (V/(Ni+V)) 252

Table 7.1: Geochemical parameters used in oil-to-source rock correlations 255

Table 7.2: Influence of thermal degradation on the vanadium-nickel fraction of a Kuwait crude oil residue. Data is from Costantinides and others (1959, p. 140) 257

Table 7.3: Comparison of the vanadium-nickel fractions in the asphaltene and non-asphaltene fractions of two crude oils 259

Table 7.4: Comparison of vanadium-nickel fractions of Kuwait crude oil and Kuwait oil residue with naturally degraded crude oils that are suspected of being derived from Kuwait crude oil (Brunnock et al., 1968) 261

Table 7.5: Experimental results showing the influence of weathering on the vanadium-nickel fraction of a Kuwait crude oil residue in open tank experiments (Davis and Gibbs, 1975) 262

Table 7.6: Vanadium and nickel concentrations and vanadium-nickel fractions of pyrolysates expelled from Woodford Shale (WD-5) by hydrous pyrolysis at different temperatures for durations of 72 hours 266

Table 7.7: Vanadium and nickel concentrations and vanadium-nickel fractions of bitumens and pyrolysates from the same rocks. Pyrolysates were generated by hydrous pyrolysis 268

CHAPTER 1

INTRODUCTION

Abnormally high concentrations of vanadium and nickel have been noted in crude oils (Hodgson, 1954; Bonham, 1956; Witherspoon and Nagashima, 1957; Ball and Wenger, 1960; and others), asphalts (Erickson et al., 1954), and black shales (Krauskopf, 1955; and Vine and Tourtelot, 1970). It has also been observed that crude oils from certain basins or formations within a given basin have a distinct vanadium to nickel proportionality (Hodgson, 1954; and Ball and Wenger, 1960). The types of metallo-organic compounds that accommodate these two metal are still not completely resolved (Beach and Shewmaker, 1957; and Dwiggins et al., 1969), but it is known that they are high molecular weight complexes (Yen, 1975a), with vanadium and nickel being covalently bound as VO^{+2} and Ni^{+2}, respectively (Saraceno et al., 1961; and Dwiggins et al., 1969).

Although the chemistry of vanadium and nickel in crude oils has been studied extensively, there are still several fundamental questions that remain unresolved. The objective of this study is to examine in detail four of these basic questions, which include the following:

1. Why are vanadium and nickel preferentially concentrated in organic substances?

2. What is the source of vanadium and nickel in organic substances?

3. What controls the vanadium to nickel proportionality in organic substances?

4. Can the vanadium to nickel proportionality be used to correlate a crude oil with the source rock from which it was expelled?

1.1 PREFERENCE, SOURCE, AND PROPORTIONALITY

It has been suggested that the answers to the first three questions may lie in the sedimentary rocks from which crude oils are expelled (Erickson et al., 1954; Bonham, 1956; Erdman et al., 1957; Hodgson et al., 1967; and Filby, 1975). Hodgson and others (1968) studied vanadium and nickel in certain metallo-organic complexes (porphyrins), that were extracted from a variety of sedimentary rock types. They concluded that the vanadium porphyrins showed no apparent relation to the nickel porphyrins, nor to the lithology, sulfur content, geological age, or level of diagenesis of the sedimentary rocks from which they were extracted. Additional factors that were not considered in their study, which may be relevant, are the type and amount of organic matter in the rocks and their environment of deposition. Theoretical considerations along with data from the literature suggest that these factors may play an important role in controlling the source, concentration, and proportionality of vanadium and nickel in the organic matter of sedimentary rocks and their expelled hydrocarbons. For this reason, vanadium and nickel

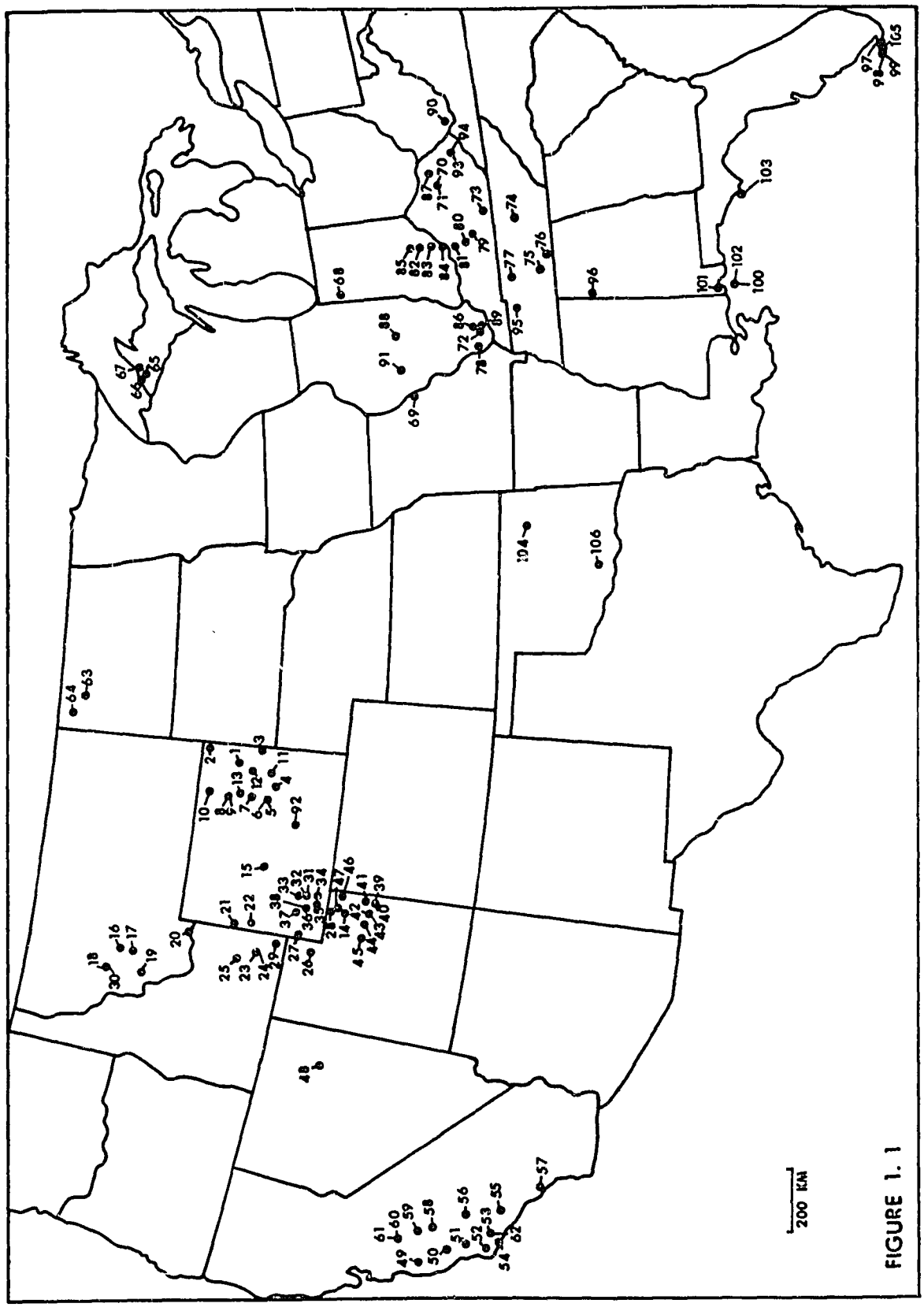

FIGURE 1. 1

concentrations in the extractable organic matter from 144 sedimentary rocks and 9 recent sediments were determined by neutron activation analysis. These samples represent a variety of depositional environments and contain several types of organic matter in varying quantities and mixtures. This data in conjunction with theoretical considerations and published data are used in dealing with the first three objectives of this study. Figure 1.1 shows the sample localities, and Table 1.1 gives the names and ages of the sampled formations. Detail descriptions of the sampling localities noted on Figure 1.1 and an inventory of the samples collected are given in Appendices I and II, respectively.

1.2 OIL-TO-SOURCE ROCK CORRELATION

Vanadium and nickel in crude oils have been used to decipher petroleum migrations paths and to correlate oils from different formations or fields (Al-Shahristani and Al-Aryia, 1972; Hodgson and Baker, 1959; and Bonham, 1956), but their use as a means to correlate crude oils to their source rocks has not been properly evaluated. The tenacious bonding of vanadium and nickel in high molecular weight organic complexes of crude oils (Sugihara et al., 1975; Rosscup and Bowman, 1967; Caughey and Corwin, 1955) suggests that once these metals are incorporated into a crude oil they remain fixed. Thermal maturation, migration, and microbial degradation of crude oils may alter the concentrations of vanadium and nickel by addition or subtraction of more labile components in crude oils, but their proportionality should remain unchanged.

Figure 1.1: Map showing sampling localities for samples used in this study.

Table 1.1: Formations sampled for this study, and their geological age and sample numbers.

Formation	Geologic Age	Sample Nos.
Nonesuch	Precambrian	NS1-NS6
Maquoketa	Ordovician	MQ1,MQ2
Woodruff	Devonian	W1-W3
New Albany	Dev.-Miss.	NA1-NA25
Chattanooga	Dev.-Miss.	CH1-CH12
Woodford	Dev.-Miss	WD5,WD7
Bakken	Dev.-Miss.	B1,B2
St. Louis	Mississippian	SL1
Manning Canyon	Pennsylvanian	MC1-MC3
Breathitt	Pennsylvanian	HA9,HA22
Pocahontas	Pennsylvanian	PO1
Carbondale	Pennsylvanian	I1
Phosphoria	Permian	P1-P31
Ellis	Jurassic	E1
Mowry	Cretaceous	M1-M43
Moreno	Cretaceous	MO1,MO2
Frontier	Cretaceous	F1,F2
Espada	CretaceousZ	ES1
Ferris	Cretaceous-Paleocene	H1
Green River	Eocene	GR1-GR39
Kreyenhagen	Eocene	K1-K6
Cozy Dell	Eocene	CD1
Monterey	Miocene	MR1-MR17
Sediment	Recent	RE1-RE9
Living Matter	Recent	LM1, LM2

The fourth objective of this study considers the potential of these two metals as a correlation parameter by comparing their proportionality in laboratory generated pyrolysates and naturally occurring hydrocarbons with their proportionality in the extractable organic matter from their source rocks.

CHAPTER 2

TYPES OF ANALYSES AND THEIR GEOCHEMICAL IMPLICATIONS

As shown in Figure 2.1, the analyses performed on the rocks and sediments of this study have been divided into two categories; organic analyses and bulk rock analyses. The organic analyses used in this study were chosen because they reveal information pertaining to amount, type, and level of thermal maturation of organic matter in the samples. The bulk analyses involved the whole rock sample and are used in this study to deduce the environment of deposition. This information combined with the vanadium and nickel concentrations in the extractable organic matter from the samples is used in evaluating the source, concentration, and proportionality of these two metals in organic matter.

The surfaces of rock samples were washed and scrubbed with tap water and a wire brush. After the rocks were completely dry they were crushed and pulverized. At least 300 grams of sample were pulverized to less than 150-micron size and stored in mason jars. Sediment samples were dried in a desiccator with sodium hydroxide pellets, and then pulverized and stored in the same way described for rock samples.

2.1 AMOUNT OF ORGANIC MATTER

Organic matter has been shown to have a significant influence on the chemistry of interstitial sediment waters and water columns (Shishkina, 1964; Siever et al., 1965; Brooks et al., 1968; Sholkovitz, 1973; and Toth and

Figure 2.1: Types of analyses performed on the rock and sediment samples used in this study.

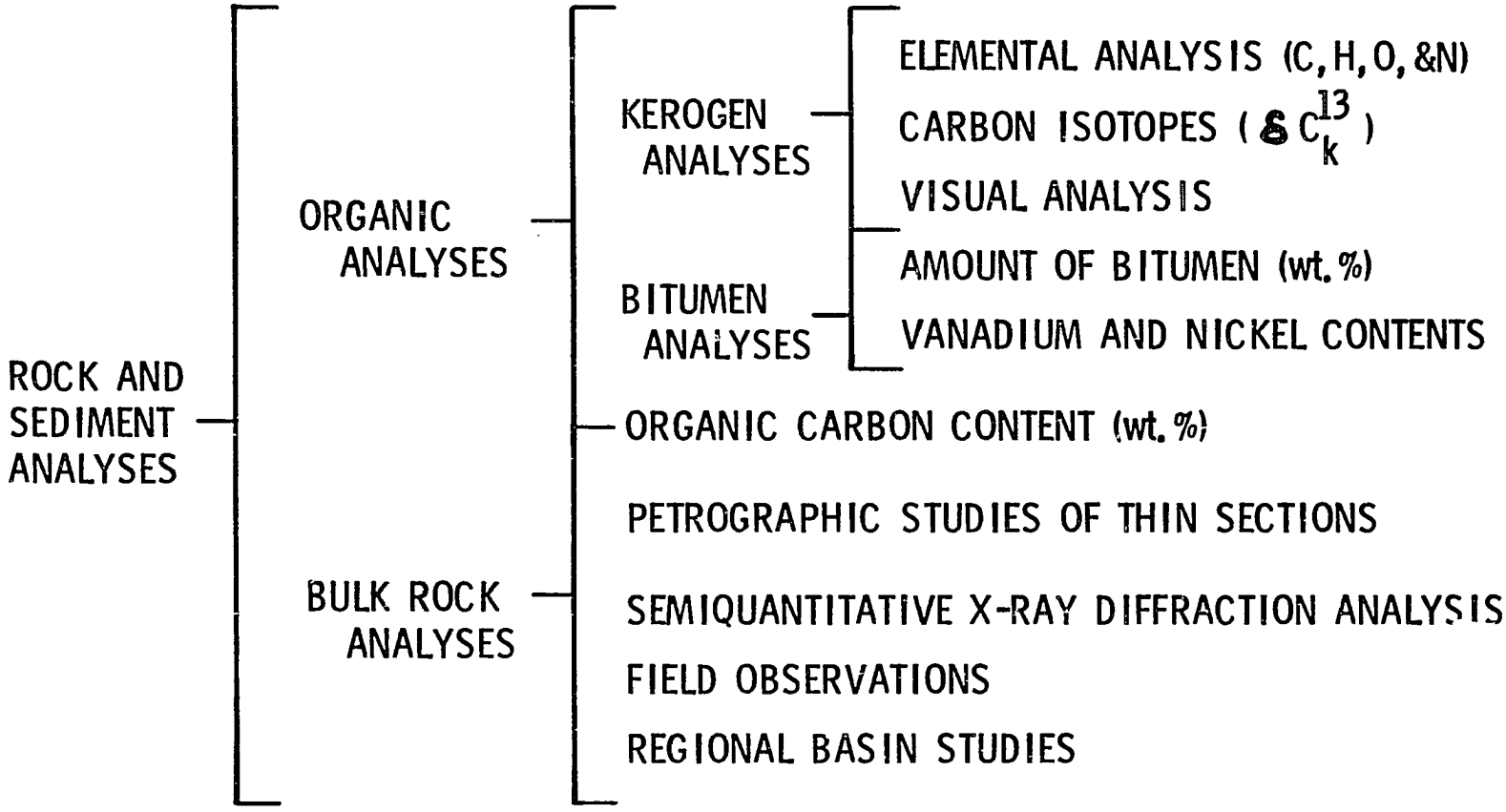

FIGURE 2.1

Lerman, 1977). Its potential effect on pH, Eh, and composition of interstitial sediment waters may play an important role in governing the geochemical behavior of vanadium and nickel in the sediments (e.g., Evans and Garrels, 1958; Hodgson and Hitchon, 1959; Gulyayeva and Lositskaya, 1967; and Szilagyi, 1972). Because of this, the amounts of organic matter in the samples of this study have been considered.

The amount of organic matter in sedimentary rocks is difficult to determine because its separation from the rock or sediment is seldom complete. Instead, a good estimate may be derived by determining the amount of carbon in the organic matter (Trask and Patnode, 1942; Ronov, 1958; Hunt, 1961; and Gehman, 1962). This is called organic carbon and can be determined readily in the laboratory. In this study organic carbon was determined by combusting the pulverized sample at 980°C in a Carlo Erba Model 1102 elemental analyzer. Inorganic carbon in the form of carbonate was removed from the samples before combustion by treating it with a warm 18% solution of hydrochloric acid. Acetanlide was used as the standard, and the method has a standard error of ±0.2 weight percent.

It should be kept in mind that the organic carbon value is only an estimate of the organic matter content of the sample. Organic carbon comprises at least 60 weight percent of the organic matter in recent sediments and approaches 100 weight percent in the organic matter of metamorphosed sedimentary rocks. Thus, the estimate becomes more accurate with increasing thermal maturation as a result of increasing carbon predominance, due to the preferential loss of the more volatile oxygen- and

hydrogen-rich components in the organic matter. For this reason care should be taken when comparing the organic carbon values of samples having drastically different levels of thermal maturation.

A verbal scale for organic richness of a sample has been devised for this study on the basis of its organic carbon content. Non-organic samples contain less than 1 weight percent organic carbon, organic samples contain 1 or more weight percent organic carbon, organic rich samples contain 5 or more weight percent organic carbon, and coaly samples contain 20 or more weight percent organic carbon. Samples containing organic carbon in quantities equal to or exceeding 50 weight percent are called coals. The organic carbon values for the samples in this study are given in Appendix IV and those for the rock samples are shown in the form of a histogram in Figure 2.2.

2.2 TYPE OF ORGANIC MATTER

Different types of organic matter in sedimentary rocks appear to be related to the source material from which they were derived (Forsman, 1963; McIver, 1967; and Staplin, 1969). Although no data have been presented on how the type of organic matter might influence the geochemical behavior of metals directly, the observations from several different studies suggests that it may play an important role. Nissenbaum (1974) has demonstrated that marine humic acids are derived from planktonic material and have a different chemical and isotopic composition than terrestrial humic acids derived from higher plant material. It is interesting that

Figure 2.2: Histogram showing the distribution of organic carbon contents in the rock samples used in this study.

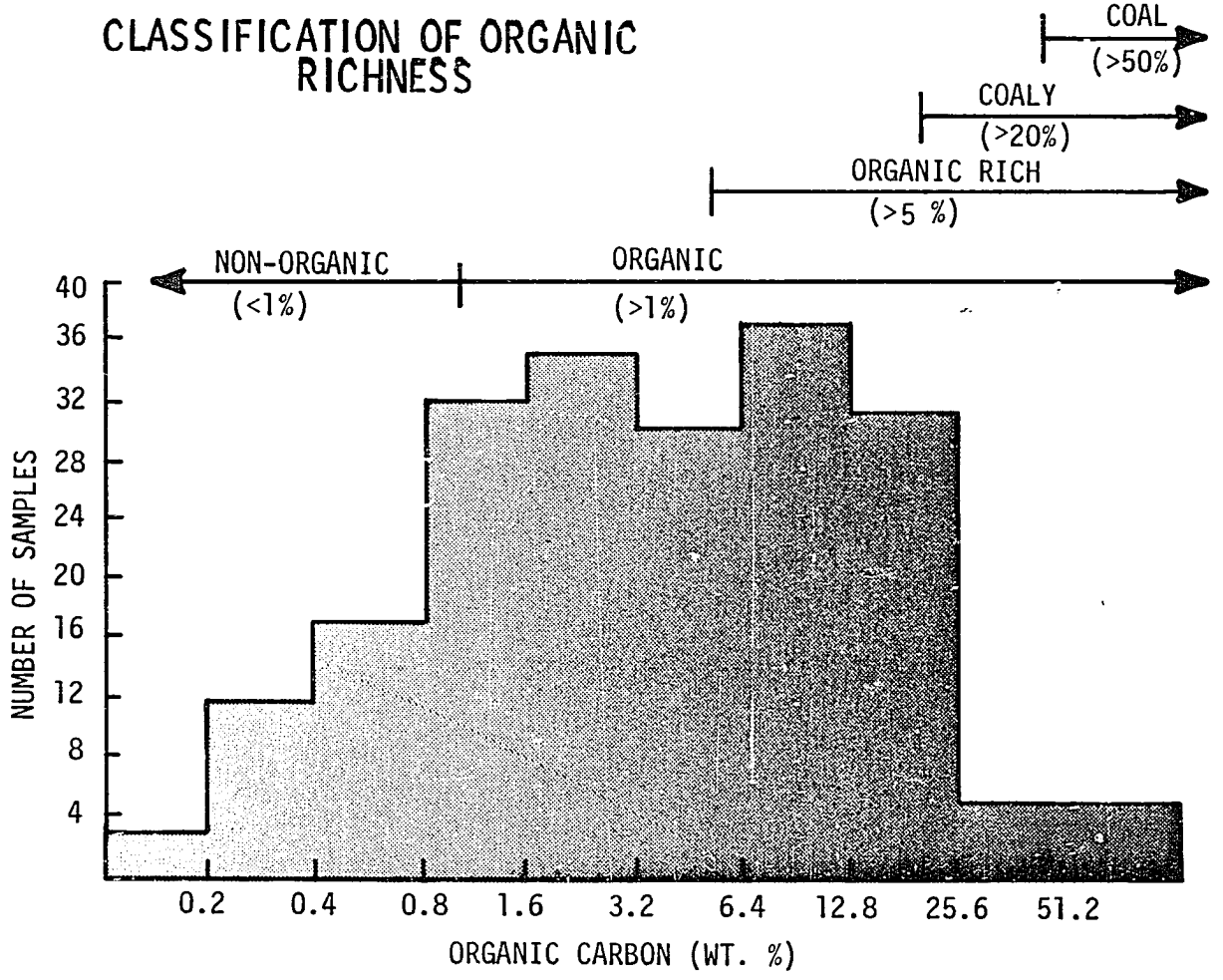

FIGURE 2.2

Rashid (1971) found that marine humic acids prefer complexing with divalent metals (e.g. Ni^{+2} and Cu^{+2}) rather than trivalent metals (e.g. Fe^{+3} and Al^{+3}), whereas Kribek and others (1977) found the reverse to be true for terrestrial humic acids. Thus, it does seem likely that the type of organic matter could control the fate of metals in a sedimentary regime, and for this reason it was considered in this study.

Organic matter in sedimentary rocks may be split into two fractions; extractable organic fraction and insoluble organic fraction. The extractable organic fraction is referred to in this study as bitumen. The bitumen is extracted from the pulverized sample by refluxing 200 milliters of a benzene-methanol mixture (70/30 volume percent, pesticide grade) through the sample for 20 hours in a soxhlet apparatus (Roberts et al., 1974). The amount of sample used depends upon its density and organic richness. The amount of bitumen extracted is given by weight in per mil ($^{o}/oo$) units, and the method has a standard error of ±0.1 per mil. In order to normalize the amount of bitumen with respect to the amount of organic matter in a sample, the amount of bitumen in a sample is divided by its organic carbon content, and in this study the quotient is called the extractability factor. Bitumen is normally not used to determine the type of organic matter in a sedimentary rock, but it has been used to correlate crude oils with their source rocks (Brenneman and Smith, 1958; Baker, 1962; and Williams, 1974). The bitumen concentrations determined for this study are given in Appendix IV.

The insoluble organic fraction is referred to in this study as kerogen and is used to identify the types of organic matter in a sedimentary rock (Staplin, 1969; Tissot et al., 1974; and Dow, 1977). The kerogen is isolated from a rock by subjecting the pulverized sample to a series of acid treatments and a heavy liquid separation. The sample is first placed in a warm 18 percent solution of hydrocloric acid, followed by a warm 52 percent solution of hydrofluoric acid, and then placed in a hot concentrated solution of hydrocloric acid. The remaining residue is then centrifuged in a zinc bromide solution with a specific gravity of 2.00. The float material is removed and placed in a soxhlet apparatus and extracted with dichloromethane for 20 hours. The insoluble residue is dried in a vacuum oven at 69°C for at least 24 hours. This material is kerogen and usually makes up the bulk of organic matter in sedimentary rocks (Eglinton, 1969).

Kerogen studies have revealed that there are three basic types of kerogen and each type is derived from a different source material (Forsman, 1963; McIver, 1967; and Staplin, 1969). Ligninic kerogen is considered to be derived from higher plants, liptinitic kerogen is considered to be derived from plankton, and sporopolleninic kerogen is considered to be derived from sporopollenin.

Microscopic studies of kerogen may be made by impregnating kerogens on glass slides with lucite. Visual examination of kerogen slides has revealed several distinct textures and morphologies for each of the three kerogen types (Staplin, 1969; Burgess, 1974). Ligninic kerogen may be equant or elongate in shape with a sharp angular outline (Plate 1). Its

PLATE 1

a. Ligninic kerogen from modern lake sediment (RE-9), very low level of thermal maturation; 212x.

b. Ligninic kerogen from Frontier coal (F-1), low level of thermal maturation; 424x.

c. Ligninic kerogen from Breathitt coal (HA-22), moderate level of thermal maturation; 424x.

d. Ligninic kerogen from Pocahontas coal (PO-1), high level of thermal maturation; 424x.

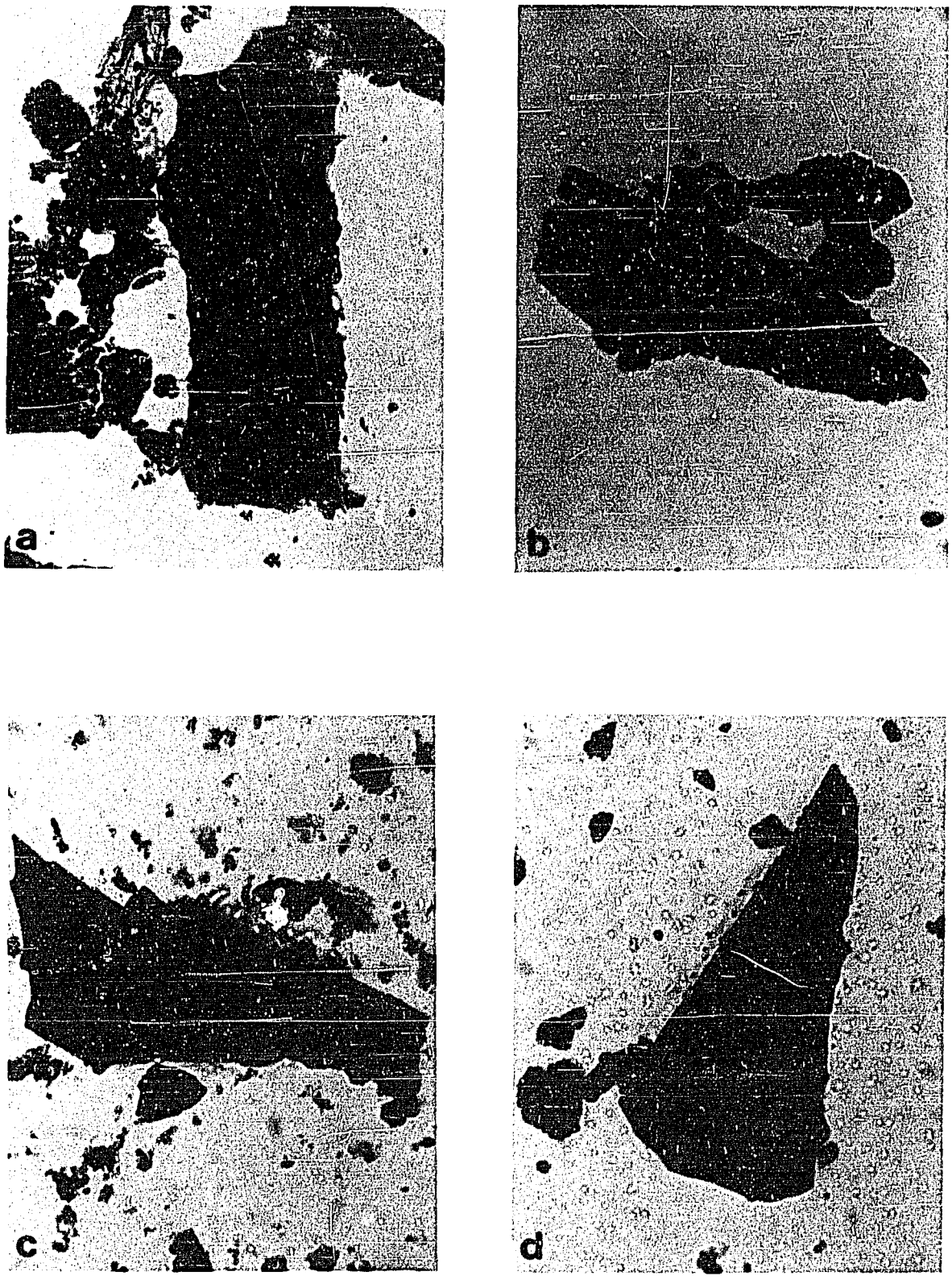

PLATE 1

texture may be fibrous or smooth, and at low to moderate levels of thermal maturation its color is a transparent amber or an opaque brown with a transparent amber border (Plate 1a thru 1c). Liptinitic kerogen has a frothy texture with an amorphous outline (Plate 2). At low to moderate levels of thermal maturation this type of kerogen has a transparent amber color and may have opaque blotches due to iron sulfide inclusions (Plate 2a thru 2c). Sporopolleninic kerogen has an equant shape with a sharp angular to rounded outline (Plate 3a and 3b), or an amorphous outline with a frothy texture similar to liptinitic kerogen (Plate 3c and 3d). The author considers the former to be derived from spore and pollen wall casings (e.g., Heslop-Harrison, 1971), while the latter is considered to be derived from the cell walls of algae (e.g., Good and Chapman, 1978; Atkinson et al., 1972). In this study the former will be designated as α-sporopolleninic kerogen and the latter will be designated as β-sporopolleninic kerogen. At low to moderate levels of thermal maturation α-sporopolleninic kerogen may be distinguished from ligninic kerogen by its transparent yellow or orange color and if not badly fragmented, its palynomorphic outline. At a low level of thermal maturation β-sporopolleninic kerogen may sometimes be distinguished from liptinitic kerogen by its transparent yellow color, but at moderate to high levels of thermal maturation no visual distinction is possible.

A semi-quantitative determination of kerogen types in the samples collected for this study were made by the Fleet grain counting method (Galehouse, 1971). For this type of analysis 200 to 250 kerogen macerals were counted per analysis, and the results are reported in number percent.

PLATE 2

a. α-Liptinitic kerogen from Monterey shale (MR-11), low level of thermal maturation; 424x.

b. β-Liptinitic kerogen from Kreyenhagen shale (K-2), low level of thermal maturation; 424x.

c. β-Liptinitic kerogen from New Albany shale (NA-4), moderate level of thermal maturation; 424x.

d. β-Liptinitic kerogen from Nonesuch shale (NS-2), high level of thermal maturation; 424x.

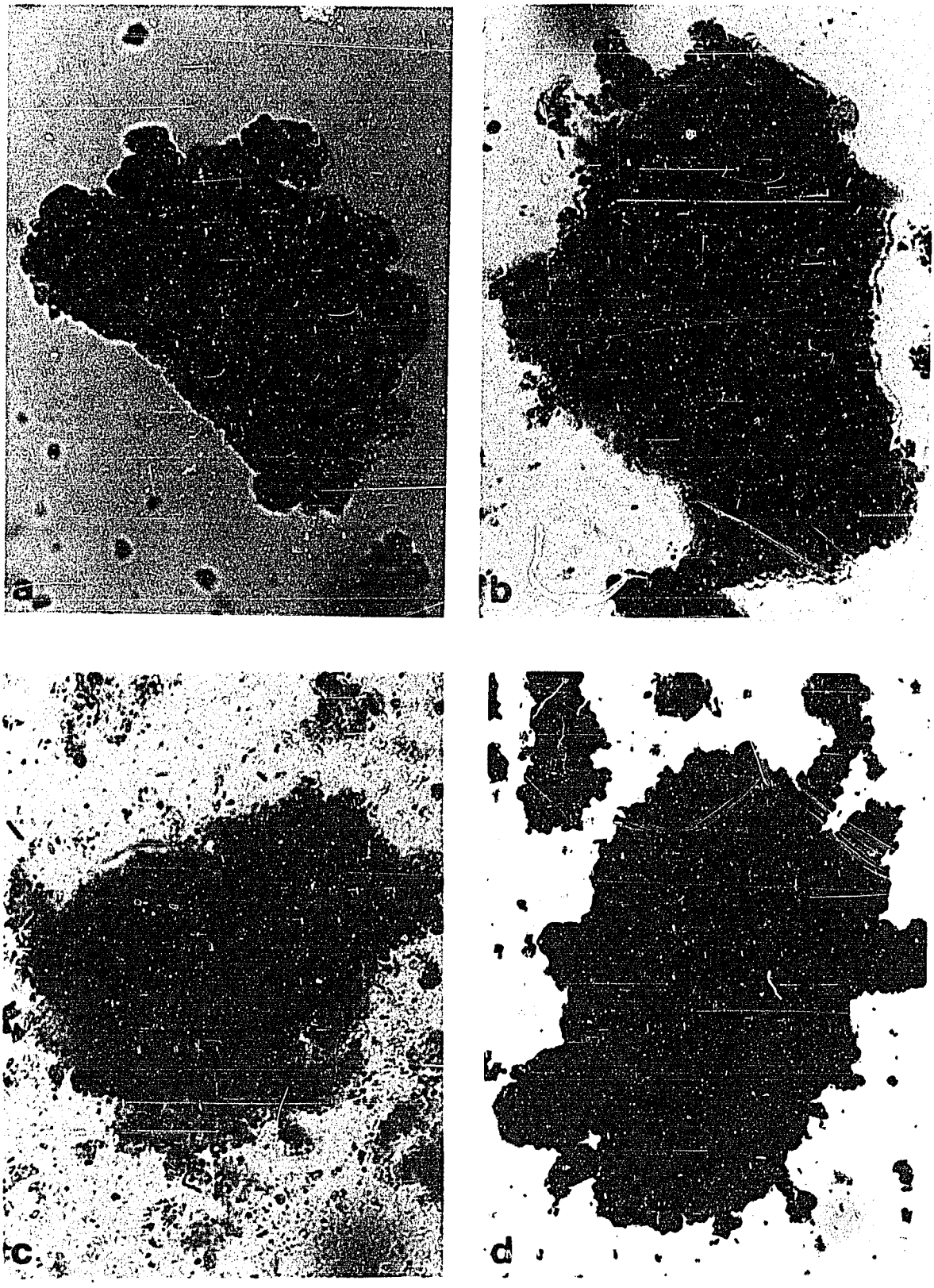

PLATE 2

PLATE 3

a. α-Sporopolleninic kerogen from New Albany shale (NA-15), moderate level of thermal maturation; 424x.

b. Thin section showing distribution of α-sporopolleninic kerogen in New Albany shale (NA-15); 212x.

c. β-Sporopolleninic kerogen from Green River shale (GR-12), low level of thermal maturation; 212x.

d. Thin section showing amorphous character of β-sporopolleninic kerogen in Green River shale (GR-4); 424x.

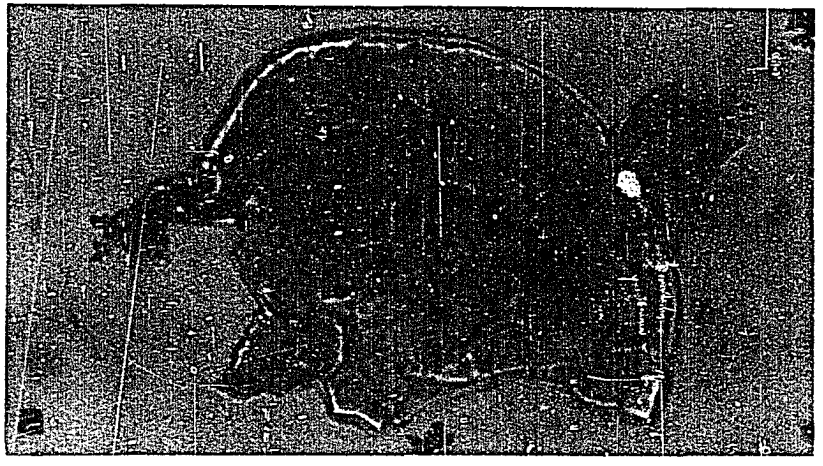

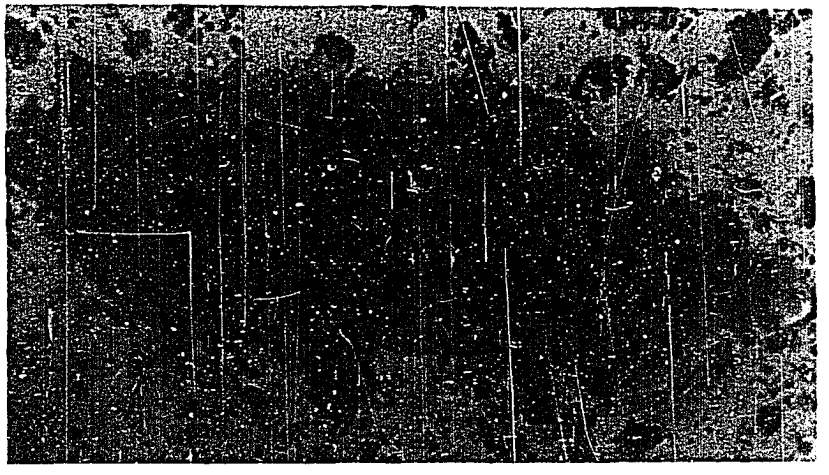

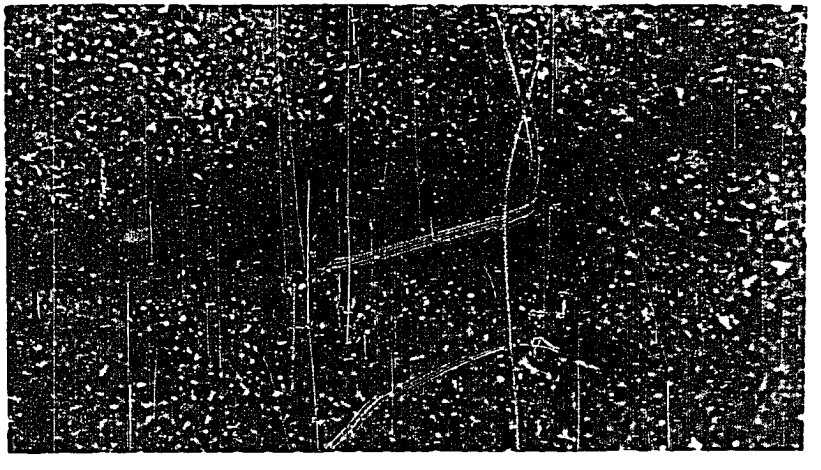

PLATE 3

More time consuming quantitative methods could have been employed (e.g., Rosiwal-Shand method), but the Fleet grain counting method proved to be adequate for this study.

The chemical composition of a kerogen is also another way of identifying the kerogen type, as well as its level of thermal maturation (Tissot et al., 1974; Dow, 1977; and Harwood, 1977). Carbon, hydrogen, nitrogen, and oxygen usually comprise more than 95 weight percent of a kerogen (McIver, 1967), and determination of these basic elements is referred to collectively as elemental analysis. The carbon, hydrogen, and nitrogen were determined in this study by combusting a kerogen at 980°C in a Carlo Erba Model 1102 elemenetal analylzer. Acetanilide was used as the standard and the method had a standard error of ±0.4 weight percent for carbon, ±0.1 weight percent for hydrogen, and ±0.1 weight percent for nitrogen. Oxygen was determined by combusting the kerogen at 950°C in a Perkin-Elmer 240 elemental analyzer. Benzoic acid was used as the standard, and the method had a standard error of ±0.5 weight percent. The elemental analyses for the samples used in this study are given in Appendix V.

The atomic hydrogen to carbon ratio (H/C) and atomic oxygen to carbon ratio (O/C) of a kerogen are commonly used to determine its type and level of thermal maturation (Tissot et al., 1974; Comer and Littlejohn, 1977; and Dow, 1977). Although other combinations of ratios and values of the elemental analyses have been employed (e.g., C-H-O ternary plots, McIver, 1967;percent carbon versus atomic H/C ratio plots, Harwood, 1977; and carbon to nitrogen ratios, Waples, 1977), the author has found the plot in

Figure 2.3 to be the most useful. At low levels of thermal maturation, Figure 2.3 shows that ligninic kerogen has the lowest atomic H/C ratio, sporopolleninic kerogen has the highest atomic H/C ratio,and liptinitic kerogen has an intermediate atomic H/C ratio. All three types approach a pure carbon end member with increasing thermal maturaiton as a result of the preferential loss of more volatile hydrogen- and oxygen-rich components in the kerogens.

These thermal maturation paths have been observed in nature and verified by pyrolysis experiments (Tissot et al., 1974). The levels of thermal maturation (high, moderate, and low) are based on the kinds of products produced by a kerogen during diagenesis. Carbon dioxide and water are the major products at low levels of thermal maturation, while liquid hydrocarbons are the major products at moderate levels of thermal maturation, and gaseous hydrocarbons are the major products at high levels of thermal maturation (Tissot et al., 1974; Dow, 1977; and Harwood, 1977). Additional thermal maturation paths may occur in positions intermediate to the three major kerogen paths as a result of mixtures. Since the elemental analyses cannot reveal which of the three kerogen types comprise the mixture, the use of visual analysis is important to their interpretation.

Although the determination of kerogen type and level of thermal maturation by elemental analyses appears to be straightforward, the author has noted that oxidation of kerogens can complicate their interpretation. The author suggests that kerogen derived from highly oxidized organic matter, regardless of its type, follows the lower most thermal maturation path in

Figure 2.3: Plot modified after Tissot and others (1974) showing the chemical evolution of the three kerogen types with increasing thermal maturation.

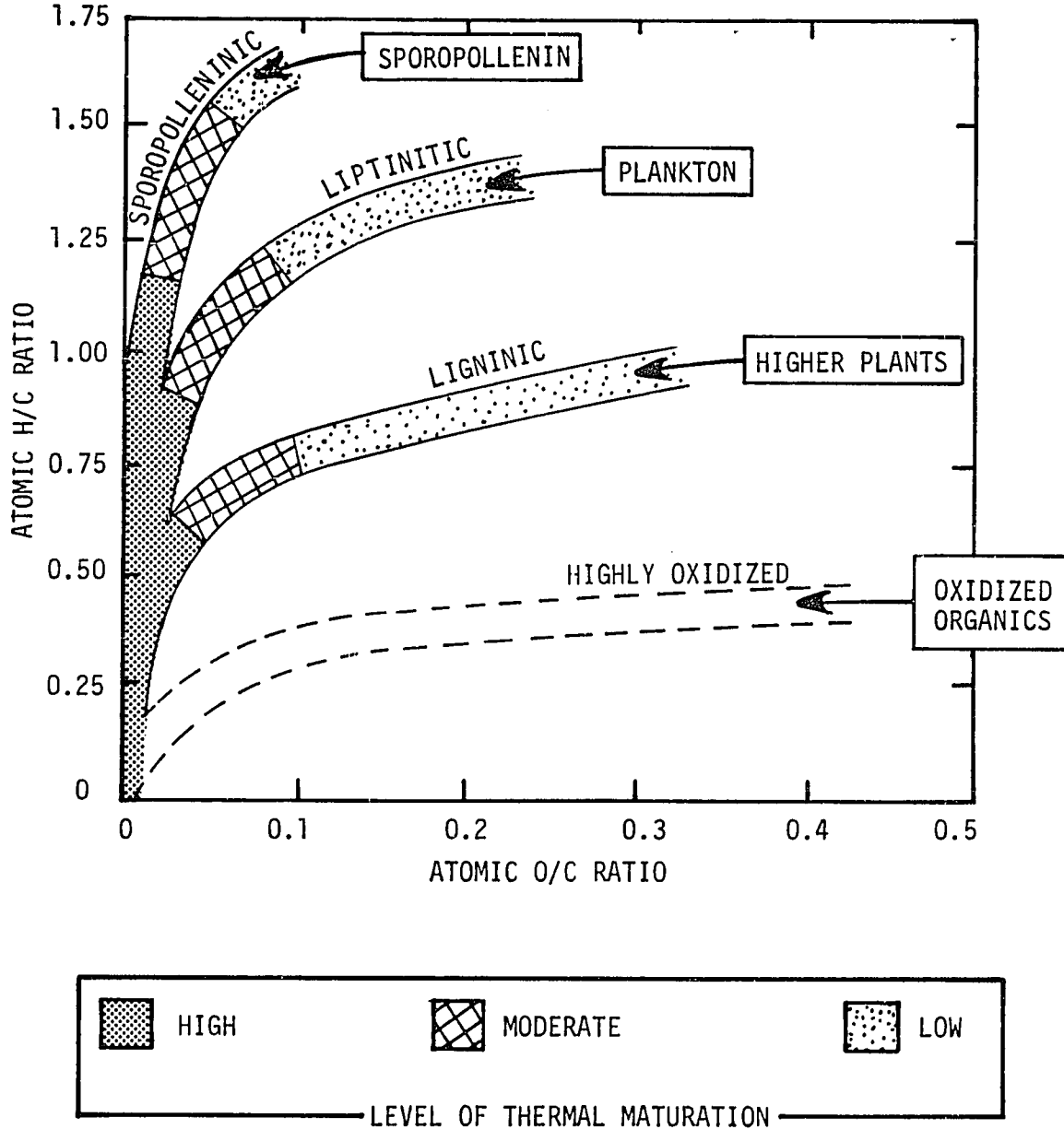

FIGURE 2.3

Figure 2.3. The thermal maturation path is hypothetical in part, and is based on the observation that a number of kerogens have compositions that occur below the thermal maturation path of ligninic kerogen (Figure 2.4). Visual analyses of these kerogens reveal that they are all opaque,and that liptinitic kerogens as well as ligninic and sporopolleninic kerogens are present. The author has interpreted these kerogens as products of oxidation in which oxygen is either retained or added to the kerogen, while hydrogen bearing components are removed from it. Aerobic conditions are the most favorable for these reactions, and the path of oxidation would run contrary to the thermal maturation paths as suggested in Figure 2.5. Different degrees of oxidation of kerogens can result in additional thermal maturation paths intermediate to the major thermal maturation paths given in Figure 2.3. In these instances, distinction by elemental analyses between a mixture of kerogen types and a partially oxidized kerogen of one type is not possible unless used in conjunction with visual analysis.

The author envisages four ways in which oxidation may occur; 1) partial combustion of organic matter by forest or peat fires (e.g., Figure 2.5, curve A), 2) oxidation of organic matter in aerobic sediments or water columns during deposition (e.g., Figure 2.5, curve B), 3) oxidation of organic matter in a sedimentary rock due to weathering (e.g., Figure 2.5, curve C), and 4) oxidation of organic matter in sedimentary rocks as a result of oxygenated hydrothermal fluids (Figure 2.5, curve C). Although this overall scheme is in part hypothetical, data on kerogen weathering support these oxidation trends (Figures 3.2 and 3.5).

Figure 2.4: Atomic H/C to O/C plot of kerogens from rock samples collected for this study. The actual values from which these ratios were calculated are given in Appendix IV.

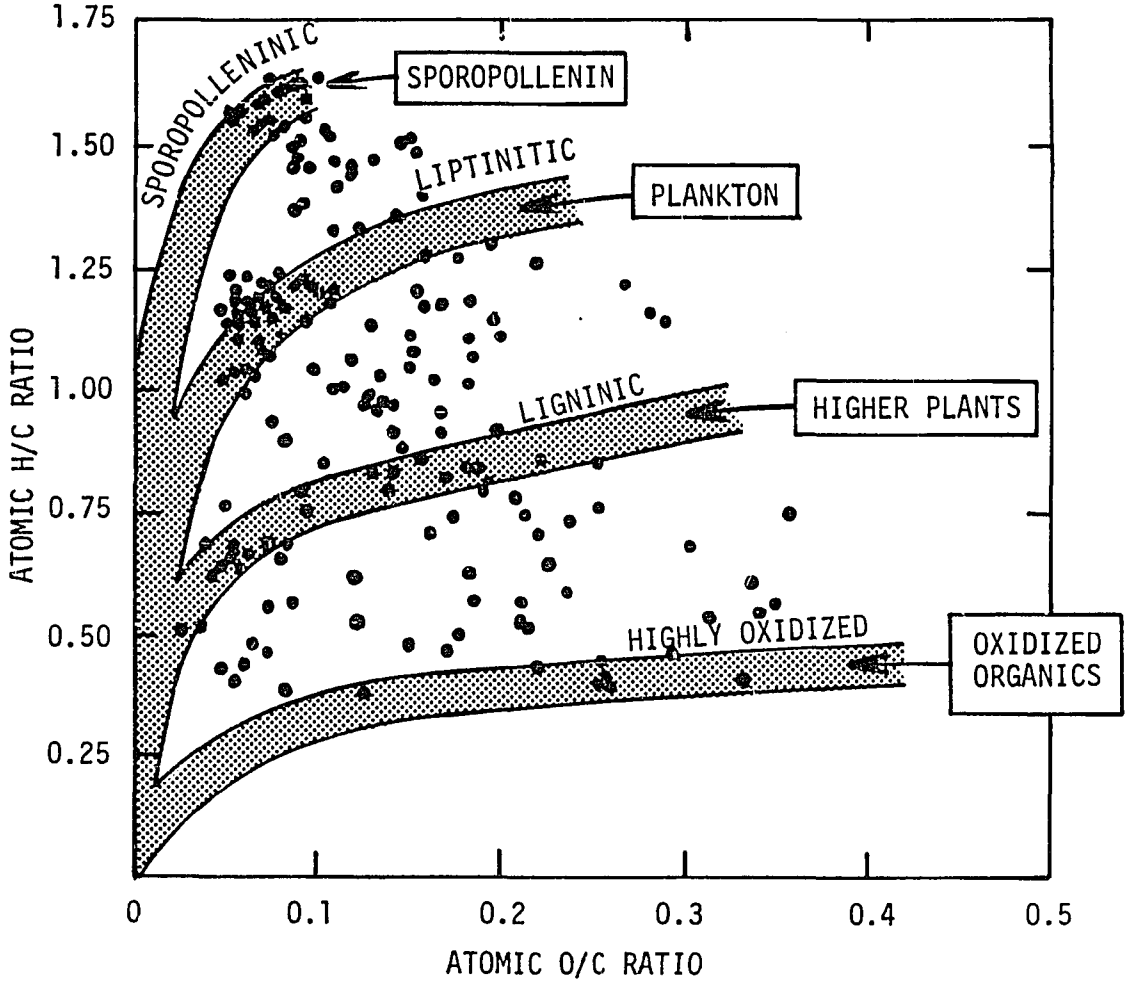

FIGURE 2.4

Figure 2.5: Atomic H/C to O/C plot showing the suggested chemical trends for kerogen oxidation. Curve A represents early oxidation of kerogen precursors, curve B represents oxidation of kerogen in sediments (pre-lithification), and curve C represents oxidation of kerogen in sedimentary rocks.

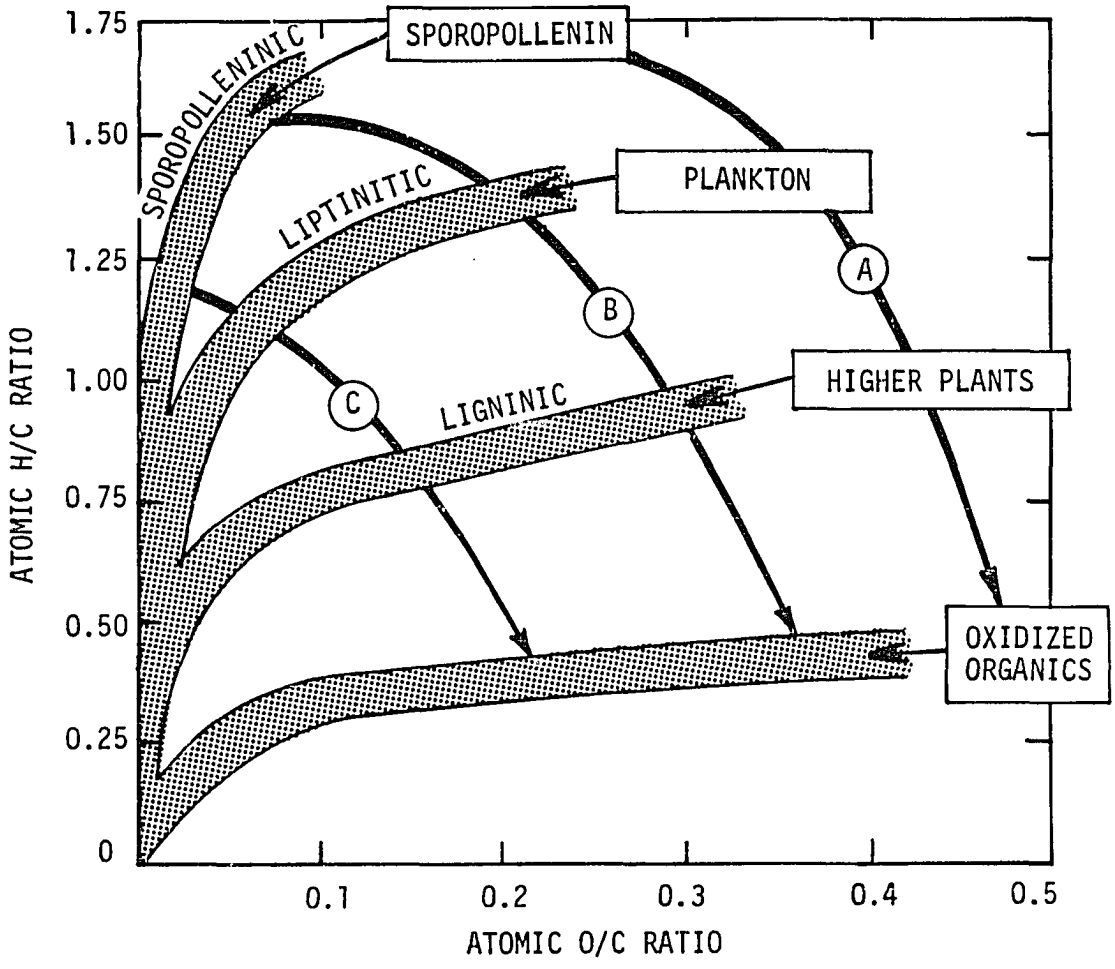

FIGURE 2.5

The stable carbon isotopes of kerogens with respect to their geological age (Jackson et al., 1978) and level of diagenesis (Baker and Claypool, 1970; and McKirdy and Powell, 1974) have been investigated, but their use in distinguishing kerogen type has not been verified. The author was encouraged to examine their potential as an indicator of kerogen type by Nissenbaum's (1974) study of humic acids. His study revealed that stable carbon isotopes could be used to distinguish humic acids derived from marine plankton from those derived from terrestrial plants. Additional encouragement came from several other studies that also employed stable carbon isotopes for differentiating sources of organic matter (Sackett and Thompson, 1963; Hedges and Parker, 1976; Stuermer et al., 1978; Rashid and Reinson, 1979).

The stable carbon isotope ratios (δC^{13}) in this study were determined at the Amoco Production Company Research Center on their Nuclide Analysis Associates ratio gas mass spectrometer, under the direction of Jack Ackley. The δC^{13} values are given in per mil units ($^{o}/oo$) relative to the Pee Dee Belemnite (PDB) standard (Craig, 1957), and the method has a standard error of ±0.1 per mil. The kerogen is introduced into the mass spectrometer as carbon dioxide, which is derived by combusting the kerogen at 860°C and then purified (Hoefs, 1973). The values determined for this study are given in Appendix V.

As shown in Figure 2.6, δC^{13} values for ligninic kerogen consistently occur between -22.0 and -26.5 per mil, which is within the range of its higher plant precursors. One exception is the C_3 category of higher

Figure 2.6: δC^{13} values of liptinitic and ligninic kerogens through the geological record, and their precursors. Plankton values from Degens and others (1968b), and Fontugene and Duplessy (1978); plant, leaves, and wood values from Craig (1953); Miocene values from Monterey samples (this study); Eocene values from Craig (1953), Cozy Dell samples (this study), and Kreyenhagen samples (this study); Paleocene-Cretaceous values from Ferris samples (this study); Cretaceous values from Craig (1953) and Frontier samples (this study); Permian values from Compston (1960) and Phosphoria samples (this study); Pennsylvanian values from Craig (1953), Breathitt samlples (this study), Pocahontas sample (this study), Carbondale sample (this study), and Manning Canyon sample (this study); Devonian values from Maynard (1979), Chattanooga samples (this study), New Albany samples (this study), and Woodruff samlples (this study); Ordovician values from Maquoketa samples (this study); Keweenawan values from Nonesuch samples (this study); and Huronian values from Barghoorn and others (1977).

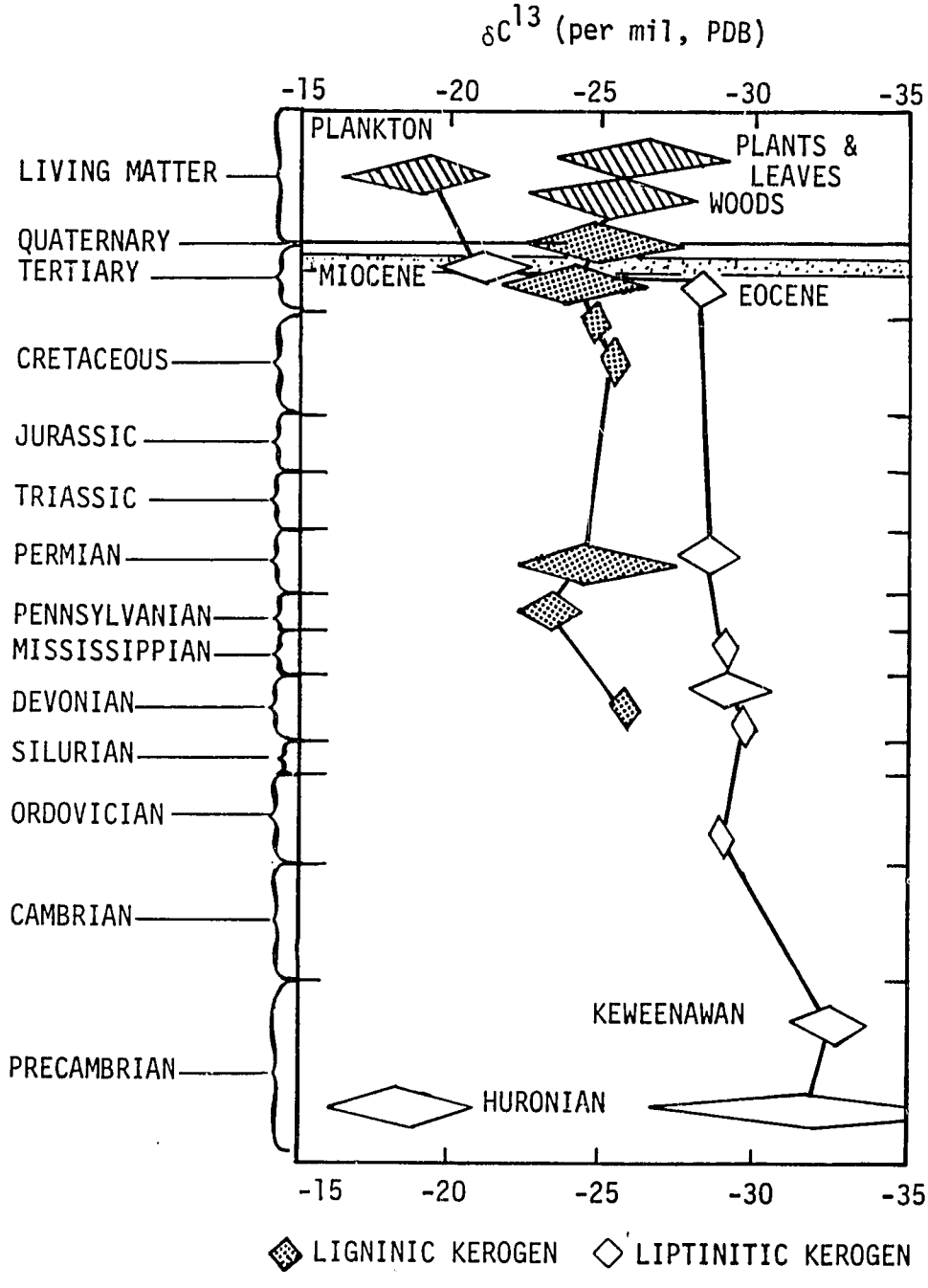

FIGURE 2.6

plants which utilize a different mechanism of photosynthesis and as a result have a δC^{13} range between -6 and -19 per mil (Smith and Epstein, 1971). C_3 plants are not common, and on the basis of Figure 2.6 their contribution to ligninic kerogens in the geological past does not appear to be significant.

There are two isotopically distinct liptinitic kerogens, which in this study are designated as α-liptinitic and β-liptinitic kerogens. α-liptinitic kerogens have δC^{13} values ranging from -16 to -23 per mil, which is similar to their plankton precursors (Figure 2.6). Two known occurrences of this type of kerogen are in the Monterey Formation of California and the Gunflint Formation of Ontario. β-liptinitic kerogen is more common in the geological record and has δC^{13} values more negative than -27.5 per mil, which is isotopically lighter than its plankton precursors. This isotopic difference between α- and β-liptinitic kerogens is significant and may reflect differences in 1) the abundance and source of carbon, 2) the level of diagenesis, or 3) the preferred preservation of organic constituents in plankton precursors.

Plankton consist of phytoplankton, zooplankton, and, bacterica, with phytoplankton comprising a major portion of the plankton biomass (Bordovskiy, 1965). The δC^{13} values for zooplankton and other animals are essentially the same as the food they consume (DeNiro and Epstein, 1978; Haines and Montague, 1979; Fry and Parker, 1979). Their primary food source is phytoplankton which is enriched in C^{12} relative to the carbon source as a result of photosynthesis (Park and Epstein, 1960). Their carbon source is

dissolved bicarbonate in the aqueous habitat (Smith and Epstein, 1971), and its isotopic carbon composition and abundance are important factors controlling the δC^{13} value of phytoplankton (Degens et al., 1968a; Calder and Parker, 1973). Degens and others (1968a) have shown that when CO_2 is abundant, phytoplankton are enriched in C^{12} by approximately 19 per mil regardless of the initial isotopic composition of the bicarbonate source. Thus, if the bicarbonate source has a δC^{13} value of 0 or -10 per mil, the phytoplankton will have a δC^{13} value of -19 or -29 per mil, respectively. The constancy of the isotopic carbon and bicarbonate concentration in sea water over the last one billion years (Keith and Weber, 1964; Holland, 1972; Mackenzie, 1975) suggests that their fluctuations are not a likely cause of the isotopic differences between α- and β-liptinitic kerogens. The only exceptions would be in lakes or small barred basis where isotopically heavier or large amounts of CO_2 were introduced by volcanic fumeroles or concentrated by evaporation. Neither of these environmental situations appears to be related to the isotopic differences between α- and β-liptinitic kerogens shown in Figure 2.6.

The δC^{13} values of organic matter do become significantly more positive at high levels of thermal maturation (Baker and Claypool, 1970; McKirdy and Powell, 1974), but this trend does not explain the more negative isotopic values of β-liptinitic kerogen relative to its precursor. It should also be noted that the α-liptinitic kerogens from the Monterey Formation are at the same low level of thermal maturation as the β-liptinitic kerogens from the Kreyenhagen Formation. Several investigators have suggested that diagenesis during early bural in sediments results in organic matter with

more negative δC^{13} values (Sackett et al., 1974; Gormly and Sackett, 1977). Although average trends have been noted in their studies, the scatter of the data suggests that other variables are equally or more important.

A more plausible explanation for the isotopic difference in liptinitic kerogens is that α-liptinitic kerogens retain more of the organic constituents of its plankton precursor than β-liptinitic kerogens. Liptinitic kerogens are considered to be a condensate of proteins, carbohydrates, and lipids derived from defunct plankton (Welte, 1974). As shown in Figure 2.7, the lipids of plankton, particularly the chloroform-extractable lipids, are isotopically more negative than the overall isotopic composition of the plankton and its other organic constitutents (Park and Epstein, 1961; Parker, 1964; Degens et al., 1968b; Sackett et al., 1974). Proteins and carbohydrates are the major organic constitutents of plankton (Table 2.1) and as a result their less negative isotopic composition predominates over the isotopically more negative lipids. In nature, proteins and carbohydrates are readily consumed by bacteria under aerobic and anaerobic conditions, whereas most lipids are only consumed by bacteria under aerobic conditions (Zobell, 1946). This suggests that in an anaerobic environment the proteins and carbohydrates of a defunct plankton would be consumed by bacteria, while the preserved lipids condense into a β-liptinitic kerogen that is isotopically more negative than its plankton precursor. Although preservation of proteins and carbohydrates is unlikely due to their high susceptibility to aerobic and anaerobic bacterial degradation, the preservation of the latter has been observed in

Figure 2.7: Carbon isotope values of major organic constituents comprising plankton (Degens et al., 1968b) and their proposed relationship with liptinitic kerogens.

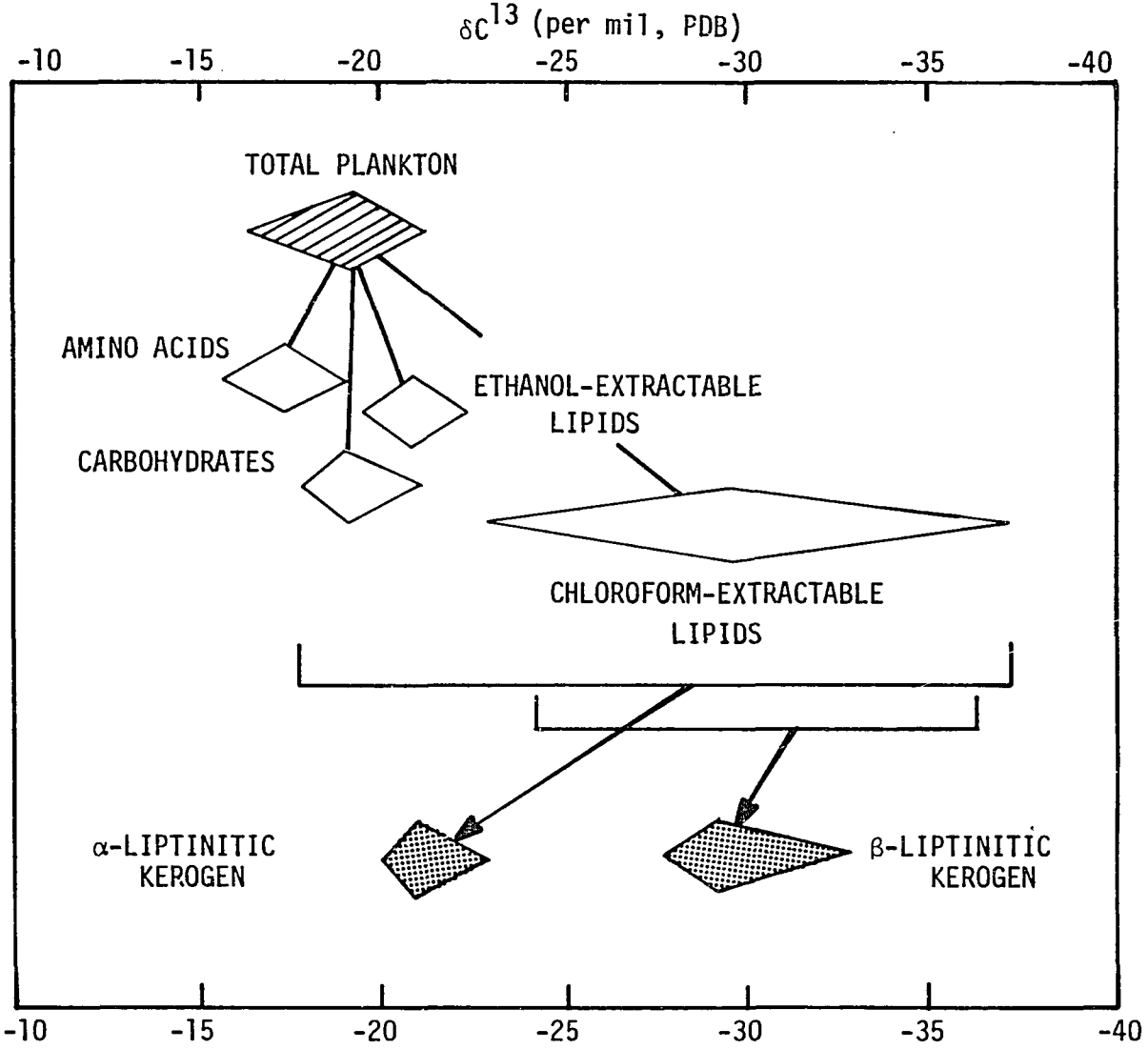

FIGURE 2.7

Table 2.1: Organic constituents of plankton in dry weight percent.*

Plankton Type	Proteins	Carbohydrates	Lipids	Ash
Phytoplankton				
Diatoms	24-48	0-31	2-10	30-59
Dinoflagellates	41-66	6-36	2-6	12-27
Zooplankton				
Copepods	71-77	0-4	4-19	4-6
Sagittae	70	14	2	16

*Data from Raymont (1963, p.534).

some cases (e.g., Morey and Morey, 1969; Wetzel, 1975, p. 542; Hatcher et al., 1977). In these cases, the preservation of carbohydrates with the less abundant lipids may result in the condensation of an α-liptinitic kerogen that has an isotopic composition similar to its plankton precursors.

The prevalence of β-liptinitic kerogen in the geological record (Figure 2.6) suggests that its conditions for formation are more easily maintained and common in natural systems than the conditions for α-liptinitic kerogen formation. Retardation of anaerobic bacterial degradation appears to be essential for the formation of α-liptinitic kerogens and two conditions favoring this include low water temperatures and rapid sedimentation. More studies on these two types of liptinitic kerogens are needed and the existence of a continum between the two cannot be determined from the available data.

Stable carbon isotope data on sporopolleninic kerogen is sparse (Brooks and Shaw, 1972; Brooks, 1978, personal communique), and the only δC^{13} values for sporopolleninic kerogen in this study are those from the Green River Formation. These kerogens are amorphous (Plate 3c) and elemental analysis indicates that they are β-sporopolleninic kerogens at a low level of thermal maturation. The δC^{13} values for these kerogens are similar to β-liptinitic kerogens and are shown as a histogram in Figure 2.8. It is interesting that the kerogens derived from smectite bearing rocks have more positive δC^{13} values than those from rocks not bearing smectite. This data needs to be studied further, but a tentative explanation is that

Figure 2.8: Histogram showing carbon isotope values of β-sporopollenic kerogen from the Green River Formation (GR-1 thru GR-39).

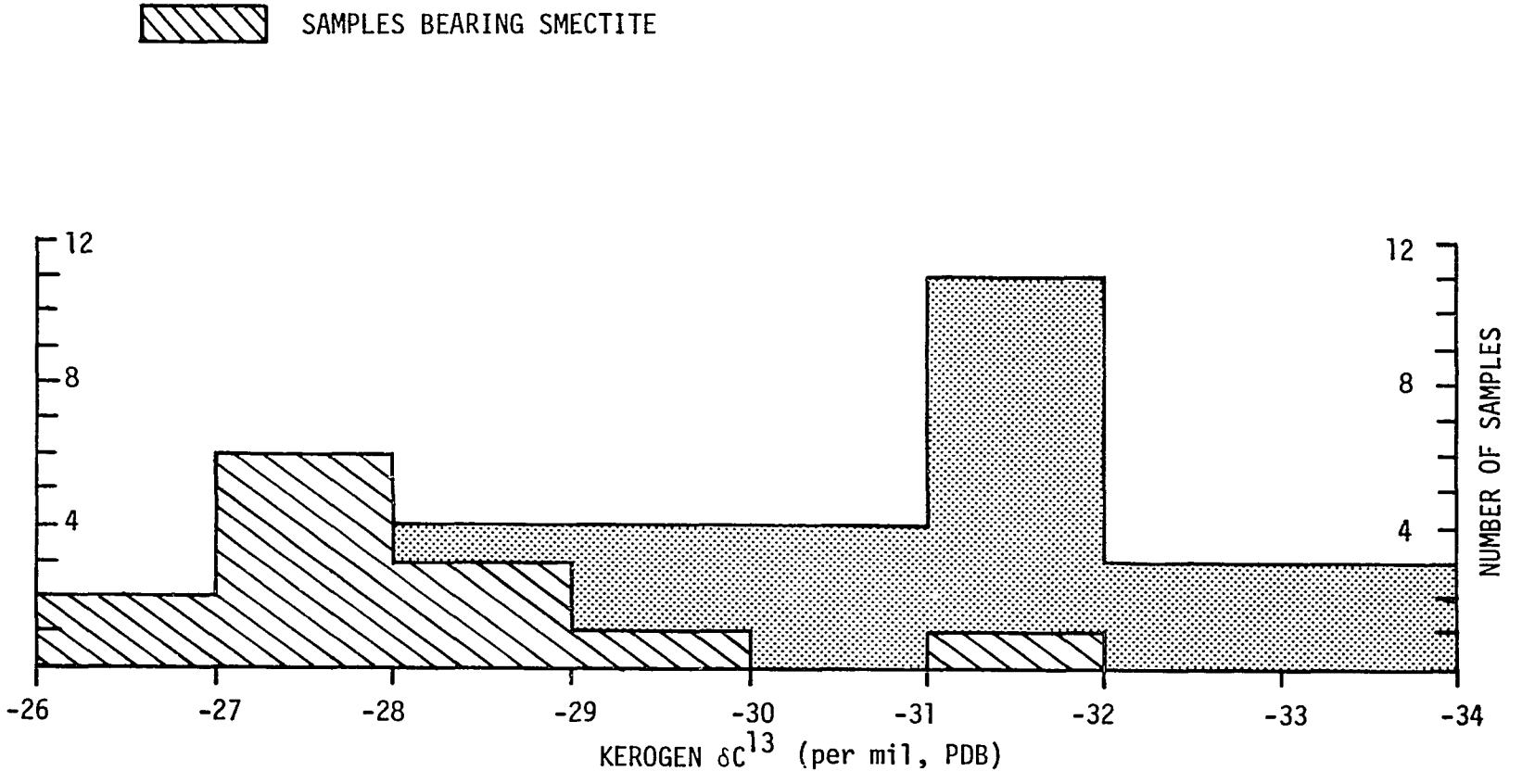

FIGURE 2.8

volcanic activity within the relatively small confines of the lacustrine regimes of the Bridger and Uinta Basins influenced the δC^{13} values of the kerogen precursors.

Although stable carbon isotopes of kerogens do reflect kerogen type to some degree, their use without visual or elemental analyses makes their interpretations tenuous. This is due to the wide range of isotopic values for each kerogen type, which hinders proper interpretations of samples bearing a mixture of kerogen types. In this study kerogen carbon isotopes were only used in conjunction with visual and elemental analyses.

2.3 VANADIUM AND NICKEL ANALYSES

Vanadium and nickel concentrations in organic matter and crude oils were determined by neutron activation analysis. The method is discussed in detail by Filby and Shah (1975), but briefly the method consists of generating radioactive elements by bombarding a sample with neutrons. The sample is then allowed to undergo radioactive decay, and the radiation associated with the metal of interest is measured. Concentrations are then determined from standards that have been run in a similar fashion. The method is accurate and precise, and its other advantages include 1) only small amounts of sample are needed because of its high sensitivity, 2) no pre-dilution or concentration procedures are necessary, 3) loss of volatile forms of metals is avoided because the sample is not heated above 40°C, and 4) interferences and matrix effects are of minimal importance (Filby and Shah, 1975).

The analyses were contracted out to the Nuclear Research Laboratory under the direction of Dr. Thomas F. Parkinson at Virginia Polytechnic Institute and State University. The samples were subjected to a thermal flux of 1.3×10^{12} neutrons per centimeter squared-second, and the maximum detection sensitivities for vanadium and nickel are 0.0017 and 1.3 micrograms, respectively (Parkinson, 1977). The concentrations are reported in parts per million, and the proportionality of vanadium to nickel is expressed as the vanadium-nickel fraction; V/(Ni+V). Usually the proportionality of these two metals is expressed as a ratio (i.e., V/Ni), but the infinite limits on such an expression make plotting and mathematical processing of the data difficult, particularly when infinity values occur. This is remedied by the vanadium-nickel fraction because of its finite limits (Lim V/(V+Ni) = 1 when Ni = 0, and =0 when V=0).

Determining the vanadium and nickel concentrations in the organic matter of a sedimentary rock is difficult because it must first be isolated from the inorganic rock matrix. Although kerogen comprises the major portion of organic matter in a rock, its isolation from the inorganic matrix requires caustic acid treatments that are likely to alter the proportionality and concentrations of the metals. Conversely, bitumen comprises a smaller portion of the organic matter in a rock, but its isolation from the inorganic rock matrix by soxhlet extraction is less caustic and less likely to alter the proportionality or concentrations of the metals. Another advantage in using bitumen rather than kerogen is that the former is more similar in composition to crude oils, and correlations between crude oils and their source rocks usually employ the bitumen of rocks

rather than their kerogens (e.g., Brenneman and Smith 1958); Hunt and Jamieson, 1958; Williams, 1974).

In Table 2.2 the proportionality and concentrations of vanadium and nickel in bitumen and kerogen are compared. Ligninic kerogens are enriched in nickel relative to the bitumens, while vanadium concentrations are essentially the same. Liptinitic and sporopolleninic kerogens are also enriched in nickel relative to the bitumens, but are depleted in vanadium. From this data it is not possible to determine whether these differences between the bitumens and kerogens are induced by the caustic acid treatment or the result of natural fractionation of the metals. In addition to this uncertainty, pyrite contamination in kerogens was found to cause significant deviations in the vanadium and nickel analyses. Table 2.3 shows that the determined nickel concentration in kerogen is definitely affected by pyrite contamination. Pyrite contamination is common in kerogens and usually accounts for 10 to 30 weight percent of the isolate kerogen. This very fine (<1 micron) pyrite is disseminated in the kerogen and is protected from acid attack by the encompassing kerogen. Nitric acid does remove most of this pyrite but its effects on the elemental and metal analyses are pronounced (Tables 2.4 and 2.5, respectively). Because of these analytical problems, the vanadium and nickel determinations were not made on the kerogens, but rather on the bitumen portions of the rocks.

The advantages in analyzing the bitumens for vanadium and nickel are 1) their extraction from the rocks is not destructive to the metallo-organic complexes, and 2) the amount of inorganic contaminants is minimal.

Table 2.2: Vanadium and nickel concentrations in bitumens and kerogens.

Kerogen Type	Vanadium (ppm) Bitumen	Kerogen	Δ	Nickel (ppm) Bitumen	Kerogen	Δ	V/(Ni + V) Bitumen	Kerogen	Δ
Ligninic									
H-1	1	1	0	0	28	-28	1.00	0.02	+0.98
I-1	12	13	-1	11	55	-44	0.53	0.19	+0.36
Liptinitic									
NA-5	330	185	+145	495	669	-174	0.40	0.22	+0.18
NA-12	1080	446	+634	497	1190	-693	0.68	0.27	+0.41
B-1	949	775	+174	688	1410	-722	0.57	0.35	+0.22
Sporopolleninic									
GR-6	7	1	+6	119	150	-31	0.06	0.01	+0.05

Table 2.3: Vanadium and nickel analyses of kerogen and the effect of pyrite contamination.

Sample and Aliquot No.	Wt. % of Added Pyrite	Vanadium (ppm) Measured	Calculated*	Δ	Nickel (ppm) Measured	Calculated*	Δ	V(Ni + V) Measured
NA-12-1**	0	446	446	0	1190	1190	0	0.27
NA-12-2	9.2	416	408	8	870	1090	-213	0.32
NA-12-3	24.9	308	357	-49	605	953	-348	0.34
NA-12-4	34.5	303	332	-29	518	885	-367	0.37

*Calculations are based on the additional weight due to the added pyrite.

**Initial sample has about 12 weight percent pyrite.

Table 2.4: Elemental analyses of kerogens before and after being treated with a 25 percent solution of nitric acid for 5 hours.

Kerogen Type	Atomic H/C Ratio			Atomic O/C Ratio			% Nitrogen*		
	Before	After	Δ	Before	After	Δ	Before	After	Δ
Ligninic									
I-1	0.81	0.66	0.15	0.14	0.37	-0.23	1.6	6.6	-5.0
Liptinitic									
NA-5	1.19	1.04	0.15	0.10	0.29	-0.19	2.5	7.2	-4.7
Sporopolleninic									
GR-6	1.54	1.51	0.03	0.10	0.23	-0.13	2.6	6.1	-3.5

*Weight percent of normalized carbon, hydrogen, oxygen, and nitrogen analyses.

Table 2.5: Vanadium and nickel analyses of kerogens before and after being treated with a 25 percent solution of nitric acid for 5

Kerogen Type	Vanadium (ppm)			Nickel (ppm)			V/Ni + V)		
	Before	After	Δ	Before	After	Δ	Before	After	Δ
Ligninic									
I-1	13	1	12	55	5	4	0.19	0.11	0.18
Liptinitic									
NA-5	185	38	147	669	171	498	0.22	0.18	0.04
Sporopolleninic									
GR-6	1	1	0	150	0	150	0.01	1.00	-0.99

A benzene-methanol mixture was used as the extraction solvent because its bitumen and metal yields were greater and more reproducible than other solvents (Table 2.6). Suspended rock powder that is occasionally rinsed into the solvent as a result of solvent flashing or leaks in the cellulose thimbles within the soxhlet apparatus is removed by filtering the solvent through a millipore filter system with 0.5 micron teflon filters. Afterwards the bitumen is isolated by evaporating off the solvent with a rotary vacuum evaporator. The bitumen is then heated in an oven at 84°C for 12 hours. This heating procedure removes the highly volatile components in the bitumen, which helps stabilize the weight of the bitumen (Figure 2.9). Although the weight of a bitumen may be significantly reduced by this procedure, it does help concentrate the metallo-organics which are not volatile at low heating temperatures (Table 2.7).

The inorganic contaminants in some bitumens are apparently dissolved out of the pulverized rock by the solvent during extraction in the soxhlet apparatus. Gypsum and native sulfur have been identified in a few of the bitumens of this study, and other possible contaminants include halite, trona, and niter. These contaminants only distort the vanadium and nickel analyses when they comprise a large portion of the extract. This usually occurs in extracts derived from rocks that are non-organic (less than 1 weight percent of organic carbon), at a high level of diagenesis, or bearing highly oxidized organic matter. These rock types have extracts that seldom exceed 0.01 weight percent of the rock and are orange, yellow, or light gray to white in color. In this study, vanadium and nickel analyses were only considered meaningful on extracts that accounted for more

Table 2.6: Vanadium and nickel analyses of bitumens extracted by different solvents from the New Albany Shale Standard No. 1*.

Solvents	Bitumen (°/oo)	Vanadium (ppm)	Nickel (ppm)	V/(Ni + V)
Toluene/Methanol** (mean of 3 samples)	2.6	262 ± 14	257 ± 80	0.52 ± 0.06
Methanol	3.3	67	88	0.43
Benzene	4.0	252	330	0.54
Benzene/Methanol** (mean of 3 samples)	6.0	341 ± 12	335 ± 8	0.51 ± 0.01

*Standard consists of a composite of samples from the Clay City outcrops (local sites 70 and 71).

**Mixtures are 70/30 volume percent.

Figure 2.9: (a) Graph showing weight loss of bitumen sample in sealed polyethylene vials with increasing exposure time to atmospheric conditions. (b) Graph showing constant weight of bitumen sample in polyethylene vial with exposure time after heating at 84°C for 24 hours.

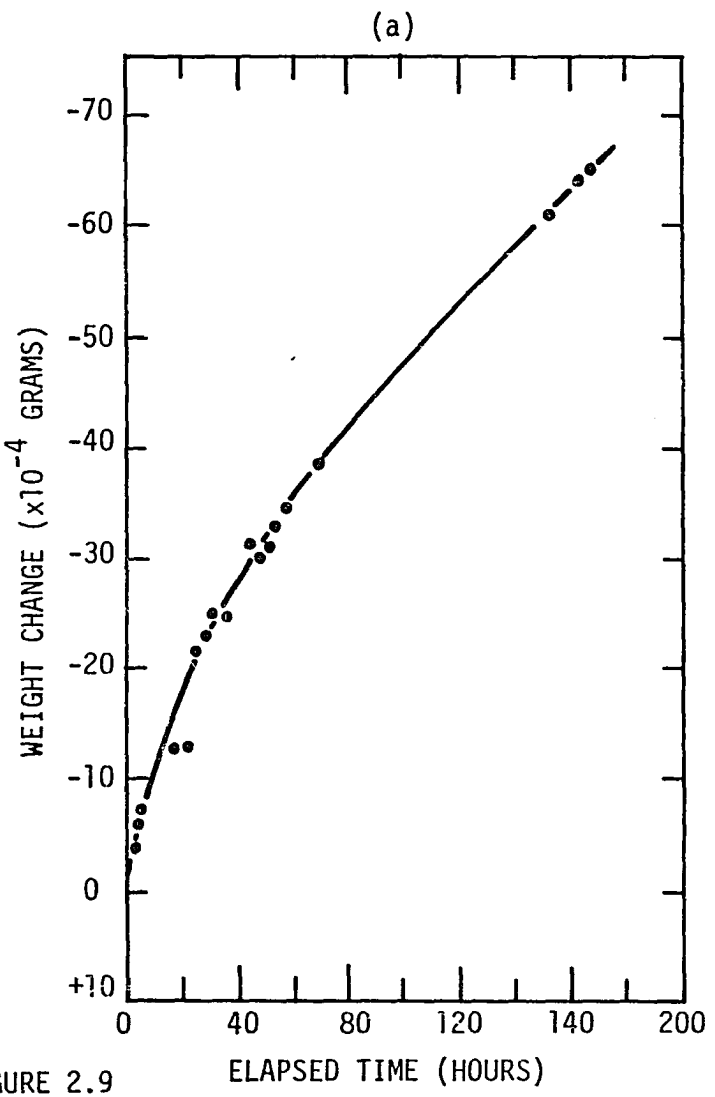

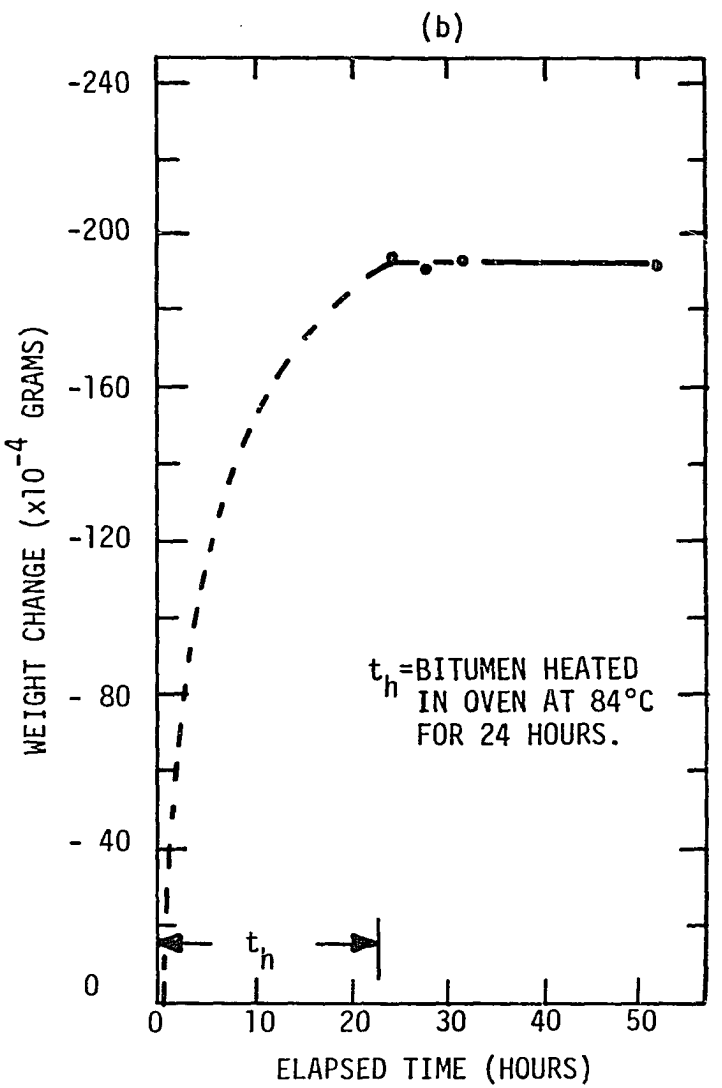

FIGURE 2.9

Table 2.7: Vanadium and nickel analyses showing the effect of heating bitumen at 96°C for 24 hours. Vales are means of 3 aliquots of Standard No. 1.

	Before Heating	After Heating
Bitumen (^{o}/oo)	4.8	2.6
Vanadium (ppm)	142 + 5	262 + 14
Nickel (ppm)	106 + 36	257 + 80
V/(Ni+V)	0.59 + 0.10	0.51 + 0.06

*Bitumen extracted with a toluene/methanol mixture.

than 0.15 weight percent of the rock and that were medium brown to black in color. This prerequisite insures that the contaminants usually comprise less than 7 weight percent of the extract, which would not cause appreciable variations in the metal analyses because of their low metal concentrations (Table 2.8). The vanadium and nickel analyses determined for this study are given in Appendix VI.

2.4 EVALUATION OF DEPOSITIONAL ENVIRONMENTS

Studies on trace elements in argillaceous sediments (Potter et al., 1963) and shales (Degens et al., 1957) have suggested that certain trace elements may be helpful in distinguishing depositional environments (e.g., fresh-water or marine environments). The results of these studies have encouraged the author to examine the possible influences that depositional environments may have on the proportionality and concentration of vanadium and nickel in the organic matter of sedimentary rocks. The depositional environment in which a sedimentary rock was deposited is manifested in part in the lithology, sedimentary textures, and regional character of the rock. These parameters were evaluated in this study by the bulk analyses shown in Figure 2.1.

The lithology of the samples was petrographically examined in thin section and analyzed by semiquantitative x-ray diffraction. The petrographic study focused on the mineralogy of laminae, identification of authigenic minerals, recognition of fossils, and determination of grain size. The semiquantitative x-ray diffraction analyses were performed at the Amoco

Table 2.8: Vanadium and nickel concentrations in inorganic contaminants.

Inorganic Contaminant	Vanadium (ppm) Mean	Range	Nickel (ppm) Mean	Range
Halite (n=7)[1]	<0.3	<0.3	2.5	1.6-3.5
Trona (n=1)[2]	<1		57.6	
Anhydrite (n=3)[1]	1.3	0.3-2.5	0.7	<0.8-1.2
Sulfur (n=3)[3]	0.08	0.2-2.0	75.5	11.0-143
Niter (n=1)[4]	0.01		<1	

1 Data from Stewart (1963).

2 Trona from Big Island Trona Mine in Wyoming.

3 Sulfur from samples from Gulf Coast Salt Dome, Michigan Evaporite, and Potzuoli Solfatara.

4 Fisher Certified ACS Grade.

n = Number of samples.

Production Company Research Center. The method was developed by Duschatko and Nash (1973) and is an expanded version of the methods described by Moore (1968) and Devine and others (1972). The semiquantitative mineralogy obtained from this method is given in Appendix VII. The nomenclature used for the lithologies in this study are in accordance with Lewan's (1978) laboratory classification of very fine-grained rocks.

Sedimentary features were noted in the outcrop and in hand specimen. The prevalent sedimentary features noted in this study were bedding characteristics. Samples were considered bedded if continuous layers were thicker than 5mm, laminated if continuous layers did not exceed 5mm, streaked if discontinuous layers had thicknesses less than 0.3 times their lengths, blebbed if discontinuous layers had thicknesses greater than 0.3 times their lengths, massive if sample appeared homogenous, and bioturbated if distinct burrows were visible or if the sample was mottled.

Regional studies including isopach maps, facies or lithology distribution maps, and correlated stratigraphic sections from the literature were used in this study. In order to maintain continuity between the data collected in this study and the published regional studies, the stratigraphic location of the samples was recorded in addition to their geographic location (Appendix II).

CHAPTER 3

SAMPLING TECHNIQUES AND THE EFFECTS OF WEATHERING

The majority of samples used in this study were collected from outcrops, and therefore the effects of weathering were considered. Clayton and Swetland (1978), and Leythaeuser (1973) have studied the effects of weathering on the organic fraction of outcrop samples, but they neglected to mention what type of kerogen was being weathered and what type of physical changes occurred in the rocks as the degree of weathering increased. Information on the latter would be helpful in establishing field criteria on which the degree of weathering would be determined on a sample during its collection. This was considered in this study along with kerogen type, and field work revealed two styles of weathering; 1) surface weathering, and 2) pedogenic weathering.

3.1 SURFACE WEATHERING

Surface weathering, as its name implies, occurs on the surface of an outcrop as a result of the interaction between the face of an outcrop and the physical, chemical, and biological agents of the atmosphere. The different stages in this style of weathering are defined by changes in the splitting character of the rock (Figure 3.1). Earthy zones consisting of loosely aggregated clods of highly weathered rock occur sporadically in depressions on the outcrop face where they are not susceptible to being washed away by rain waters. The earthy zone grades inward into a fissile zone, which is the outer most exposed zone of the

Figure 3.1: Conceptional cross-sectional view of surface weathering zones.

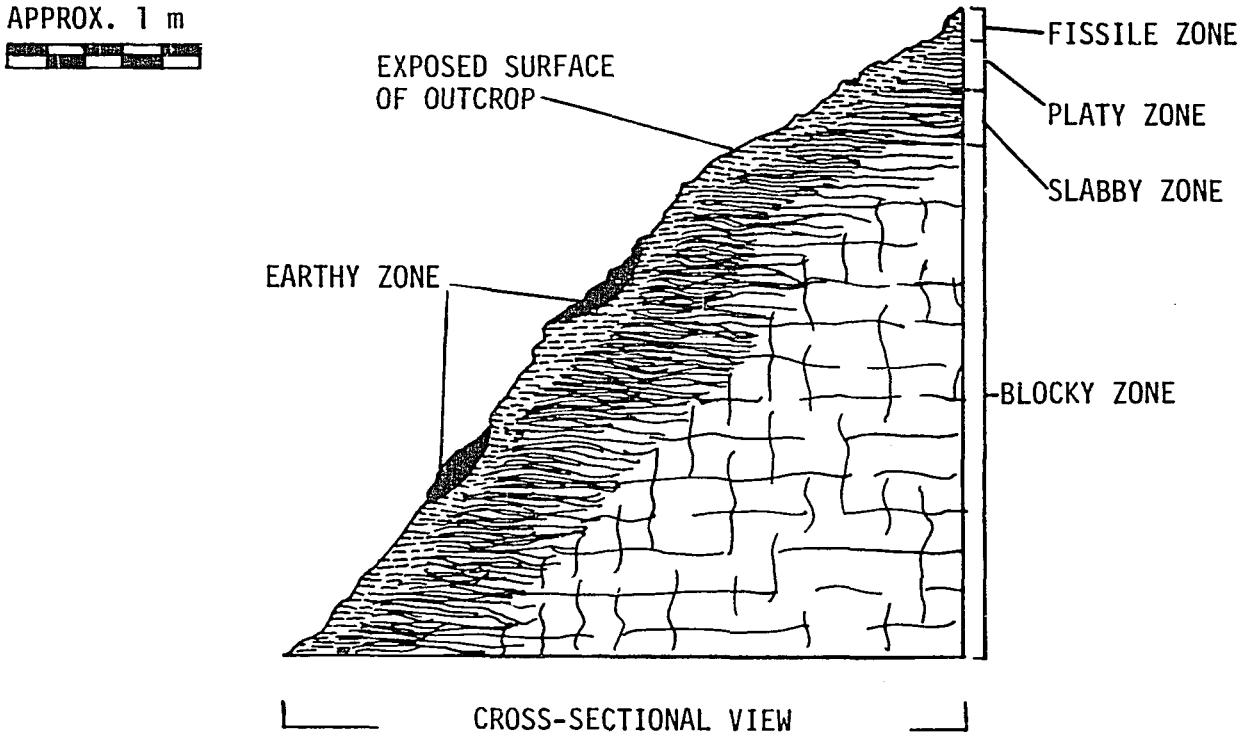

FIGURE 3.1

outcrop surface where the earthy zone has been washed away. The fissile zone consists of chips and planes of rock less than 2mm thick. This zone grades into a platy zone that consists of rock plates ranging in thickness from 2 to 5mm. This zone grades into a slabby zone consisting of rock slabs that exceed 5mm in thickness, and this grades into a blocky zone consisting of equant masses of rock. The lateral depth of this surface weathering series seldom exceeds one meter, and the width of each zone depends on the texture of the rock, its composition, and the intensity of weathering in the region. This surface weathering series has been observed in humid and arid climates and has been observed on a variety of rock types (i.e., claystone, marlstone, and oil shale) with massive, bioturbated, and laminated bedding features.

A faint discoloration of the rock is sometimes observed in the platy zone of the outcrop, but intense discoloration is usually observed in the fissile and earthy zones of the outcrop. Usually the discoloration involves an increase in the lightness value of the unweathered color and an increase in its chroma.

The chemical changes accompanying the physical changes in the rock during surface weathering, appear to occur predominantly in the organic fraction, rather than in the inorganic fraction of the rock. Table 3.1 shows that the mineralogy of the surface weathered samples does not change significantly. Conversely, within the organic fraction the kerogen and bitumen are significantly altered by surface weathering.

Table 3.1: Mineralogy of surface weathered shales and their unweathered equivalents. Values given in weight percent.*

Mineral	M-23 Slabby	M-24 Fissile	GR-7 Blocky	GR-8 Fissile	GR-12 Blocky	GR-14 Earthy
Quartz	49	54	19	19	12	10
Feldspars	1	3	3	3	21	25
Analcite	nd	nd	44	46	nd	nd
Illite	12	13	21	21	tr	21
Smectite	27	19	nd	nd	nd	nd
Kaolinite	11	10	nd	nd	nd	nd
Dolomite	nd	nd	13	11	67	44
Pyrite	nd	1	nd	nd	nd	nd
Total	100	100	100	100	100	100

*Mineralogy determined by semiquantitative x-ray diffraction analysis.

nd = not detected
tr = trace amounts (<1%)

Visually the morphology, transparency, and color of kerogen does not appear to change significantly with surface weathering. Table 3.2 shows that the carbon isotope values do not change significantly, but there does appear to be a slight enrichment in C^{13} in the weathered sporopolleninic kerogens, while the liptinitic and ligninic kerogens show a slight enrichment in C^{12}.

Elemental analyses of kerogen show the most obvious chemical changes that occur during surface weathering. Based on the data given in Figure 3.2, two types of chemical alteration occur during the surface weathering of kerogen; 1) oxidation and 2) dehydrogenation. Oxidation of the kerogen is suggested by the increase in the atomic O/C ratio. This apparent oxidation commences in the platy zone and increases in intensity through the fissile and earthy zones. Dehydrogenation is suggested by the decrease in the atomic H/C ratio, and commences in the fissile zone and continues through the earthy zone. The chemical alteration trend resulting from these two types of alteration is shown conceptually in the insert in Figure 3.2. Although the data is limited, this surface weathering trend appears to be valid for all three kerogen types.

In addition to the kerogen being influenced by surface weathering, the amount of bitumen and total organic carbon content in a rock are also influenced by surface weathering. Figure 3.3 shows that surface weathering initiates a decrease in total organic carbon content in the platy zone, and this decrease continues into the fissile and earthy zones.

Table 3.2: Carbon isotope values of kerogens from surface weathered rocks and their unweathered equivalents.

	M-23 Slabby	M-24 Fissile	MR-12 Blocky	MR-13 Platy	GR-7 Blocky	GR-8 Fissile	GR-12 Blocky	GR-14 Earthy
Kerogen Type	β-Lipnitic + Ligninic		α-Lipnitic		β-sporopoleninic		β-sporopolleninic	
Kerogen δC^{13} ($^{o}/oo$, PDB)	-24.6	-24.1	-22.8	-22.6	-31.7	-32.0	-30.9	-31.5

Figure 3.2: H/C versus O/C plot of kerogen alteration resulting from surface weathering.

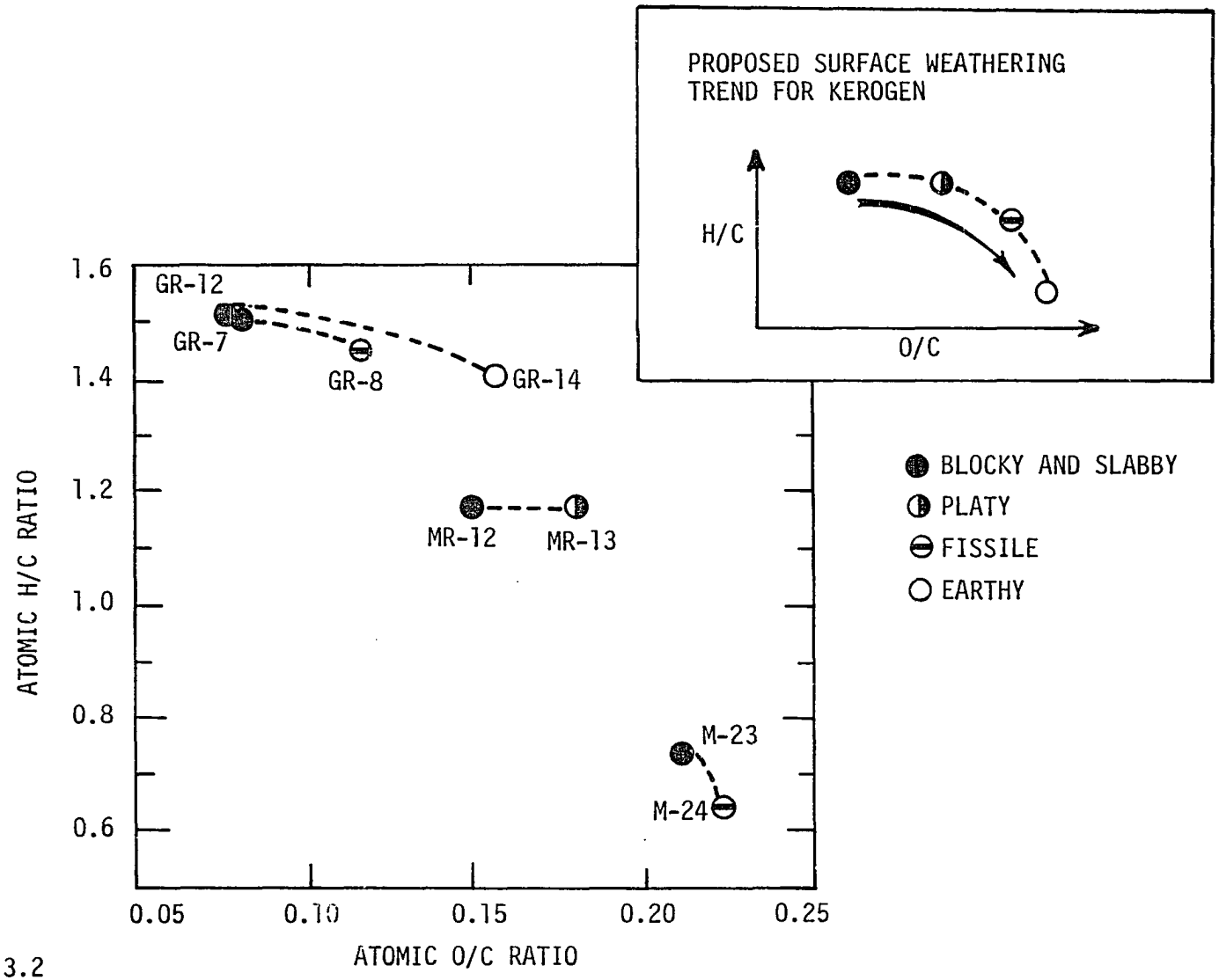

FIGURE 3.2

Figure 3.3: Plot showing alteration of the total organic carbon and the extractability factor (bitumen/total organic carbon) of a rock as a result of surface weathering.

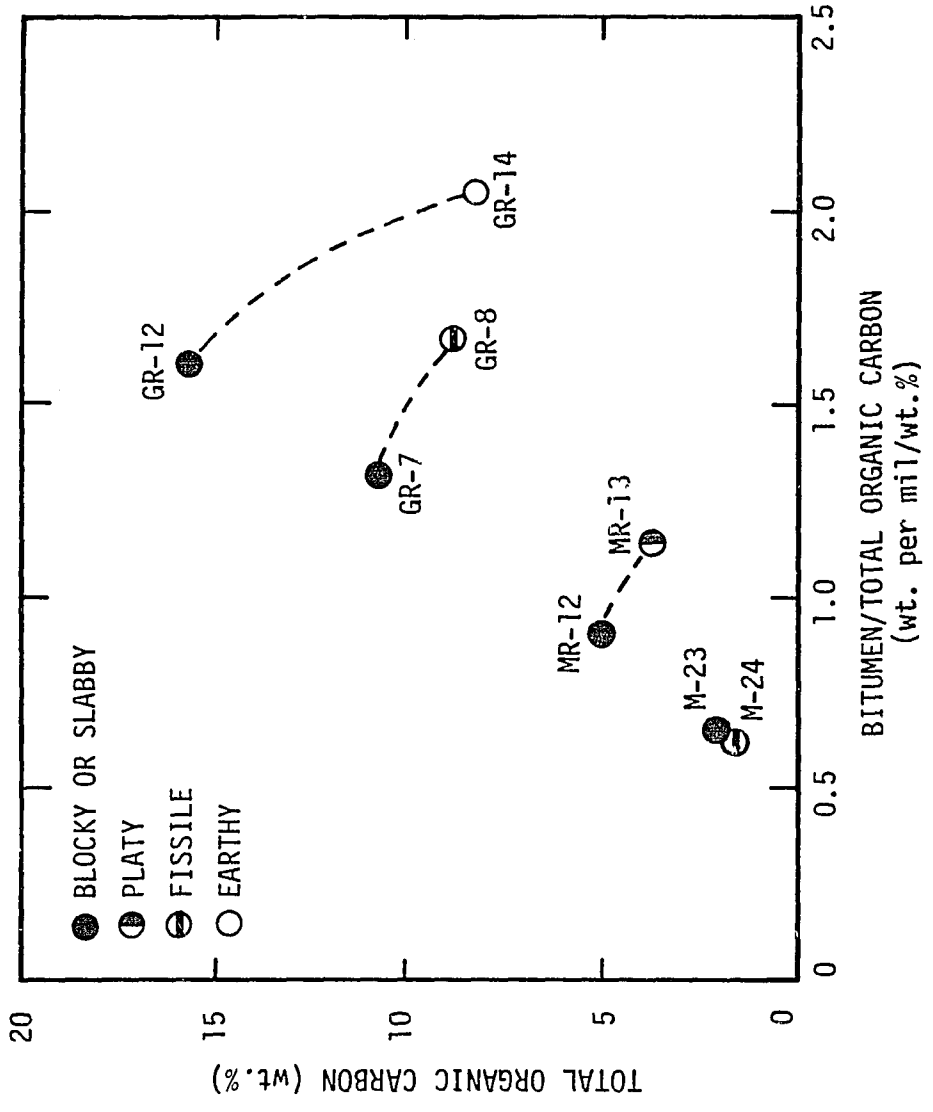

FIGURE 3.3

Accompanying this decrease is an apparent increase in the amount of bitumen with respect to the total organic carbon content of the rock. The bitumen to total organic carbon ratio is a measure of extractability, and its increase with increasing surface weathering may be due to the chemically altered portions of the kerogen becoming more susceptible to extraction with increasing weathering. This weathering mechanism suggests that while some portions of the organic matter are being removed from the rock system, other portions are being transferred from the kerogen phase of the rock system to its bitumen phase.

3.2 PEDOGENIC WEATHERING

The second style of weathering is referred to as pedogenic weathering, and it is the result of meteoric waters weathering rocks into residual soils (Figure 3.4). Outcrops exposed along river banks and road cuts sometimes exhibit a residual soil profile outlining the topography of the outcrop. The A and B horizons of the profile are the actual soil and show no color or textural resemblance to the original rock. The underlying C horizon consists of highly weathered rock and is referred to in this study as the saprolite horizon. Although the rock in this horizon is discolored and more friable than the original rock, the textural fabric of the original rock is usually preserved. The saprolite horizon grades downward into the transition horizon, which consists of rock ellipsoids encompassed by friable, discolored rock. The encompassing rock is similar to the highly weathered rock in the saprolite zone and is referred to as saprolite rinds. The rock ellipsoids are

Figure 3.4: Conceptual cross-sectional view of pedogenic weathering horizons.

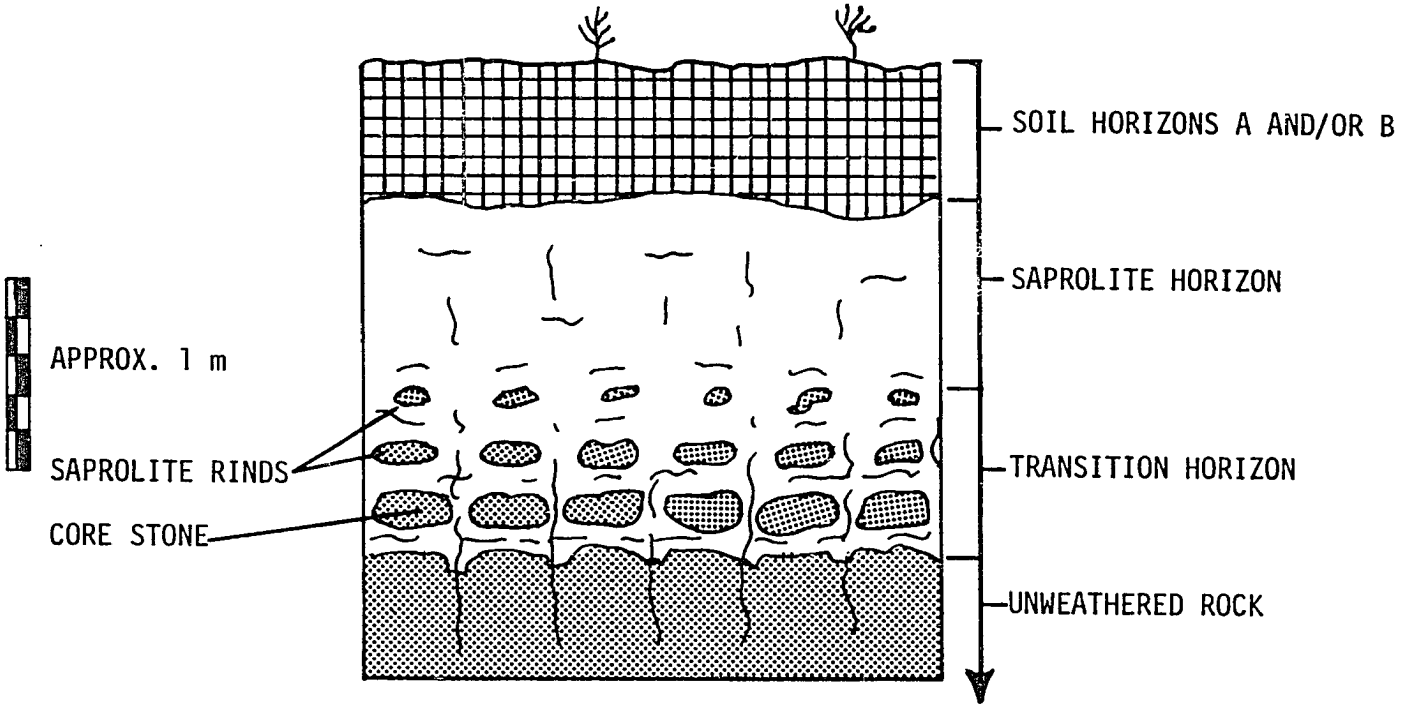

FIGURE 3.4

usually not discolored and are referred to as core stones. As the transition zone grades downward into the unweathered rock, the saprolite rinds become thinner and the core stones become larger. Minerals, such as limonite, hematite, gypsum, and jarosite, sometimes occur as coatings on the fracture and parting surfaces of the unweathered rock below the transition horizon. It appears as though these minerals precipitate out of the downward percolating meteoric waters, which have leached the necessary chemical components from the weathered rocks in the overlying horizons. In some cases the saprolite horizon may abruptly penetrate the transition and unweathered zones along abrupt high permeability zones like clastic dikes and fault planes.

The thickness of each horizon and the depth at which they occur depends on the intensity of weathering in an area and the composition of the original rock. The intensity of the weathering depends on a number of variables including climate, topography, soil biota, and duration of weathering. The best measure of intensity of this style of weathering is the degree of discoloration. The greater the discoloration the greater the intensity of the pedogenic weathering.

Unlike surface weathering, the inorganic phases of rocks are altered during pedogenic weathering. As shown in Table 3.3, the clinoptilolite, pyrite, and clay minerals are altered significantly by this style of weathering, particularly in the saprolite horizon and the saprolite rinds of the transition horizon. The actual mineralogical changes vary with the chemistry of the percolating meteoric waters in an area.

Table 3.3: Mineralogy of pedogenic weathered shales and their unweathered equivalents. Values given in weight percent.*

Mineral	Kreyenhagen Shale Unweathered Horizon	Kreyenhagen Shale Saprolite Horizon	M-43 Unweathered Horizon	M-41 Transition Horizon Core	M-42 Saprolite Rim
Quartz	22	21	50	48	48
Feldspars	10	9	1	1	1
Clinoptilolite	10	1	nd	nd	nd
Illite	26	20	6	9	16
Smectite	25	40	28	30	25
Kaolinite	5	9	3	4	5
Chlorite	nd	nd	2	nd	nd
Dolomite	nd	nd	8	5	6
Pyrite	2	nd	2	3	nd
Total	100	100	100	100	100

*Mineralogy determined by semiquantitative x-ray diffraction analysis.

**Values represent the mean of 7 samples from the unweathered zone and 7 samples from the saprolite zone (Lewan, 1975).

nd = not detected

The elemental composition of kerogen responds to pedogenic weathering in the same manner as it does to surface weathering (Figure 3.5). Oxidation of the kerogen begins in the core stones of the transition horizon and continues through the saprolite horizon. Dehydrogenation of the kerogen commences in the saprolite rinds of the transition horizon and continues through the saprolite horizon. Although the elemental composition of a pedogenic weathered kerogen follows the same trend as surface weathered kerogen, the former has a much more drastic effect on liptinitic kerogen. Visual examination of pedogenic weathered kerogen reveals a preferential leaching of liptinitic kerogen with respect to ligninic kerogen in the saprolite horizon. The preferential leaching of liptinitic kerogen in this horizon results in a relative increase in the ligninic kerogen, which may have only made up a minor portion of the total kerogen in the unweathered rock. This process is also reflected in the carbon isotope values of the total kerogens as shown in Table 3.4. As the isotopically heavier ligninic kerogen increases relative to the leached isotopically lighter β-liptinitic kerogen, the carbon isotopes values of the total kerogen becomes heavier.

Data on the pedogenic weathering effects on total organic carbon and amount of bitumen in a rock are shown in Figure 3.6. Although the data is not complete, the author feels that the pedogenic weathering trend from the unweathered horizon through the saprolite rinds of the transition horizon are probably similar to the trend observed in surface weathering. As mentioned previously, this trend involves the loss of total organic carbon and an increase in the amount of bitumen with

Figure 3.5: H/C versus O/C plot of kerogen alteration resulting from pedogenic weathering.

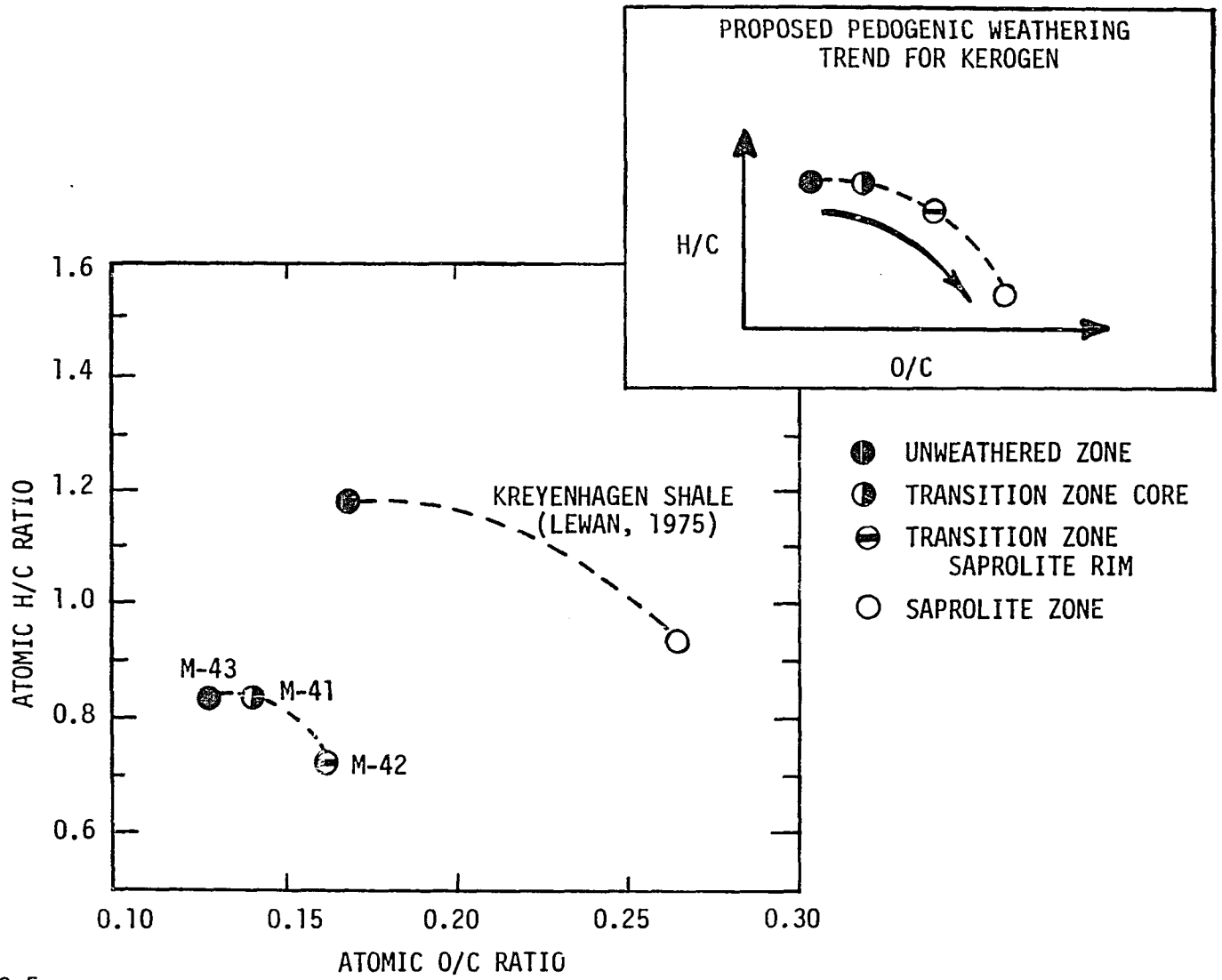

FIGURE 3.5

Table 3.4: Carbon isotope values of kerogens from pedogenic weathered rocks and their unweathered equivalents.

	Kreyenhagen Shale*		M-43	M-41	M-42
	Unweathered Horizon	Saprolite Horizon	Unweathered Horizon	Transition Core Stone	Horizon Saprolite Rim
Kerogen Type	α-Lipnitic + Minor Ligninic	α-Lipnitic + Ligninic	Ligninic + Lipnitic	Ligninic + Lipnitic	Ligninic + Lipnitic
Kerogen δC^{13} ($^{o}/oo$, PDB)	-31.2	-28.7	-25.2	-25.4	-24.7

*Data from Lewan (1975).

Figure 3.6: Plot showing the alteration of the total organic carbon and the extractability factor (bitumen/total organic carbon) of a rock as a result of pedogenic weathering.

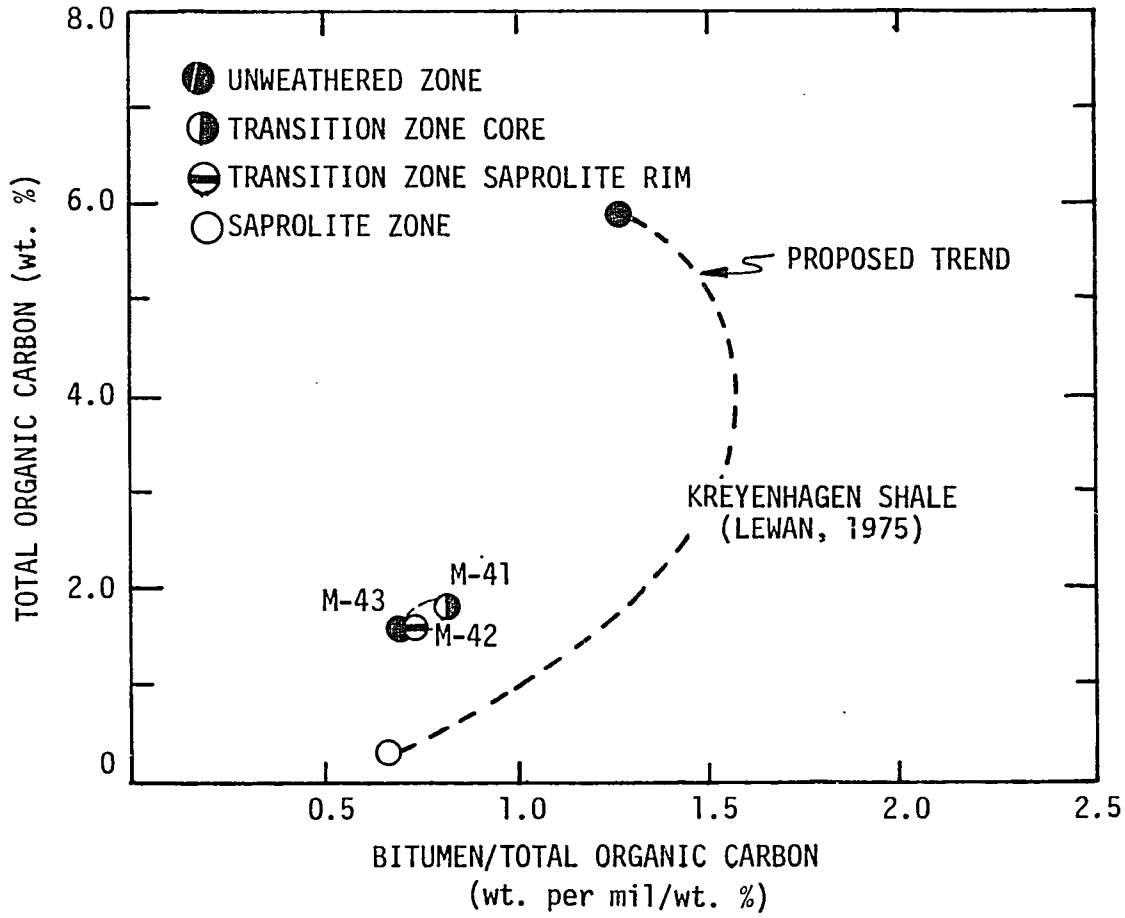

FIGURE 3.6

increasing weathering intensity. This trend is altered significantly in the saprolite horizon where the amount of bitumen as well as the total organic carbon are drastically reduced. This deviation in the trend is probably the result of liptinitic kerogen being leached from the system. Currently it is not known how organics in rocks bearing sporopolleninic kerogen will react to pedogenic weathering, and additional studies in this area are needed.

3.3 DISCUSSION

Data on the effect of weathering on the concentrations and proportionality of vanadium and nickel in bitumen are limited due to the difficulty in extracting sufficient quantities of bitumen from highly weathered rocks. The available data in Table 3.5 shows that the concentrations of these two metals do fluctuate with the degree of weathering for both surface and pedogenic weathering, but their proportionality is only altered in sporopolleninic kerogen bearing rocks in the fissile through earthy zones of surface weathering. The proportionality of the metals in bitumens from liptinitic kerogen bearing rocks does not appear to be altered in platy zones of surface weathering or in saprolite rinds of pedogenic weathering.

Figure 3.7 summarizes some of the physical and chemical changes that occur to a rock during surface and pedogenic weathering. It has not been the intent of this discussion to explain the specific mechanisms and reactions responsible for these changes. Instead the intent has

Table 3.5: Data on the effect of weathering on the concentration and proportionality of vanadium and nickel in bitumen.

Sample Number	Kerogen Type	Weathering Type	Degree of Weathering	Vanadium (ppm)	Nickel (ppm)	V Ni+V
GR 12	β-Sporopolleninic	Surface	Blocky	5.2	74.8	0.07
GR 14		Weathering	Earthy	1.0	48.3	0.02
GR 7	β-Sporoppoleninic	Surface	Blocky	5.4	40.5	0.12
GR 8		Weathering	Fissile	1.9	67.0	0.03
MR 12	α-Liptinitic	Surface	Blocky	7.9	239	0.03
MR 13		Weathering	Platy	3.3	162	0.02
MR 43	β-Liptinitic +	Pedogenic	Unweathered	8.7	78.0	0.10
MR 41	Ligninic	Weathering	Core Stone	9.7	133.0	0.07
MR 42			Saprolite Rind	6.3	67.1	0.09

Figure 3.7: Graphs showing types of alteration and their occurrence through surface weathering zones (a) and pedogenic weathering horizons (b).

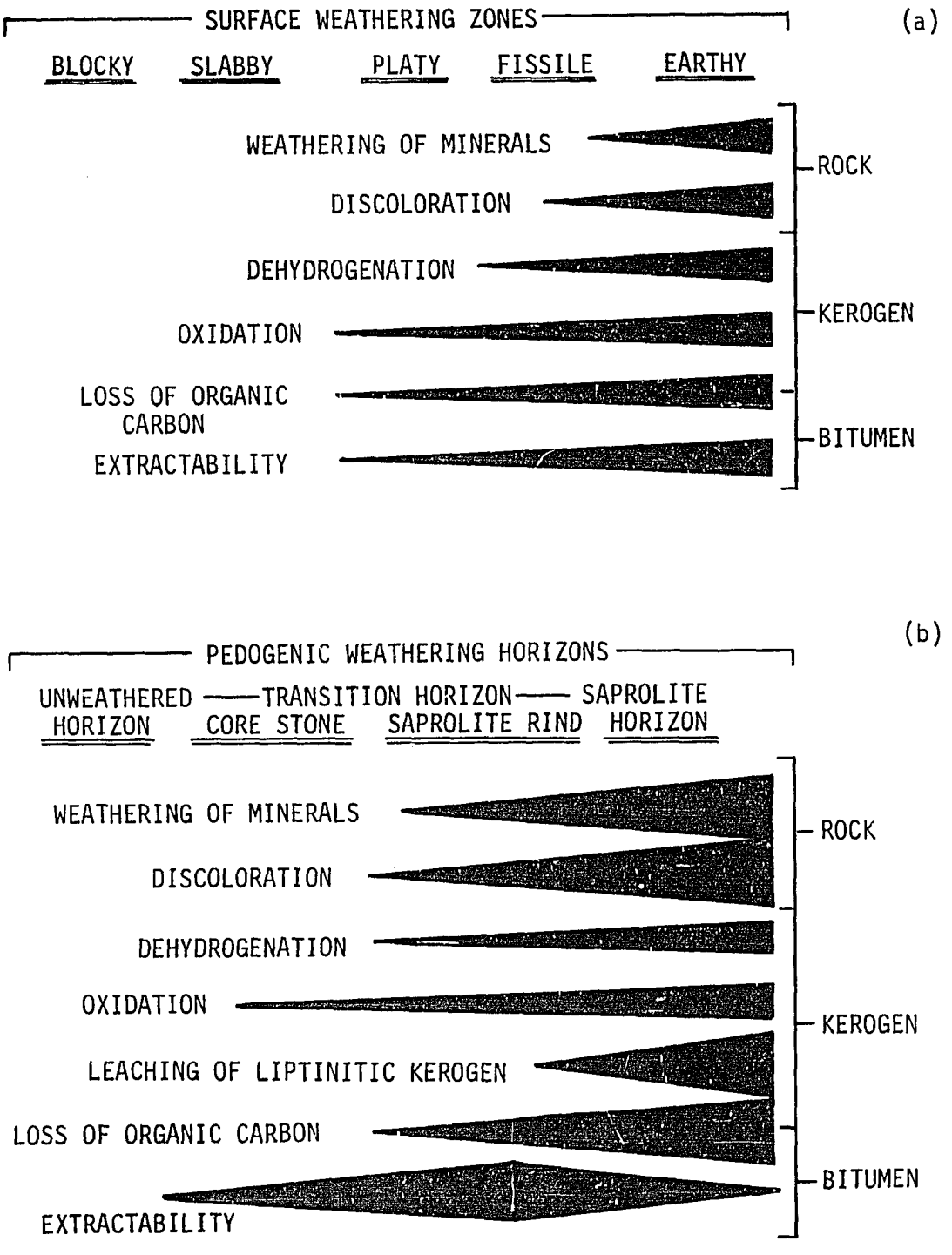

FIGURE 3.7

been to establish field criteria that will enable one to determine the degree and style of weathering in an outcrop, and from this determine what portions of the outcrop are suitable for sampling. In this study an outcrop was initially examined and evaluated with respect to the two styles of weathering before sample collection. As suggested by Figure 3.7, blocky and slabby rock samples from surface weathered portions of an outcrop were collected because they are the least likely to show weathering effects. In pedogenic weathered portions of an outcrop the sampling was done in the areas with the least discoloration, preferably the unweathered horizon rather than the core stones of the transition horizon. It should be noted that pedogenic and surface weathering are commonly superimposed on one another along the margin of the topographic outline of an outcrop (Figure 3.8). In some cases this may be the only portion exposed in an outcrop, and in these cases no samples should be collected. A general rule for sampling is that all samples should be blocky or slabby with no signs of saprolite rinds.

Figure 3.8: Conceptual drawing of the superimposition of surface weathering on pedogenic weathering of the Kreyenhagen shale at the Skunk Hollow Outcrop (Local No. 59).

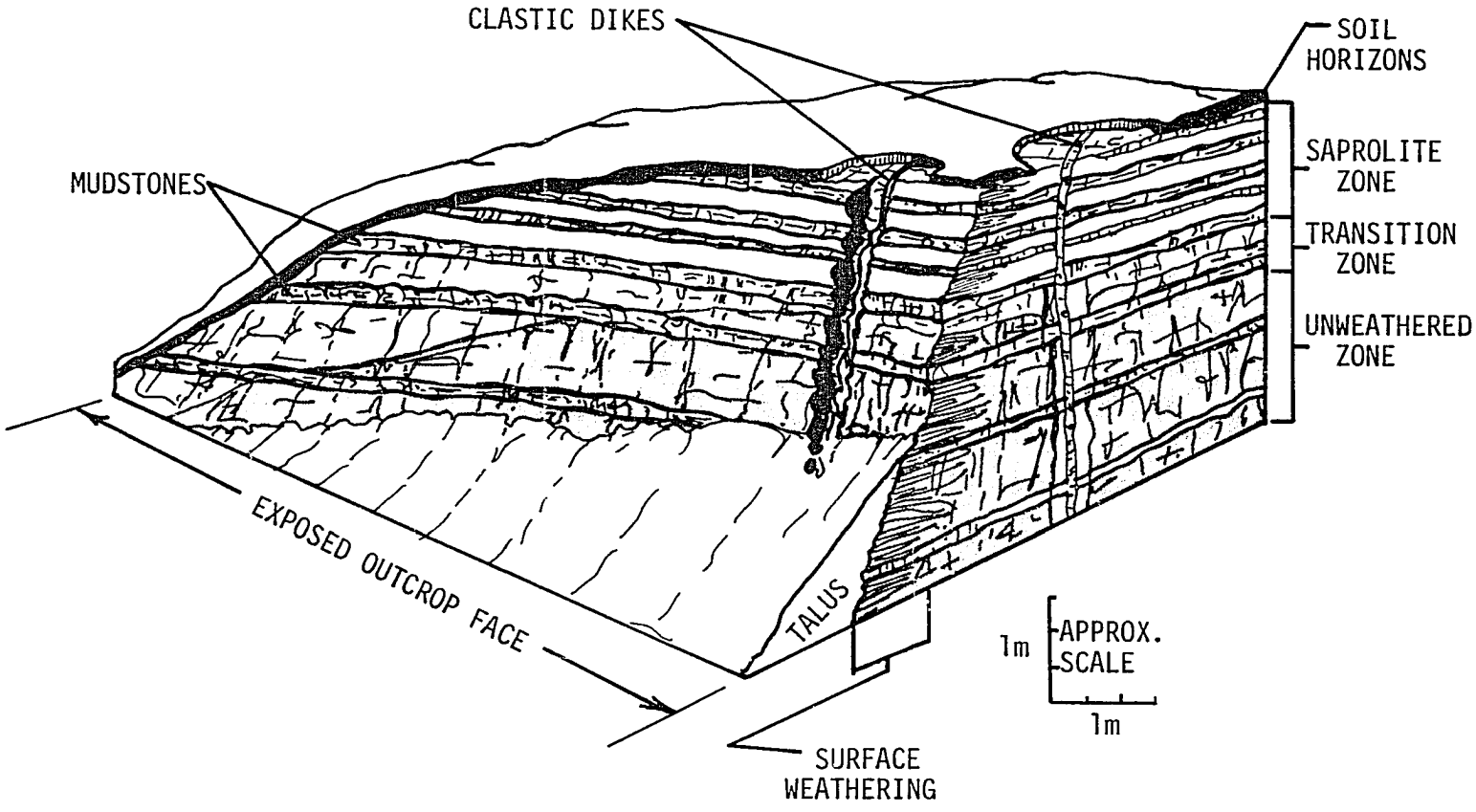

FIGURE 3.8

CHAPTER 4

NATURALLY OCCURRING VANADIUM- AND NICKEL-ORGANIC COMPLEXES

High vanadium and nickel concentrations in naturally occurring organic substances are attributed to metallo-organic complexes. These complexes usually have high molecular weights (>400), and their structural complexity renders them difficult to study. In spite of this difficulty, numerous investigations concerning their structure and chemical behavior have been published. Based on these investigations, there appear to be three major classes of naturally occurring vanadium-and nickel-organic complexes; 1) tetrapyrrole complexes, 2) mixed ligand tetradendate complexes, and 3) humate complexes.

4.1 TETRAPYRROLE COMPLEXES

The basic framework of tetrapyrrole complexes consists of four pyrrole molecules bound together at their alpha positioned carbons by four methines (Figure 4.1). Within the center of this conjugated complex only two of the pyrroles contain imine hydrogen atoms. Under the proper conditions these two hydrogen atoms may be easily replaced by bivalent cations, such as Mg^{+2}, Fe^{+2}, Co^{+2}, Cu^{+2}, Ni^{+2}, or VO^{+2}. Tetrapyrrole complexes with this basic framework are referred to as porphyrins, and a variety of functional groups may be bound to their peripheral carbon atoms (Figure 4.1). Different types and amounts of these functional groups result in a homologous series of porphyrins (Hodgson, Strosher,

Figure 4.1: Basic framework of tetrapyrrole complex and modifications resulting from the addition of peripheral functional groups.

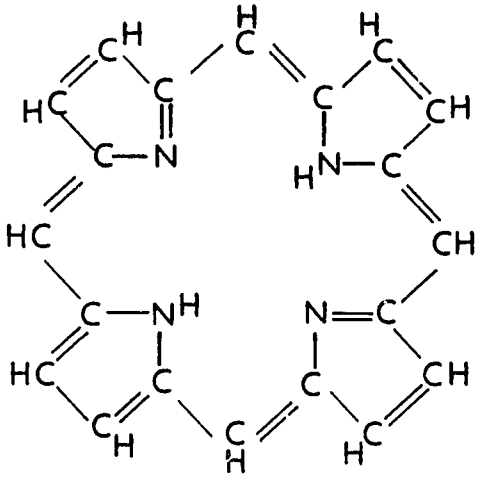

BASIC FRAME WORK OF
TETRAPYRROLE COMPLEX
(PORPHIN)

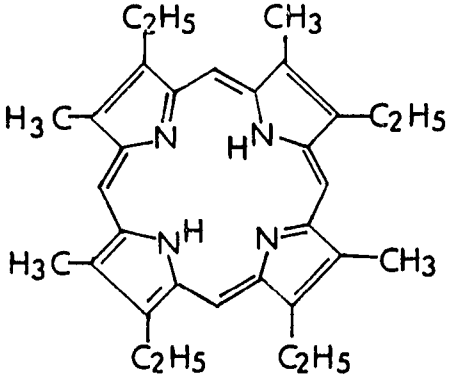

BASIC FRAME WORK WITH
ALKYL FUNCTIONAL GROUPS
(ETIO PORPHYRIN)

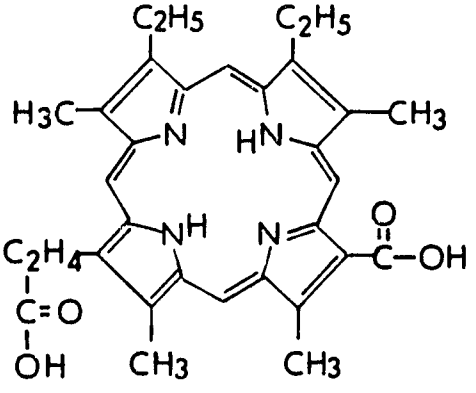

BASIC FRAME WORK WITH
ALKYL AND CARBONAL
FUNCTIONAL GROUPS
(RHODOPORPHYRIN)

FIGURE 4.1

and Casagrande, 1972; Casagrande and Hodgson, 1974). Other types of modifications that may occur to the basic framework include increasing or decreasing its aromaticity. Increasing the aromaticity of the basic conjugated frameworks results in highly aromatic tetrapyrrole complexes, while decreasing the aromaticity of the basic conjugated framework results in pseudoaromatic tetrapyrole complexes (Figure 4.2). These two types of tetrayrrole complexes are collectively referred to as nonporphyrins, which also includes mixed ligand tetradendate complexes and humate complexes.

Chlorophyll and heme pigments in living matter appear to be the most likely precursors of tetrapyrrole complexes found in crude oils, sediments, and sedimentary rocks (Hodgson et al., 1960; Blumer and Snyder, 1967; Yen, 1975). Heme pigments are porphyrins with iron substituting for the two centrally located imine hydrogen atoms. Although heme pigments are present in all organisms with the exception of anaerobic clostrida and lactic acid bacteria (Metzler, 1977, p. 563), their most significant concentrations occur in animals. Chlorophyll pigments are pseudoaromatic tetrapyrrole complexes with magnesium substituting for the two centrally located imine hydrogen atoms. Chlorophyll pigments are restricted to oxygen evolving photosynthetic organisms, where they are much more prevalent than the heme pigments. Although heme pigment may be a significant precursor in a few cases (e.g. Shiobara and Taguchi, 1975), the wider distribution and higher concentrations of chlorophyll pigment in the biosphere make it the more likely precursor (Corwin, 1959).

Figure 4.2: Types of conjugated configurations in tetrapyrrole complexes.

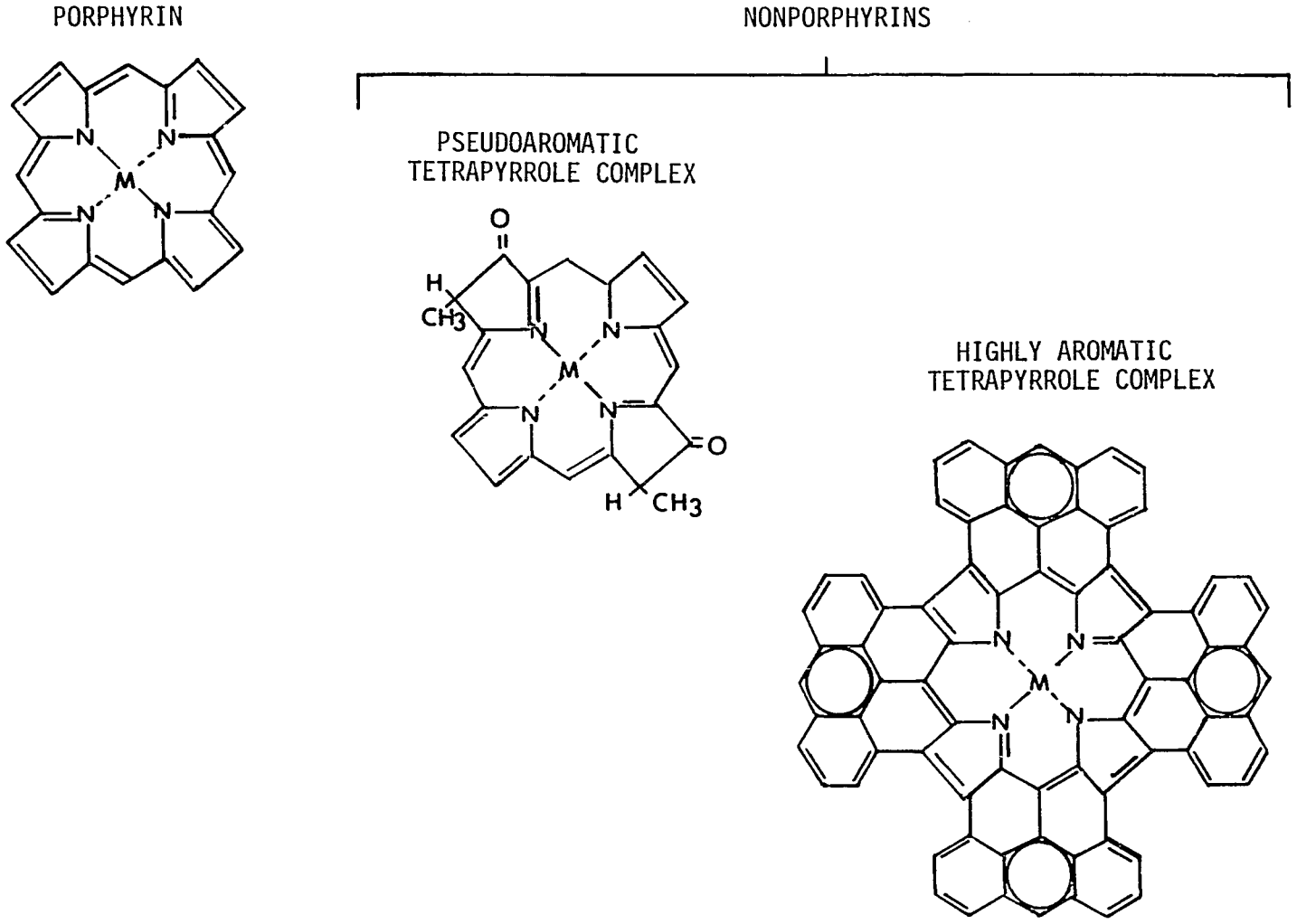

FIGURE 4.2

Conversion of chlorophylls to tetrapyrrole complexes similar to those found in crude oils, sediments, and sedimentary rocks appears to involve a series of reactions (Orr et al., 1958; Baker and Smith, 1973; Yen, 1975), of which only a few have been well documented. Most of the proposed reaction series are concerned with the conversion of chlorophyll to insular porphyrins, similar to those observed in crude oils. Although these proposed reaction series may take place in part, they do not include the possibility of chlorophyll derivatives being assimilated into kerogens during the early stages of diagenesis as suggested by Blumer and Snyder (1967). Later at moderate to high levels of thermal maturation, these assimilated tetrapyrrole complexes may be released from the kerogen contemporaneously with the generation of crude oil. With this possibility in mind, the following three-stage series for the conversion of chlorophylls to tetrapyrrole complexes in sedimentary rocks and crude oils is proposed.

4.1.1 Stage I: From Water Column to Sediment Surface

Stage I involves the interaction between chlorophylls and water as the pigments settle through a water column or rest on the sediment-water interface. The two major types of reaction that may occur in this setting are demetallation and decomposition. Available data indicates that the former occurs in the upper portions of a water column, while the latter occurs at the sediment-water interface, as well as within the water column.

Demetallation is the result of two hydrogen atoms replacing the centrally located divalent magnesium cation in the chlorophylls. This reaction occurs readily in dilute acid solutions (Joslyn and Mackinney, 1938; Hoff, 1964, p. 3) and results in the formation of pheophytins (Figure 4.3). Studies by Yentsch (1965) and Lorenzen (1967) indicate that demetallation is essentially complete within the upper 200 meters of most marine water columns. Thus in most cases, pheophytin rather than chlorophyll is deposited on the sediment-water interface (Orr et al., 1958; Baker and Smith, 1973; Baker and Smith, 1974; Yen, 1975). In the few cases where minor amounts of chlorophyll are detected in sediments, the environment of deposition is characterized by high detritus sedimentation rates (e.g. deltaic environments; Corcoran, 1957), water with high magnesium concentrations (e.g. hypersaline environments; Nissenbaum et al., 1972), and high organic matter accumulation rates (e.g. lacustrine environments; Koyama et al., 1968; Daley and Brown, 1973a).

Although it has been demonstrated in the laboratory that demetallation may occur inorganically in dilute acid solutions (Lamort, 1956; Hodgson and Hitchon, 1959; Daley and Brown, 1973a), the grazing effect of zooplankton appears to be the major cause of demetallation in lacustrine (Daley, 1973) and marine (Lorenzen, 1967) water columns. This is based on the observation that demetallated tetrapyrroles are common in the feces of zooplankton (Currie, 1962), and laboratory experiments show total conversion of chlorophyll to pheophytin and lesser amounts of pheophorbide by zooplankton digestion (Daley, 1973). The demetallation

Figure 4.3: Formation of pheophytin as a result of the demetallation of chlorophyll.

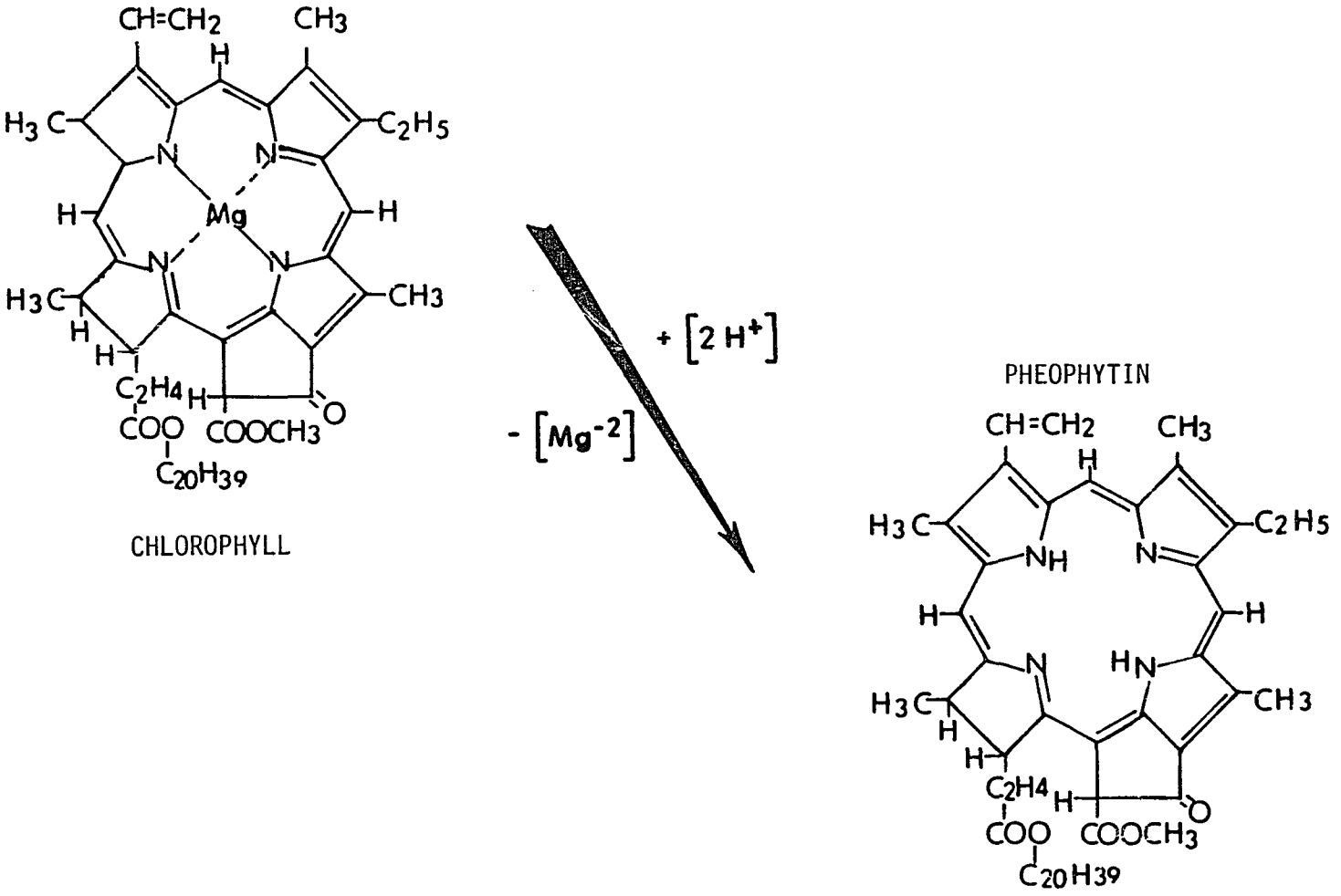

CHLOROPHYLL

FIGURE 4.3

is attributed to the acid conditions within the digestive tract of the zooplankton (Daley, 1973).

Pheophytin may also be produced biochemically in preference to chlorophyll when phytoplankton are subjected to long periods of darkness (Yentsch, 1965). Although phytoplankton in the darker portions of the euphotic zone in a water column may produce some pheophytin, the mechanism offers no explanation for the demetallation of chlorophylls produced in the more favorable portions of the euphotic zone. It has also been noted by Daley (1973) that pheophytin production during long periods of darkness is not common to all phytoplankton.

Decomposition of tetrapyrroles is the second type of reaction that may occur in a water column, and it involves the complete rupturing of the tetrapyrrole structure (Daley and Brown, 1973). Decomposition of tetrapyrroles and accompanying organic matter is severe in marine water columns below depths of 50 to 100 meters (Figure 4.4) and may be the result of aerobic bacterial degradation or photochemical oxidation. The effectiveness of bacteria in degrading organic matter under aerobic conditions (Waksman and Carey, 1935; Zobell, 1946; Oppenheimer, 1960; Volkmann and Oppenheimer, 1962; Koyama and Tomino, 1967) and the concentration of bacteria in marine water columns below 50 meters (Zobell, 1946; Jannasch and Jones, 1959) suggests that aerobic bacterial degradation is a possible mechanism for decomposition (Figure 4.4). Photochemical oxidation is also a possible mechanism for decomposition of tetrapyrroles (Rabinowitch, 1945; Daley and Brown, 1973) and would appear to be most

Figure 4.4: Plots showing organic variables in the offshore southern California water column. Data from (a) Jannasch and Jones (1959), (b) and (c) Holm-Hansen (1969). Shaded area represents zone of phytoplankton concentration (Sleggs, 1927).

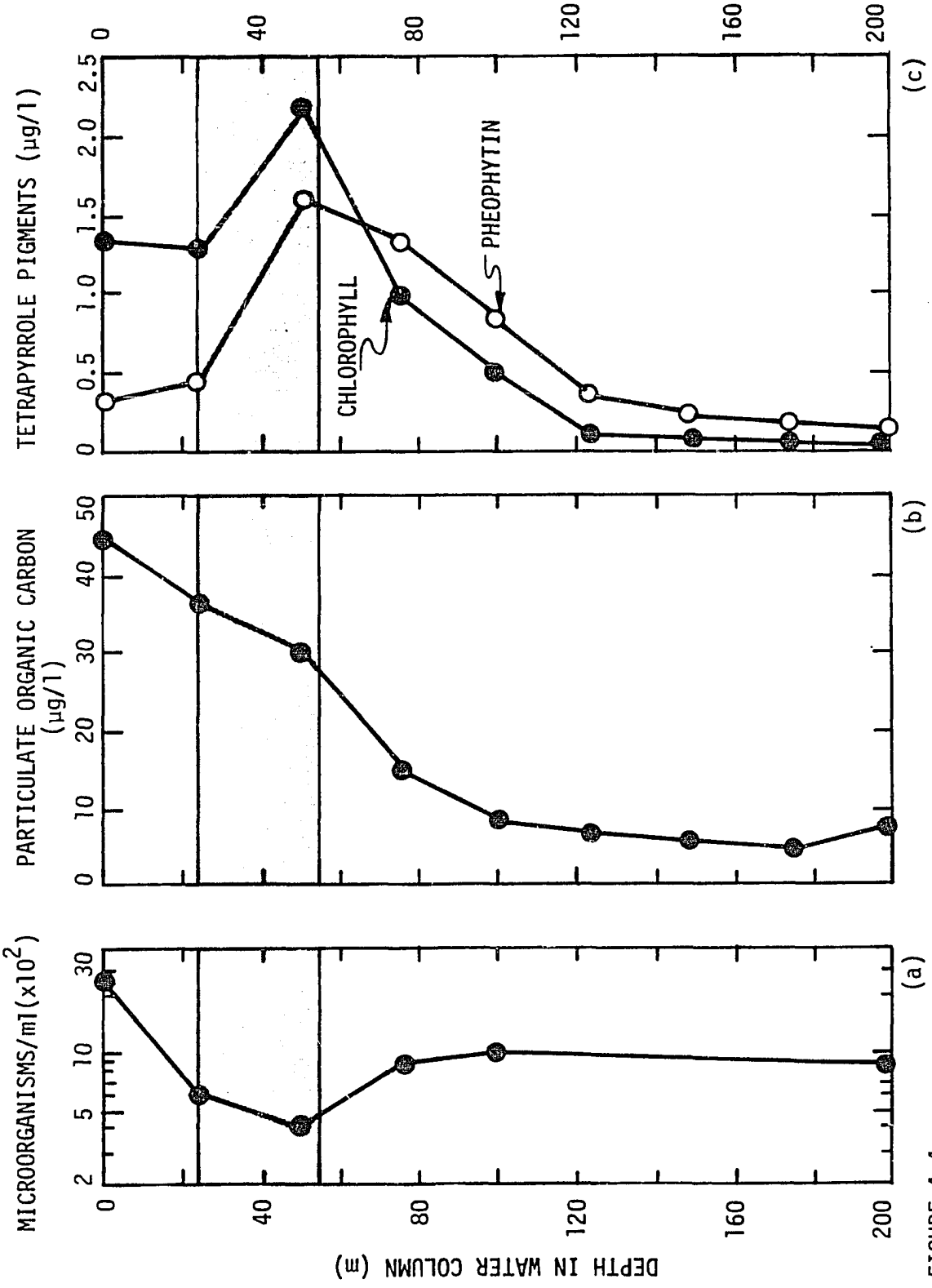

FIGURE 4.4

effective in the aerobic portions of the euphotic zone of water columns. Experimental results presented by Daley (1973) suggest that photochemical oxidation is more salient to tetrapyrrole decomposition than aerobic bacterial degradation, but additional research on the later mechanism is needed (Kallio, 1979).

The availability of oxygen within a water column appears to be crucial to tetrapyrrole decomposition, and as a result, anaerobic conditions favor the preservation of tetrapyrroles (Brongersma-Sanders, 1951; Gorham and Sanger, 1967; Drozdova and Gorskly, 1972; Drozdova, 1975; Didyk et al., 1978). Preservation of the organic matter accompanying tetrapyrroles is also favored under anaerobic conditions (Zobell, 1946; Koyama and Tomino, 1967; Didyk et al., 1978), but its rate of decomposition under aerobic conditions appears to be slower than the rate of decomposition for tetrapyrroles. This preferred decomposition of tetrapyrroles has been documented for photochemical oxidation (Daley and Brown, 1973), but has not been verified for aerobic bacterial degradation. Although the mechanism is not completely understood, preferential decomposition of tetrapyrroles has been noted in marine water columns (Figure 4.5a), lacustrine sediments (Figure 4.5b; Koyama et al., 1973),and decaying leaves (Sanger, 1968, 1971a, 1971b).

Preferred decomposition of this type suggests that the amount of tetrapyrroles retained in an accumulation of organic matter is a function of its exposure time to aerobic conditions and the oxygen level of the aerobic conditions encountered. The tetrapyrrole content should be low

Figure 4.5: Plots showing the preferred decomposition of tetrapyrrole pigments relative to total organic carbon in (a) a marine water column (Holm-Hansen, 1969) and (b) a lake sediment (Koyama et al., 1968).

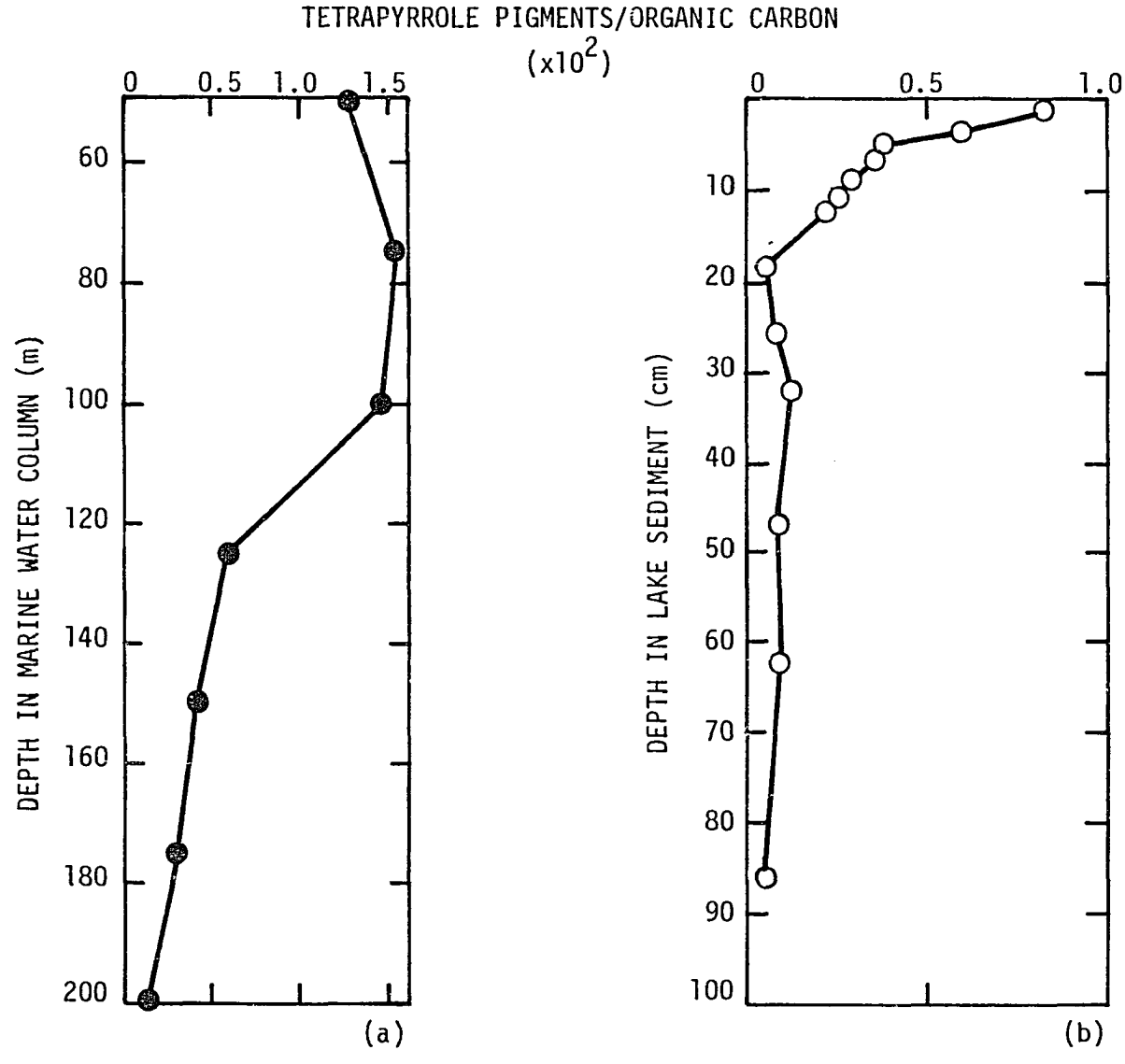

FIGURE 4.5

in organic matter that has settled through long aerobic water columns or has been exposed to aerobic conditions on the sediment-water interfaces for a long duration. Conversely, the tetrapyrrole content should only be partially reduced in organic matter that has encountered anaerobic waters early in its descent through a water column or rapidly buried to anaerobic conditions within a sediment column. This can be demonstrated in part by examining the offshore basins of southern California. The height of the water columns overlying these basins varies with basin depth, which may range from 627 meters in the Santa Barbra Basin to 4800 meters or more in the open ocean basin (Emery, 1960). Figure 4.6 shows that the concentration of pheophytin in the organic matter from the surface sediments of these basins decreases as their approximate settling distance through the aerobic and dysaerobic portions of the water column increases. The scatter in this general trend may be explained by two additional factors that were not considered in the plot; 1) the oxygen levels of the water columns are not the same in all of the basins and 2) the exposure time of organic matter on the sediment-water interfaces may vary with the sedimentation rates of each basin.

4.1.2 Stage II: From Sediment Surface to Sediment Lithification

Stage II represents the diagenetic setting from the time organic matter is buried in unconsolidated sediments to the time of sediment lithification. Decomposition of organic matter, as described in Stage I, continues in the upper aerobic portions of sediments that are overlain by aerobic waters. Conversely, decomposition is restrained in anaerobic

Figure 4.6: Concentration of pheophytin in organic matter from surface sediments of offshore southern California versus height of water column above sediment. The sediments plotted have median grain diameters equal to or less than 10 microns. Data from Orr and others (1958).

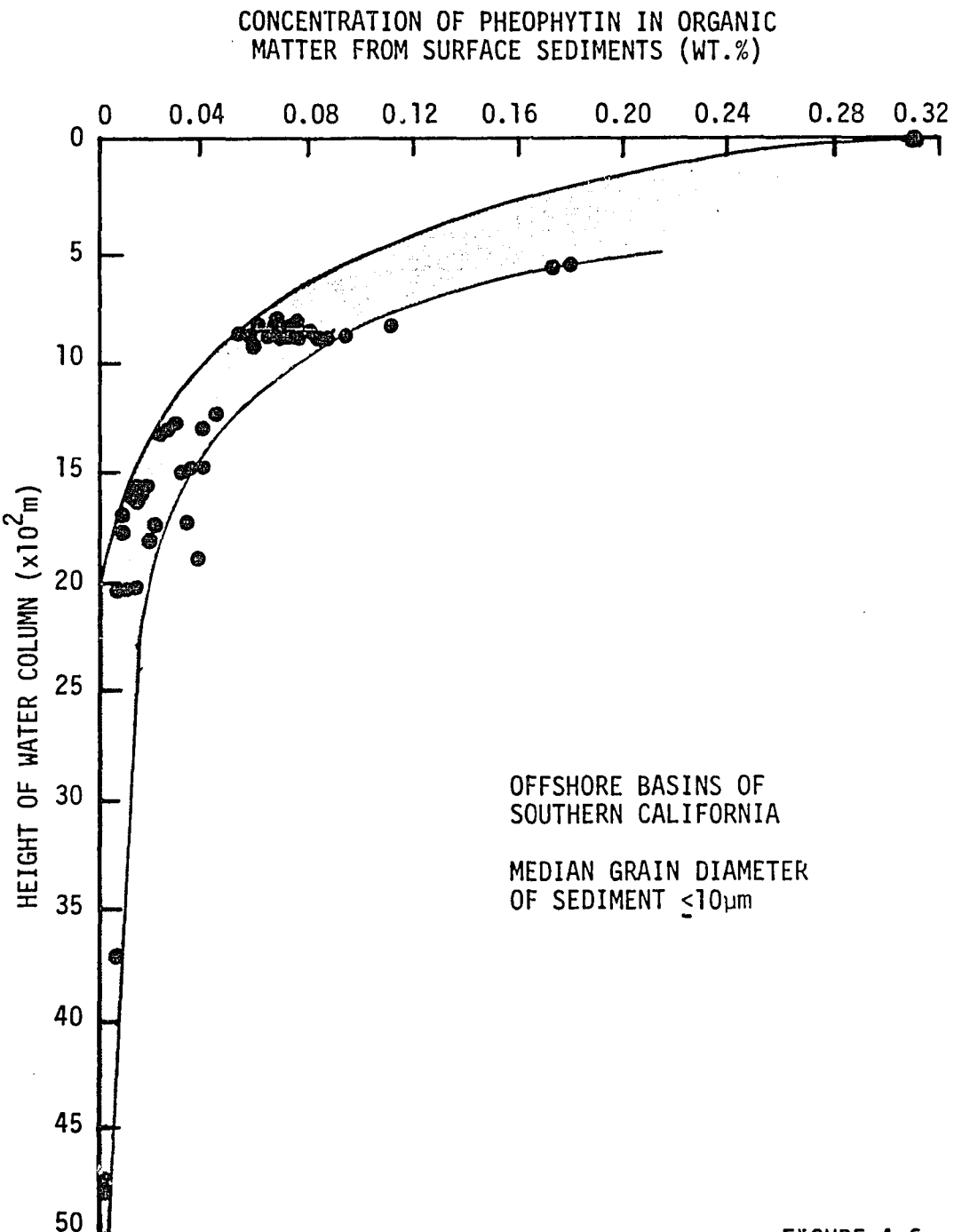

FIGURE 4.6

sediments, and under these reducing conditions a series of reactions involving the modification of tetrapyrrole pigments occur. Five major reactions suggested by Baker and Smith (1973, 1974) include allomerization, dealkenylation, reduction, aromitization and metallation. In addition to these reactions, assimilation as suggested by Blumer and Snyder (1967) will also be considered in this discussion. Although diagenetic sequences for some of these reactions have been postulated (Baker and Smith, 1973; Baker et al., 1977), data from a recent sediment study by Brown and others (1977) indicates that depth of burial is not a critical factor in the upper 250 cm of a sediment column.

Aerobic conditions usually prevail in the upper portions of sediment columns that are overlain by aerobic waters (Didyk et al., 1978, Fig. 1a; Thiede and Van Andel, 1977, Fig. 1). With increasing depth of burial, these sediments gradually become dysaerobic and eventually anaerobic (Zobell, 1942; Zobell, 1946b; Brooks et al., 1968). Rapid burial of sediments in this setting to anaerobic depths is a critical factor in the preservation of organic matter and its tetrapyrrole pigments (Didyk et al., 1978; Richards, 1970). Failure to meet this condition results in non-organic sediments (<1 wt.% organic carbon), which are typical of Holocene sediments in the major oceanic basins (Hunt, 1973; Heath et al., 1978). Within these non-organic sediments, the surviving trace amounts of tetrapyrrole pigments may be modified by allomerization during their exposure to aerobic conditions.

Allomerization in this situation involves the opening of the isocyclic ring in pheophytin by oxidation (Conant et al., 1931). An abbreviation of the numerous steps suggested by Yen (1975) and Baker and Smith (1973, 1974) for this reaction is shown in Figure 4.7. The resulting open ringed pseudo-aromatic tetrapyrroles are referred to as chlorins. Although this reaction is prominent in aerobic sediments (Daley and Brown, 1973; Brown et al., 1977), the dependency on oxygen of this reaction makes it unlikely in anaerobic sediments. Under anaerobic conditions the prominent reactions include dealkenylation, reduction, aromitization, and assimilation.

Dealkenylation involves the elimination of the phytol side chain from a tetrapyrrole pigment, and the preservation of the double bond in the chain is critical to the reaction (Figure 4.8). Once this double bond has been reduced, the resulting alkyl side chain will remain relatively stable until higher levels of diagenesis are reached (Baker and Smith, 1973, 1974; Aizenshtat et al., 1979). Regardless of the exact timing and mechanism of these reactions, the data shown in Figure 4.9 suggests that factors related to burial or lithification may be critical to the removal of the aliphatic portions of ester side groups. The small percentage of dealkenylated tetrapyrroles (pheophorbides) that do occur in the surface sediments is probably the result of zooplankton digestion of chlorophyll (Currie, 1962; Daley, 1973).

If anaerobic conditions persist with burial depth, the 2-vinyl double bond may be reduced to an ethyl side chain, and the 9-keto group may be

Figure 4.7: Formation of purpurin and chlorin as a result of the allomerization of pheophytin.

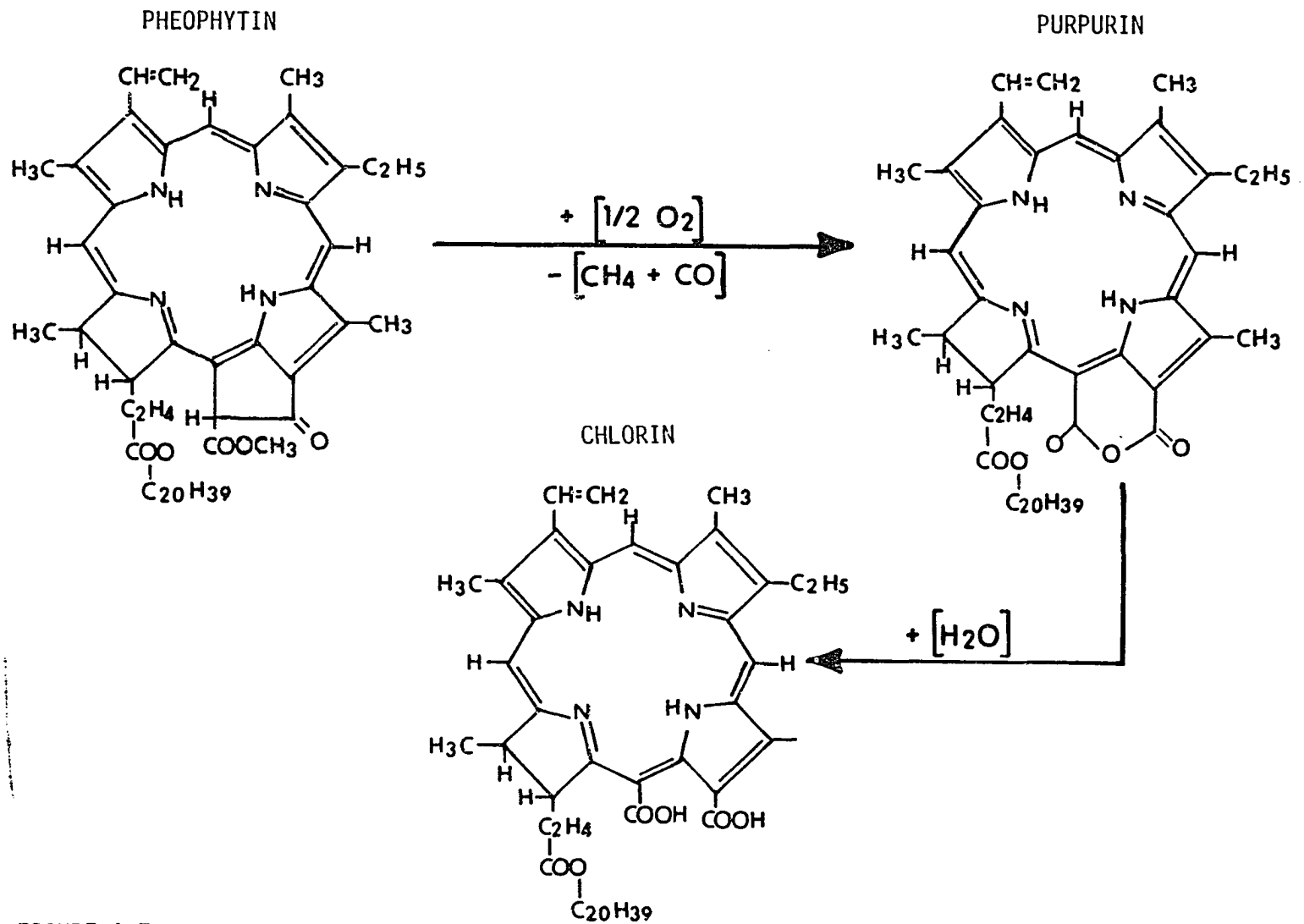

FIGURE 4.7

Figure 4.8: a) Reduction of phytol double bond, and
b) dealkenylation of phytol side chain.

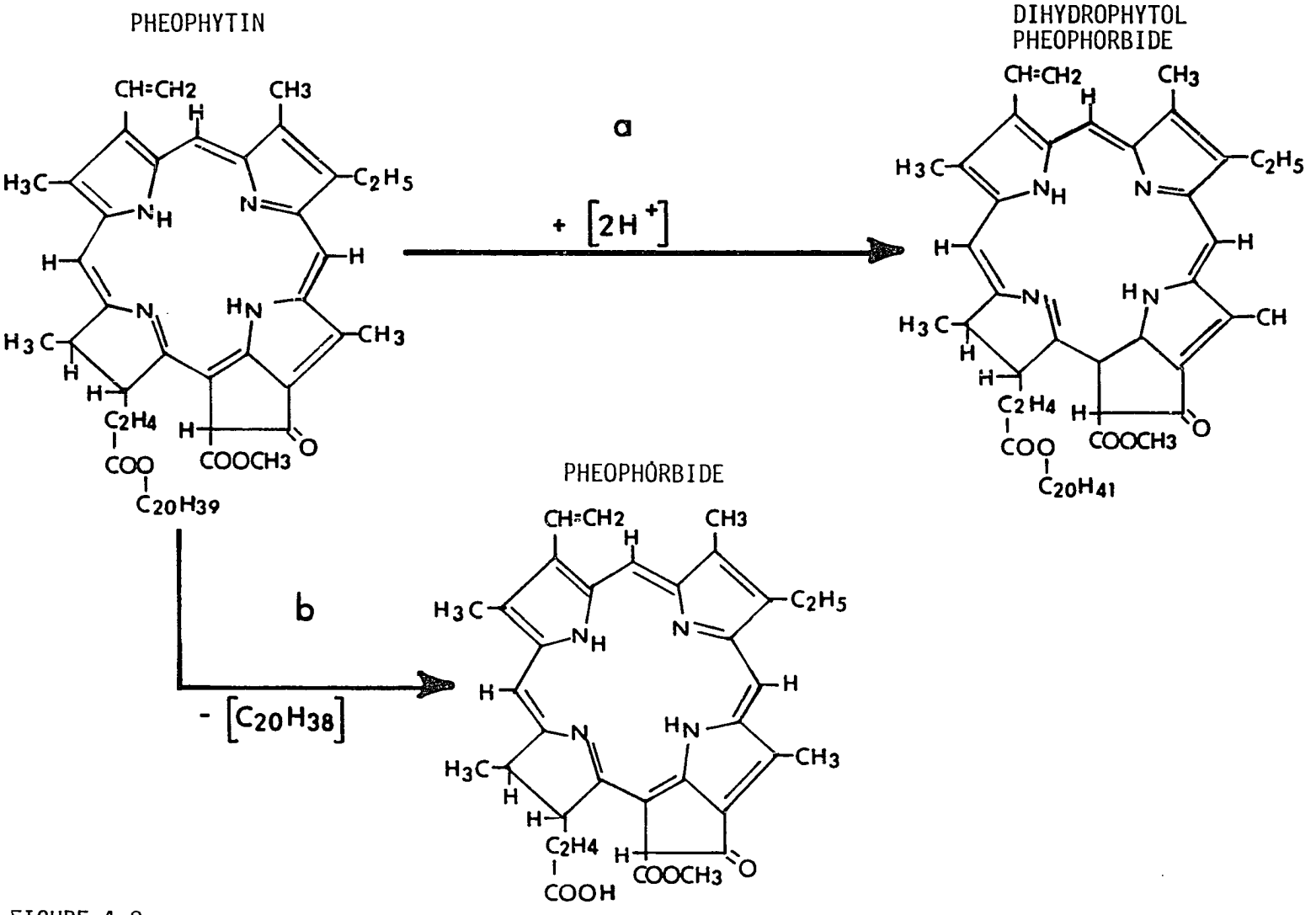

FIGURE 4.8

Figure 4.9: Comparison of the amounts of deestrified tetrapyrroles in surface sediments with those in lithified sediments. Data from Baker and Hodgson (1968) and Shiobara and Taguchi (1975).

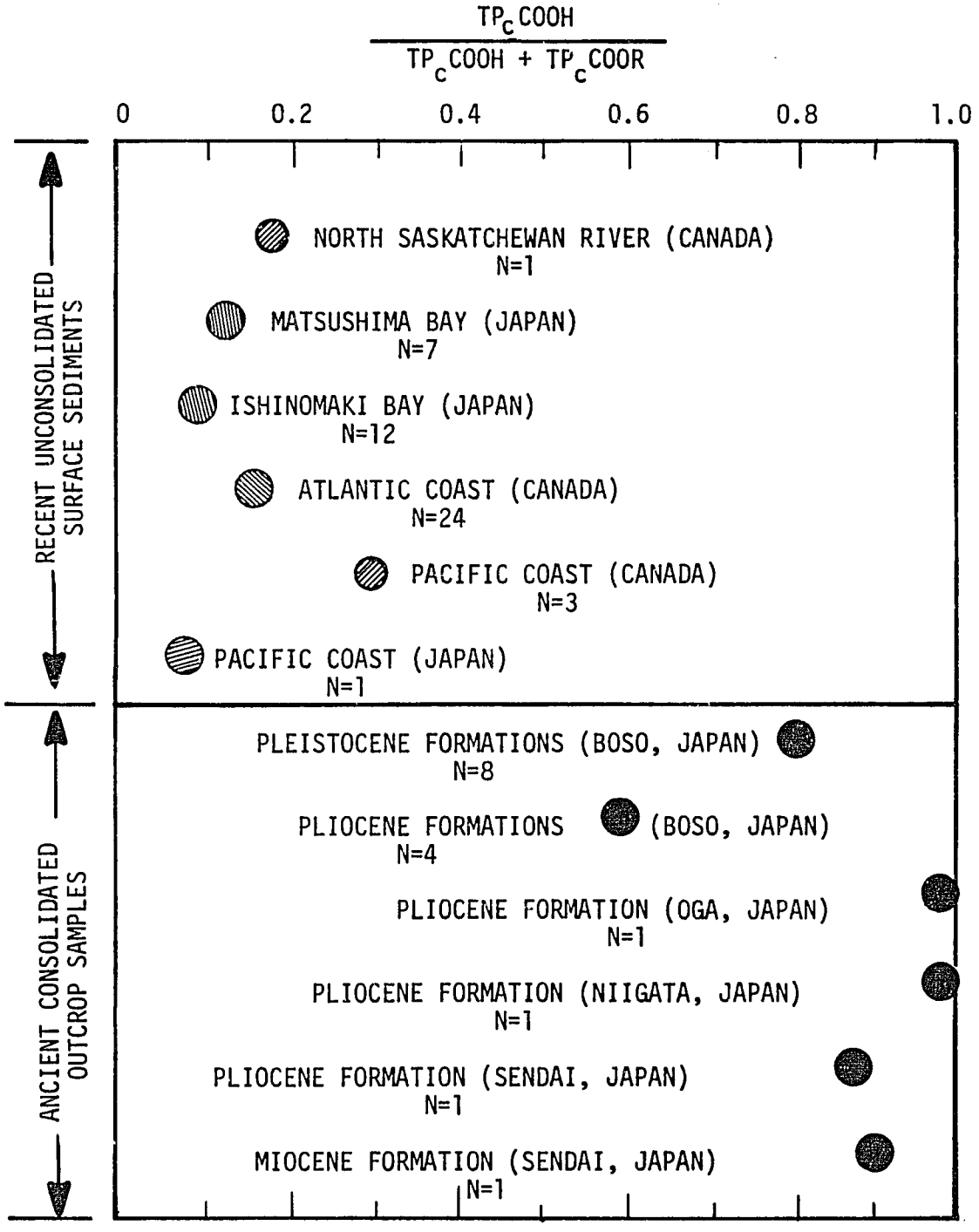

TP_cCOOH=TETRAPYRROLES WITHOUT ESTER LINKAGES

TP_cCOOR=TETRAPYRROLES WITH ESTER LINKAGES

N=NUMBER OF SAMPLES

FIGURE 4.9

reduced to methylene (Baker and Smith, 1974). Some of the hydrogen needed for these reduction reactions may be derived from aromitization of the tetrapyrrole, which up to now has been pseudoaromatic. The result of these reactions is a porphyrin that is insular with respect to the accompanying organic matter (Figure 4.10). It is also possible that the porphyrin or its precursors may be assimilated into kerogen as it forms in the buried sediment (Blumer and Snyder, 1967; Oehler et al., 1974). Three likely sites where linkage between kerogen and porphyrin may occur are the 2-vinyl, 9-keto, and carboxyl groups (Figure 4.11). The chemical and structural character of the organic matter surrounding tetrapyrroles are probably critical factors in determining what types of linkages may occur in assimilation, as well as whether or not assimilation may occur. The chemical and structural complexity of kerogen suggests that a variety of situations may exist between tetrapyrroles and organic matter in a sediment. And as a result, insular and assimilated porphyrins probably coexist in the same organic accumulations. The prevalence of one of these porphyrin types over the other cannot be determined from available data and additional research in this area is needed.

Metallation of tetrapyrroles appears to occur throughout Stage II regardless of the peripheral modifications that may be occurring to the tetrapyrroles (e.g. deestrification, allomerization, reduction, aromitization, and assimilation). The reaction is confined to the two centrally located imine hydrogen atoms of the tetrapyrrole (Figure 4.12a), and as a result the reaction may involve pheophytins as well as

Figure 4.10: Three reactions involving the reduction of the 2-vinyl double bond to an ethyl side chain, reduction of the 9-keto group to methylene, and the aromitization of the pheophorbide structure to a porphyrin.

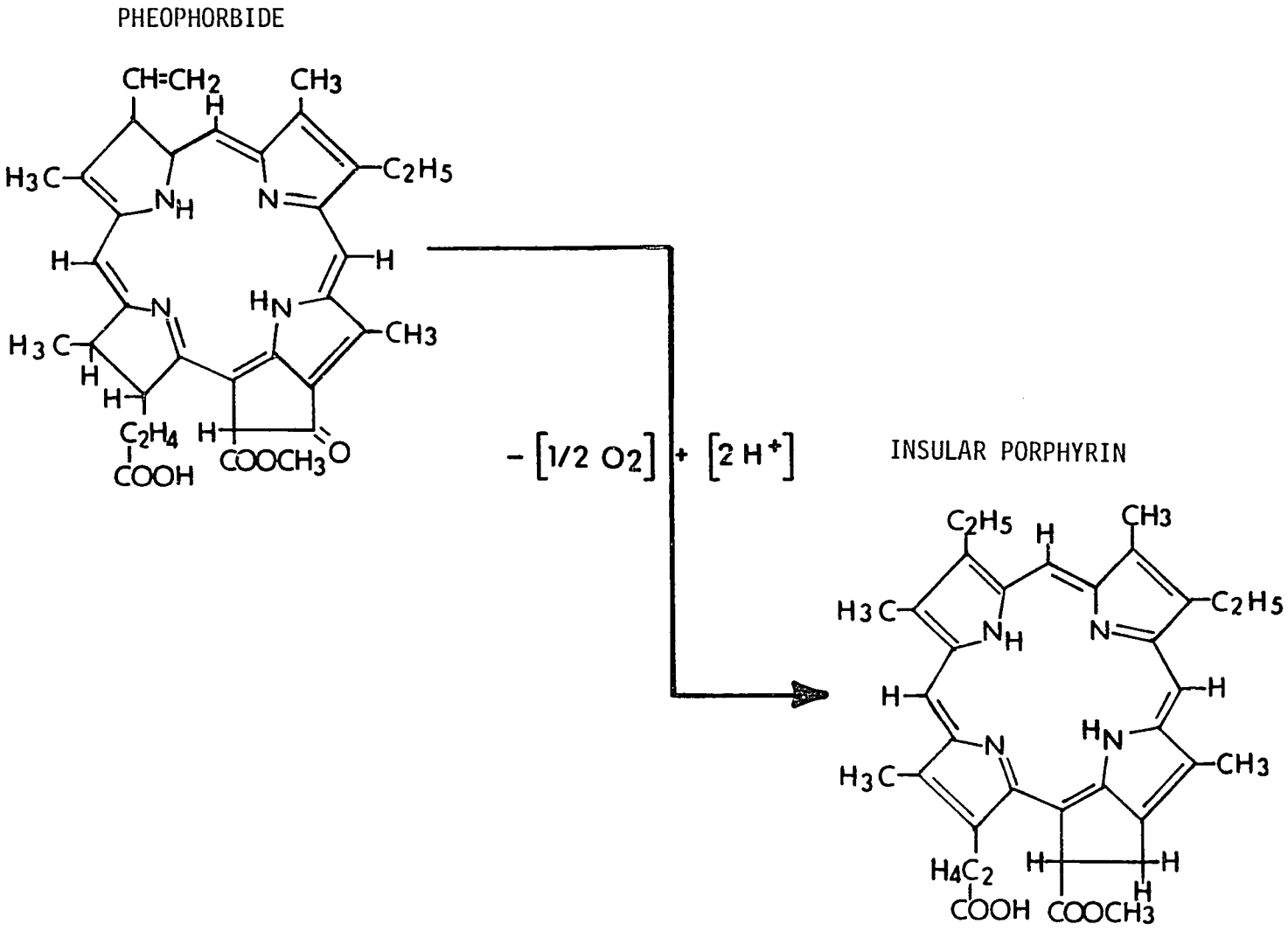

FIGURE 4.10

Figure 4.11: Assimilation of pheophorbide into the kerogen structure. Kerogen linkages designated as K_1, K_2, and K_3.

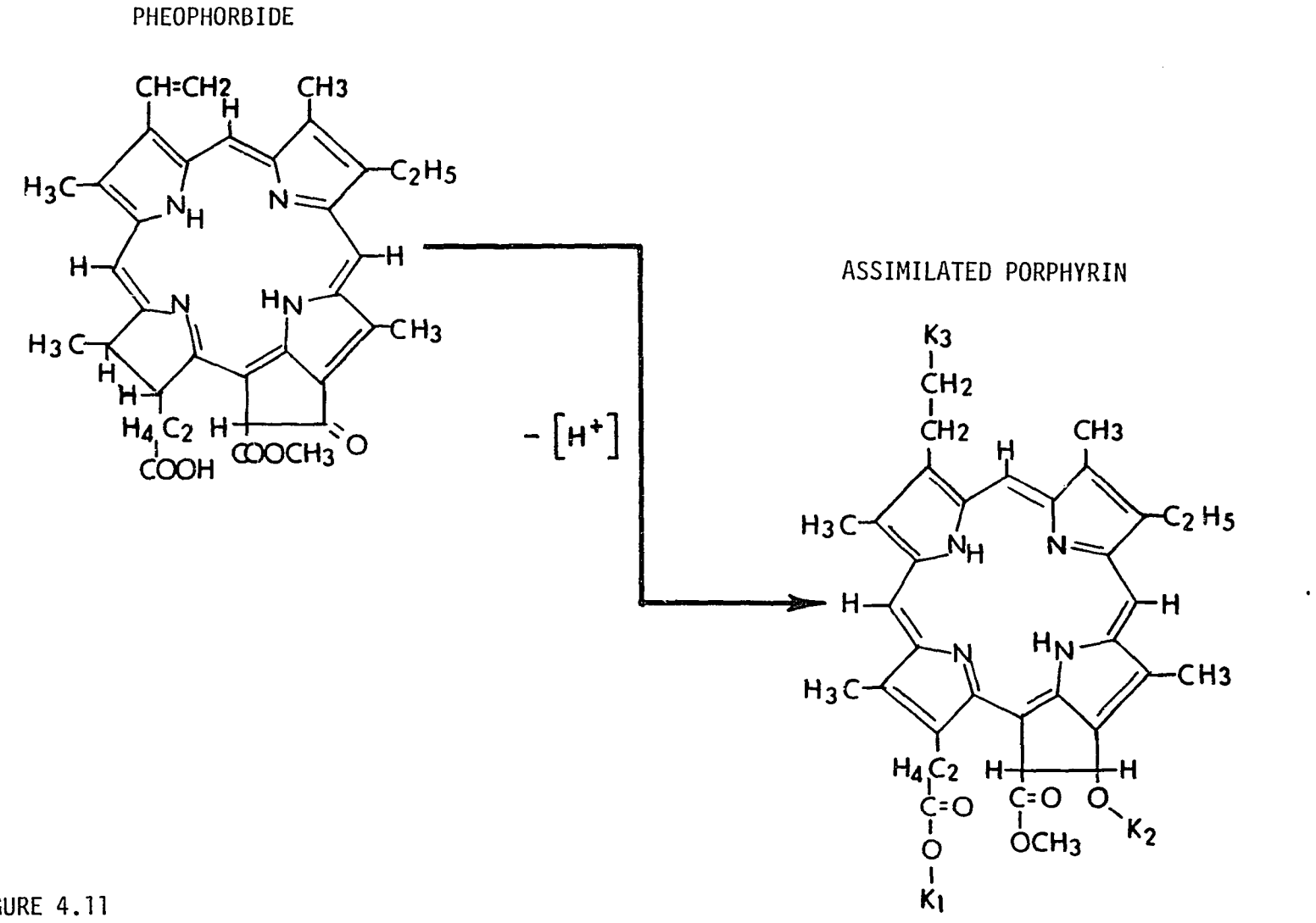

FIGURE 4.11

Figure 4.12: a) Plan view of metallation site in tetrapyrroles for a bivalent metal (M^{+2}); b) perspective view of nickelous (Ni^{+2}) metallation site; and c) perspective view of vanadyl (VO^{+2}) metallation site.

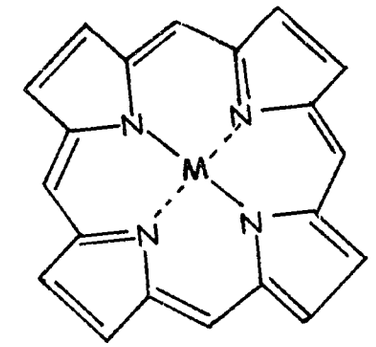

a

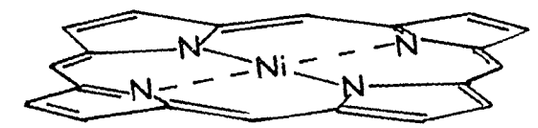

b

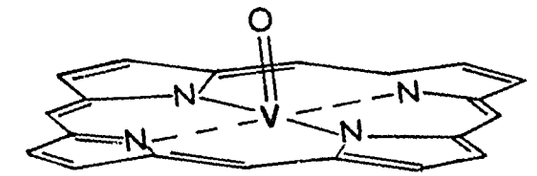

c

FIGURE 4.12

porphyrins, or any of the intermediates (Orr et al., 1958; Hodgson et al., 1967, p. 239; Shiobara and Taguchi, 1975). The bonding is largely covalent in character (Lemberg and Legge, 1949; Barnes and Dorough, 1950), and involves opposite nitrogen atoms sharing one of their electrons with a bivalent metal cation. Bonding of this type with some of the metals from the first transition series of elements (e.g. V, Mn, Fe, Co, Ni, Cu, and Zn) results in tenacious bonds that require concentrated sulfuric acid for cleavage (Caughey and Corwin, 1955; Dean and Girdler, 1960). These tenacious bonds also prevent exchange reactions from occurring between bonded metals and metal cations in the surrounding media (Barnes and Dorough, 1950). In addition, these bonds have a relatively high thermal stability and usually remain stable at temperatures in excess of 300°C (Erdman et al., 1956a; Hodgson and Baker, 1957; Morandi and Jensen, 1964). Thus, once a tetrapyrrole has been metalled with one of the transition metals mentioned, it is unlikely that the bond will be cleaved under most diagenetic conditions.

Although the stability of tetrapyrroles is enhanced by metallation (Hodgson and Baker, 1957; Corwin, 1959), the scarcity of metallated tetrapyrroles in the surface sediments of recent marine environments (Baker and Hodgson, 1968; Shiobara and Taguchi, 1975) suggests that time and burial conditions may be critical to the reaction. Laboratory studies on metallation of pheophytin indicate that the reaction rate increases with increasing temperature and decreasing pH (Corwin, 1959; Hodgson et al., 1960; Baker and Hodgson, 1961). The combined influence of these two variables and their changes with burial depth probably control the

timing of metallation in the sediment column, but the thousands of years available for the reaction insures its completion under most sedimentary conditions (Hodgson et al., 1960). Extrapolation of experimental data by Hodgson and others (1960) indicates that at temperatures as low as 10°C only a few decades are necessary for complete metallation.

The more than sufficient time alloted for metallation during Stage II suggests that the amount of metallated tetrapyrroles in a lithified sediment may be a function of the amount of suitable metal cations available for metallation during its burial as a sediment. Thus, the varying degree of metallation observed in some lithified sedimentary sections (e.g. Figure 4.13) may be the result of varying amounts of available metal cations suitable for metallation during Stage II of their burial history. The basic premise is that sedimentary conditions favoring high metal cation concentrations relative to the amount of preserved tetrapyrroles will result in complete metallation, while sedimentary conditions favoring low metal cation concentrations relative to the amount of preserved tetrapyrroles will result in partial metallation. Specifics on the influence of sedimentary conditions is discussed later in the text (Chapter 5.2.3).

Small bivalent cations form the most stable bonds with tetrapyrroles (Dunning et al., 1953; Caughey and Corwin, 1955; Erdman et al., 1957). Although the cations of the first transition-series of elements meet these requirements, naturally occurring tetrapyrroles are almost exclusively bound to nickel or vanadium cations (Hodgson et al., 1968; Filby,

Figure 4.13: Variations in the amount of metallated tetrapyrroles through a lithified sedimentary section on the Boso Peninsula, Japan (Shiobara and Taguchi, 1975).

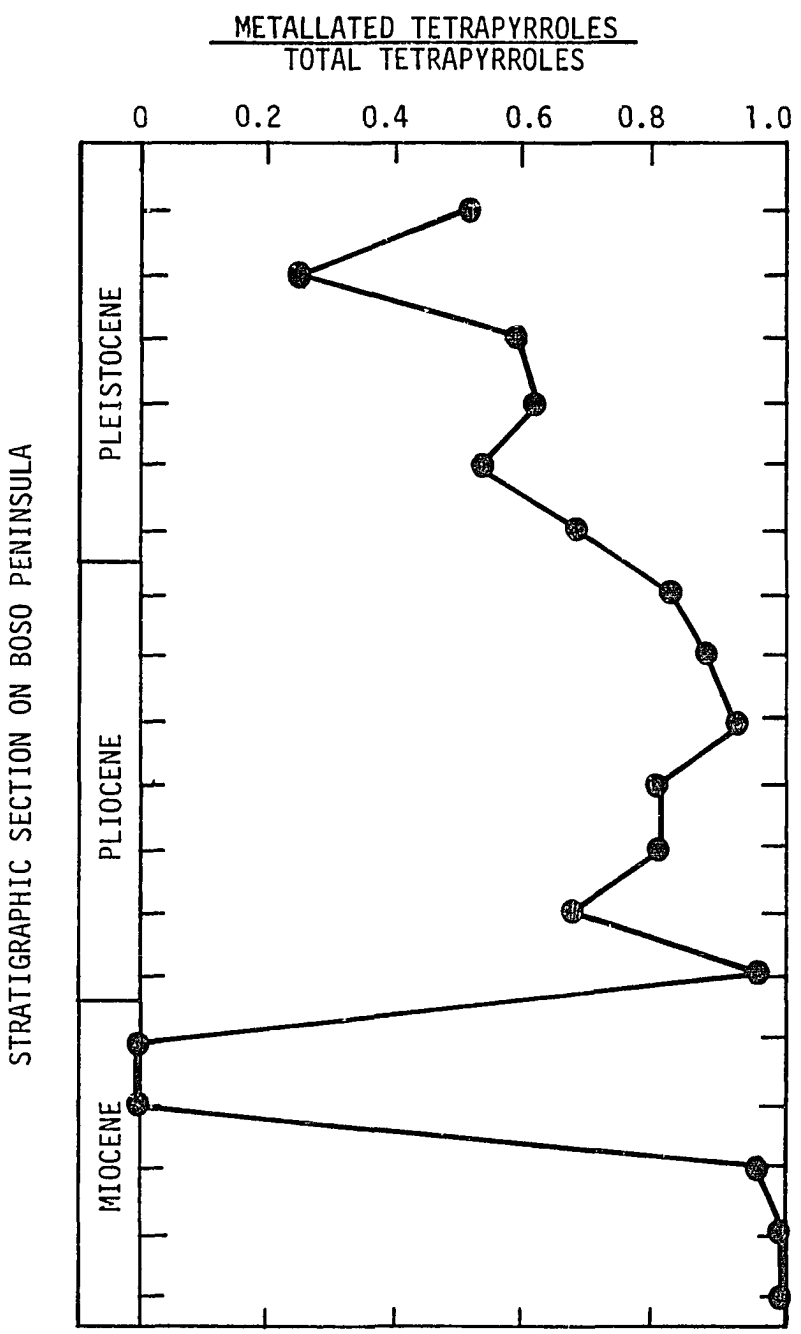

FIGURE 4.13

1975). Nickel is bound as a bivalent nickelous cation (Ni^{+2}) within the tetrapyrrole (Figure 4.12b; Fleischer, 1963). Quadrivalent vanadium is bound to the two opposite nitrogen atoms of the tetrapyrrole as a bivalent vanadyl cation (VO^{+2}) with its covalently bound oxygen extending outside of the structure (Figure 4.12c; Erdman et al., 1956b). The preference for these two metal cations appears to be the result of three factors; 1) their availability in nature as a bivalent cation, 2) their small ionic radii, and 3) their favorable electron configuration.

All of the elements of the first transition-series form bivalent cations, but only certain ones exist under the conditions favorable for preservation of tetrapyrroles. As stated earlier, anaerobic conditions are the most favorable for preservation of organic matter and its accompanying tetrapyrroles. These conditions are characteristic of reducing environments with Eh values usually being less than zero (Krumbein and Garrels, 1952). An Eh-pH stability field for the preservation of tetrapyrroles in nature may be approximated by superimposing the upper Eh limit of zero on the Eh-pH field for marginal marine and marine sediments as observed by Bass Becking and others (1960). This approximated stability field is shown in Figure 4.14, as the outlined stippled areas in the series of Eh-pH diagrams, constructed for sea water concentrations of the bivalent cations of the first-transition series of elements. This series of Eh-pH diagrams indicates that bivalent cations of copper, chromium, and titanium are not likely to be available within the approximated stability field for tetrapyrrole preservation. Conversely, nickel, vanadium, cobalt, scandium, manganese, zinc, and iron do have

Figure 4.14: Eh-pH diagrams showing approximated stability field for tetrapyrrole preservation (stippled area) and stability field for bivalent cations of the first transition-series of elements (hatched area). Average sea water concentrations were used for the total dissolved metal concentrations (Goldberg, 1961).

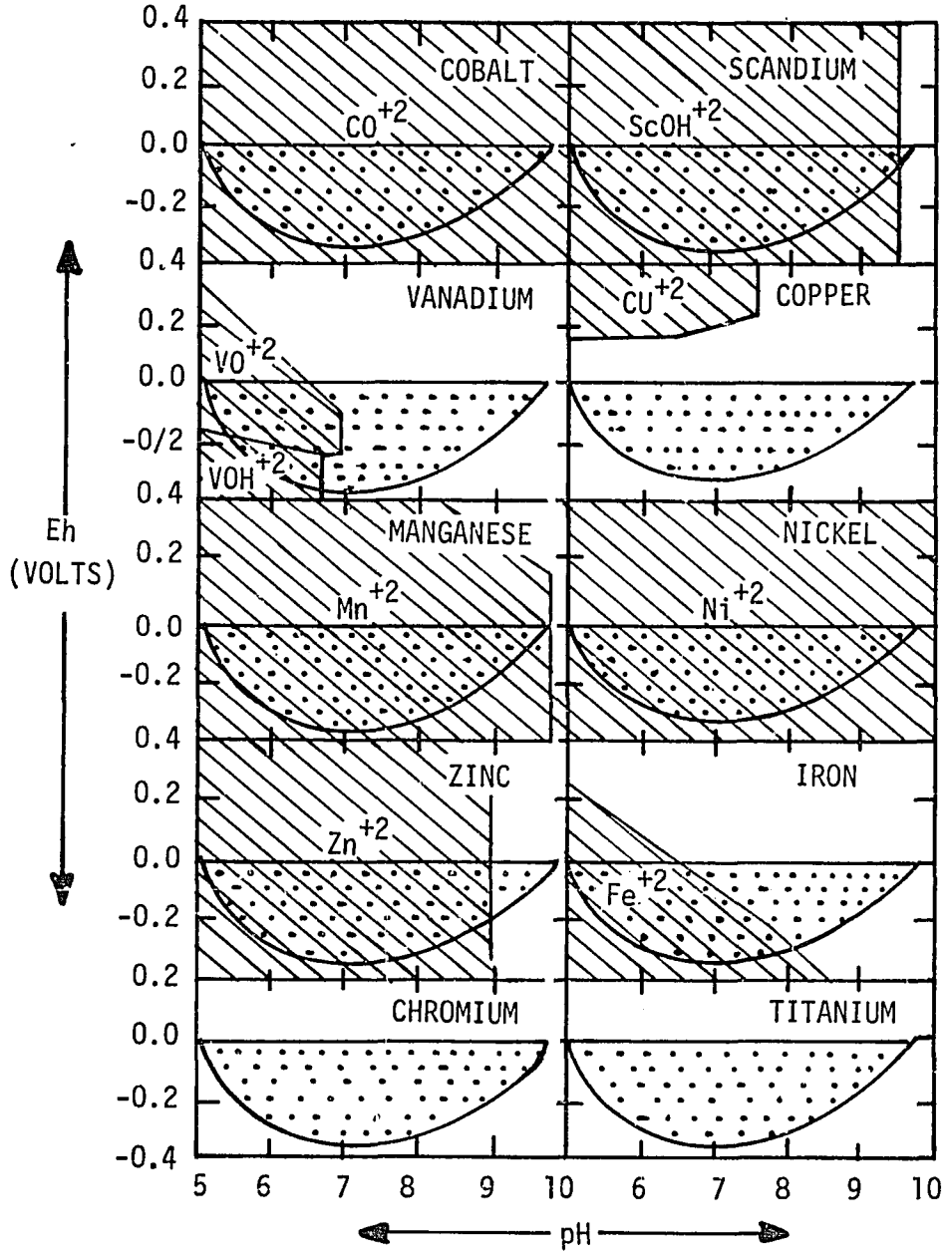

FIGURE 4.14

bivalent cations that are available within the approximated stability field for tetrapyrrole preservation.

The distance between opposite nitrogen atoms in a tetrapyrrole is limited (Table 4.1), and because of this the size of a bonding bivalent cation is also critical to metallation. In general, the smaller the size of a bivalent cation, the greater its stability will be within a tetrapyrrole (Dunning et al., 1953; Caughey and Corwin, 1955; Erdman et al., 1957). The relatively small ionic radii of the metals in the vanadyl and nickel cations (Table 4.2) indicate that these two cations have a distinct physical advantage over the other available bivalent cations.

In addition to this physical advantage, vanadyl and nickel cations are also more advantageous from an energy standpoint. Although the Gibbs free energies for metallation of the different bivalent cations would be more informative than their ligand field stabilization energies (Glasby, 1975; McKenzie, 1975), the lack of thermodynamic data on the metallation of tetrapyrroles (Sugihara, 1975) encourages the use of the ligand field theory. A detail discussion of this theory will not be attempted in this text, but a good review of the concept is given by Cotton (1964). In general, the ligand field theory is concerned with the distribution of electrons in orbitals at different energy levels within a bound cation. The resultant energy is referred to as the ligand field stabilization energy, and it increases with the stability of a bound cation.

Table 4.1: Distance between opposite nitrogen atoms in tetrapyrroles.

	Phthalocyanine (Robertson, 1936)	Ni-phthalocyanine (Robertson and Woodward, 1937)	Ni-etioporphyrin I (Fleischer, 1963)	Ni-etioporphyrin II (Crute, 1959)
Distance (Å)	3.82	3.66*	3.91*	3.68*

*Distance between nickel and nitrogen multiplied by two.

Table 4.2: Ionic radii of metals (6 fold coordination) in bivalent cations of the first transition series.

Cation	Radius (Å)*
V^{+2}	0.88
$ScOH^{+2}$	0.81
Mn^{+2}	0.80
Fe^{+2}	0.74
Zn^{+2}	0.74
VOH^{+2}	0.74
Co^{+2}	0.72
Ni^{+2}	0.69
VO^{+2}	0.63

*Data from Ahrens (1952, Table 16)

In order to employ the ligand field theory, the bonding orbitals, spin state, and coordination of a cation must be determined. The bonding of bivalent cations of the first transition series of elements is restricted to their outermost d orbitals (Burns, 1970). The weak ligand field produced by a tetrapyrrole suggests that all of the d orbitals of a cation will be filled before electron pairing commences (Hodgson et al., 1967) and this constitutes a high spin state. As shown in Figure 4.15, the coordination of a bivalent cation in a tetrapyrrole structure may be considered eitehr octahedral or square planar. The octahedral coordination suggests that unpaired electrons in the solvent, which bears the tetrapyrrole, act as ligands (Figure 4.15 a and b), whereas square planar coordination suggests that the solvent is inert (Fiugre 4.15c). Both types of coordination have been considered in this study, and the relation between the energy levels of their orbitals is shown in Figure 4.16. Ligand field stabilization energies for the bivalent cations of the first transition series of elements were calculated from this information and the results are shown in Table 4.3. Vanadyl, vanadium hydroxide, and nickel cations have the highest stabilization energies for both types of coordination, which indicates that they form the most stable bonds with tetrapyrroles.

4.1.3 Stage III: From Sediment Lithification to Metamorphism

Stage III represents the diagenetic setting in which organic matter, in lithified sediment, undergoes thermal maturation (Figure 2.3). During thermal maturation, a number of major modifications to the tetrapyrroles

Figure 4.15: The coordination of a bivalent cation in a tetrapyrrole may be considered octahedral (a and b) or square planar (c).

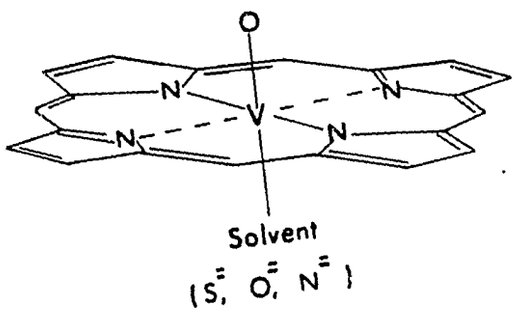

a

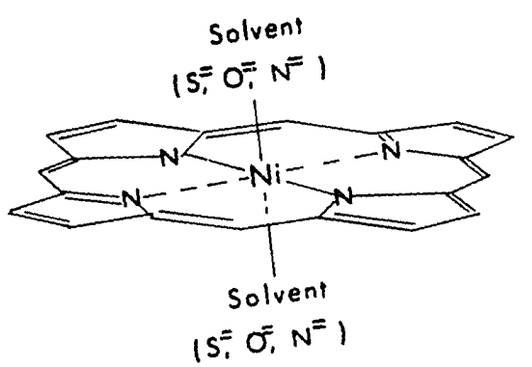

b

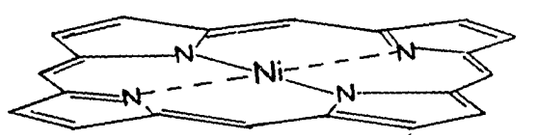

c

FIGURE 4.15

Figure 4.16: Energy level diagrams showing the ligand field splitting patterns for d orbitals of cations in octahedral and square planar coordination. Values are from Krishnamurthy and Schaap (1969).

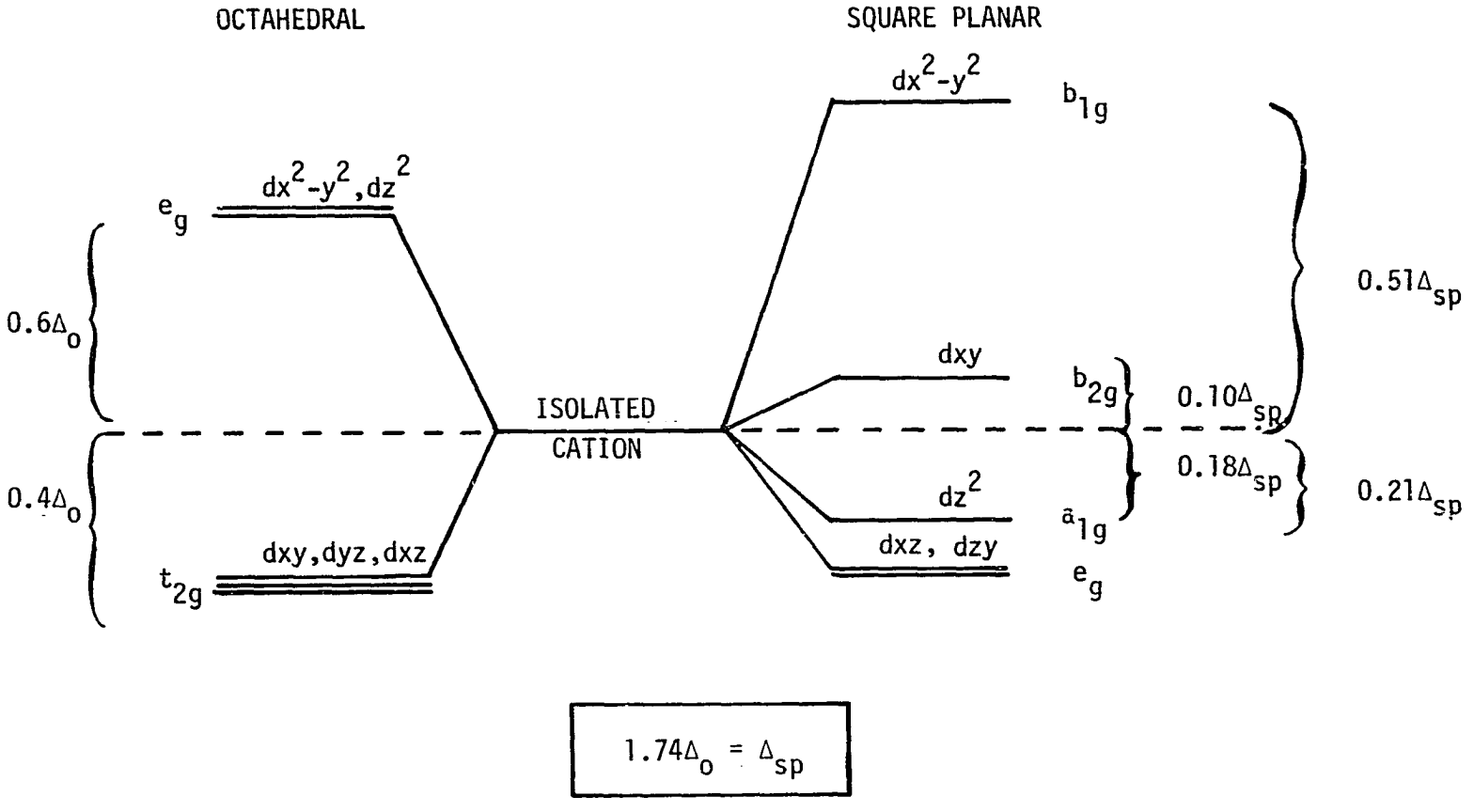

FIGURE 4.16

Table 4.3: Electron distribution and ligand field stabilization energies for high spin state, bivalent cations of the first transition series of elements in octahedral and square planar coordination.

Number of 3d Electrons	Bivalent Cation	Octahedral t_{2g}	Octahedral e_g	LFSE (Δ_o)	Square Planar e_g	Square Planar a_{1g}	Square Planar b_{2g}	Square Planar b_{1g}	LFSE (Δ_o)
0	Ca^{+2}	— — —	— —	0	— —	—	—	—	0
1	$ScOH^{+2}$	↑ — —	— —	$0.40\Delta_o$	↑ —	—	—	—	$0.37\Delta_o$
2	Ti^{+2}, TiO^{+2}	↑ ↑ —	— —	$0.80\Delta_o$	↑ ↑	—	—	—	$0.75\Delta_o$
3	VO^{+2}, $V(OH)^{+2}$	↑ ↑ ↑	— —	$1.20\Delta_o$	↑ ↑	↑	—	—	$1.06\Delta_o$
4	Cr^{+2}	↑ ↑ ↑	↑ —	$0.60\Delta_o$	↑ ↑	↑	↑	—	$0.89\Delta_o$
5	Mn^{+2}	↑ ↑ ↑	↑ ↑	0	↑ ↑	↑	↑	↑	0
6	Fe^{+2}	↓↑ ↑ ↑	↑ ↑	$0.40\Delta_o$	↓↑ ↑	↑	↑	↑	$0.37\Delta_o$
7	Co^{+2}	↓↑ ↓↑ ↑	↑ ↑	$0.80\Delta_o$	↓↑ ↓↑	↑	↑	↑	$0.75\Delta_o$
8	Ni^{+2}	↓↑ ↓↑ ↓↑	↑ ↑	$1.20\Delta_o$	↓↑ ↓↑	↓↑	↑	↑	$1.06\Delta_o$
9	Cu^{+2}	↓↑ ↓↑ ↓↑	↑ ↑	$0.60\Delta_o$	↓↑ ↓↑	↓↑	↓↑	↑	$0.89\Delta_o$
10	Zn^{+2}	↓↑ ↓↑ ↓↑	↓↑ ↓↑	0	↓↑ ↓↑	↓↑	↓↑	↓↑	0

occur, and they include dealkylation, decarboxylation, ring scission, thermal cracking, aromitization, and condensation. Although the order of these reactions has not been conclusively established, a logical progression is postulated in the following discussion.

Dealkylation involves the elimination of the alkyl portion of ester side chains that occur on the tetrapyrroles (Figure 4.17a). The carboxyl portion of the esters remains on the tetrapyrrole and the fate of the cleaved alkyl group depends on the physiochemical conditions of the environment (Didyk et al., 1978, Figure 3). Included in this reaction are those tetrapyrroles in Stage II that avoided dealkenylation by early reduction of their double carbon bond in the phytol side chain (Figure 4.8). The low percentage of aliphatic chains on the carboxyls of tetrapyrroles extracted from outcrop samples of relatively young lithified sediments (Figure 4.9) suggests that dealkylation occurs at low levels of thermal maturation.

Decarboxylation probably follows dealkylation and involves the elimination of carboxyl groups from the tetrapyrroles (Figure 4.17b) and accompanying organic matter. Carbon dioxide is produced by decarboxylation, and this type of reaction appears to be typical at low levels of thermal maturation which are characterized by the generation of carbon dioxide and water (Tissot et al., 1974).

Ring scission involves the opening of the isocyclic pentane ring on a tetrapyrrole (Figure 4.18), and it probably occurs during oil generation

Figure 4.17: Modifications to tetrapyrroles during low levels of thermal maturation; a) dealkylation and b) decarboxylation.

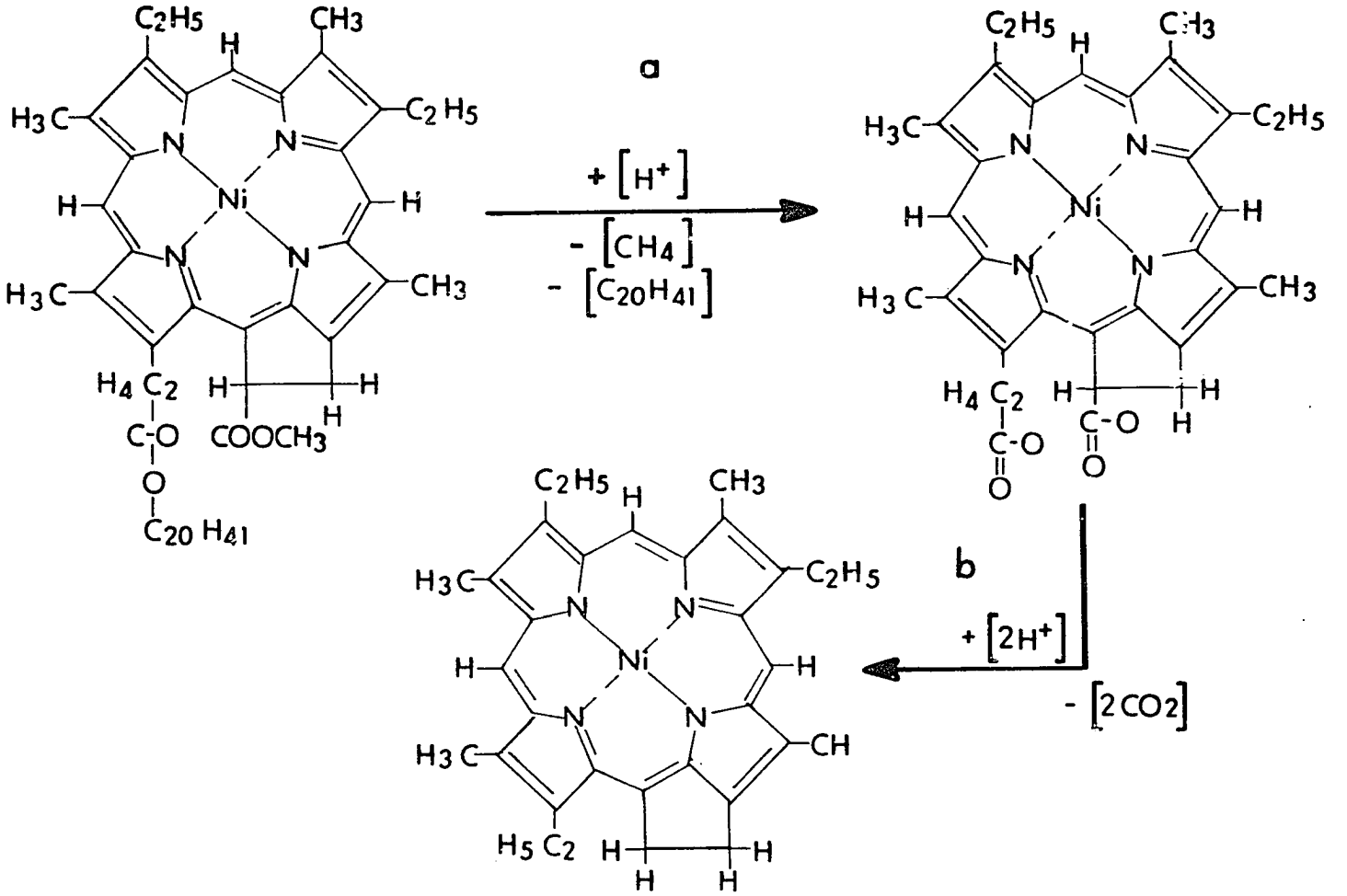

FIGURE 4.17

Figure 4.18: Ring scission of the isocyclic pentane ring at moderate levels of thermal maturation.

NICKEL-DEOXOPHYLLOERYTHRO-
ETIOPORPHYRIN (Ni-DEPE)

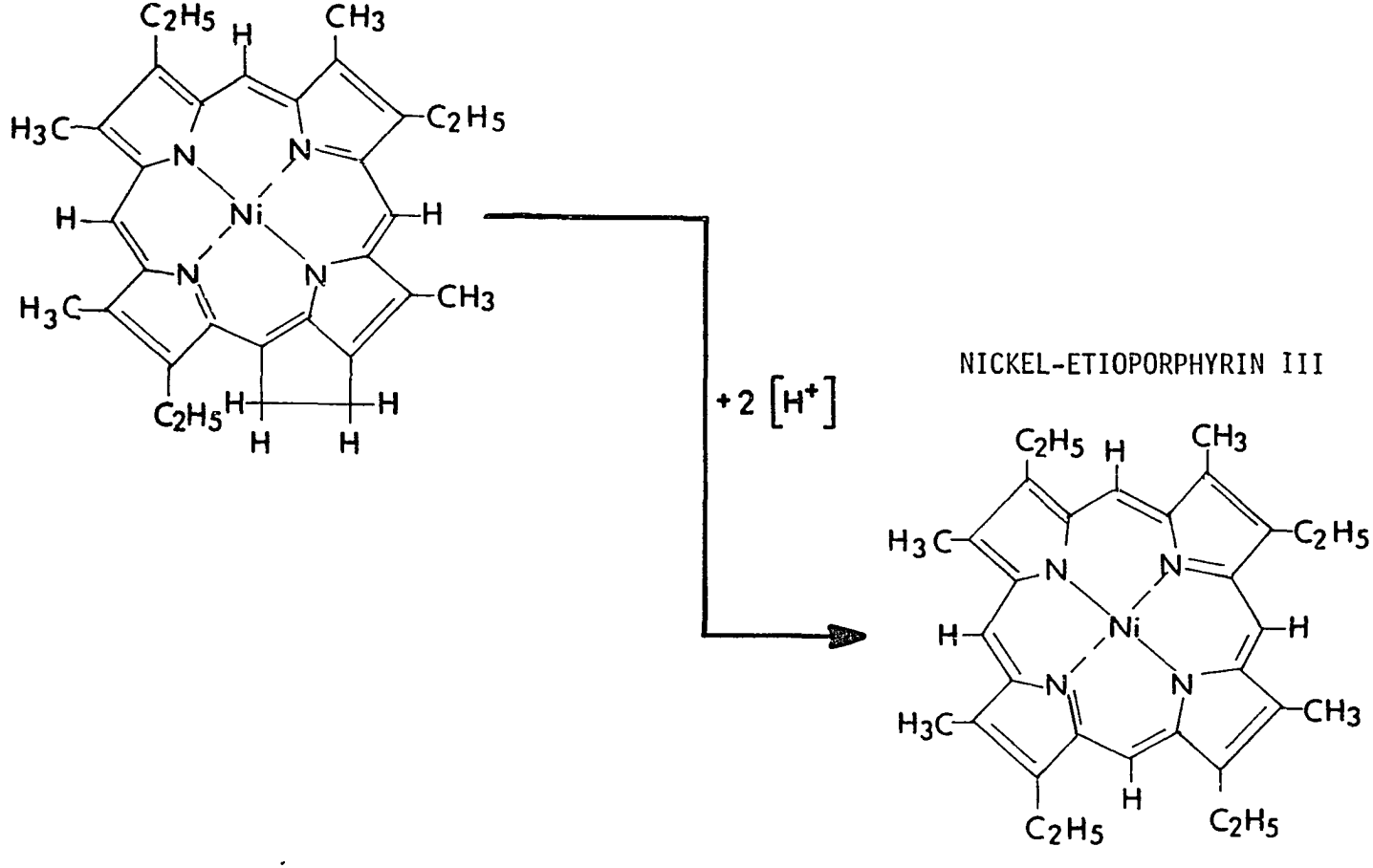

FIGURE 4.18

at moderate levels of thermal maturation. Data from natural oil occurrences (Yen and Silverman, 1969) and laboratory experiments (Didyk et al., 1975) indicate that ring scission increases with thermal maturation, and has been proposed as a good index for determining the thermal maturity of crude oils.

During oil generation at moderate levels of thermal maturation, it appears possible for assimilated tetrapyrroles to develop into insular prophyrins or highly aromatic tetrapyrroles that may be insular or assimilated (Figure 4.19). The type of reaction in which an assimilated tetrapyrrole will participate is probably determined by factors related to its chemical environment and linkage types within a kerogen. The complexity of kerogen suggests that assimilated tetrapyrroles may experience a variety of chemical environments and linkage types in any one kerogen. As a result, it appears possible that thermal cracking and aromitization may occur simultaneously. Thermal cracking of assimilated tetrapyrroles results in insular porphyrins, and variations in their linkage types may give rise to the homologous series observed in crude oils and bitumens (Dean and Whitehead, 1963; Thomas and Blumer, 1964; Morandi and Jensen, 1964; Baker, 1966; Baker et al., 1967; Didyk et al., 1975). This suggests that the frequency distributions of homologous series in crude oils and bituments may reflect in part the abundance of linkage types in a kerogen. Aromitization results in highly aromatic tetrapyrroles, which have been identified in the high molecular weight portion of crude oils and bitumens (Vaughan et al., 1970; Blumer and Rudrum, 1970; Yen, 1975). As high levels of thermal maturation are

Figure 4.19: Examples of tetrapyrroles that may occur at moderate to high levels of thermal maturation; a) insular porphyrin, b) highly aromatic insular tetrapyrrole, and c) highly aromatic tetrapyrrole condensed within a kerogen (K).

a

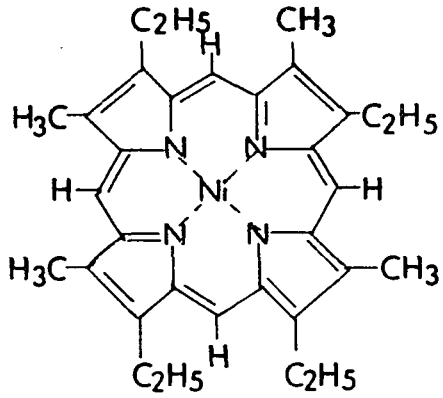

b

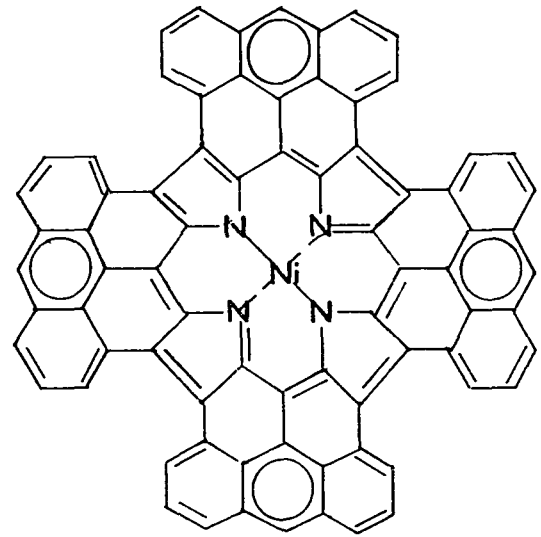

c

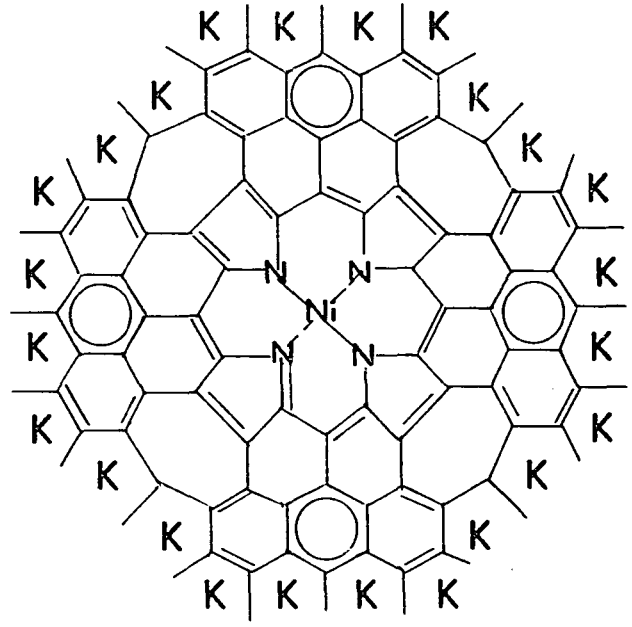

FIGURE 4.19

approached, the highly aromatic tetrapyrroles that remain assimilated may be condensed into large aromatic complexes that begin to dominate the structure of the maturing kerogen. These will eventually take on graphite-like properties and such tetrapyrroles have been detected in rocks exposed to high levels of thermal maturation (Yen, 1975).

4.1.4 SUMMARY

The preceding discussion on the conversion of tetrapyrrole pigments to insular and assimilated tetrapyrroles in crude oils, bitumens, and kerogens, presents the major reactions involved. The sequence and overlapping relationships of these reactions are shown conceptually in Figure 4.20. Although the mechanisms and timing for some of these reactions still require further research, three important points in this reaction sequence should be emphasized:

1) The amount of tetrapyrroles available for bonding with bivalent vanadium and nickel cations is determined by the exposure time to and the oxygen level of aerobic environments encountered by accumulating organic matter during Stage I.

2) Bivalent vanadium and nickel cations are preferred in tetrapyrroles, and their metallation occurs during early periods of diagenesis (i.e. Stage II).

Figure 4.20: Proposed reaction sequence for conversion of tetrapyrrole pigments to insular and assimilated tetrapyrroles in crude oils, bitumens, and kerogens.

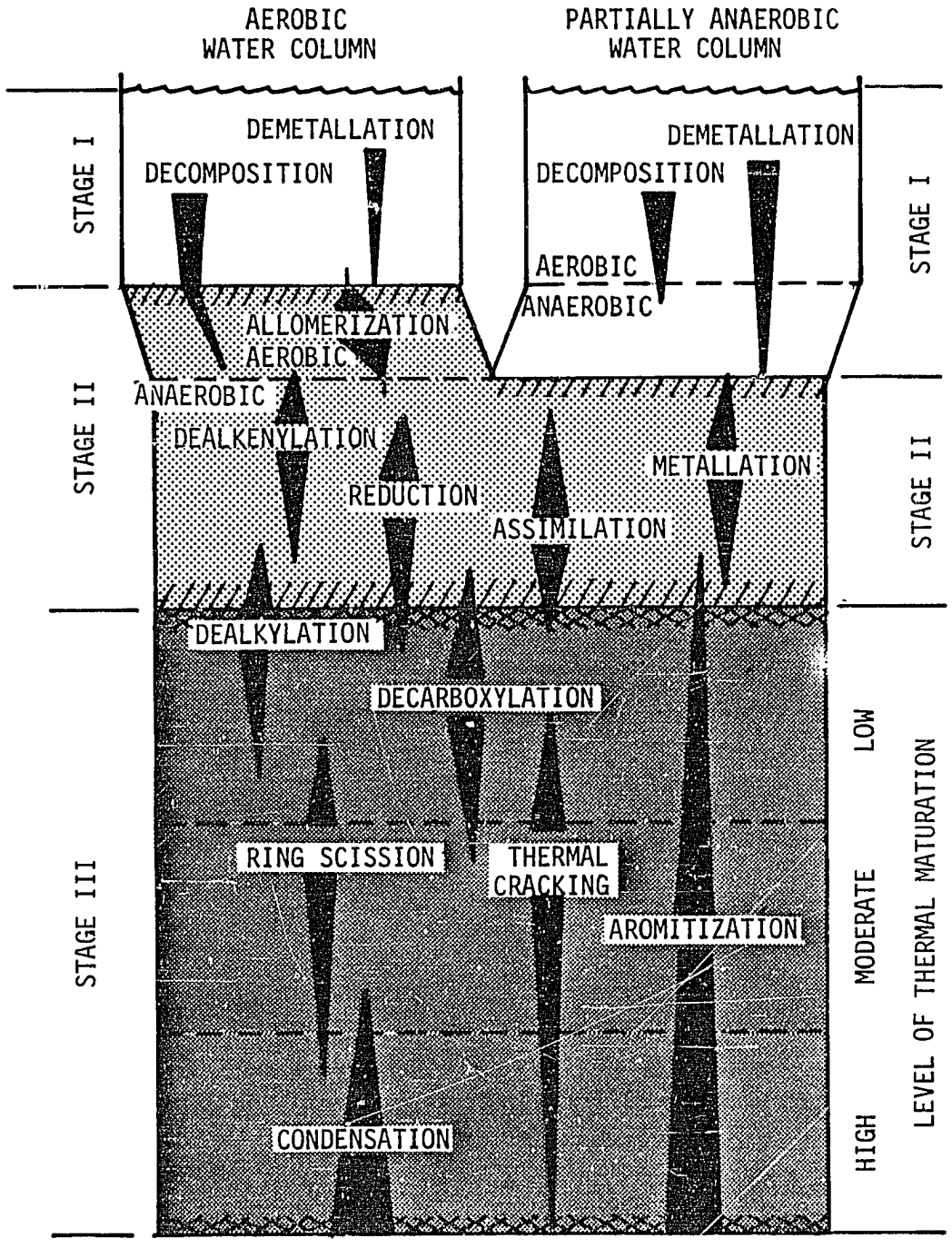

FIGURE 4.20

3) Tetrapyrrole bonds with bivalent vanadium and nickel cations are tenacious and their cleavage is not likely under most diagenetic conditions.

4.2 MIXED LIGAND TETRADENTATES

The framework of mixed ligand tetradentates may be variable as shown in Figure 4.21. The ligands available for bonding with metals may involve numerous combinations of sulfur, nitrogen, and oxygen (Yen, 1975). Similar to tetrapyrroles, these compounds require bivalent cations for metallation, but unlike tetrapyrroles, the metal coordination is not square planar or octahedral (Martin and Ramaiah, 1965; Boucher and Yen, 1968 and 1969; Boucher et al., 1968). Distortion of the ligands around the bound metals results in less stable coordinations such as tetrahedral or square-pyramidal (Table 4.4). As a result, demetallation of mixed ligand tetradentates occurs readily in dilue acid (Yen, 1975), and they are therefore susceptible to demetallation during diagenesis. Studies concerning mixed ligand tetradentates in nature are scarce, and currently their occurrence in nature appears to be limited to a minor constituent in some crude oils.

4.3 HUMATE COMPLEXES

In this study, metallo-organic complexes with oxygen atoms acting as ligands in the bonding of metal cations are referred to as humate complexes. Naturally occurring humate complexes are common in humic

Figure 4.21: Several examples of mixed ligand tetradentate complexes (M = metal cation).

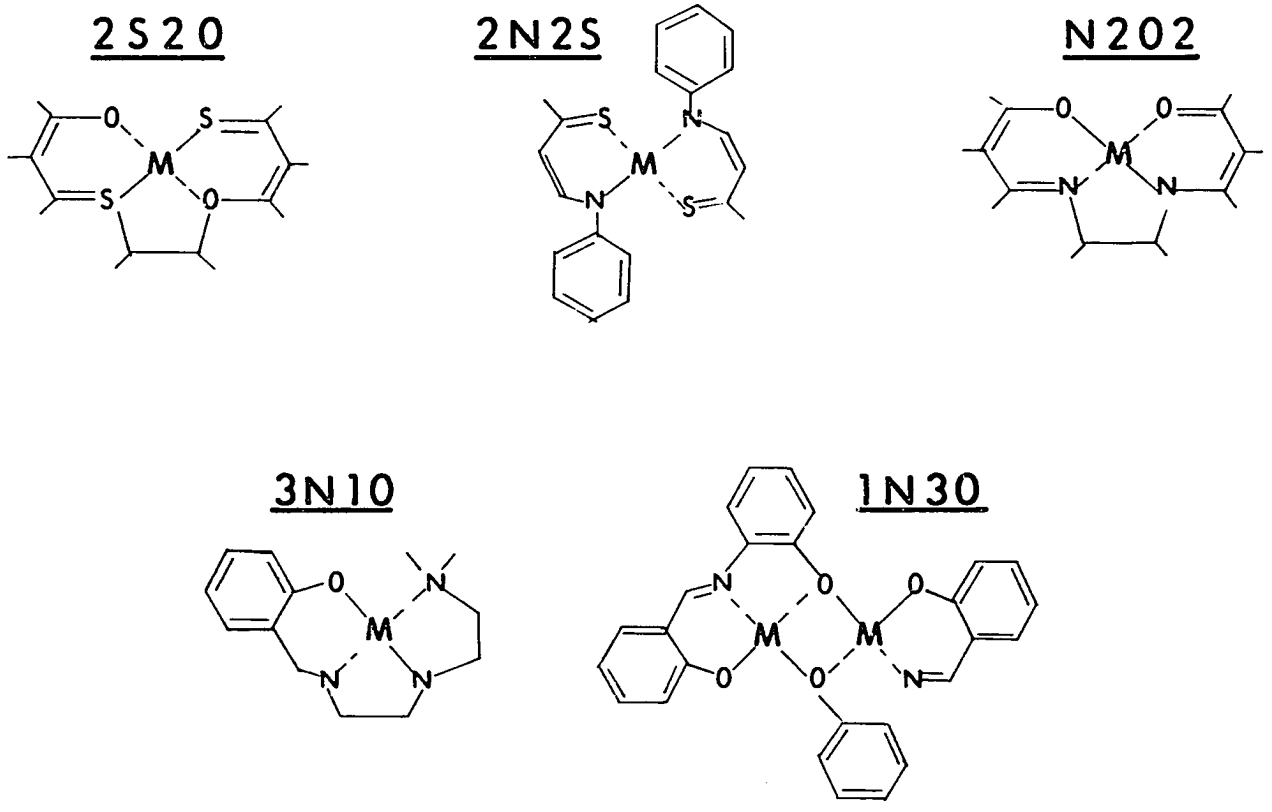

FIGURE 4.21

Table 4.4: Ligand field stabilization energies for high spin, bivalent cations of the first transition series of elements.

Number of 3rd Electrons	Bivalent Cations	Ligand Field Stabilization Energies*				
		Octahedral	Square Planar	Square Pyramidal	Cubic	Tetrahedral
0	Ca^{+2}	0	0	0	0	0
1	$ScOH^{+2}$	0.40	0.37	0.40	0.53	0.26
2	Ti^{+2}	0.80	0.75	0.79	1.07	0.53
3	VO^{+2}	1.20	1.06	0.88	0.71	0.35
4	Cr^{+2}	0.60	0.89	0.79	0.36	0.17
5	Mn^{+2}	0	0	0	0	0
6	Fe^{+2}	0.40	0.37	0.40	0.53	0.26
7	Co^{+2}	0.80	0.75	0.79	1.07	0.53
8	Ni^{+2}	1.20	1.06	0.88	0.71	0.35
9	Cu^{+2}	0.60	0.89	0.79	0.36	0.17
10	Zn^{+2}	0	0	0	0	0

*All values expressed as decimal fractions of the ligand field stabilization for octahedral coordination (Δ_o).

substances and usually involve the oxygen in carboxyl or phenolic hydroxide functional groups (Van Dijk, 1971; Schnitzer and Khan, 1972; Gamble and Schnitzer, 1973; MacCarthy and Mark, 1976). As shown in Figure 4.22, several combinations of these two functional groups may be envisaged for bonding of metal cations. Although indirect evidence does suggest phenolic hydroxide functional groups are involved to some degree in bonding of metal cations (MacCarthy and Mark, 1976), it is generally accepted that carboxyl functional groups are the prominant participants in humate complexes (Vinkler et al., 1976).

The bonding of a metal cation in a humate complex may be ionic, covalent, or a combination of the two (Schnitzer and Hoffman, 1967). Infrared spectroscopic investigations of humic substances by Vinkler and others (1976) indicated that cations with small ionic radii (e.g. Al^{+3}, Cr^{+3}, VO^{+2}, and Co^{+2}) form covalent humate complexes, cations with large ionic radii (e.g. Mg^{+2}, Mn^{+2}, Na^{+} and Ca^{+2}) form ionic humate complexes and cations with intermediate ionic radii (e.g. Cu^{+2}, Zn^{+2}, and Fe^{+2}) form ionic-covalent transitional humate complexes.

Metal cations are tightly bound in humate complexes under most neutral and basic conditions, but acid conditions increase the effectiveness of hydrogen as a competitor for bonding sites (Schnitzer and Khan, 1972). Although significant quantities of VO^{+2} and Ni^{+2} may form humate complexes at low pH values (Szalay and Szilagyi, 1967; Szabo, 1958; McBride, 1978), their stabilities are considerably lower than trivalent cations, such as Fe^{+3} and Al^{+3} (Van Dijk, 1971; Schnitzer and Khan,

Figure 4.22: Examples of types and reactions of humate complexes (M = metal cation).

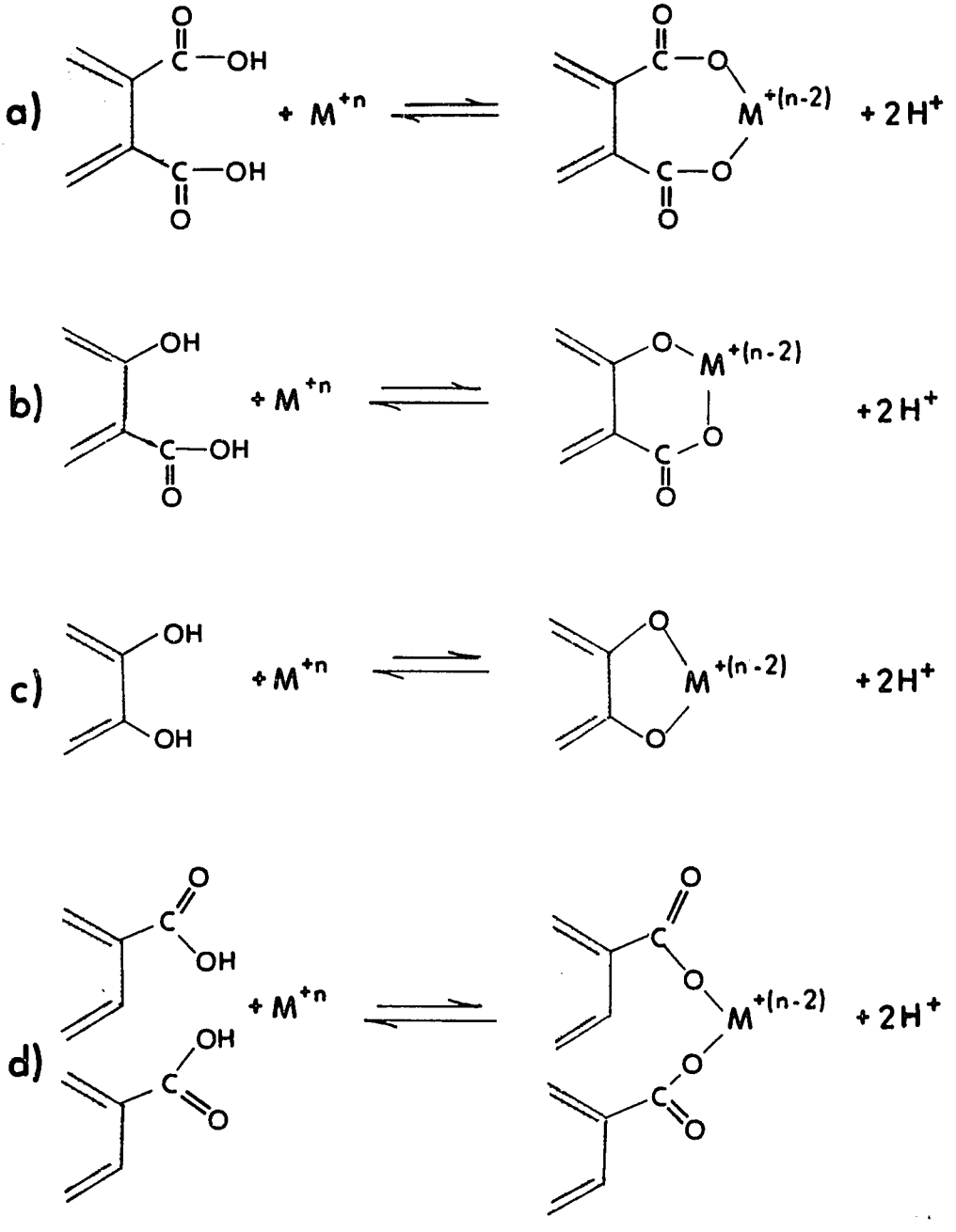

FIGURE 4.22

1972; Kribek et al., 1977), which are usually more abundant in natural environments. This is supported by the observation that concentrations of iron and aluminum are considerably higher in naturally occurring humic substances than nickel or vanadium (Figure 4.23). Exceptions have been noted in some marine humic substances, which have higher concentrations of divalent cations than trivalent cations (Rashid, 1971). These exceptions appear to be related to more nitrogen and sulfur functional groups in some marine humic acids, which may also act as ligands in addition to oxygen functional groups (Nissenbaum and Swaine, 1976). This may result in the formation of mixed ligand tetradentates, which apparently prefer divalent cations.

It has been proposed that during early diagenesis, humic substances may become primary constituents of some kerogens (Tissot and Welte, 1978, p. 90). Humate complexes would probably be incorporated into these kerogens, but their preservation with burial appears unlikely. The development of reducing conditions with burial could result in demetallation of humate complexes by hydrogen replacement at low pH conditions or by sulfide formation. Pauli (1975) has shown that demetallation of humate complexes occurs in the presence of hydrogen sulfide and results in the formation of metal sulfides. Although some humate complexes may persist through these reducing conditions, it appears unlikely that they would survive decarboxylation when subjected to low levels of thermal maturation.

Figure 4.23: Plot showing the amount of iron and aluminum in humic substances relative to their vanadium and nickel content; circles represent humic acid fractions, triangles represent fulvic acid fractions, and squares represent total humic substances.

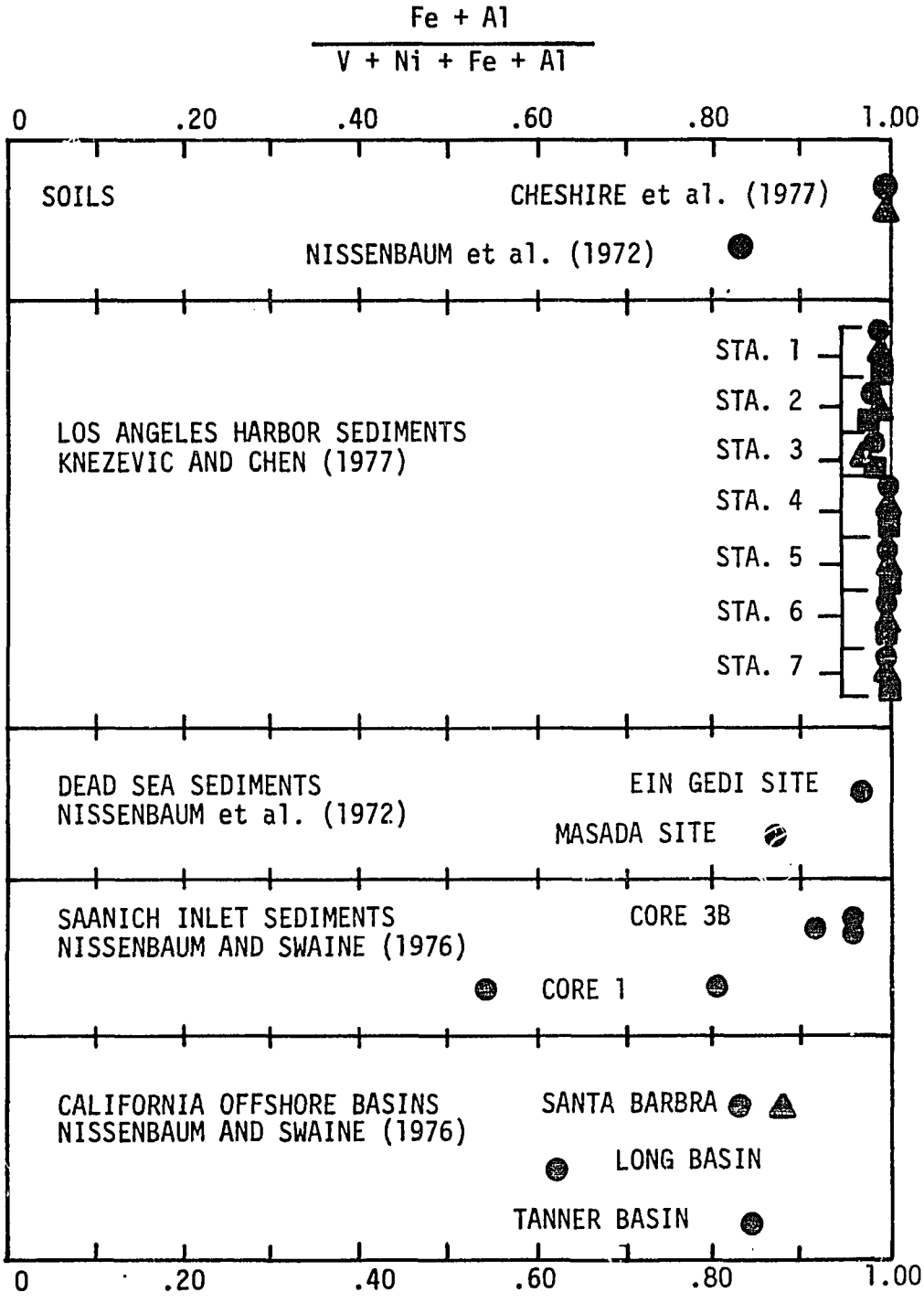

FIGURE 4.23

4.4 DISCUSSION

Although vanadium and nickel are capable of occurring in all three of the metallo-organic complexes described, their greatest stability and preference in nature at surface and diagenetic conditions is as vanadyl- and nickelous-tetrapyrrole complexes. Vanadium and nickel are usually concentrated in the high molecular weight fraction of crude oils and asphalts (Corbett, 1967; Dwiggins et al., 1969; Branthaver and Dorrence, 1978), with porphyrins accommodating as much as 50 weight percent of the two metals and highly aromatic tetrapyrrole complexes accommodating the remainder (Vaughan et al., 1970; Costantinides et al., 1959). In bitumens, these two metals also occur predominantly in tetrapyrrole complexes, but highly aromatic tetrapyrrole complexes are likely to be much more dominant than porphyrins (Blumer and Snyder, 1967; Blumer and Rudrum, 1970; Rho et al., 1973).

As stated earlier, VO^{+2} and Ni^{+2} form tenacious bonds with tetrapyrroles, and their cleavage from these bonds requires extreme conditions that are not likely under most diagenetic settings. The stability of these two metals in bitumen has been demonstrated by subjecting bitumens from the same rock to different concentrations of sulfur acid at 150°C for seven hours in a teflon lined digestion bomb. The results in Table 4.5 show that demetallation does occur, as expected, when the bitumen is subjected to concentrated sulfuric acid (37N), but demetallation does not occur when the bitumen is subjected to an 18.5N solution of sulfuric acid. Even this latter condition exceeds the limits of

Table 4.5: Vanadium and nickel concentrations in bitumens from the New Albany shale standard No. 1, which have been subjected to 18.5N and 37N solutions of sulfuric acid at 150°C for 7 hours.

Sulfuric Acid Concentration	Vanadium (ppm)	Nickel (ppm)	V/(Ni+V)
0*	344	324	0.51
18.5N	357	339	0.51
37.0N	38	49	0.44

*This sample was not subjected to 150°C for 7 hours.

natural diagenetic conditions with a pH of 0.3 at 25°C. In addition to withstanding chemical and thermal decomposition within the diagenetic realm, the highly aromatic character of these high molecualr weight complexes makes them less susceptible to microbial degradation (Bailey et al., 1973) and weathering (Brunnock et al., 1968; Blumer et al., 1973; Zsolnay, 1978). Thus, once vanadium and nickel are bound to tetrapyrrole complexes it appears unlikely that demetallation will occur under most diagenetic and reservoir conditions.

CHAPTER 5

SOURCES OF VANADIUM AND NICKEL IN NATURALLY OCCURRING ORGANIC SUBSTANCES

The source of vanadium and nickel in the organic matter of sediments and sedimentary rocks is critical to understanding the factors controlling their concentrations, as well as their proportionality to one another. The two most likely sources of these two metals are the endemic metals in the living matter from which an organic accumulation was derived or the dissolved metals in the interstitial waters of the sediments which are associated with an organic accumulation. In this chapter, both possible sources will be considered.

5.1 LIVING MATTER

It has been suggested that the vanadium and nickel concentrations detected in the organic matter of sediments and sedimentary rocks are endemic to the living matter from which the organic matter was derived (e.g., Vinogradov, 1936; Manskaya and Drozdova, 1968, p. 219; Yen, 1975). Endemic metal concentrations have been shown to be highly variable for different types of organisms (Noddack and Noddack, 1939), for the same species at different seasons (Black and Mitchell, 1952), and for individuals of the same species (Bertrand, 1950). In order to evaluate this possible source properly, the endemic concentrations of the

major sources of organic matter in sediments and sedimentary rocks will be considered individually, and these include higher plants, plankton, and sporopollenin.

5.1.1 Higher Plants

Higher plants are the most likely precursors of ligninic kerogen (Tissot and Welte, 1978, p. 145), which is usually the prominent kerogen type in peats, lignites, and coals. In addition to occurring in these concentrated forms, ligninic kerogen may also be disseminated in sediments and sedimentary rocks. The endemic vanadium and nickel concentrations in higher plants appear to be controlled primarily by the amount of soluble vanadium and nickel in the medium in which they are growing, and their ability to accumulate vanadium and nickel from the growing medium. Generally, plants growing in soils with high metal concentrations are usually more enriched in metals than those growing in soils with low metal concentrations (Cannon, 1963; Bertrand, 1950; Brooks et al., 1977). This is particularly true for the roots of plants, which usually have higher metal concentrations than the aerial parts of plants (Cannon, 1963; Bertrand, 1950). The actual amount of vanadium and nickel that can be extracted from the growing medium and incorporated into a plant varies with species. The fungus, Amanita muscaria is capable of concentrating 60 to 181 ppm of vanadium (dry weight basis), while on the same soil other species of this genus only concentrate 0.1 to 2.4 ppm of vanadium (dry weight basis; Bertrand, 1950). Similarly, Brooks and others (1977) have noted that certain plant species of the genera

Dicoma, Geissois, Alyssum, Homalium, Hybanthus, Psychotria, and Sebertia incorporate nickel at concentrations in excess of 1000 ppm (dry weight basis) when grown in a medium that has a relatively high nickel concentration (e.g., residual soils on ultrabasic rocks). These high endemic metal concentrations for higher plants are not common, and average endemic concentrations range from 0.1 to 32 ppm for vanadium (Figure 5.1) and from 1 to 45 ppm for nickel (Figure 5.2).

Figures 5.1 and 5.2 show that the vanadium and nickel concentrations in bitumens from rocks bearing ligninic kerogen fall within the observed ranges for endemic concentrations in higher plants. Similarly, the vanadium and nickel concentrations in whole peats and coals are also within the observed ranges for endemic concentrations (Figures 45 and 46). In coals and some peats, the vanadium and nickel concentrations tend to occur in the higher end of these endemic ranges, and this appears to be due to the inclusion of inorganic phases, which may contain appreciable quantities of metals. Data from studies by Cameron and Wright (1977), and Ruch and others (1974) show that the vanadium and nickel concentrations increase as the amount of inorganic phases included in the analyses increases (Figure 5.3, Ref. 1 and Ref. 2; Figure 5.4, Ref. 1 and Ref. 4). Thus with this deviation in mind, it appears that the vanadium and nickel concentrations in coals and peats occur well within the observed range for endemic metal concentrations of higher plants.

Figure 5.1: Vanadium concentrations in bitumen from rocks and sediments bearing ligninic kerogen, and precursory organic substances (Ref. 1, Bertrand, 1950; Ref. 2, Boyle, 1977; Ref. 3, Cannon, 1952, Table 7). Number of samples given in parentheses.

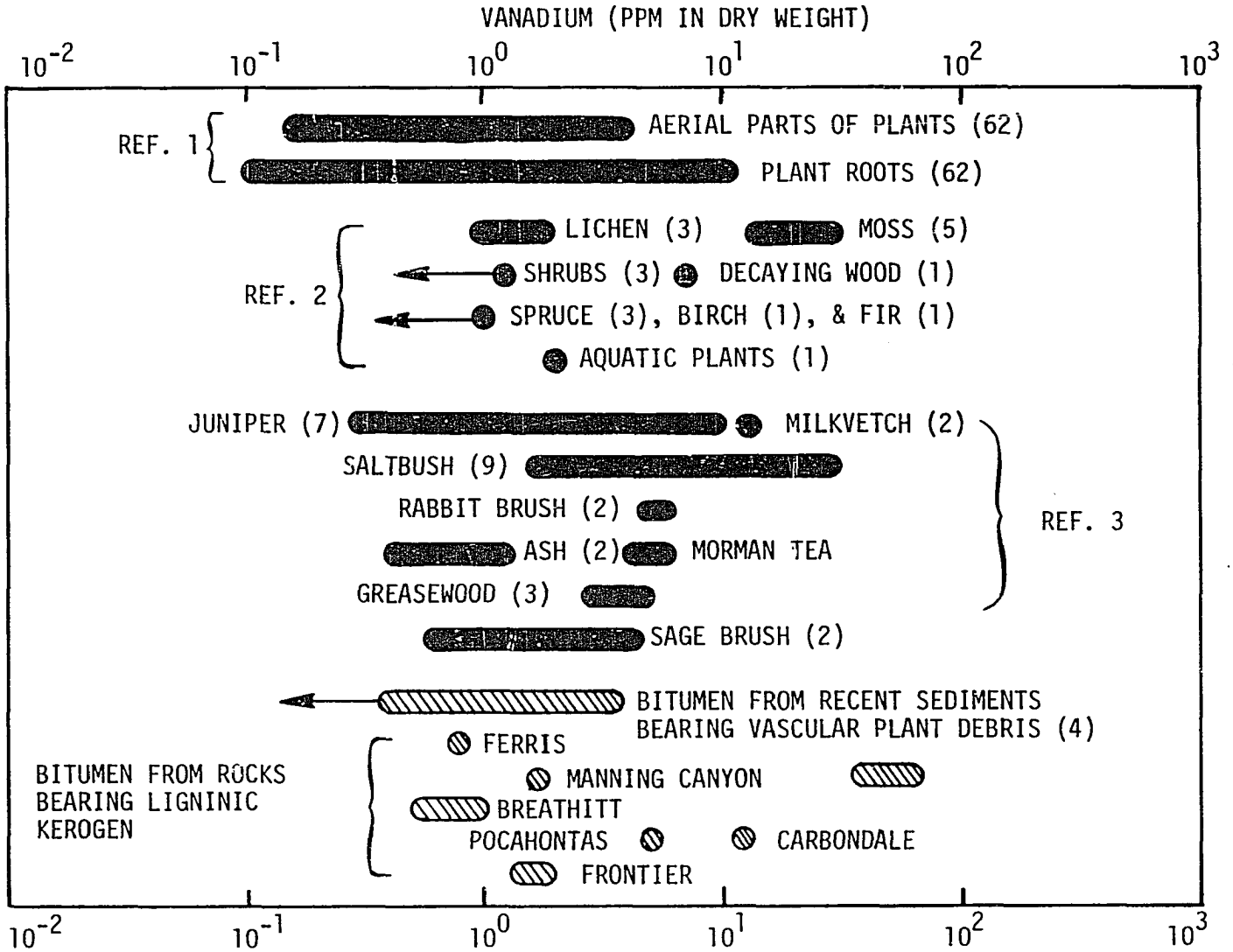

FIGURE 5.1

Figure 5.2: Nickel concentrations in bitumens from rocks and sediments bearing ligninic kerogen, and precursory organic substances (Ref. 1, Boyle, 1977; Ref. 2, Kovdi et al., 1959; Ref. 3, Cannon, 1960, whole plant values were calculated by assuming ash values between 5.4 and 23.4 percent by weight). Number of samples given in parentheses.

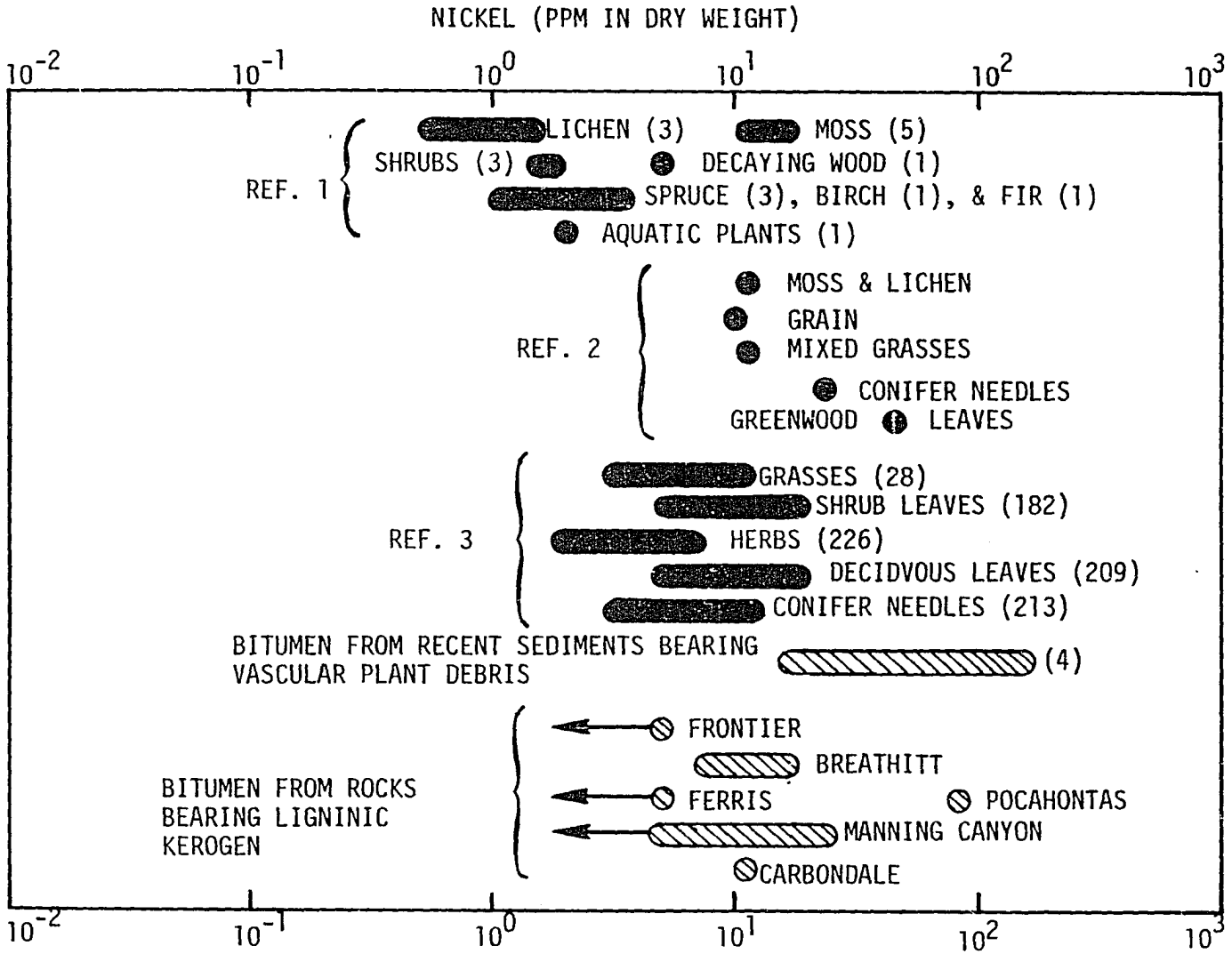

FIGURE 5.2

Figure 5.3: Vanadium concentrations in higher plants, peats, and coals (Ref. 1, Cameron and Wright, 1977; Ref. 2, Kochenov and Kreshtapova, 1967; Ref. 3, Ruch et al., 1974; Ref. 4, Zubovic et al., 1960a; Ref. 5, Abernethy et al., 1969; Ref. 6, Zubovic et al., 1960b.; Ref. 7, Szilagyi, 1971; Ref. 8, Swaine, 1975; Ref. 9, Yudovich et al., 1972). Number of samples given in parentheses.

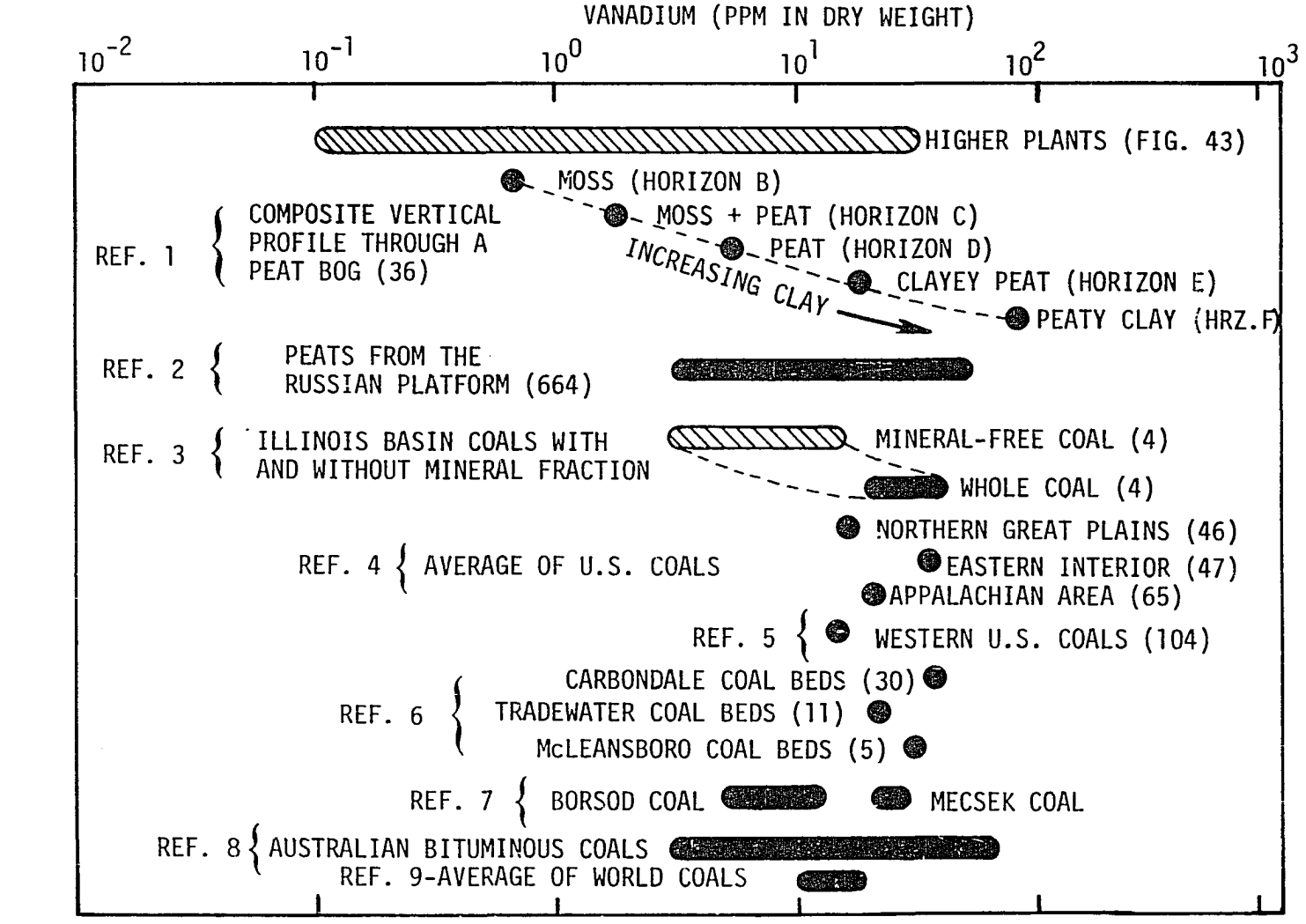

FIGURE 5.3

Figure 5.4: Nickel concentrations in higher plants, peats, and coals (Ref. 1, Cameron and Wright, 1977; Ref. 2, Casagrande and Erchull, 1977; Ref. 3, Kochenov and Kreshtapova, 1967; Ref. 4, Ruch et al., 1974; Ref. 5, Zubovic et al., 1960a.; Ref. 6, Abernethy et al., 1969; Ref. 7, Zubovic et al., 1960b.; Ref. 8, Swaine, 1975; Yudovich et al., 1972). Number of samples given in parentheses.

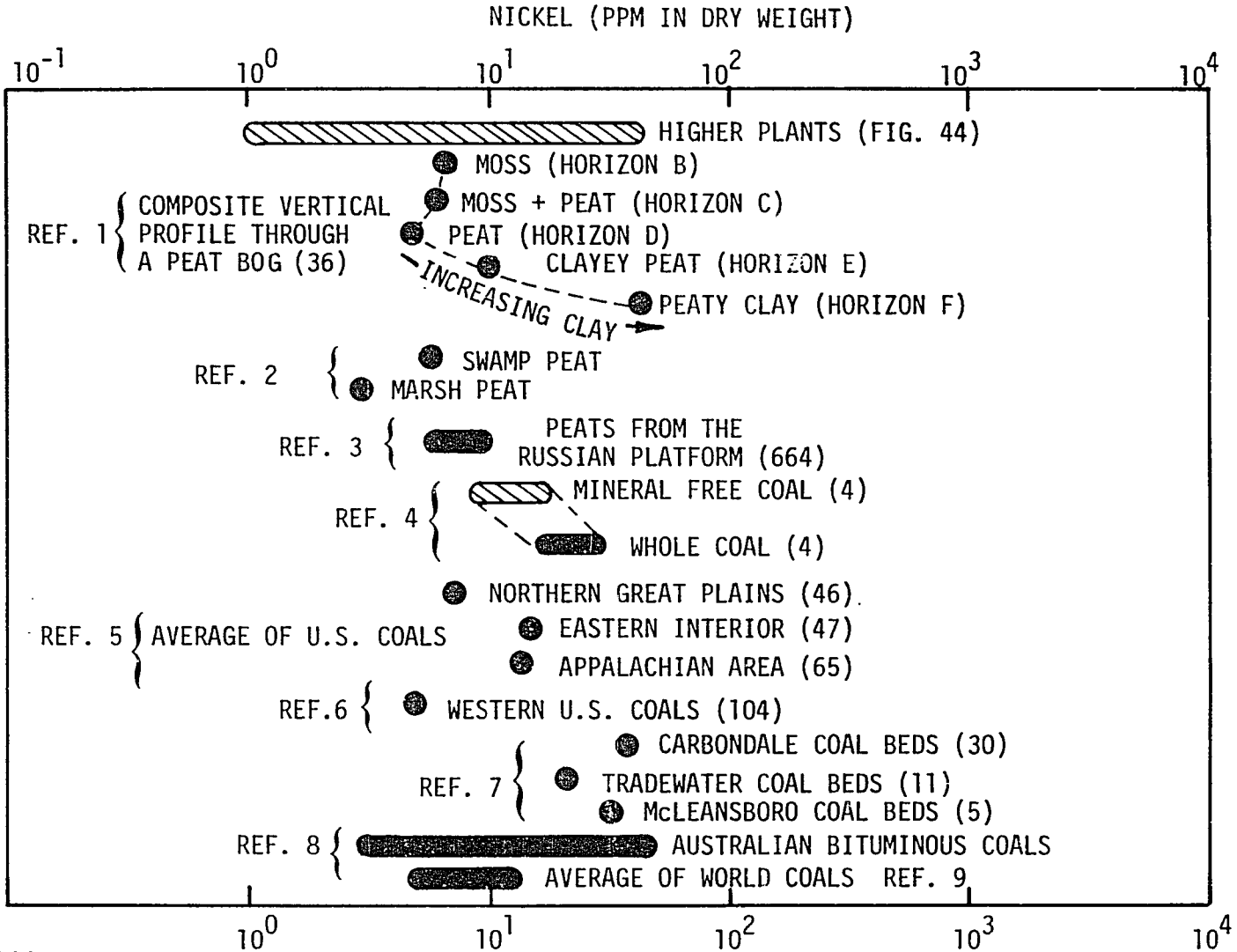

FIGURE 5.4

Although laboratory studies have shown that vanadium may be reduced and concentrated by defunct higher plant debris (Pommer, 1958; Szalay and Szilagi, 1967 and 1969; Bloomfield and Kelso, 1973; Wilson and Weber, 1979), the humate complexes responsible for this enrichment usually prefer trivalent iron or aluminium cations (see Chapter 4.3 Humate Complexes). A major exception to this occurs in sandstone-type uranium deposits, which consist of concentrations of uranium and lesser amounts of vanadium on decayed higher plant debris in the form of humate complexes and mineral precipitates (Haji-Vassiliou and Kerr, 1973). In this situation the higher plant debris usually occurs in fluvial sandstones, through which oxygenated uranium- and vanadium-bearing waters flow (Rackley, 1972; Alder, 1964; Wright, 1955). Under these conditions it appears that aqueous uranium and vanadium are reduced by the decaying plant debris and are then bound into humate complexes or precipitated as mineral oxides. Distinction between this type of secondary enrichment and endemic concentrations of vanadium can be made readily by the anomalously high uranium and vanadium concentrations in the former and their geological settings. Figures 43 through 46 indicate that vanadium and nickel in ligninic kerogen and its associated bitumen are usually endemic to the higher plants from which they were derived.

5.1.2 Plankton

Plankton include phytoplankton, zooplankton, and microplankton (bacteria). Collectively these passively floating or weakly motile organisms are considered to be the precursors of liptinitic kerogens

(Tissot and Welte, 1978, p. 144). These sources of organic matter are sometimes referred to as marine in origin, but the abundance of plankton in eutrophic lakes (Wetzel, 1975, p. 335) makes such labelling misleading and therefore it will not be used in this discussion. Similar to higher plants, the amount of endemic vanadium and nickel in plankton is controlled primarily by the amount of vanadium and nickel in the medium in which they are growing and their ability to accumulate these two metals. The laboratory study by Riley and Roth (1971) demonstrated that phytoplankton grown in waters with high metal concentrations were more enriched in metals than those grown in waters with low metal concentrations. They also showed that the ability to accumulate metals varied with species and type of metal. The data in Figures 5.5 and 5.6 suggest that the endemic metal concentrations for plankton ranges from 0.3 to 13 ppm for nickel and from less than 4 to 16 ppm for vanadium, respectively.

Figure 5.5 shows that the nickel concentrations in extracts from algae and algal-bearing sediment occur within the vicinity of the observed endemic nickel concentrations. Conversely, the bitumens from rocks bearing liptinitic kerogen show a distinct enrichment of nickel relative to the observed endemic nickel concentrations. This data indicates that endemic nickel concentrations are not sufficient to account for the nickel concentrations in bitumens derived from liptinitic kerogens and another source of nickel is needed.

Figure 5.5: Nickel concentrations in bitumens from rocks and sediments bearing liptinitic kerogen, extracts from brown and green algae, and precursory organisms (Ref. 1, Martin and Knauer, 1973; Ref. 2, Fowler, 1977; Ref. 3, Young and Langille, 1958; Ref. 4, Bollingberg, 1975; Ref. 5, Vinogradov, 1953, p. 121).

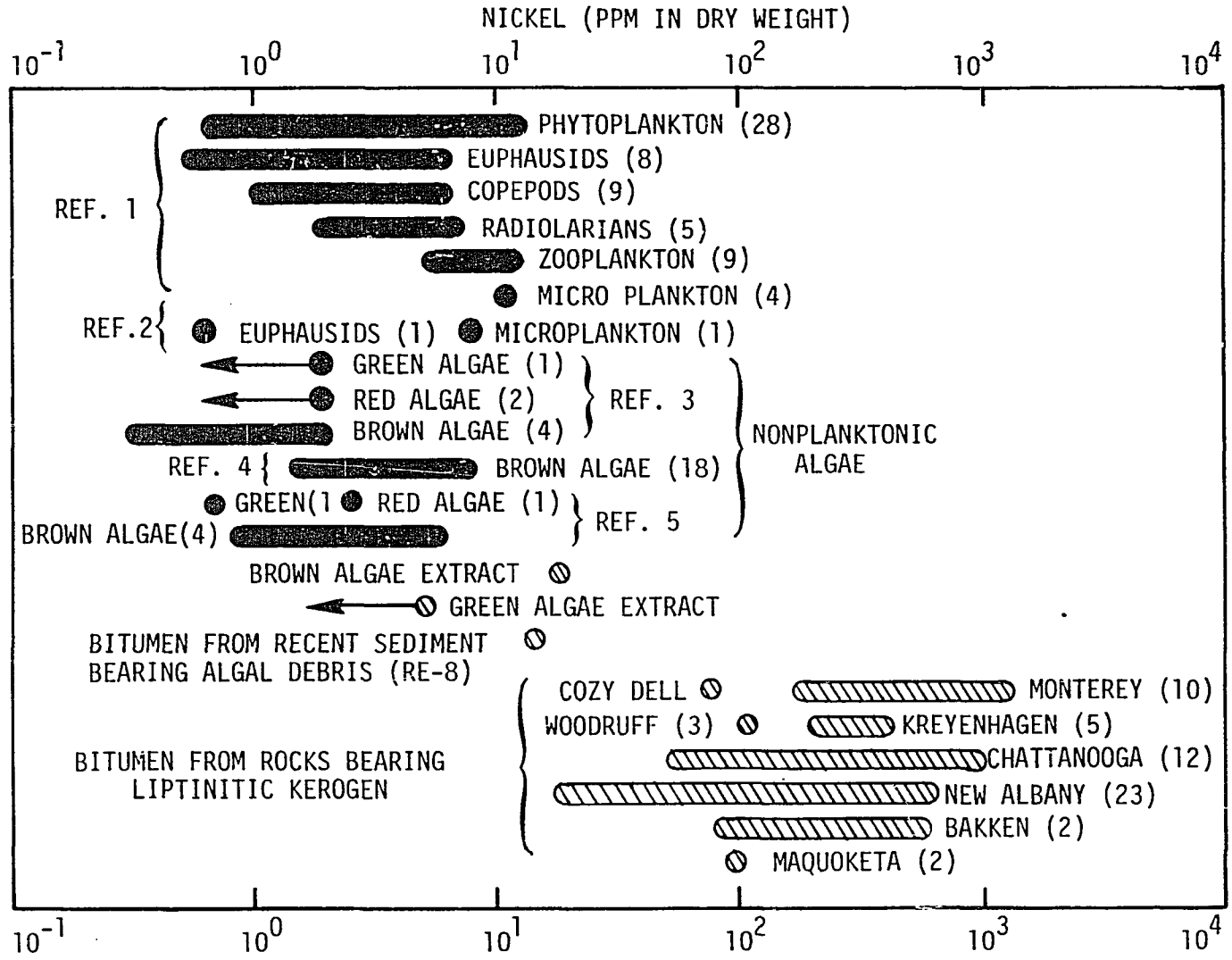

FIGURE 5.5

Figure 5.6: Vanadium concentrations in bitumens from rocks and sediment bearing liptinitic kerogen,extracts from brown and green algae, and precursory organisms (Ref. 1, Ostroumov and Silina, 1952; Ref. 2, Nicholls et al., 1959; Ref. 3, Martin and Knauer, 1973).

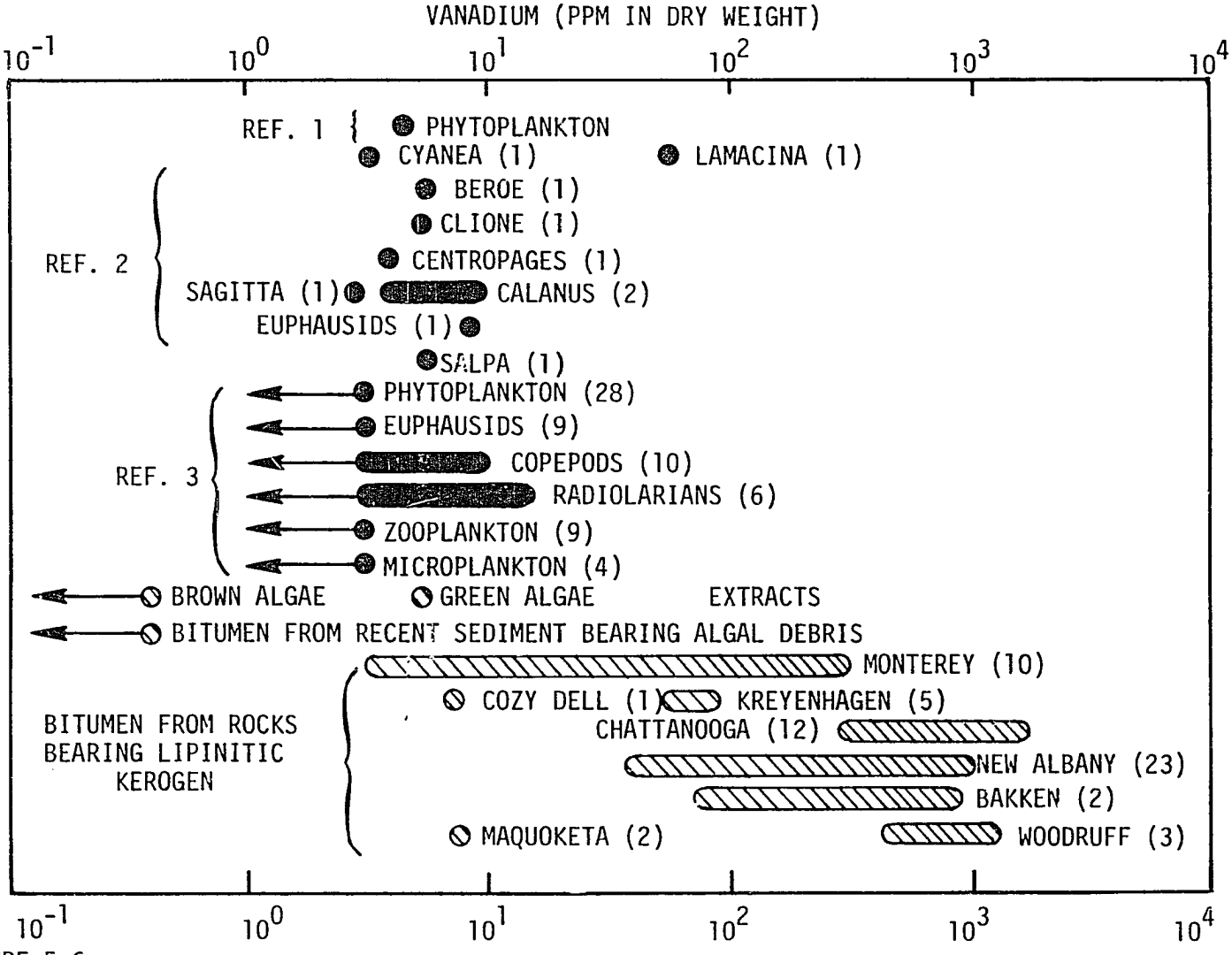

FIGURE 5.6

Figure 5.6 shows that the vanadium concentrations in extracts from algae and algal-bearing sediment also occur within the observed endemic vanadium range. But unlike nickel, the vanadium concentrations in bitumens from rocks bearing liptinitic kerogen vary from the observed endemic vanadium concentrations to higher concentrations that suggest enrichment. Some investigators (e.g., Vinogradov, 1936; Manskaya and Drozdova, 1968, p. 219; Yen, 1975) have suggested that the incorporation of certain vanadium-rich marine animals into an organic accumulation may explain the high vanadium concentrations sometimes observed. The marine animal most often cited as a possible cause of vanadium enrichment in an organic accumulation is ascidia from the suborder phlebobranchiata in the subphylum tunicata. Although the presence of this type of tunicate would increase the endemic vanadium concentration range significantly (Figure 5.7), the presence of this sessile, aerobic respiring organism is highly improbable in the anaerobic bottom waters observed for the preservation of organic accumulations. Thus the high vanadium concentrations in some bitumens derived from rocks bearing liptinitic kerogen are not endemic to their plankton sources and for these bitumens another source is needed.

5.1.3 Sporopollenin

Spores and pollen are usually protected from chemical attack by a resistant wall composed of a material referred to as sporopollenin (Brooks and Shaw, 1972). A large amount of data has been published on this resistant material (e.g., Books et al., 1971), and it appears to be the

Figure 5.7: Vanadium concentrations in plankton, aquatic animals (Ref. 1, Bertrand, 1950; Ref. 2, Blotcky et al., 1979; Ref. 3, Nicholls et al., 1959; Ref. 4, Vinogradov, 1953, p. 425) and bitumens from rocks bearing liptinitic kerogens. The data on tunicata from Ref. 3 and Ref. 4 were classified according to Berrill (1950). Number of samples given in parentheses.

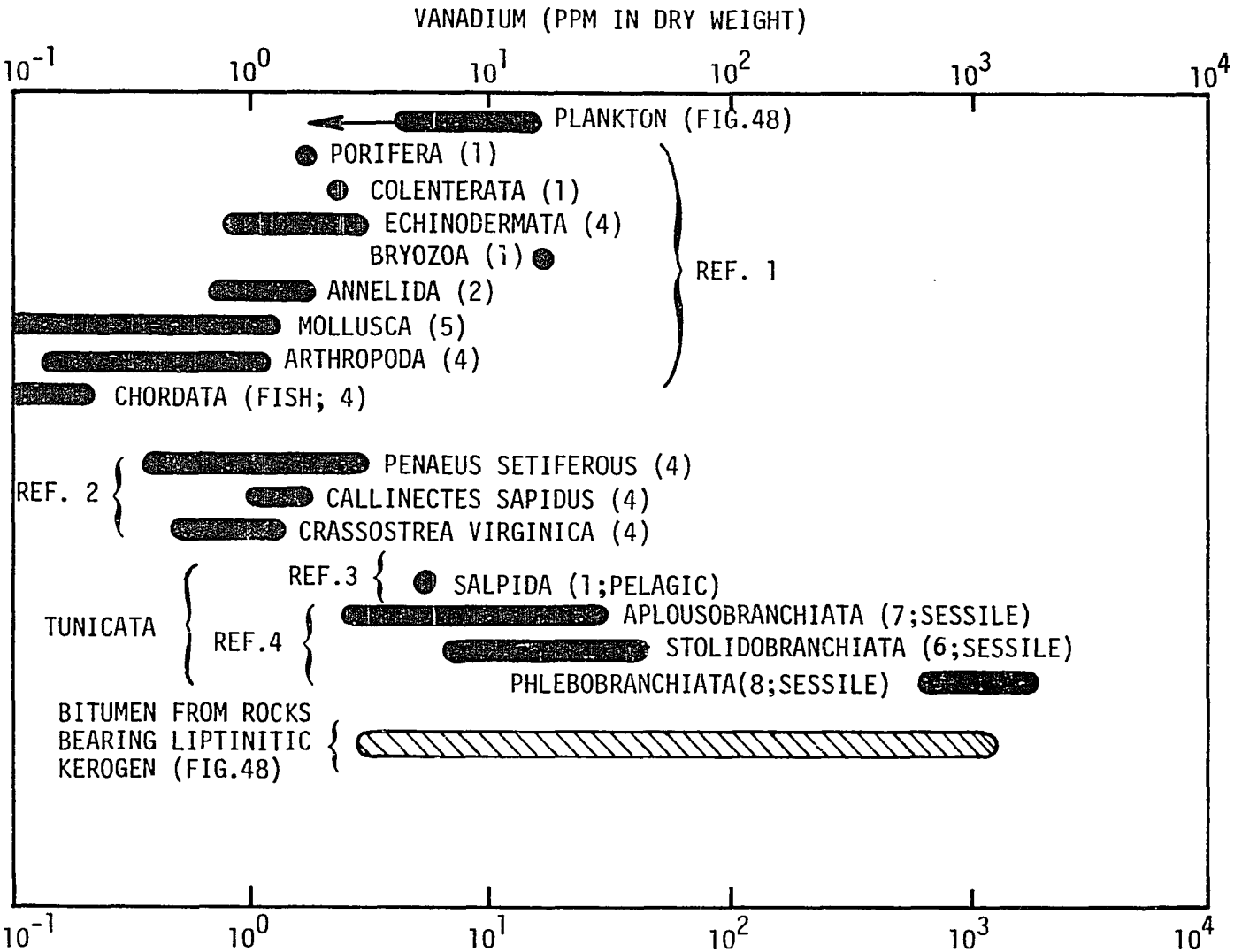

FIGURE 5.7

most likely precursor of sporopolleninic kerogen (Brooks and Shaw, 1968 and 1970). Several studies on trace elements in sporopollenin have been published (Fawcett et al., 1971, 1973, and 1974), but unfortunately vanadium and nickel concentrations were not determined in these studies. The lack of this data makes it difficult to determine the endemic vanadium and nickel concentrations in sporopollenin, which, in turn, makes it difficult to assess the enrichment of these two metals in sporopolleninic kerogens and their bitumens. In order to get around this problem, the endemic vanadium and nickel concentrations in sporopollenin will be assumed to be within the combined endemic vanadium and nickel concentrations of higher plants and plankton, from which sporopollenin is derived. It should be noted that this is only an approximation, and more trace element studies on sporopollenin are necessary before this approximation is improved.

Rocks bearing kerogen that consists mainly of sporopolleninic kerogen are rare compared to the other kerogen types (Tissot and Welte, 1978, p. 144). The only samples representing rocks with sporopolleninic kerogens in this study are those from the Green River Formation in the Uinta and Green River Basins. Figure 5.8 shows that the nickel concentrations in the bitumens of the Green River Formation are definitely enriched relative to the endemic nickel concentrations in planton, but vary from enriched to endemic concentrations relative to the endemic nickel concentrations in higher plants. Vanadium concentrations in these same bitumens vary from enriched to endemic concentrations relative to higher plants. Although the data is limited, it suggests that vanadium and

Figure 5.8: Comparison of vanadium and nickel concentrations in bitumens and kerogen of the Green River Formation with their endemic concentrations in higher plants and plankton.

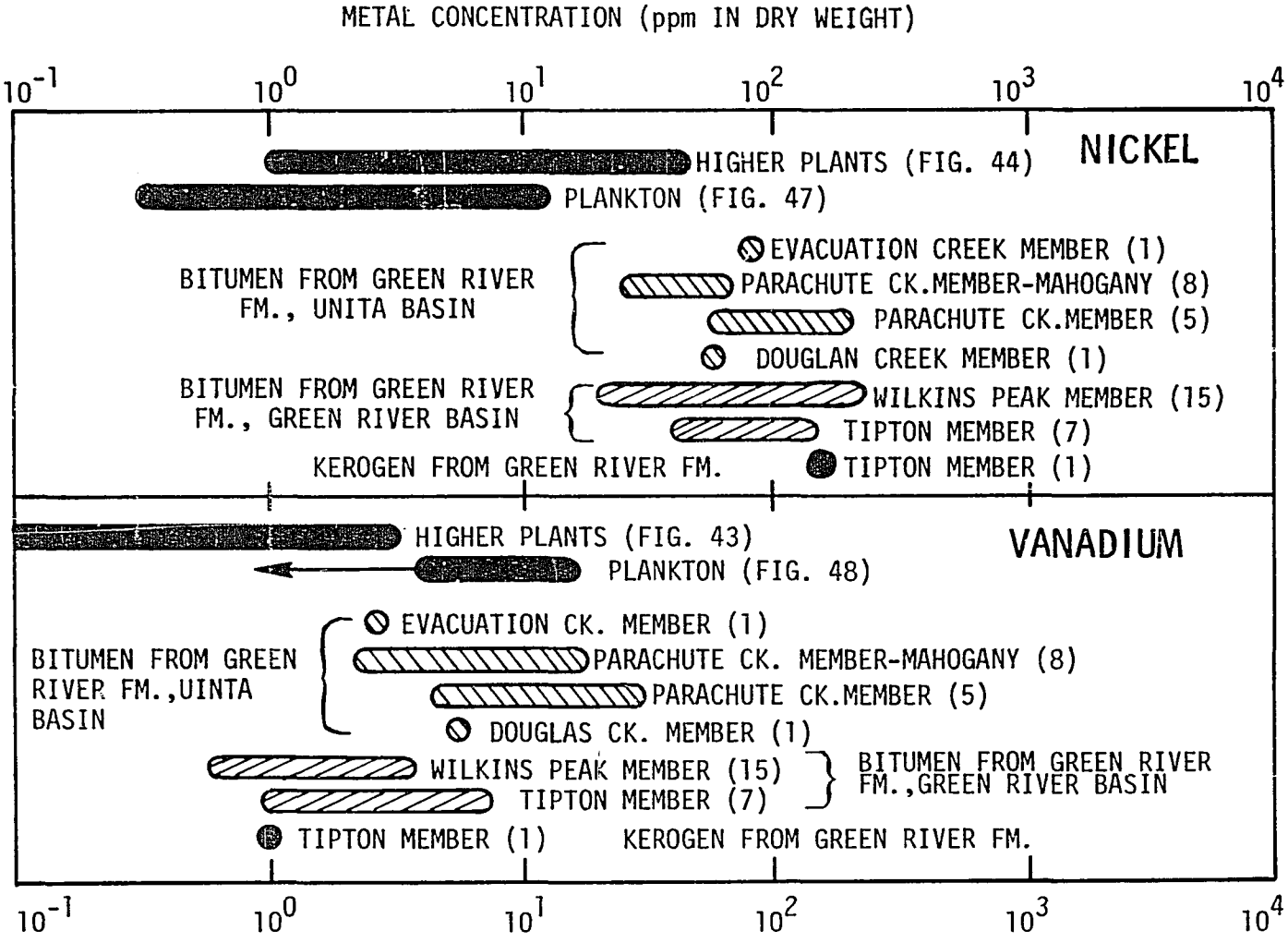

FIGURE 5.8

nickel concentrations in bitumens from rocks bearing sporopolleninic kerogen may be enriched or endemic to the sporopollenin source. Thus, in the enriched bitumens, another source of vanadium and nickel is needed.

5.1.4 Summary

The general conclusions are summarized in Table 5.1. Ligninic bitumens are not enriched in vanadium or nickel, and they usually reflect the endemic concentrations of their higher plant precursors. Conversely, liptinitic bitumens and to a lesser extent sporopolleninic bitumens may be enriched in vanadium and nickel. It should also be noted that nickel always appears to be enriched in liptinitic bitumen, but vanadium may vary from enriched to endemic concentrations.

5.2 INTERSTITIAL WATER

The enriched concentration of vanadium and nickel in liptinitic and sporopolleninic bitumens may be derived from the interstitial waters that accompany the organic matter during burial in the sediment column. The metal concentrations of interstitial waters are usually different than the metal concentrations of the overlying water body (e.g., Brooks et al., 1968; Presley et al., 1972). This difference in composition is the result of a number of processes operating in the sediment column. Several of the salient processes include desorption and dissolution of metals from minerals or organic matter, sorption and precipitation of

Table 5.1: A summary of the nature of vanadium and nickel in bitumens from rocks bearing different types of kerogen.

Metal	Ligninic	Sporopolleninic	Liptinic
Vanadium	Endemic	Endemic-Enriched	Endemic-Enriched
Nickel	Endemic	Endemic-Enriched	Enriched

metals with minerals or organic matter, exchange of metals between interstitial water and minerals or organic matter, and diffusion of metals from and to the overlying water body. Although these processes may control the composition of interstitial waters, their ability to concentrate vanadium or nickel in interstitial waters seldom exceeds 100 ppb (Figures 5.9 and 5.10). An exception to this is subsurface water in tuffaceous rocks which may obtain vanadium concentrations up to 700 ppm (Ref. 7, Figure 5.9). The critical factor that appears to determine the effectiveness of interstitial waters as a source of enriched vanadium or nickel in organic matter is the openness of the sediment column with respect to the overlying water body.

5.2.1 Closed Sediment System

A closed sediment system is defined in this study as a volume of sediment that is not involved in ion diffusion with its overlying water body and surrounding sediments. In this system the vanadium and nickel concentrations in the interstitial waters are limited, and they are not likely to be sufficient as a source for enriched vanadium and nickel concentrations in organic matter. The two graphs in Figure 5.11 show that an interstitial water with a vanadium or nickel concentration of 10 ppb could only enrich the organic matter of a closed sediment system with less than 1 ppm of either metal (red construction lines a and a_1). This amount of metal is insignificant relative to the endemic metal concentrations in the organic matter, and it becomes less significant as the amount of organic matter in the sediment increases (Figure 5.11, red

Figure 5.9: Vanadium concentrations in fresh surface waters (solid dots and bars; Ref. 1, Livingstone, 1963; Ref. 2, Konovalov, 1973), sea water (cross hatched dots and bars; Ref. 3, Riley, 1965; Ref. 4, Goldberg, 1965; Ref. 5, Angino, 1964; Ref. 6, Black and Mitchell, 1952), and subsurface waters (hatched bars; Ref. 7, Denson and Gill, 1965; Ref. 8, Sugawara, Naito, and Yamada, 1956). Number of samples given in parentheses.

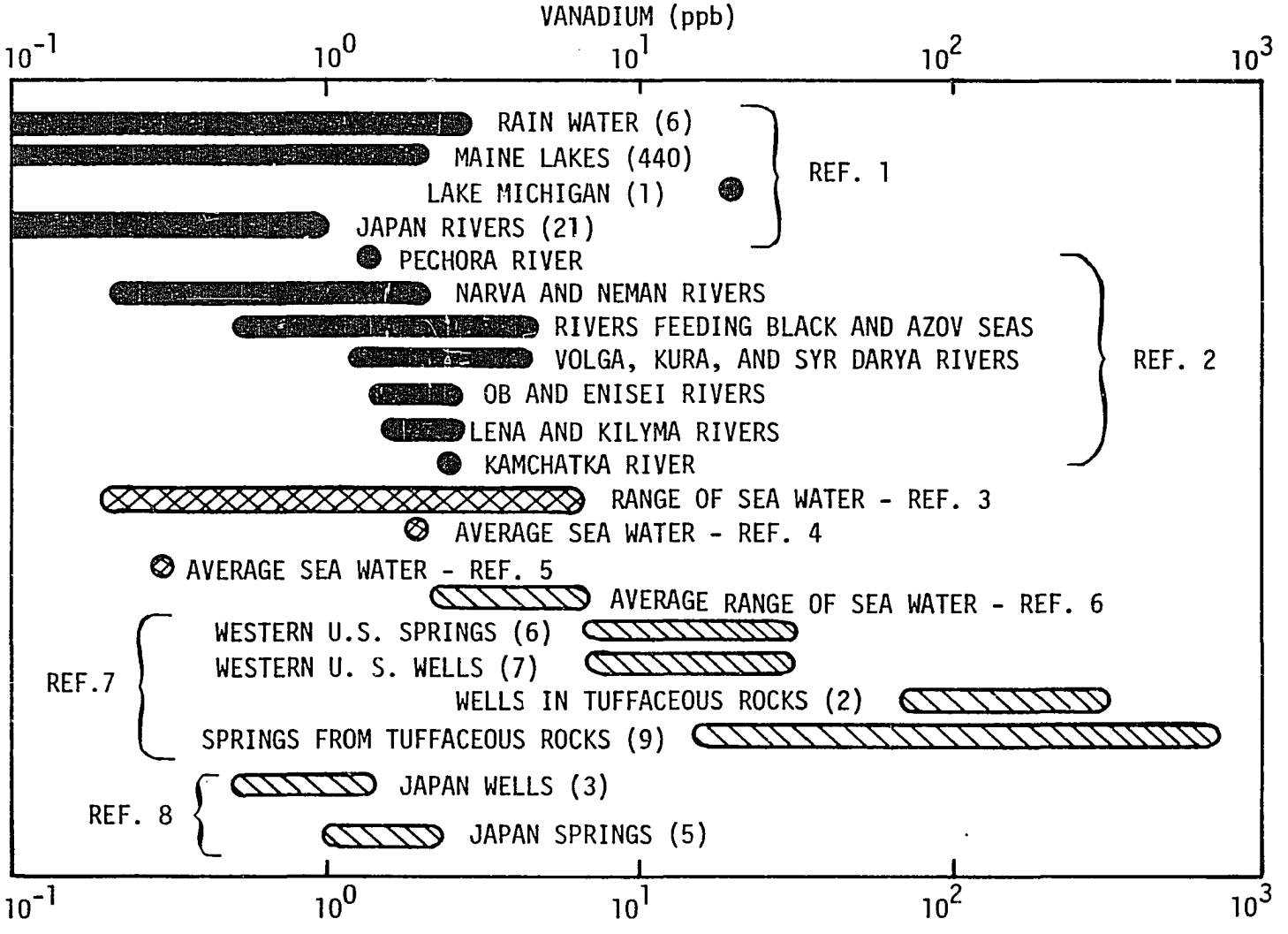

FIGURE 5.9

Figure 5.10: Nickel concentrations in fresh surface waters (solid dots and bars; Ref. 1, Livingston, 1963, Table 90; Ref. 2, Andelman, 1973; Ref. 3, Konovalov, 1973), sea water (cross hatched dots and bars; Ref. 4, Sclater et al., 1976; Ref. 5, Brewer and Spencer, 1974; Ref. 6, Goldberg, 1965; Ref. 7, Black and Mitchell, 1952), and subsurface waters (hatched dots and bars; Ref. 8, Denson and Gill, 1965; Ref. 9, Naboko et al., 1973). Number of samples given in parentheses.

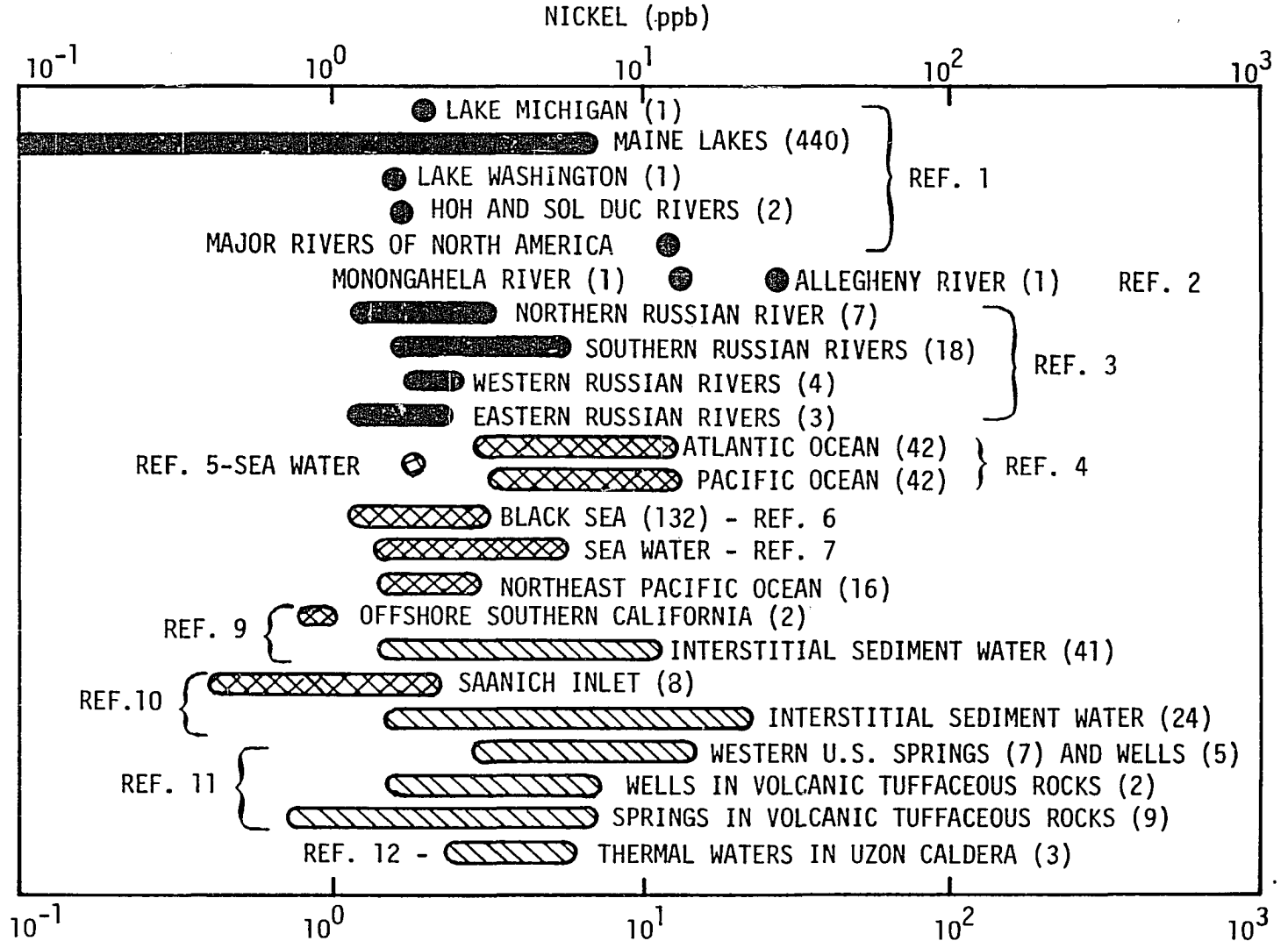

FIGURE 5.10

Figure 5.11: Graphs showing the maximum metal concentration that may occur in the organic matter of a sediment in a closed system. Calculations are based on 1 m^3 of sediment, and the parameters considered are percent water by volume, concentration of metal in interstitial water, and grams of organic matter in sediment. The dried sediment is assumed to have a density of 2.5 grams/cm^3. Graph A shows the dependence of grams of dissolved metal per cubic meter of sediment on percent water by volume in the sediment and concentration of metal in the water. Graph B shows the dependence of maximum metal concentration possible in the organic matter of a sediment on grams of dissolved metals per cubic meter of sediment and grams of organic matter per cubic meter of sediment. Numbers in parentheses represent the weight percent of organic matter on a dry weight basis for 1 cubic meter of sediment with 25, 50, and 75 percent water by volume, respectively.

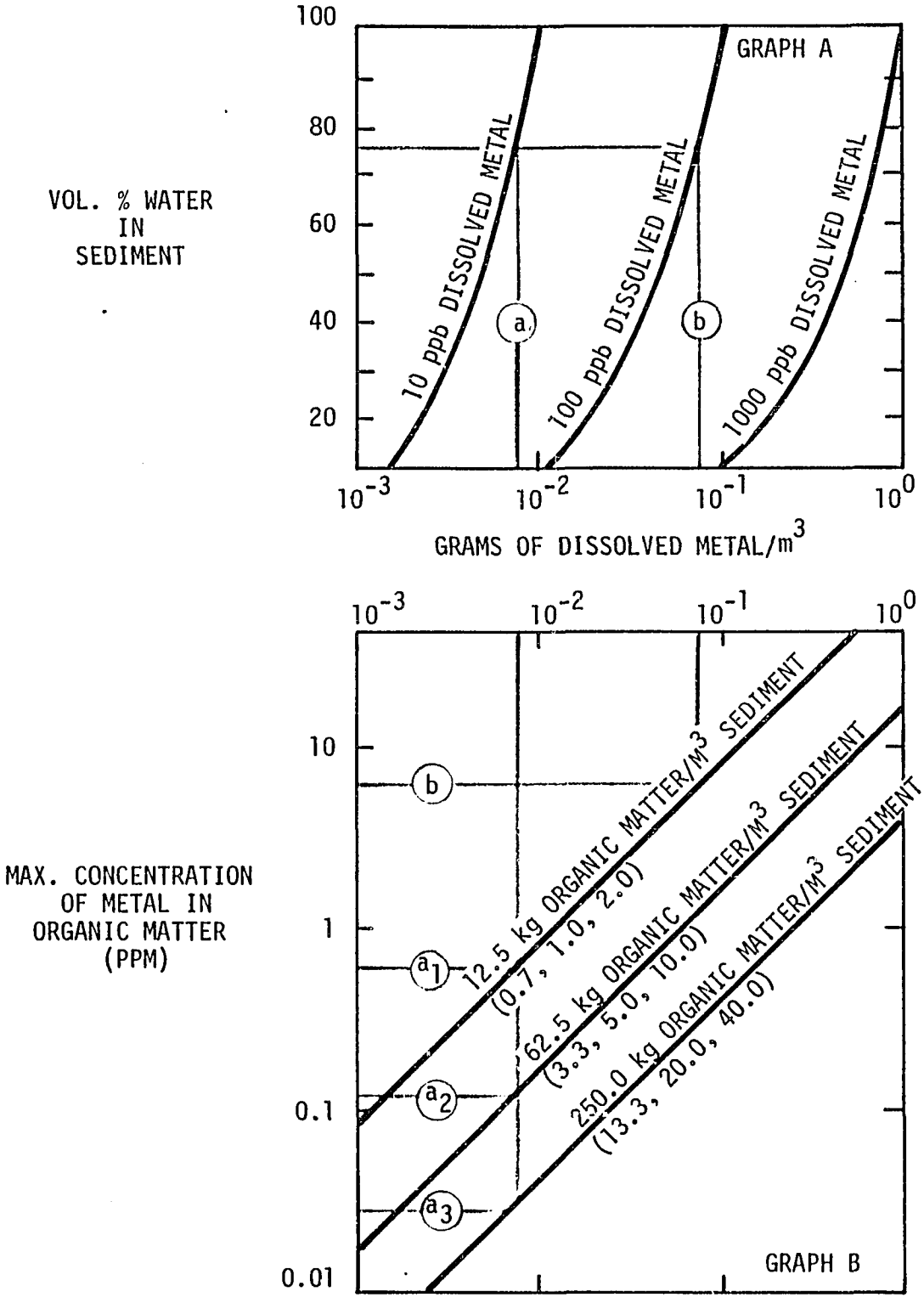

FIGURE 5.11

construction lines a, a_1, a_2, and a_3). Even with metal concentrations as high as 100 ppb in an interstitial water, the maximum metal enrichment of the organic matter would still be indistinguishable from endemic concentrations (Figure 5.11, red construction line b).

5.2.2 Open Sediment System

An open sediment system is defined in this study as a volume of sediment that is involved in ion diffusion with its overlying water body and surrounding sediments. In this type of system, the dissolved vanadium and nickel in the overlying water body are available as a source for their enrichment in organic matter in a sediment column. As vanadium or nickel in an interstitial water react to form metallo-organic complexes in the organic matter of a sediment column, additional vanadium or nickel diffuses downward from the overlying water body to replace the extracted metals. This type of open sediment system would allow significant amounts of vanadium and nickel to concentrate as metallo-organic complexes in the sediment column. Diffusion of ions through open sediment systems have also been used to explain concentrations of sedimentary iron sulfides (Berner, 1969) and manganese oxides (Bonatti et al., 1972).

5.2.3 Open-To-Closed Sediment System

In nature a sediment column is usually an open sediment system at and near its sediment-water interface and becomes a closed sediment system

at some depth as a result of compaction. The depth at which a closed sediment system occurs is dependent on the compaction rate of a sediment, which, in turn, is dependent on a variety of sediment properties (Meade, 1966). In this type of open-to-closed sediment system the duration of the open sediment system becomes a critical factor that determines the effectiveness of interstitial water as a source for enriched vanadium and nickel concentrations in organic matter.

Although the rate of metallation of metallo-organic complexes does not appear to pose a significant time dependence (Hodgson et al., 1960), the rate at which bonded metal is replaced by diffusion in the interstitial water does appear to pose a significant time dependence. Concentration gradients for nickel in interstitial waters from marine sediments down to depths of 34 meters were calculated from published data (Brooks et al., 1968; Presley et al., 1972). The results gave a range of concentration gradients between 10^{-7} and 10^{-6} μmoles/cm^4. Using this range of concentration gradients and published diffusion coefficients for nickel (Li and Gregory, 1974), an approximation of the flux of nickel in marine sediments was calculated by Fick's first law (Berner, 1971, p. 25). The result of these approximations gave a range of flux values between $10^{-12.5}$ and 10^{-11} μmoles/cm^2/sec. As shown in Figure 5.12, flux values of this order of magnitude suggest that an open sediment system would have to be operative for over 7000 years in order to obtain an enriched metal concentration of 1000 ppm in organic matter that comprises 10 percent by weight of the sediment (red construction lines a, a_1, and a_2). At low to moderate sedimentation rates (10 to 100 cm/1000 years), the

Figure 5.12: Graphs showing approximately the enriched metal concentrations that may be obtained by organic matter from interstitial waters in an open sediment system. Calculations are based on a sediment slab that has a surface area of $1cm^2$ and a depth of 1 mm. The densities of the organic and inorganic fraction of the sediment slab are assumed to be 1.5 and 2.5 g/cm^3, respectively. Graph A shows approximately the minimal amount of metal required to pass through a sediment slab in order to obtain a specified enriched metal concentration in the organic matter of the sediment slab. The lines labeled OM represent sediment slabs with different amounts of organic matter, which are expressed in weight percent of the whole sediment slab. Graph B shows approximately the amount of time the sediment system must be open in order to obtain a specified enriched metal concentration in the organic matter. The lines labeled J represent different metal flux values, which are expressed in $\mu moles/cm^2 sec$. Graph C shows the burial depth of a sediment slab after a specified time. The lines labeled ω represent different sedimentation rates, which are expressed in cm/1000 years. The red lines labeled a, a_1, a_2, b, b_1, and b_2 are construction lines which are referred to in the text.

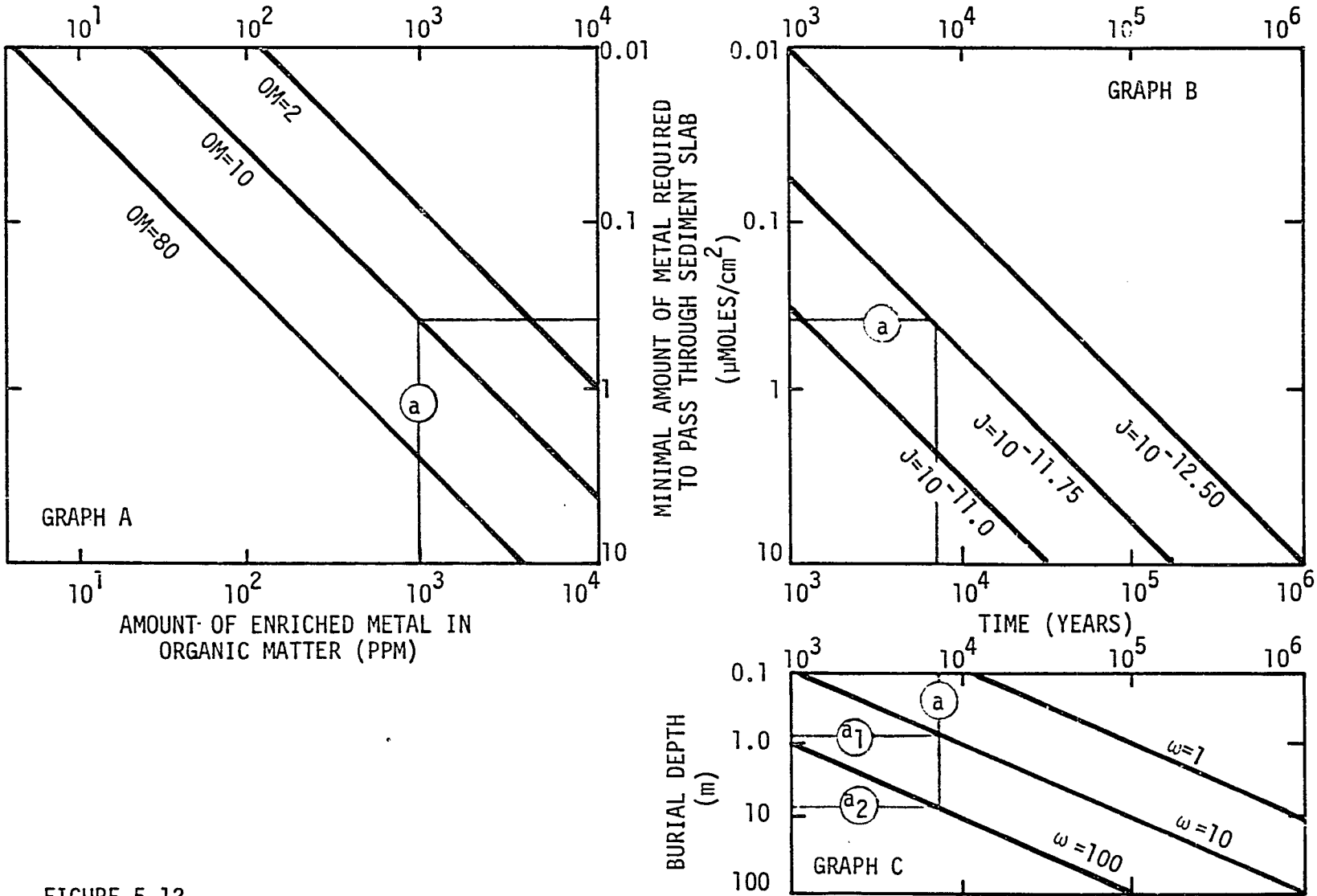

FIGURE 5.12

open sediment system would have to remain operative down to depths of 1 to 10 meters. The large amounts of water retained by most sediments at these depths (>50 percent by volume of sediment; e.g., Meade, 1966; Emery, 1960, p. 258), suggests that an open sediment system is likely to be maintained.

Continuous and homogeneous sedimentation operates for varying amounts of time in nature, and the introduction of evaporites, welded tuffs, volcanic flows, or a different type of sediment at a higher sedimentation rate (e.g., >500 cm/1000 years) could result in the early development of a closed sediment system within a sediment column. Under this condition, complete metallation of potential metallo-organic complexes may not occur. Thus, variations in the degree of metallation of potential metallo-organic complexes downward through a sediment column (e.g., Figure 4.13), may reflect variations in the metal flux or duration of the open sediment system during the history of the sediment column. It should also be noted that as the amount of potential metallo-organic complexes in a sediment become more abundant, the metal flux or duration of an open sediment system must increase accordingly in order to insure their complete metallation.

5.2.4 Summary

The dissolved vanadium and nickel in interstitial waters could be the source of their enriched concentrations in organic matter. This source may only be effective in an open sediment system where the reacted

metals are replaced by diffusion of metals from the overlying sediment and water body. In the event that a sediment column should develop a closed sediment system early in its history, incomplete metallation of its potential metallo-organic complexes may occur. The degree of metallation appears to be dependent on the amount of potential metallo-organic complexes, metal flux, and duration of the open sediment system.

5.3 DISCUSSION

Interstitial water appears to be the most likely source for enriched vanadium and nickel concentrations in liptinitic and sporopolleninic bitumens. The exclusion of ligninic bitumens from vanadium or nickel enrichment may be explained by the difficulty in preserving tetrapyrrole complexes in organic matter derived from higher plants. Tetrapyrrole complexes are the most preferred and stable metallo-organic complexes of vanadium and nickel, and the preservation of their chlorophyll precursors is critical to their occurrence in the organic matter of sediments and sedimentary rocks (Chapter 4.1). Similar to phytoplankton, higher plants also contain significant amounts of chlorophyll, (Table 5.2), but unlike the subaqeous habitat of phytoplankton, the intense light and highly aerobic subaerial habitat of higher plants insures rapid and complete decomposition of chlorophyll at death.

Preferential decomposition of chlorophyll occurs during the late stages of senescence before the death of a plant (Bidwell, 1974, pp. 483-493), and as a result complete decomposition of chlorophyll usually occurs

Table 5.2: Concentrations of tetrapyrrole pigments in phytoplankton and higher plants.

Substance	Pigment	*Concentration	Reference
Phytoplankton	Chlorophylls	3,000-67,000	Vallentyne (1960)
Phytoplankton	Chlorophylls	30,000	Didyk et al. (1978)
Phytoplankton (Diatoms)	Chlorophylls	23,270	Pace (1941)
Hazel Leaves (Green on Tree)	Chlorophylls	9,680	Sanger (1968)
Aspen Leaves (Green on Tree)	Chlorophylls	4,650	Sanger (1968)
Oak Leaves (Green on Tree)	Chlorophylls	5,450	Sanger (1968)
Falling Oak Leaves (During Autumn)	Chlorophylls Pheophytins	0 300	Sanger (1971b)
Fallen Oak Leaves (Over-wintering on the ground)	Chlorophylls Pheophytins	0 100	Sanger (1971b)

*Concentrations based on dry weight of substance in ppm.

before a plant is masticated, uprooted, or macerated. Studies on deciduous trees by Sanger (1968, 1971a, 1971b) have shown that decomposition of chlorophyll in leaves is rapid and essentially complete before the leaves are detached from their stems. Thus it appears that kerogens and bitumens derived from higher plants are likely to be deficient in tetrapyrrole complexes and as a result are not likely to be enriched in vanadium and nickel.

Although preferential decomposition of chlorophyll also occurs in defunct phytoplankton as they settle through a water column, the less severe conditions of their subaqueous habitat provides a greater probability for preservation of their chlorophyll (Chapter 4.1). Indirect evidence for the preservation of greater amounts of tetrapyrrole complexes in organic matter derived from plankton as compared to organic matter derived from higher plants is the low nitrogen contents in ligninic kerogens (Waples, 1977). Figure 5.13 shows that liptinitic kerogens have a greater nitrogen content than ligninic kerogens, and this difference corresponds with the ability of their bitumens to be enriched in vanadium and nickel. The intermediate character of sporopolleninic bitumens and kerogens suggests that minor amounts of tetrapyrrole complexes may be incorporated into some sporopollenins. Although this would be unlikely for the low nitrogen bearing sporopollenins derived from spores or pollens (atomic N/C ratio$\leq$0.011; Brooks, 1971), it would be possible for sporopollenin derived from the cell walls of green algae (e.g., Good and Chapman, 1978; Atkinson et al., 1972) where chlorophyll would be more accessible. Thus, liptinitic organic matter appears to be

Figure 5.13: Plot comparing the atomic N/C ratio of the three kerogen types with the vanadium plus nickel concentrations in their bitumens. The samples used include I-1, F-1, F-2, and H-1 for ligninic kerogen bearing rocks, MR-5 thru MR-10, MR-12, MR-13, and K-1 thru K-5 for liptinitic kerogen bearing rocks, and GR-1, GR-3 thru GR-7, GR-10 thru GR-13, GR-15 thru GR-21, GR-25 thru GR-27, GR-29, GR-30, GR-32, GR-34, and GR-37 thru GR-39 for sporopolleninic kerogen bearing rocks.

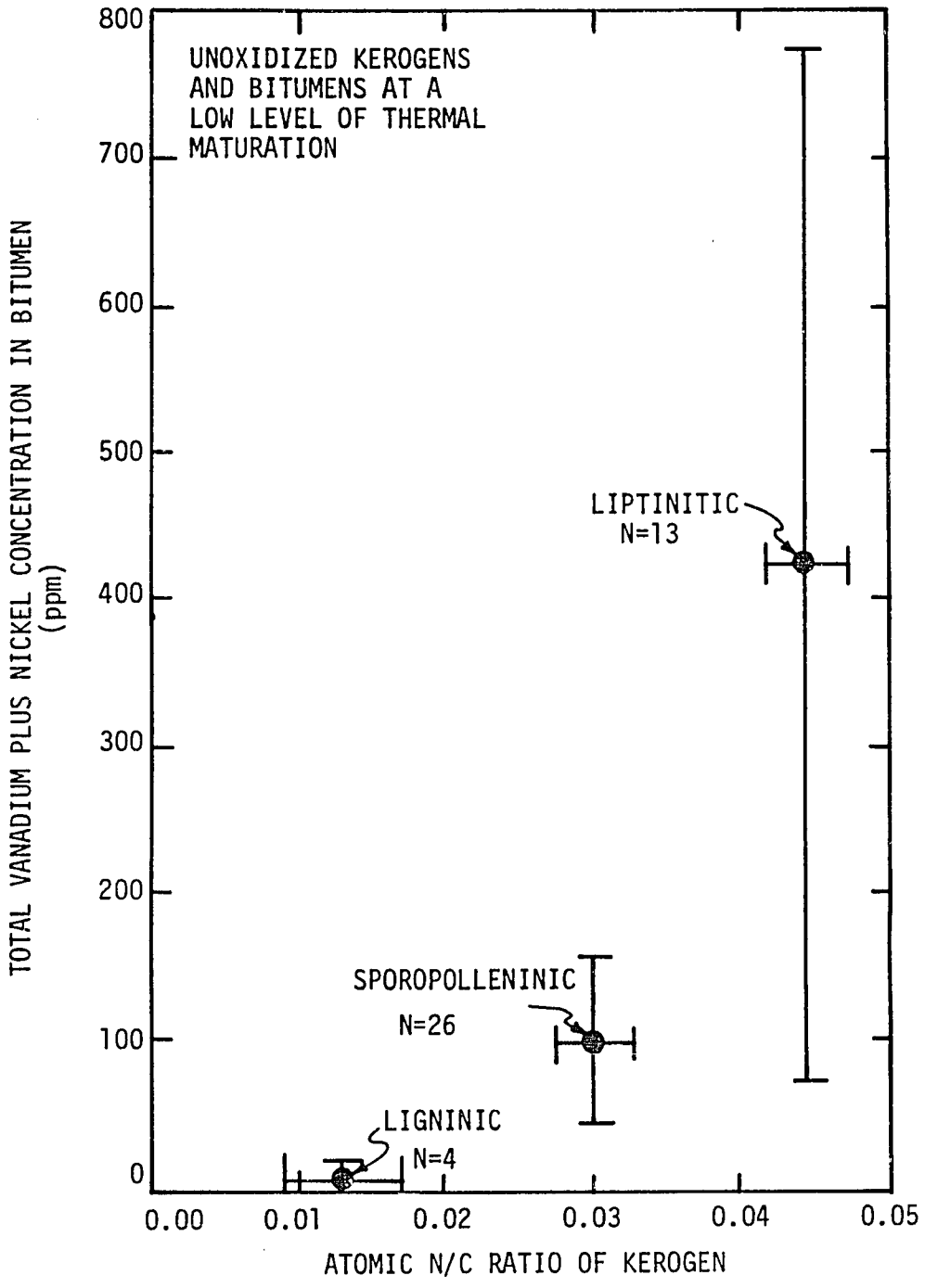

FIGURE 5.13

the most favorable for concentrating vanadium and nickel because of the higher chlorophyll content of its precursors relative to sporopolleninic organic matter, and the higher probability of tetrapyrrole preservation in the habitat of its precursors relative to ligninic organic matter.

In summary, the amount of vanadium and nickel concentrated in organic matter appears to be dependent on three primary factors; 1) amount of tetrapyrrole complexes in an accumulation of organic matter, 2) flux of metals through a sediment column, and 3) duration of an open sediment system. A list of these primary factors and some of the salient variables that control them are given in Table 5.3. In this study the amount and percent of metallated tetrapyrroles were not determined, and as a result a proper evaluation of the importance and interrelations of these three factors in specific cases could not be undertaken. In future studies, the determination of amount and percent of metallated tetrapyrroles could allow the assessment of the other two primary factors and their controlling variables. In addition, the amount of tetrapyrroles preserved in the organic matter of a sedimentary rock may reveal information on the conditions of the overlying water column. Studies of this type have been and are being undertaken on recent sediments (Brown, 1979, personal communique; Daley et al., 1977; Sanger and Gorham, 1970; Brown, 1969) and their application to organic matter in sedimentary rocks may prove to be useful in evaluating the conditions of paleoenvironments.

Table 5.3: Primary factors determining the amount of vanadium and nickel concentrated in organic matter and their controlling variables.

Primary Factors	Controlling Variables
1. Amount of Tetrapyrrole Complexes	a. Amount and type of organic matter
	b. Exposure time to aerobic conditions
	c. Oxygen concentration of aerobic conditions
2. Metal Flux in Sediment Column	a. Metal concentration in overlying water body
	b. Mineralogy of sediment column
	c. Tortuosity of diffusion path
3. Duration of Open Sediment System	a. Compaction rate of sediment column
	b. Rate of sedimentation
	c. Depositional frequency of impermeable beds in the sediment column

CHAPTER 6

FACTORS CONTROLLING THE PROPORTIONALITY OF VANADIUM AND NICKEL

The most likely control on the proportionality of vanadium to nickel in tetrapyrrole complexes is the relative availability of vanadyl (VO^{+2}) to nickelous (Ni^{+2}) cations in the interstitial waters during metallation. The three factors that appear to exert the greatest influence on their availability are the redox potential, hydrogen ion activity, and biogenic sulfide activity in the sediment system. The influence and interrelationships of these three factors are most easily envisaged with Eh-pH diagrams.

6.1 CONSIDERATIONS IN THE CONSTRUCTION AND NATURAL LIMITS OF Eh-pH DIAGRAMS

The Eh-pH diagrams presented in this chapter were constructed in accordance with the thermodynamic relationships described by Garrels and Christ (1965). The total dissolved element concentrations used in the construction of the diagrams were those found in average sea water as reported by Goldberg (1961; i.e., in moles per liter $\Sigma V=10^{-7.41}$, $\Sigma N.=10^{-7.48}$, $\Sigma S=10^{-1.56}$, and $\Sigma C=10^{-2.63}$). The diagrams constructed with these concentrations are also applicable to fresh waters and interstitial waters, whose deviations from these values do not cause appreciable variations in their stability fields. This is demonstrated by comparing

Eh-pH diagrams for vanadium at normal sea water concentrations ($10^{-7.48}$ moles/liter) with concentrated vanadium in evaporated sea water that has lost 95 weight percent of its water ($10^{-6.13}$ moles/liter). As shown in the Eh-pH diagram in Figure 6.1, the difference between these two diverse concentrations is not appreciable, with a maximum pH variation of 0.75 units in the VO^{+2} - $VO(OH)_2$ boundary and a maximum Eh variation of 0.9 volts in the V^{+3} - $V(OH)_3$ boundary. The Gibbs free energies and reactions considered in constructing the Eh-pH diagrams are given in Appendices IX and X, respectively. All of the diagrams represent conditions at 298°K and 1 ATM, and appreciable variations in the stability fields are not likely for conditions with temperatures from 0 to 50°C (Evans and Garrels, 1958) and pressures in the tens of atmospheres (Garrels and Christ, 1965, p. 261). Stage II of the tetrapyrrole diagenesis series occurs well within these limits,and suggests that the diagrams are reasonable approximations of the stability fields that occur during metallation of the tetrapyrroles in sediment systems.

Sulfide and carbonate reactions were considered in the construction of Eh-pH diagrams for nickel but not for vanadium. This is because vanadium carbonates and sulfides are not common in nature and thermodynamic data is not available on their formation. Patronite (VS_4) and Sulvanite (Cu_3VS_4) are the two known vanadium sulfides (Evans, 1970), and their rarity in nature supports the non-chalcophilic character of terrestrial vanadium proposed by Goldschmidt (1954, p. 25).

Figure 6.1: Eh-pH diagrams showing the difference between the stability fields for a total dissolved vanadium concentration of $10^{-6.13}$ moles/liter (dashed lines) and those for a total dissolved vanadium concentration of $10^{-7.48}$ moles/liter.

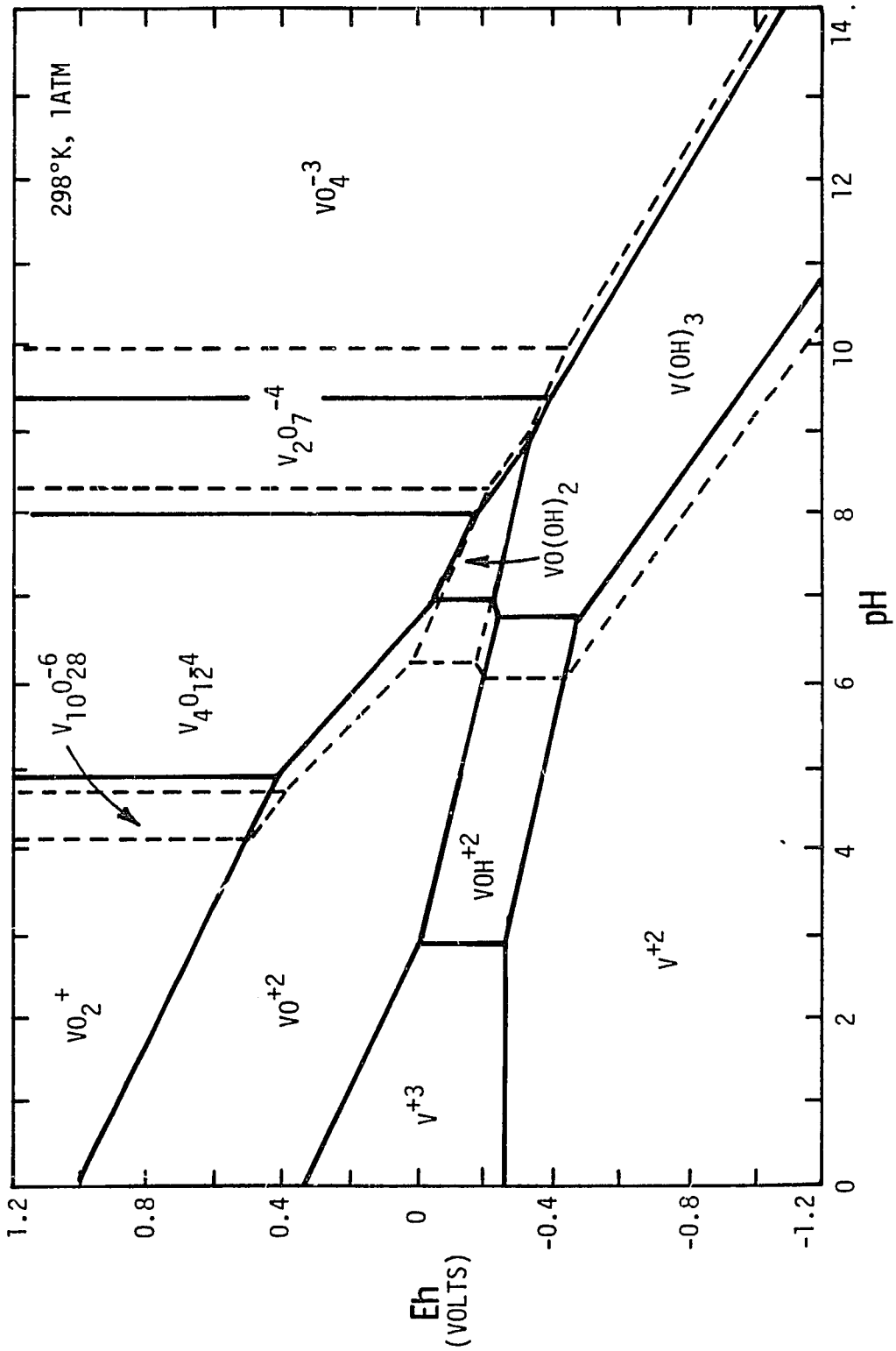

FIGURE 6.1

Although α-NiS is considered a high temperature polymorph of millerite (β-NiS; Kullerud and Yung, 1962), its Gibbs free energy of formation was used in constructing the Eh-pH diagram for nickel. The choice of the α-polymorph is based on its higher Gibbs free energy and the premise that under diagenetic conditions nickel sulfides behave similar to iron sulfides. Berner (1964a, and 1967) has found that metastable iron sulfide precipitates with high Gibbs free energies form prior to the more stable pyrrhotite and pyrite, which have lower Gibbs free energies (Table 6.1). The inclusion of metastable diagenetic phases in an Eh-pH diagram is important in achieving an accurate conception of a chemical system in nature (Berner, 1964b), and the use of α-NiS is the most likely choice from this standpoint.

The natural limits for surface and diagenetic conditions are considered to be the stability field for water (Krauskopf, 1967). In Figure 6.2, the outlines of data compiled by Baas Becking and others (1960) shows that more confined stability fields exist for interstitial waters of marine and marginal marine sediments. These stability fields may be reduced further by considering only organic sediments, which usually occur in or induce negative Eh conditions (Krumbein and Garrels, 1952). These conditions are represented by the stippled area in Figure 6.2 and will be considered to be representative of the natural stability field for organic sediments in the following discussions.

Table 6.1: Gibbs free energies of formation for iron and nickel sulfides at 298°K and 1 ATM. Values were obtained from references cited in Appendix IX.

IRON SULFIDES

Low Temperature Phase	ΔG_f° (kcal)	High Temperature Phase	ΔG_f° (kcal)
Black Precipitate (FeS)	-21.3	Trolite (FeS)	-22.9
Mackinawite (FeS)	-22.3		
Pyrrhotite (FeS)	-24.2		
Marcasite (FeS_2)	-37.9		
Pyrite (FeS_2)	-38.3		

NICKEL SULFIDES

Low Temperature Phase	ΔG_f° (kcal)	High Temperature Phase	ΔG_f° (kcal)
Millerite (β-NiS)	-20.6	α-NiS	-17.7
γ-NiS	-27.3		
Vaesite (NiS_2)	-34.0		

Figure 6.2: Natural stability fields for water (solid lines; Krauskopf, 1967, pp. 245-246), marine sediments (dotted-solid line; Baas Becking, et al., 1960), marginal marine sediments (dashed line; Baas Becking, et al., 1960), and organic sediments (shaded area; Krumbein and Garrels, 1952).

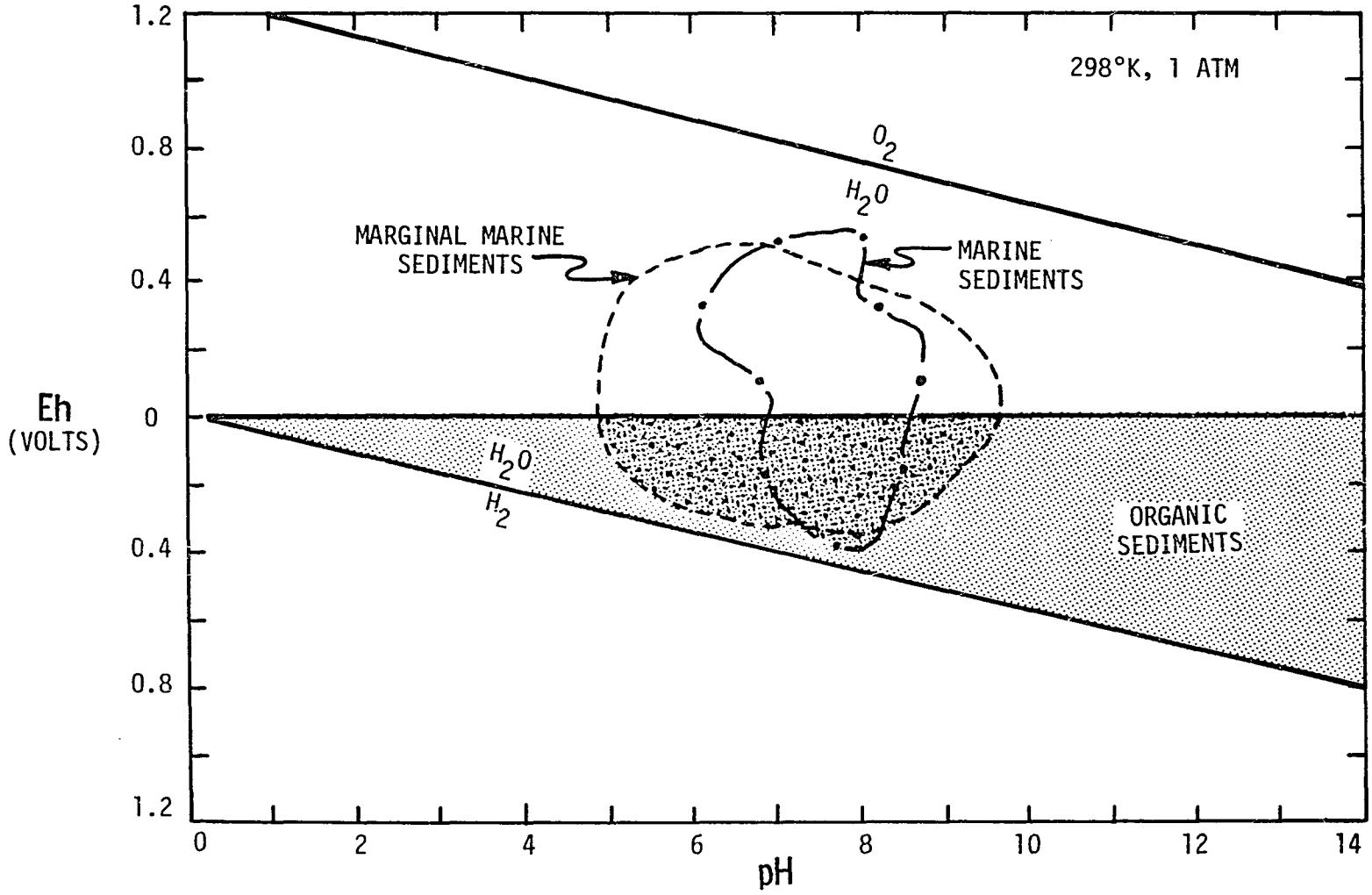

FIGURE 6.2

6.2 SIGNIFICANCE OF THE STABILITY FIELDS FOR VO^{+2} AND Ni^{+2}

As stated in Chapter 4, vanadyl and nickelous cations are the most preferred metal cations for bonding with tetrapyrrole complexes. Based on their similar ionic radii, ligand field stabilization energies, thermal stability, and resistance to highly acidic solutions (Table 6.2), these two cations appear to have an equal affinity for bonding with tetrapyrrole complexes. This suggests that the proportionality of vanadium to nickle bound to tetrapyrrole complexes in a sediment column is controlled by the proportionality of VO^{+2} to Ni^{+2} in the interstitial waters. This proportionality is controlled by the total dissolved concentration of both metals, redox potential (Eh), hydrogen ion activity (pH), and biogenic sulfide activity in the interstitial waters. When considering similar rock types of a particular age in a given basin, the total dissolved concentration of vanadium and nickel may be assumed constant with Eh, pH, and biogenic sulfide activity being the primary factors controlling variations in the proportionality of vanadium to nickel in the organic matter. When considering different rocks (e.g. claystone, marlstone, and micstone) in the same basin or similar rock types in different basin, this assumption may not be true, and should be evaluated.

6.2.1 Stability Field for VO^{+2}

The Eh-pH diagram representing vanadium under surface and mild diagenetic conditions is shown in Figure 6.3. As stated in Chapter 4,

Table 6.2: Parameters reflecting stability of vanadyl and nickelous cations in tetrapyrrole complexes.

Parameter	VO^{+2}	Ni^{+2}
Ionic Radius of Metal in Cation (A; Ahrens, 1952, Table 16)	0.63	0.69
Activation Energy for Removal of Metal from Porphyrin (kcal/mole; Hodgson and Baker, 1957)	58.6	57.5
Ligand Field Stabilization Energy (Δo; Table 4.3)	1.20	1.20
Amount of Metal Leached from Bitumen by Concentrated Sulfuric Acid at 150°C (Wt.%; Table 4.5)	88.95	84.88

Figure 6.3: Eh-pH diagram for vanadium at sea water concentrations under surface and mild diagenetic conditions ($\Sigma S = 10^{-2.63}$ mol/liter and $\Sigma CO_2 = 10^{-2.63}$ mol/liter. Hatched area represents the stability field for vanadyl species. Explanation of stippled area and broken lines is given in Figure 6.2.

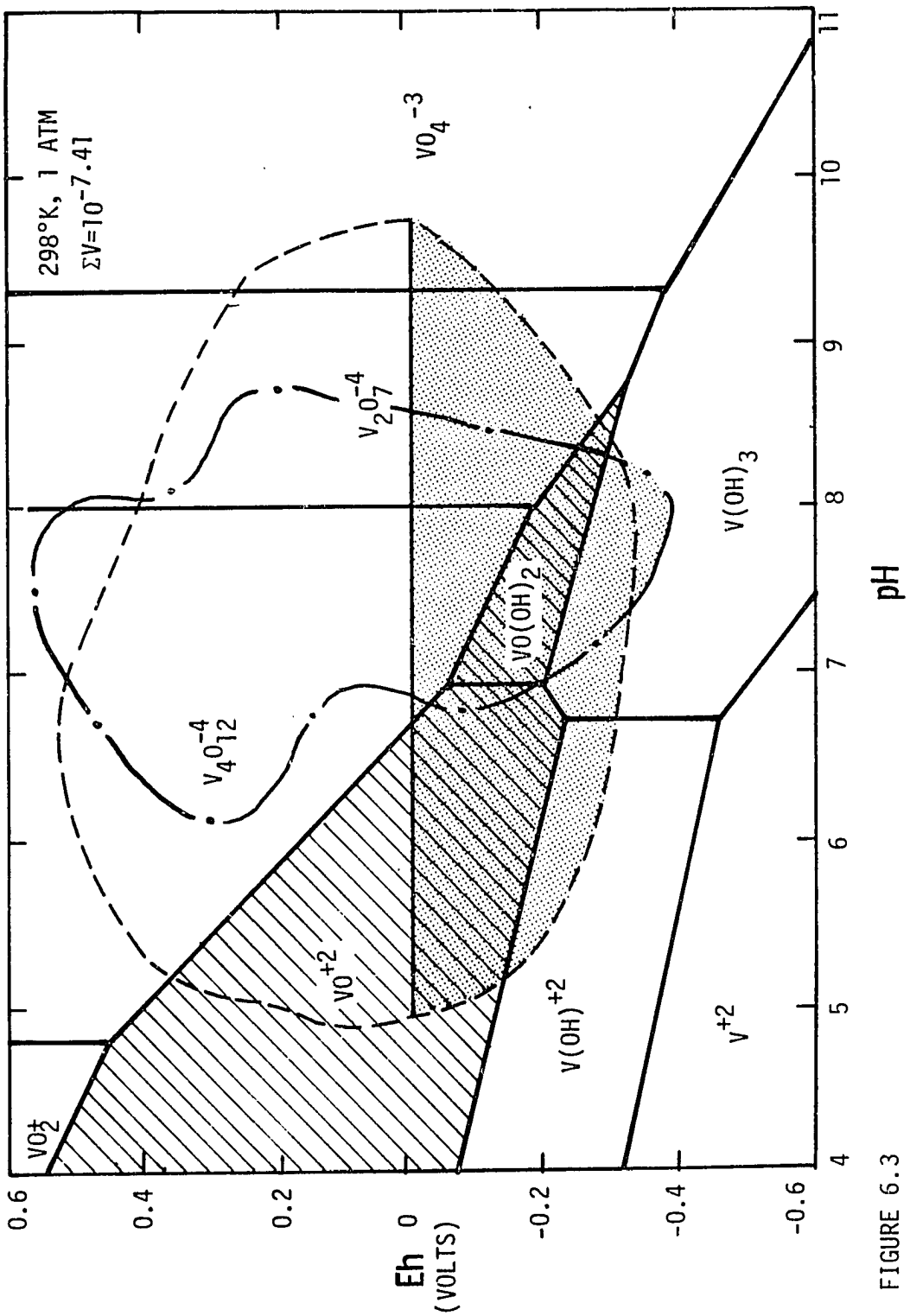

FIGURE 6.3

quadrivalent vanadium in the form of the vanadyl cation (VO^{+2}) is the species bound in tetrapyrrole complexes. Quinquivalent vanadium is unacceptable in bonding with tetrapyrrole complexes because of its polynuclear and anionic character in the aqueous state (e.g. $V_4O_{12}^{-4}$, $V_2O_7^{-4}$, and VO_4^{-3}). Conversely, trivalent vanadium in the aqueous state is mononuclear and cationic in character (eg. VOH^{+2}), but its existence under surface and mild diagenetic conditions is limited, and its presence in naturally occurring organic substances has not been reported.

As shown in Figure 6.3, the stability field for the vanadyl species becomes tapered with increasing pH and consists of two species; 1) VO^{+2} as a free cation and 2) VO^{+2} as a hydroxide ($VO(OH)_2$). Under acid conditions (pH<6.93, Reaction (2), Appendix IX) the free vanadyl cation (VO^{+2}) will be available for bonding with tetrapyrrole complexes. Under more basic conditions (pH>6.93) the vanadyl cation will be associated with hydroxide ions ($VO(OH)_2$) and this may hinder its ability to bond with tetrapyrrole complexes. Energetic considerations suggest that vanadyl hydroxide ($VO(OH)_2$) should precipitate out of solution in this stability field, but kinetic considerations suggest that this would be unlikely at these very dilute concentrations ($\Sigma V=10^{-7.41}$ moles per liter). Instead, the vanadyl cation in this field is more likely to exist as an aqueous hydroxide, whose stability would increase with increasing pH. Although the spectrochemical series (i.e., $I^-<B_r^-<Cl^-<F^-<OH^-<NCS^-<NH_3 <NO_2^-<CN^-$; Baes and Mesmer, 1976, p. 197) indicates that vanadyl cations would prefer the nitrogen ligands of the

tetrapyrrole complexes rather than hydroxide ligands, the increase in the stability of neutral aqueous vanadyl hydroxides with increasing pH is likely to cause an increase in the hindrance of vanadyl cation bonding to tetrapyrrole complexes.

Thus, it is postulated that within the free VO^{+2} stability field, the bonding of the vanadyl cation to tetrapyrrole complexes will occur readily and unhindered, while within the $VO(OH)_2$ stability field an increasing hindrance on the bonding of the vanadyl cation to tetrapyrrole complexes will become more pronounced with increasing pH. The aqueous vanadyl species that occurs in the $VO(OH)_2$ stability field is probably $VO(OH)_3^-$ with the oligomer $V_4O_9^{-2}$ being less likely (Iannuzzi and Rieger, 1975). The actual stability field for $VO(OH)_3^-$ anion represents the most hydroxylate species of vanadyl in basic solutions, and less hydroxylated species (i.e, $VO(OH)_2^o$ and $VO(OH)^+$) may occur as the pH is lowered.

6.2.2 Stability Field for Ni^{+2}

The Eh-pH diagram representing nickel under surface and mild diagenetic conditions is shown in Figure 6.4. The stability field for the nickelous cation (Ni^{+2}) in organic sediments is tapered in the direction of decreasing pH values (hatched-stippled area, Figure 6.4). Within this field the nickelous cation will be available for bonding with tetrapyrrole complexes, provided the activity of biogenic sulfide generated by sulfate-reducing bacteria is low. In modern sediments, sulfate-reducing

Figure 6.4: Eh-pH diagram for nickel at sea water concentrations under surface and mild diagenetic conditions ($\Sigma S = 10^{-1.56}$ mol/liters and $\Sigma CO_2 = 10^{-2.63}$ mol/liters). Hatched area represents the stability field for the nickelous cation (Ni^{+2}). Explanation of stippled area and broken lines is given in Figure 6.2.

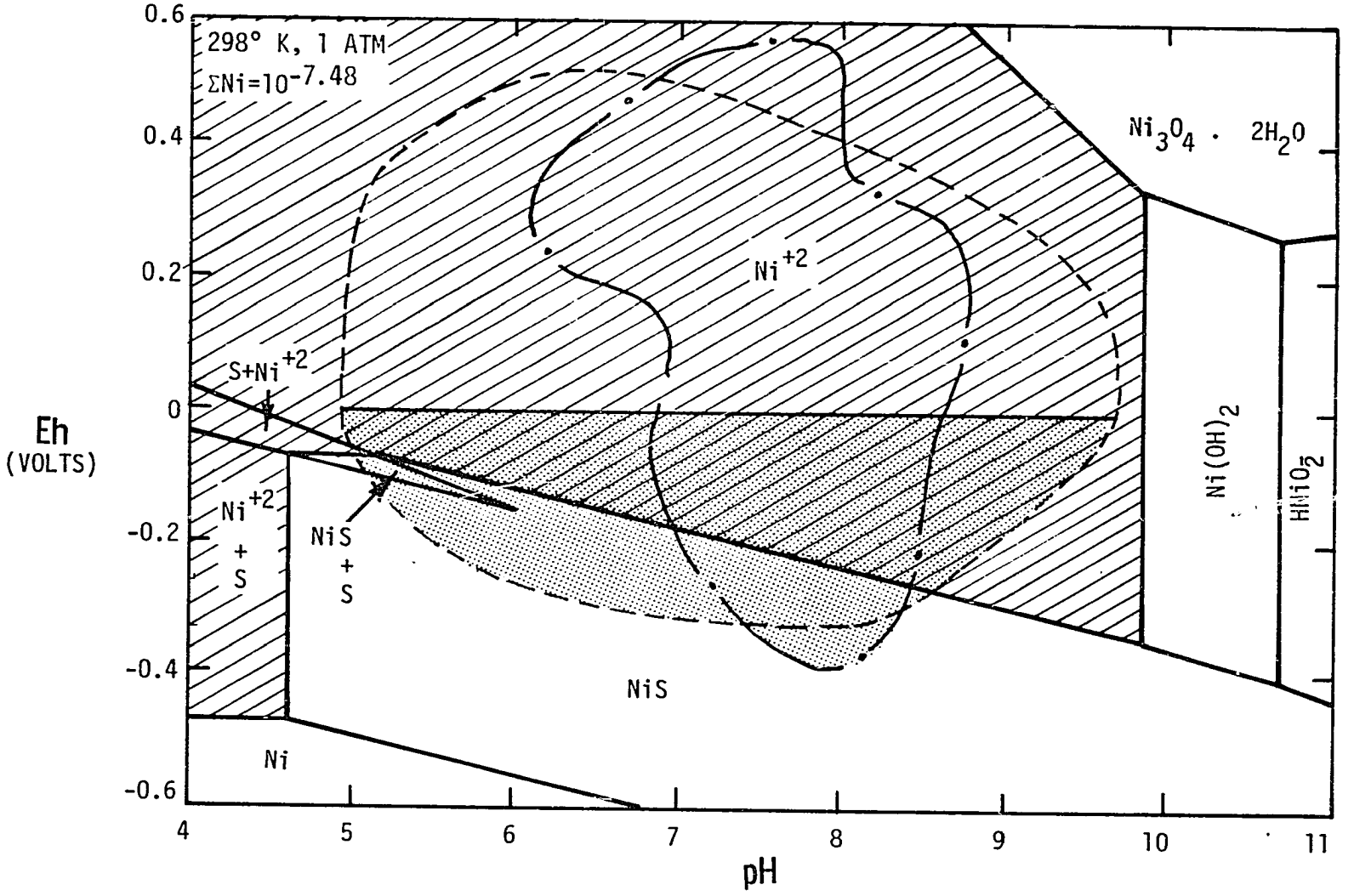

FIGURE 6.4

bacteria, such as Desulfovibrio and Desulfotomaculum, are common in anaerobic environments containing sulfate (Stanier et al., 1976, p. 710). The hydrogen sulfide they produce usually reacts with dissolved iron and results in the precipitation of iron sulfides (Berner, 1970 and 1972; and Goldhaber and Kaplan; 1975). As shown by the negative Gibbs free energies for iron- and nickel-sulfide reactions in Table 6.3, the nickelous cation has a greater affinity for sulfide than ferrous iron. Therefore in the presence of biogenic sulfide, it would appear likely that nickelous cations would form aqueous sulfide complexes or coprecipitate with iron sulfides. As the activity of biogenic sulfide increased in the interstitial water of a sediment, the ability of nickelous cations to bond with tetrapyrrole complexes is expected to decrease. The activity of biogenic sulfide is primarily dependent on the reduction rate of the sulfate reducing bacteria. Numerous investigations on the factors controlling sulfate reduction of bacteria have been conducted (Harrison and Thode, 1958; Mechalas and Rittenberg, 1960; Kaplan and Rittenberg, 1964; Kemp and Thode, 1968; Ramm and Bella, 1974; McCready, and Kaplan, 1974; and McCready, 1975), and from these investigations there appear to be four prominent factors that control the rate of bacterial sulfate reduction; 1) temperature, 2) sulfate concentration, 3) amount of organic matter, and 4) type of organic matter.

Laboratory experiments with Desulfovibrio have shown that their rate of sulfate reduction increases significantly with increasing temperature (Harrison and Thode, 1958; Kaplan and Rittenberg, 1964; Kemp and Thode, 1968; and McCready, 1975). McCready (1975) showed that the rate of

Table 6.3: Reactions between iron- and nickel-sulfides and their Gibbs free energy of reaction (ΔGr). Values based on Gibbs free energies of formation given in Appendix IX.

Reaction	ΔG_r^o (kcal)
Ni^{+2} + FeS (Precipitate) $\rightleftarrows$ α-NiS + Fe^{+2}	-5.17
Ni^{+2} + FeS (Mackinawite) $\rightleftarrows$ NiS (Millerite) + Fe^{+2}	-7.07
Ni^{+2} + FeS (Pyrrhotite) $\rightleftarrows$ α-NiS + Fe^{+2}	-11.87
Ni^{+2} + FeS_2 (Marcasite) $\rightleftarrows$ NiS_2 (Vaesite) + Fe^{+2}	-4.87
Ni^{+2} + FeS_2 (Pyrite) $\rightleftarrows$ NiS_2 (Vaesite) + Fe^{+2}	-4.47

*Values based on Gibbs free energies of formation given in Appendix IX.

sulfate reduction by Desulfotomaculum nigrificans increased by a factor of 5 between 38° and 55°C. In nature the temperature of the interstitial water of a sediment will be controlled primarily by the temperature of the overlying water body, which, in turn will be controlled by the climate, water depth, and water circulation.

The integration of laboratory results by Harrison and Thode (1958) and Kaplan and Rittenberg (1964) suggests that the rate of sulfate reduction by Desulfovibrio is unchanged by the sulfate concentration within the range of 10^{-3} to 10^{-1} moles of sulfate per liter, but does decrease as sulfate concentrations increase towards 10^{-3} moles per liter and as sulfate concentrations increase from 10^{-1} moles per liter. The initial concentration of sulfate in interstitial water will be controlled primarily by the sulfate concentration in the overlying water. The concentrations in Table 6.4 suggest that in normal marine sediments the concentration of sulfate is not likely to exert a significant control on the rate of bacterial sulfate reduction, but in fresh water sediments and sediments associated with evaporites and brines, the concentration of sulfate may exert a significant control on the rate of bacterial sulfate reduction.

The rate of bacterial sulfate reduction is sensitive to the type and amount of organic matter available (Table 6.5), which have been emphasized as important factors by several investigators (Kaplan and Rittenberg, 1964; McCready, 1975; and Goldhaber and Kaplan, 1975; Lyons and Gaudette, 1979). Anaerobic bacterial degradation is restricted

Table 6.4: Sulfate concentrations in natural waters.

Type of Water	log $M_{SO_4}^{-2}$ (mol/l)
Average sea water (Goldberg, 1961)	-1.54
Average river water (Berner, 1971, p.42)	-3.93
Range for lake water (Livingstone; 1963)	<-5.00 to -0.58
Evaporite water at gypsum precipitation (calculated)	-0.82
Range of brines (Collins, 1975, p. 413)	<-5.00 to -1.47

Table 6.5: Effect of type and amount of metabolite on rate of bacterial sulfate reduction.

Metabolite (Hydrogen Donor)	Concentration of Metabolite (mol/l)	Rate of Sulfate Reduction (M_{H_2S}/cell/hr x 10^{-6})
Hydrogen[1]	0.001	5.5
Ethanol[1]	0.1	4.2
Lactate[1]	0.1	4.0
Mannose[1]	0.1	0.3
Mucin[1]	?	~0.2
Glucosame[1]	0.1	~0.1
Dextrose[1]	0.1	~0.1
Lactate[2]	0.096	5.9
Lactate[2]	0.084	5.3
Lactate[2]	0.075	4.9
Lactate[2]	0.063	5.5
Lactate[2]	0.052	5.6
Lactate[2]	0.021	4.6
Lactate[2]	0.010	4.8
Lactate[2]	0.0021	1.1
Lactate[2]	0.0010	0.7
Lactate[2]	0.0007	0.4

[1] Kemp and Thode (1968, Table 4, 35.5°C)

[2] Kaplan and Rittenberg (1964, Table 2, 30°C)

primarily to the proteinaceous and carbohydrate constituents in organic matter (Zobell, 1946a) and their character and quantities determine the types and amounts of metabolites available for sulfate-reducing bacteria (Goldhaber and Kaplan, 1974, and 1975). Although favorable metabolites are made available in laboratory experiments, their availability in nature appears more variable due to their high susceptibility to aerobic bacterial degradation (Zobell, 1946a). Thus, organic matter that has been subjected to high levels of aerobic bacterial degradation before encountering anaerobic conditions will be deficient in proteinaceous compounds and carbohydrates, and as a result the rate of bacterial sulfate reduction will be low. Conversely, organic matter that has been subjected to low levels of aerobic bacterial degradation before encountering anaerobic conditions will retain appreciable quantities of proteinaceous compounds and carbohydrates, and as a result the rate of bacterial sulfate reduction will be high. A continuum between these two extremes is likely to occur in nature, with the level of aerobic bacterial degradation being controlled by temperature, height of aerobic water column, rate of sedimentation, and oxygen content of encountered aerobic conditions. The relationships between these variables at a constant temperature are shown conceptually in Figure 6.5. Decreasing temperature would retard aerobic bacterial degradation (Stanier et al., 1976, p. 306).

As shown in Figure 6.4, the stability field for the nickelous cation in organic sediments is limited at low Eh values by the inorganic formation of nickel sulfide. Sulfate does not exist within this stability field

Figure 6.5: Conceptual view of relationships between height of aerobic water column, rate of sedimentation, oxygen content of encountered aerobic conditions, and probability of carbohydrate preservation. Oxygen levels are classified in accordance with Rhoads and Morse (1971, Figure 5; aerobic $\geq$ 1.0 ml O_2/liter, dysaerobic = 0.1 to 1.0 ml O_2/liter, and anaerobic < 0.1 ml O_2/liter).

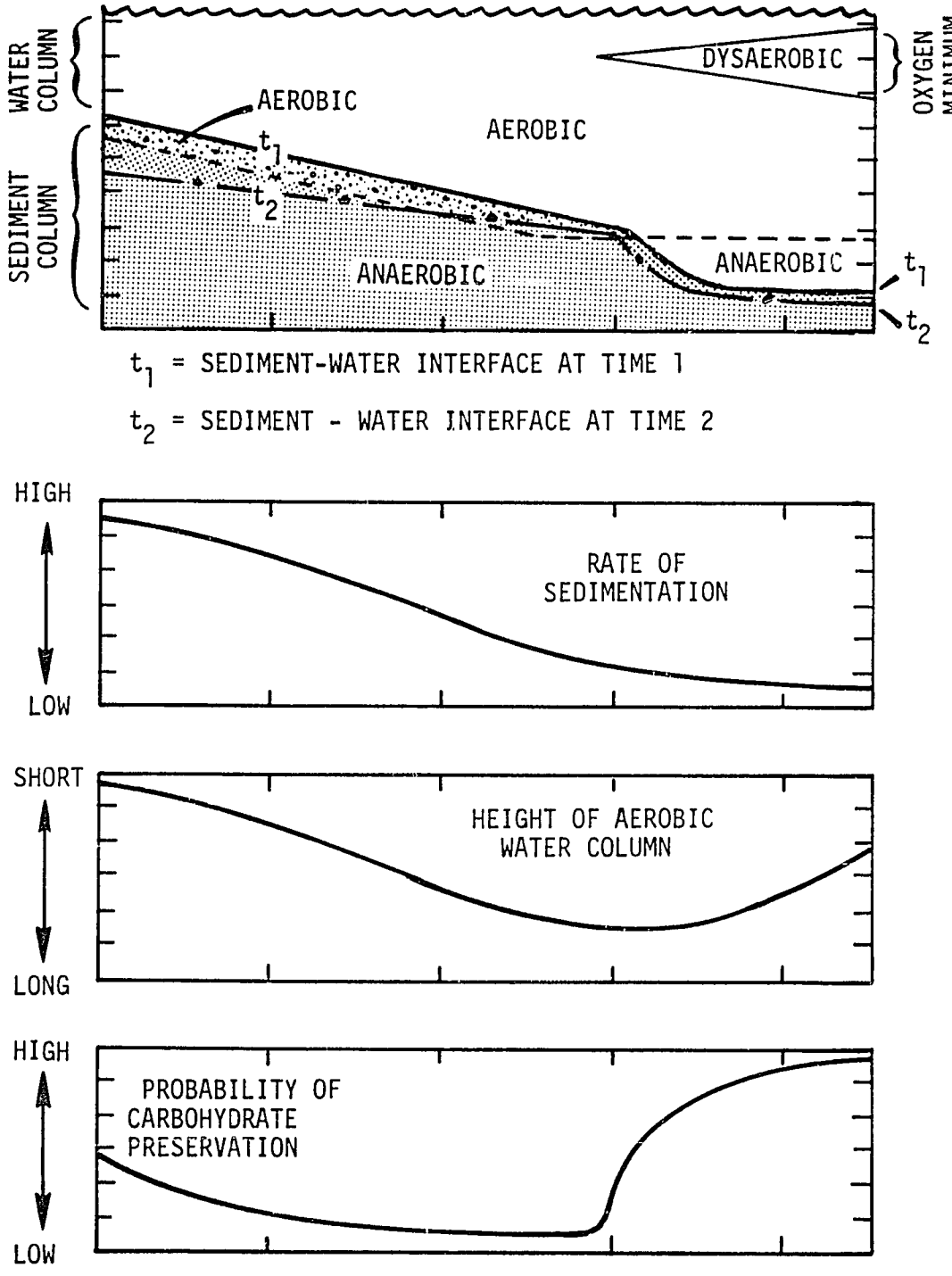

FIGURE 6.5

because of its inorganic reduction to sulfide, and as a result the activity of sulfate-reducing bacteria is terminated. Essentially all the sulfur in the interstitial waters will exist as sulfide under these conditions, and the high affinity of nickel for sulfide (Table 6.3) suggests that the development of nickel sulfide complexes or precipitates is likely to prevent the bonding of nickelous cations to tetrapyrroles.

6.3 DISCUSSION

The proportionality of vanadium and nickel in interstitial waters and tetrapyrrole complexes may be qualitatively evaluated by superimposition of the vanadium and nickel Eh-pH diagrams in Figures 6.3 and 6.4, respectively. This has been done in Figure 6.6, and for organic sediments the diagram may be categorized into six Eh-pH fields.

Eh-pH Field I represents conditions under which vanadium will occur as quinquivalent anions (eg. $V_4O_{12}^{-4}$, $V_2O_7^{-4}$, and VO_4^{-3}), which are not suitable for bonding with tetrapyrrole complexes. Conversely, nickel will be available for bonding with tetrapyrrole complexes in the form of nickelous cations. The generation of biogenic sulfide under these conditions may hinder the amount of nickel that will bond with tetrapyrrole complexes, but the complete unavailability of vanadyl cations suggests that the vanadium-nickel fraction will be very low ($V/(Ni+V) \leq 0.10$).

Eh-pH Field II represents conditions under which vanadyl cations will be available for bonding with tetrapyrrole complexes, but their availa-

Figure 6.6: Eh-pH diagram resulting from the superimposition of vanadium and nickel Eh-pH diagrams in Figures 6.3 and 6.4, respectively. Roman numerals designate major Eh-pH fields under which organic sediments may accumulate.

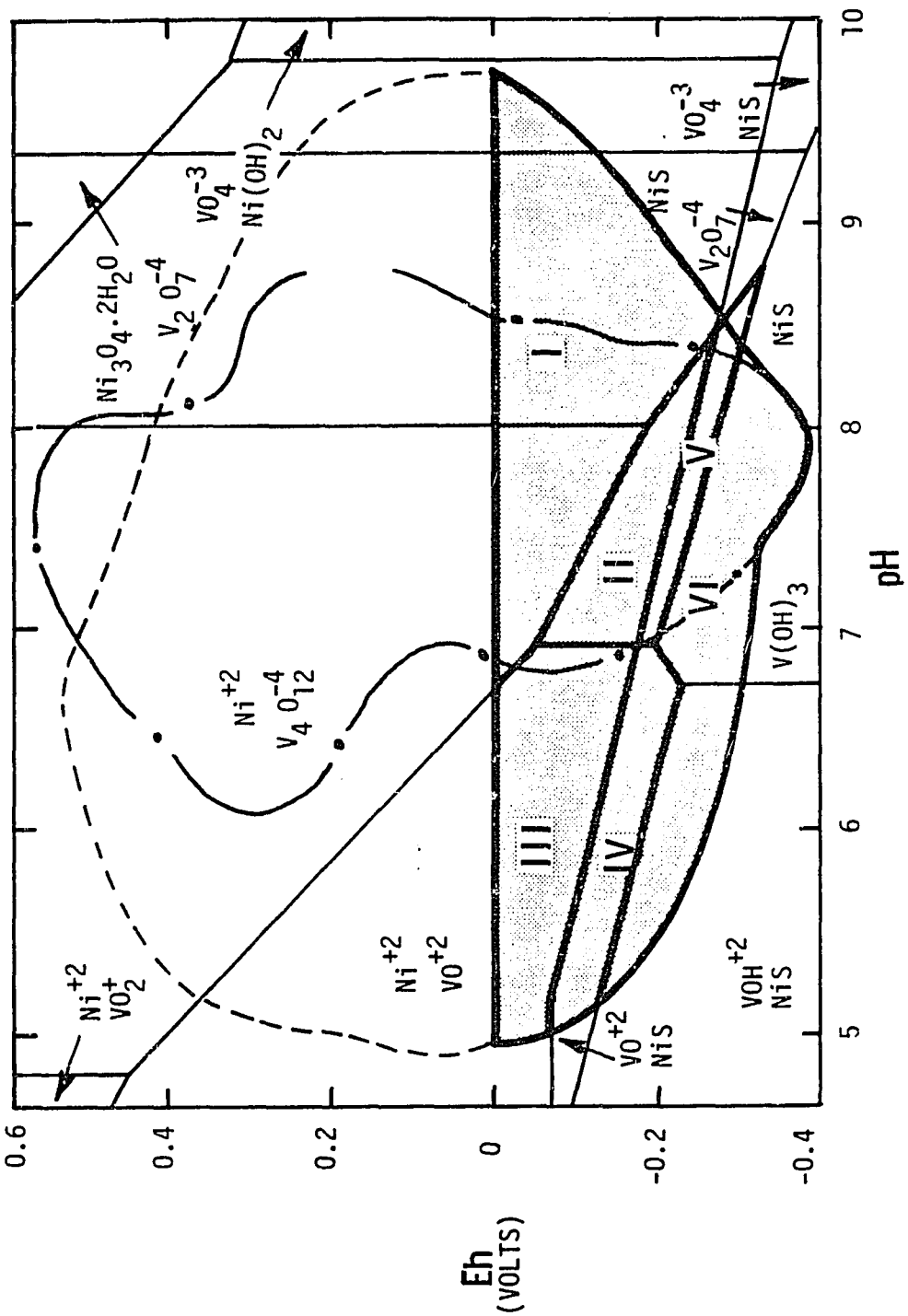

FIGURE 6.6

bility is expected to decrease with increasing pH within the field as a result of an increase in hydroxyl complexing. Nickelous cations will be available for bonding with tetrapyrrole complexes under these conditions provided the biogenic sulfide activity is low. The vanadium-nickel fraction of organic matter in Eh-pH Field II is likely to vary from moderate to low values (V/(Ni+V)=0.50 to 0.10).

Eh-pH Field III represents conditions under which both vanadyl and nickelous cations will be available for bonding with tetrapyrrole complexes. In this case, their proportionality will be controlled by the proportionality of dissolved vanadium and nickel in the interstitial waters, as well as the biogenic sulfide activity. The vanadium-nickel fractions for organic matter under these conditions could vary over the entire range of values (V/(Ni+V)=0.90 to 0.10).

Eh-pH Fields IV and V represent conditions under which nickelous cations will be unavilable for bonding with tetrapyrrole complexes because of their affinity to form inorganic sulfide complexes or precipitates. Conversely, vanadyl cations will be available for bonding with tetrapyrrole complexes, and will only be hindered by hydroxyl complexing as the pH increases within Eh-pH Field V. Vanadium will predominate under these conditions and the vanadium-nickel fraction is expected to be high ($V/(Ni+V) \leq 0.90$).

Eh-pH Field VI represents conditions under which nickel will be unavailable for bonding with tetrapyrrole complexes because of its affinity for

inorganic sulfides. Vanadium will occur as trivalent hydroxides (VOH^{+2} and $V(OH)_3$), which ligand field stabilization energies suggest are favorable for bonding in tetrapyrrole complexes (Table 4.3). Although this form of vanadium has not been reported in natural organic substances, it may account for the non-quadrivalent portion (11 to 29 weight percent) of vanadium in the unique Bachaquero and Lagunillas crude oils (Saraceno et al., 1961). If future investigations reveal that this unresolved vanadium is trivalent, then these unique crude oils may have been expelled from rocks that were derived from sediments bordering Eh-pH Field VI. The unavailability of nickel for bonding with tetrapyrrole complexes under these conditions suggests that the vanadium-nickel fraction will be very high ($V/(Ni+V) \leq 0.90$) provided bonding of trivalent vanadium to tetrapyrrole complexes occurs.

A summary of the chemistry of the Eh-pH fields described above is given in Table 6.6. With this in mind, the following sections will examine and interpret the vanadium-nickel fraction of bitumens from different organic rock types in the context of their geological settings.

6.4 GREEN RIVER FORMATION

The Green River Formation is of Eocene age (Wasatchian through Bridgerian; Gazin, 1959 and 1965) and occurs predominantly in four Tertiary basins; Green River Basin, Washakie Basin, Uinta Basin, and Piceance Creek Basin (Figure 6.7). Within these basins the Green River Formation was deposited in lacustrine environments that were surrounded in part by

Table 6.6: Summary of the vanadium and nickel species that are available and unavailable for bonding with tetrapyrrole complexes under different conditions as categorized in Figure 6.6.

Eh-pH	Vanadium		Nickel		Expected
Field	Available	Unavailable	Available	Unavailable	V/(Ni+V)
I	-	$V_4O_{12}^{-4}$, $V_2O_7^{-4}$, VO_4^{-3}	Ni^{+2}	$Ni^{+2}\cdot[S^{=}]_{Bio}$	$\leq$0.10
II	VO^{+2}	$VO(OH)^{+}$, $VO(OH)_2$	Ni^{+2}	$Ni^{+2}\cdot[S^{=}]_{Bio}$	0.10-0.50
III	VO^{+2}	-	Ni^{+2}	$Ni^{+2}\cdot[S^{=}]_{Bio}$	0.10-0.90
IV	VO^{+2}	-	-	NiS, NiS_2	$\geq$0.90
V	VO^{+2}	$VO(OH)^{+}$, $VO(OH)_2$	-	NiS, NiS_2	$\geq$0.90
VI	VOH^{+2}	$V(OH)_3$	-	NiS, NiS_2	$\geq$0.90

Bio = Biogenic

Figure 6.7: Tertiary basins in which Green River Formation occurs (modified from Van West, 1972).

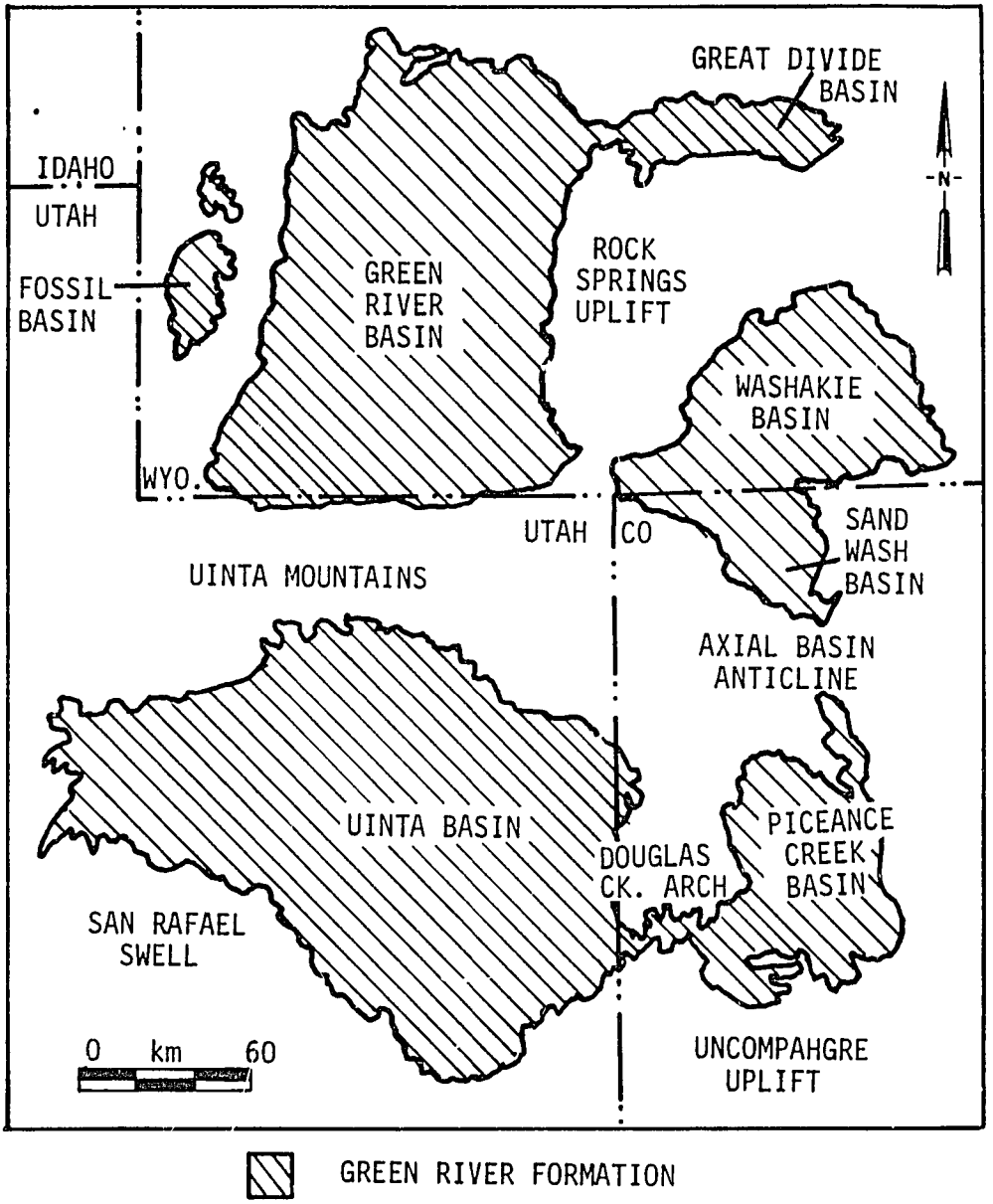

FIGURE 6.7

marginal fluvial and deltaic environments (Surdam and Wolfbauer, 1975; Ryder et al., 1976; Stanley and Surdam, 1978). Lake Gosiute and Lake Uinta were the two major lacustrine systems in which the Green River Formation was deposited. Lake Gosiute consisted of the Green River basin and Washakie Basin which apparently were not divided by the Rock Srings uplift during the deposition of the Green River Formation (Roehler, 1965). In this lacustrine system, evaporite beds of trona and halite are abundant (Bradley and Eugster, 1969) and suggest that Lake Gosiute was actually a playa-lake complex (Eugster and Surdam, 1973; Surdam and Wolfbauer, 1975; Eugster and Hardie, 1975). Lake Uinta consisted of the Uinta Basin with periodic communication with the Piceance Creek Basin being restricted by the Douglas Creek Arch (Surdam, 1979, personal communique). The relative abundance of fossils (Ryder et al., 1976) and the absence of bedded evaporites in Lake Uinta (Fahey, 1962) suggest that playa conditions were not prevalent in this lacustrine system. Although oil shales were deposited in both Lake Uinta and Lake Gosiute, it appears that they evolved independent of one another, and for this reason are discussed separately.

6.4.1 Lake Gosiute

The Green River Formation in Lake Gosiute has been divided into three members; Tipton, Wilkins Peak, and Laney Shale (Bradley, 1964; Figure 6.8). The Tipton Member occurs near the base of the Green River Formation and consists predominantly of oil shale and claystone (Roehler, 1968), which only contain fossils in the lower portion of the unit

Figure 6.8: Geological map and stratigraphic section of the Green River Formation in the Green River Basin of Wyoming (map modified after Van West, 1972). Sampling locality numbers correspond with those given in Appendix I.

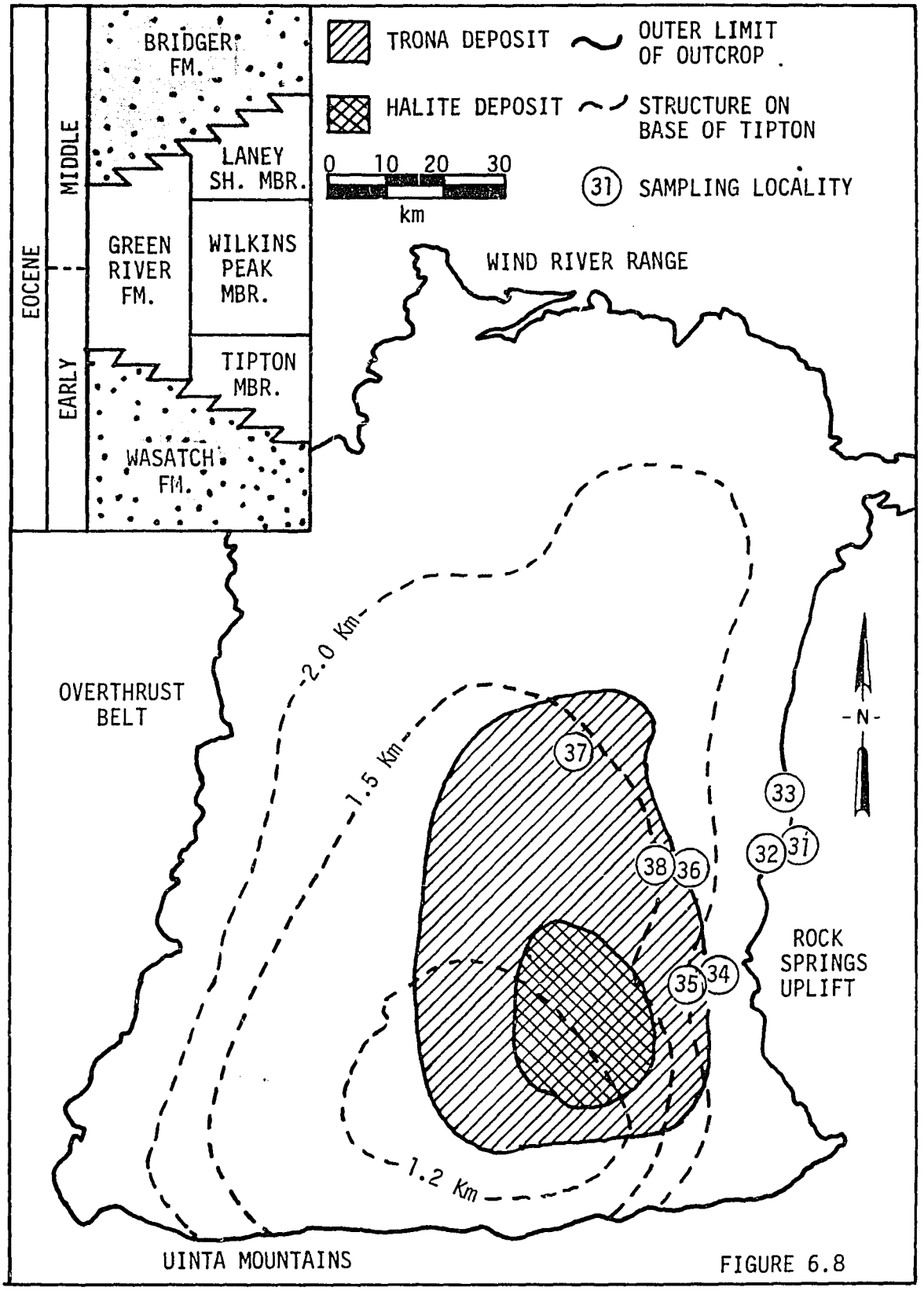

FIGURE 6.8

(Surdam and Wolfbauer, 1975). The middle and upper portions of the unit contain an abundance of analcime and are thought to have been deposited in high alkaline waters, which developed in Lake Gosiute as a result of excessive evaporation (Surdam and Wolfbauer, 1975). The evaporation and alkalinity appear to have increased during the deposition of the overlying Wilkins Peak Member, which contains bedded evaporites of trona and halite with interbedded marlstone and oil shale (Bradley and Eugster, 1969; Culbertson, 1971; Deardorff and Mannion, 1971; Eugster and Hardie, 1975). Following this Playa Lake condition, the alkalinity of Lake Gosiute appears to have decreased in its culminating phase (Surdam and Stanley, 1979). This is represented by the marlstone and oil shale of the overlying Laney Shale Member, which contain an abundance of fossil catfish (Lundberg and Case, 1970; Buchheim and Surdam, 1977).

In this study, sampling was confined to organic rich shales and to a lesser extent organic shales (Figure 6.9) from the Tipton Member and the Wilkins Peak Member in the eastern half of the Green River Basin (Figure 6.8). The kerogens from the Green River Formation in the Uinta Basin and Piceance Creek Basin have been reported to be primarily sporopolleninic kerogens (Tissot et al, 1978; Smith, 1974). In this study, visual and elemental analyses of kerogens from the Wilkins Peak Member and the Tipton Member show them to be the same type of kerogen. Visual analyses of these kerogens shows that they are greater than 95 percent β-sporopolleninic kerogen (Plate 3c). Although the source of these kerogens appears to be uniform, their elemental analyses suggest that they have experienced different degrees of oxidation. Figure 6.10 shows that

Figure 6.9: Organic carbon content of samples used in this study, and classification of their organic richness. Samples are from the Green River Formation in the Green River Basin.

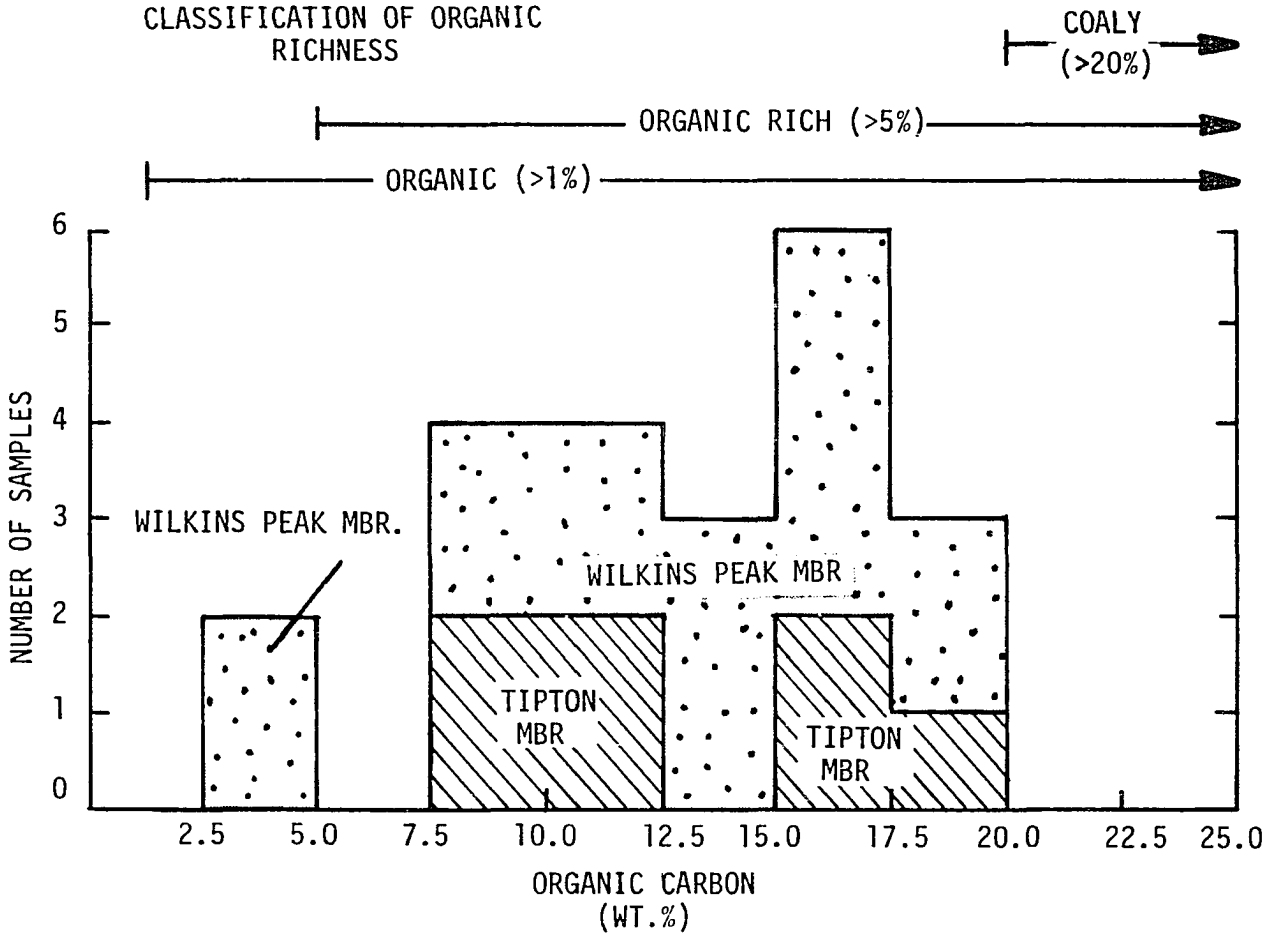

FIGURE 6.9

Figure 6.10: Atomic H/C ratio versus atomic O/C ratio plot of kerogens from the Green River Formation in the Green River Basin. Thermal maturation pathways for the three kerogen types are the same as those presented in Figure 2.3

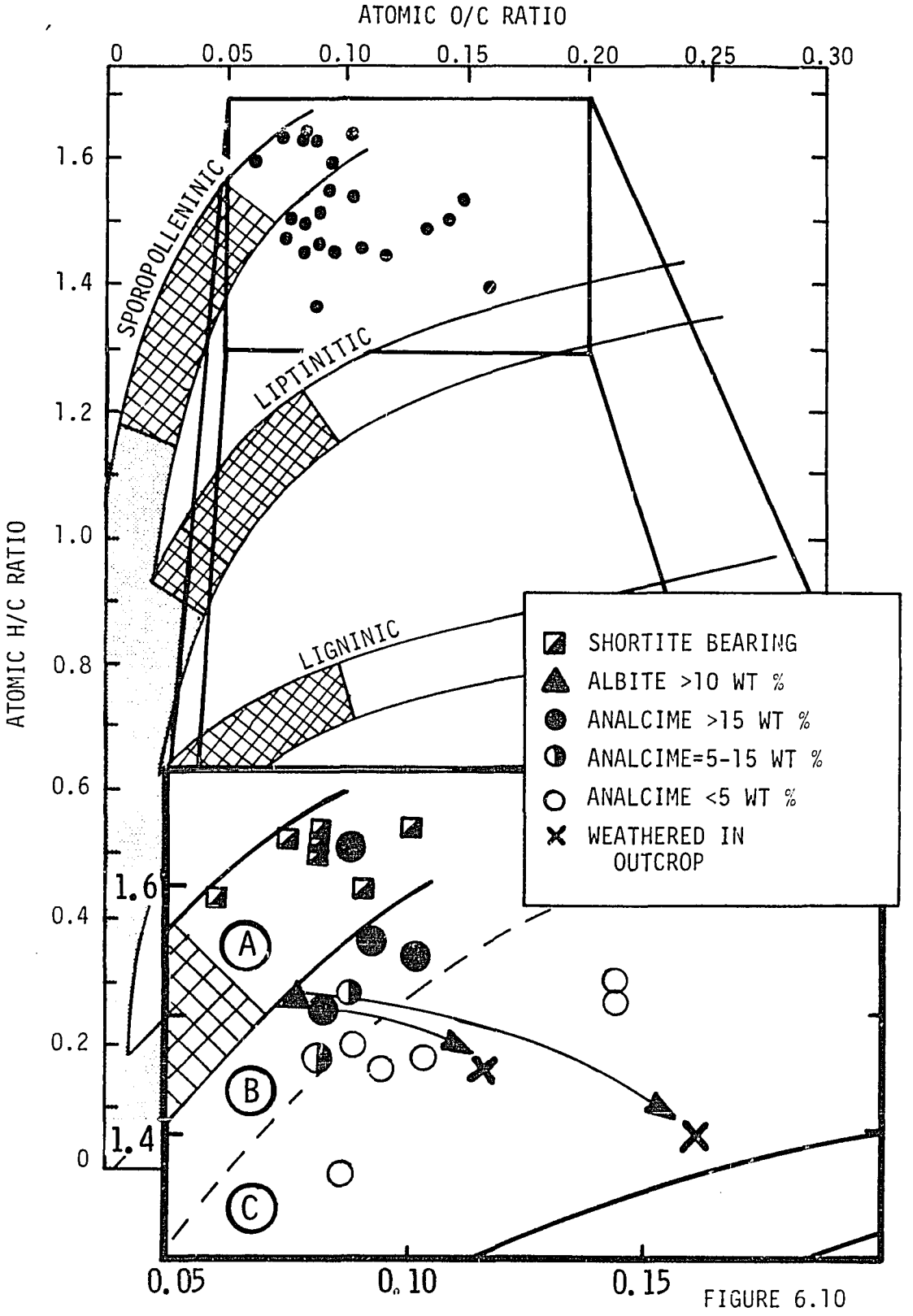

FIGURE 6.10

the kerogens in pathway A are unoxidized, while those in pathways B and C show a progressive increase in oxidation, respectively. The two weathering trends from Figure 3.2 have been superimposed on Figure 6.10 to illustrate that oxidation does proceed in the direction of pathways B and C. Based on the criteria established in Chapter 3, these samples in pathways B and C are not weathered, and are therefore interpreted to be the result of oxidation in their depositional environment. Kerogens in pathway C are interpreted to be derived from organic matter that has settled through long aerobic water columns before entering anaerobic conditions or has been exposed to aerobic or dysaerobic bottom waters for long periods of time. Conversely, kerogens in pathway A are interpreted to be derived from organic matter that has not experienced long durations in aerobic or dysaerobic conditions. Kerogens in pathway B are interpreted to represent intermediate conditions. It is worth noting, as shown in Figure 6.10, that the unoxidized kerogens in pathway A occur in the rocks of the Wilkins Peak Member, which are thought to have been deposited in highly alkaline waters.

The mineralogy of the samples is given in Figure 6.11 and they have been classified into 8 rock types as shown in Table 6.7. Dolomitic marlstones predominate in the Wilkins Peak Member and zerolite bearing claystones predominate in the Tipton Member. In the Wilkins Peak Member the marlstones may be grouped into 5 facies representing increasing alkalinity as evaporation of Lake Gosiute approaches a playa condition (Table 6.8). The presence of volcanic ash in most of these samples supplies a sufficient amount of silica to the sediment, so that a distinct

Figure 6.11: Ternary diagrams showing mineralogy of the Tipton Member and Wilkins Peak Member of the Green River Formation. Plots are based on data given in Appendix VII.

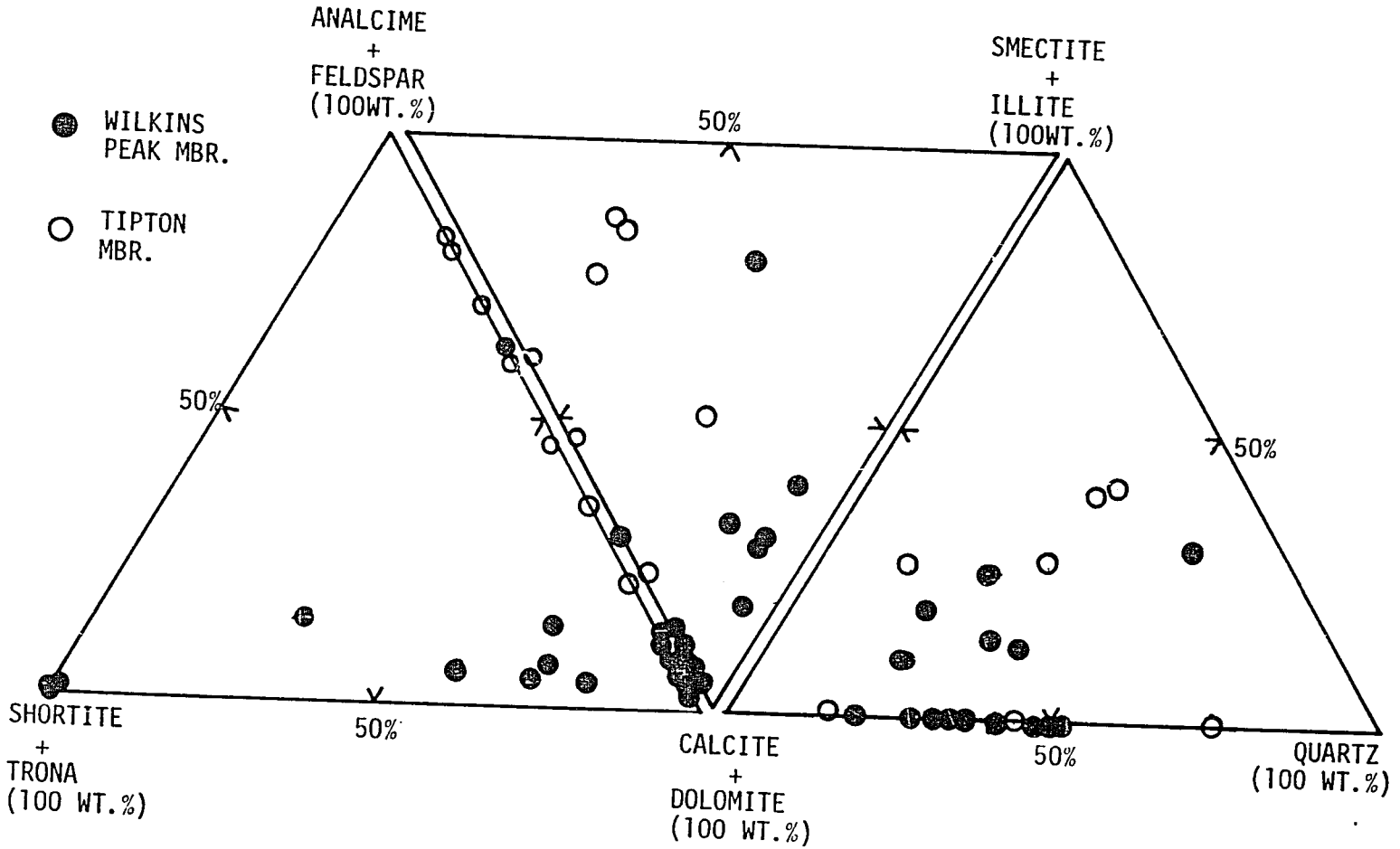

FIGURE 6.11

Table 6.7: Classification of rock types in the Wilkins Peak and Tipton members of the Green River Formation.

Rock Name*	Classified Samples	Number of Samples	
		Wilkins Peak	Tipton
Argillaceous Claystone	GR-3	1	0
Argillaceous Marlstone	GR-10, GR-14	1	1
Tektosiliceous Claystone	GR-11	0	1
Tektosiliceous Marlstone	GR-5	0	1
Zeolitic Claystone	GR-6, GR-7, GR-8	0	3
Dolomitic Marlstone	GR-1, GR-2, GR-4, GR-9, GR-13 GR-16, GR-17, GR-18, GR-20, GR-21, GR-23	11	1
Calcitic Marlstone	GR-15, GR-24	2	0
Trona Evaporite	GR-19, GR-22	2	0

*Nomenclature in accordance with Lewan (1978).

Table 6.8: Description of playa-lake facies sequence in the Wilkins Peak Member and the corresponding carbon isotope values of their kerogens and vanadium-nickel fractions of their bitumens.

Alkalinity	Facies	Description of Facies	*Kerogen δC_{13}	V/(Ni+V)
High	1	Shortitic calcareous marlstones with interbedded trona evaporites (diagnostic minerals = trona + shortite; N=6)	-31.4 ± 0.3	0.02 ± 0.01
Increasing Na^+/H^+	2	Calcareous marlstones with interbedded shortitic calcareous marlstone (diagnostic mineral = shortite; N=2)	-31.8 ± 0.9	0.09 ± 0.01
	3	Analcimic dolomitic marlstones (diagnostic mineral = analcime; N=4)	-29.0 ± 1.9	0.16 ± 0.05
	4	Dolomitic marlstones (diagnostic mineral = dolomite; N=2)	-28.6 ± 1.3	0.29 ± 0.02
Low	5	Argillaceous marlstones (diagnostic minerals = quartz and clay minerals; N=1)	-27.1 ± 0.0	0.36 ± 0.00

*Relative to PDB in per mil.
N = number of samples

mineral paragenesis sequence (smectite→zeolite→feldspar→salts) may be assigned to the increasing alkalinity in the system. Similar mineral paragenesis sequences in other volcanic ash bearing sedimentary rocks have also been attributed to increasing alkalinity (eg. Sheppard and Gude, 1968 and 1969; Boles and Surdam, 1979).

The evaporitic facies sequence suggested in Table 6.8 is also supported by the carbon isotope values of the kerogens from each facies. It has been demonstrated that the fractionation of carbon isotopes by algae becomes significantly more negative as the concentration of dissolved carbon dioxide in their environment increases (Degens et al., 1968a; Calder and Parker, 1973; Chapter 2.1.2). As the evaporation of a water body proceeds, the concentration of dissolved carbon dioxide will increase and the carbon isotopes of the algae in the system will become more negative. As shown in Table 6.8 this trend does correspond with the evaporitic facies sequence. The slight deviation of facies 1 in this trend is probably due to the decrease in dissolved carbon dioxide resulting from the precipitation of sodium carbonates (i.e., shortite and trona).

The vanadium-nickel fractions of the bitumens from the facies also correspond to an increase in alkalinity from Eh-pH Field II through Eh-pH Field I, as shown in Figure 6.12. At the lower alkalinity of facies 5, vanadyl cations would be competitive with nickelous cations for tetrapyrrole bonding sites, but as alkalinity increased in facies 4 and 3, the increase in the hydroxylation of vanadyl cations would reduce its

Figure 6.12: Interpreted trend of the playa-lake facies sequence of the Wilkins Peak Member on the Eh-pH diagram presented in Figure 6.6. Numbers on shaded trend correspond to the facies given in Table 6.8.

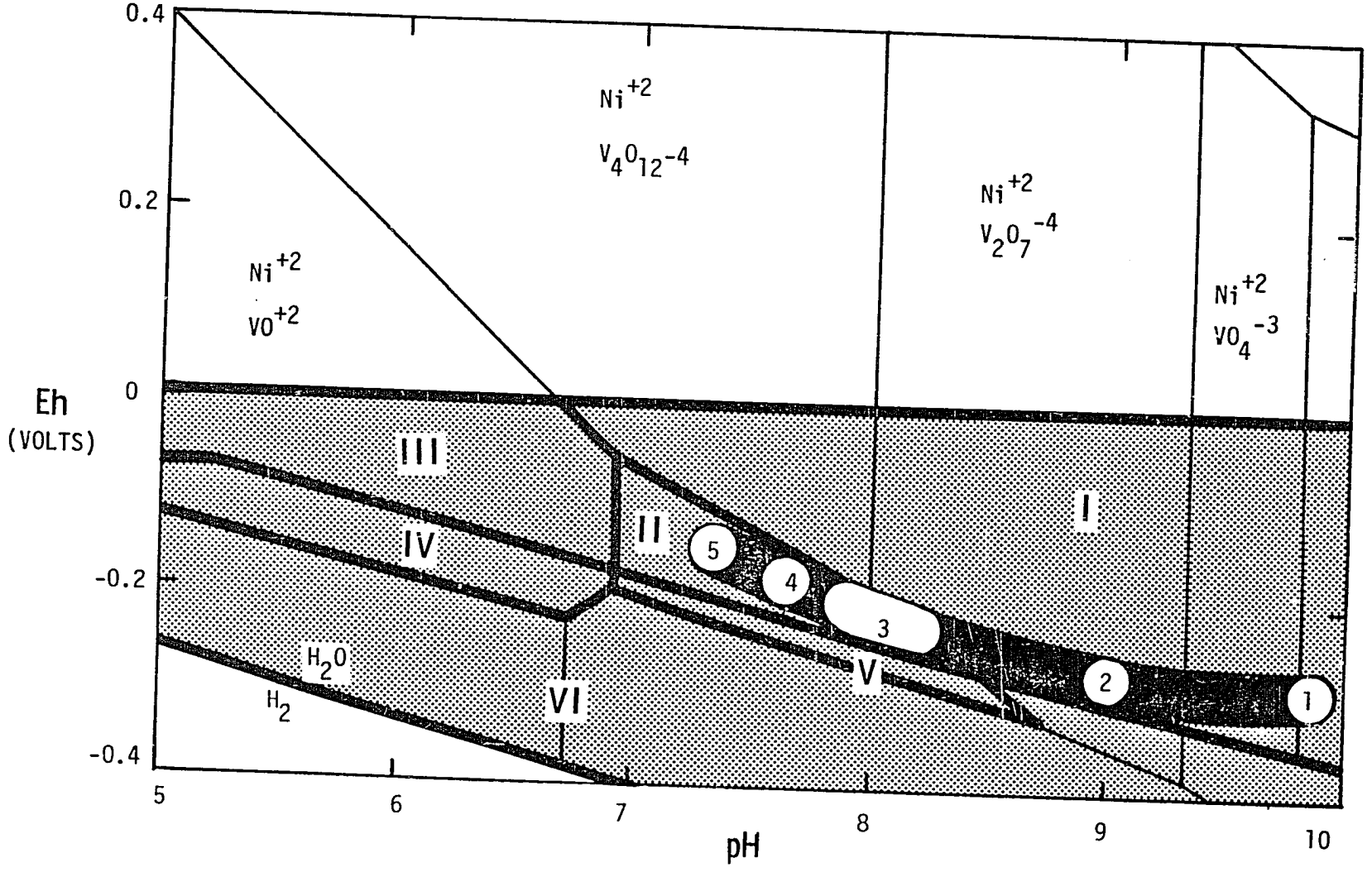

FIGURE 6.12

competitiveness relative to the nickelous cations. As the alkalinity increases into Eh-pH Field I the vanadyl cations would be oxidized to a quinquivalent anion and would be completely noncompetitive with nickelous cations. This trend suggests a decreasing vanadium-nickel fraction, which is shown in Table 6.8.

As shown in Table 6.9, the limited number of samples collected in the Tipton Member reveal only two facies. Their authigenic silicates, kerogen carbon isotopes, and vanadium-nickel fractions suggest that they occur in Eh-pH Field I between facies 1 and 2 of the Wilkins Peak Member.

6.4.2 Lake Uinta

The Green River Formation in the eastern and central portions of the Uinta Basin has been subdivided into three members; Douglas Creek, Parachute Creek, and Evacuation Creek (Bradley, 1931; Figure 6.13). The Douglas Creek Member occurs at the base of the Green River Formation and consist primarily of sandstone, siltstone, shale, and limestone (Cashion, 1967). The common occurrence of oolitic, algal, and ostracodal limestones and the presence of mollusk shells, turtle remains, and fish bones (Cashion, 1967; Ryder et al., 1976) suggest that during this time Lake Uinta was a well oxygenated shallow lake with a tolerable alkalinity. During the deposition of the overlying Parachute Creek Member, Lake Uinta is thought to have fluctuated periodically from shallow to deep water (Cashion, 1967). Although high alkalinity in Lake

Table 6.9: Description of playa-lake facies sequence in the Tipton Member and the corresponding carbon isotope values of their kerogens and vanadium-nickel fractions of their bitumens.

Alkalinity	Facies	Description of Facies	*Kerogen δC_{13}	V/(Ni+V)
High	1	Feldspathic dolomitic marlstones with authigenic feldspar comprising more than 20 wt % of the inorganic fraction (diagnostic mineral = feldspar; N=2)	-31.2 ± 0.3	0.04 ± 0.04
Na^+/H^+ Increasing				
	2	Analcimic tektosiliceous claystones with authigenic analcime comprising more than 20 wt. of the inorganic fraction (diagnostic mineral=analcime; N=5).	-32.7 ± 0.9	0.05 ± 0.04
Low				

*Relative to PDB in per mil.
N = number of samples.

Figure 6.13: Geological map and stratigraphic section of the Green River Formation in the Uinta Basin of Utah (modified after Van West, 1972; and Cashion, 1967, Figure 8). Sampling locality numbers correspond to those given in Appendix I.

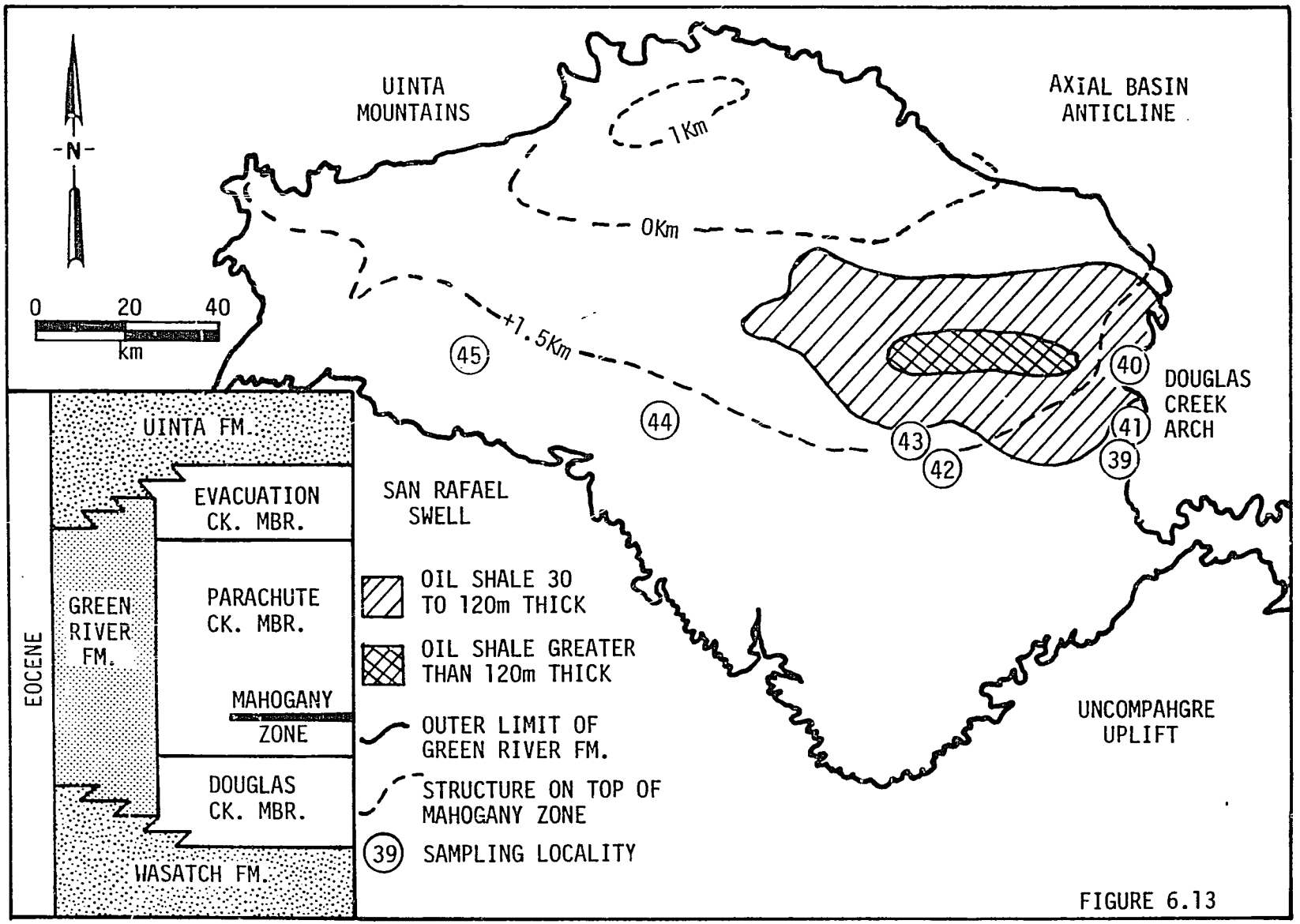

FIGURE 6.13

Uinta may have occurred periodically (Erickson, 1952; Fahey, 1962), the amount of evaporation never achieved an alkalinity that was high enough for the formation of bedded evaporites (Fahey, 1962; Cashion, 1967). The Parachute Creek Member consists primarily of marlstone and oil shale, and includes the prominent ledge forming Mahogany zone (Bradley, 1931). During the culminating phase of Lake Uinta, shallow water prevailed and is represented by the marlstone and siltstone of the Evacuation Creek Member (Cashion, 1967).

The sampling localities used in this study are shown in Figure 6.13, and sampling was confined to organic and organic rich shales from the Parachute Creek Member (Figure 6.14). Visual and elemental analyses indicate that β-sporopolleninic kerogen comprises more than 95 percent of the kerogen in these samples. Based on the criteria established in Chapter 3, none of the kerogens have been weathered, and Figure 6.15 suggests that only three of the kerogens have been subjected to oxidation in their depositional environments. Thus, it appears that anaerobic conditions were prevalent in the water column and sediment during the deposition of the majority of these samples.

The mineralogy of these samples is given in Figure 6.16, and the samples have been classified into four rock types as shown in Table 6.10. Based on the authigenic silicates and kerogen carbon isotopes of these samples, a sequence of five facies is proposed in Table 6.11. As indicated, this facies sequence suggests an increase in the alkalinity of Lake Uinta. The samples in facies 1, 2, and 3 cannot be distinguished

Figure 6.14: Histogram showing organic carbon content of smaples used in this study, and classification of their organic richness. Samples are from the Green River Formation in the Uinta Basin.

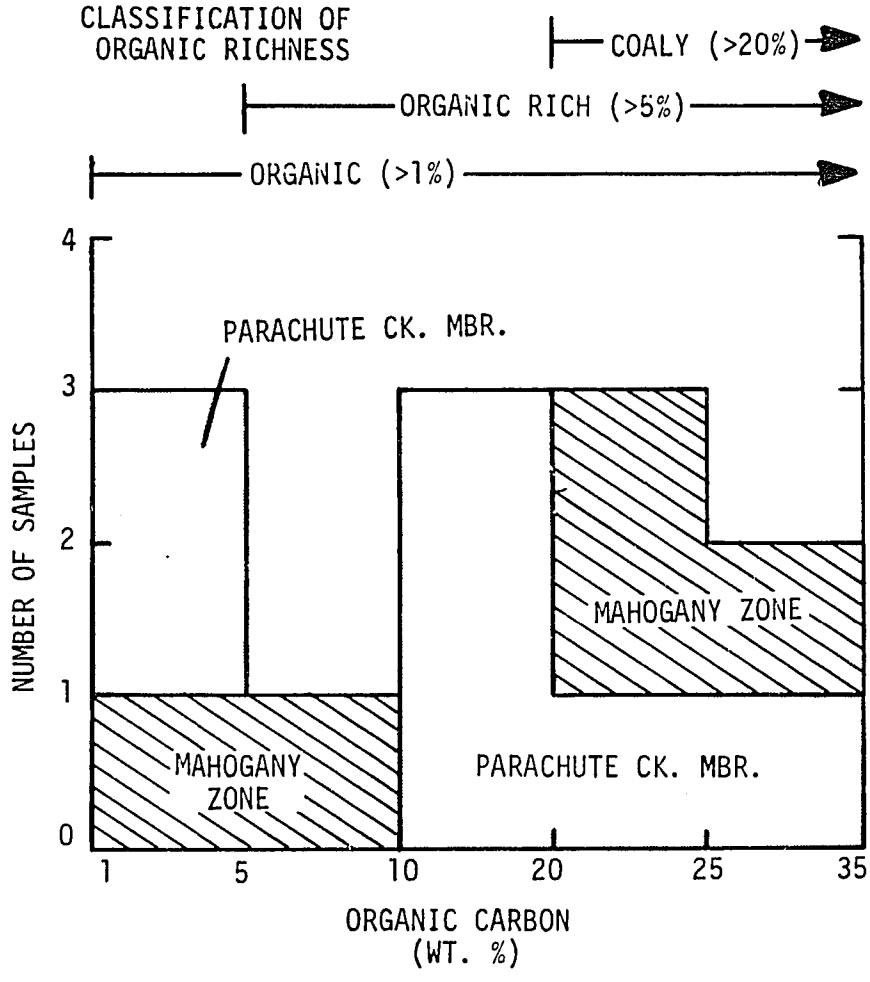

FIGURE 6.14

Figure 6.15: Atomic H/C ratios versus atomic O/C ratio plot of kerogens from the Green River Formation in the Uinta Basin. Thermal maturation pathways for the three kerogen types are the same as those presented in Figure 2.3

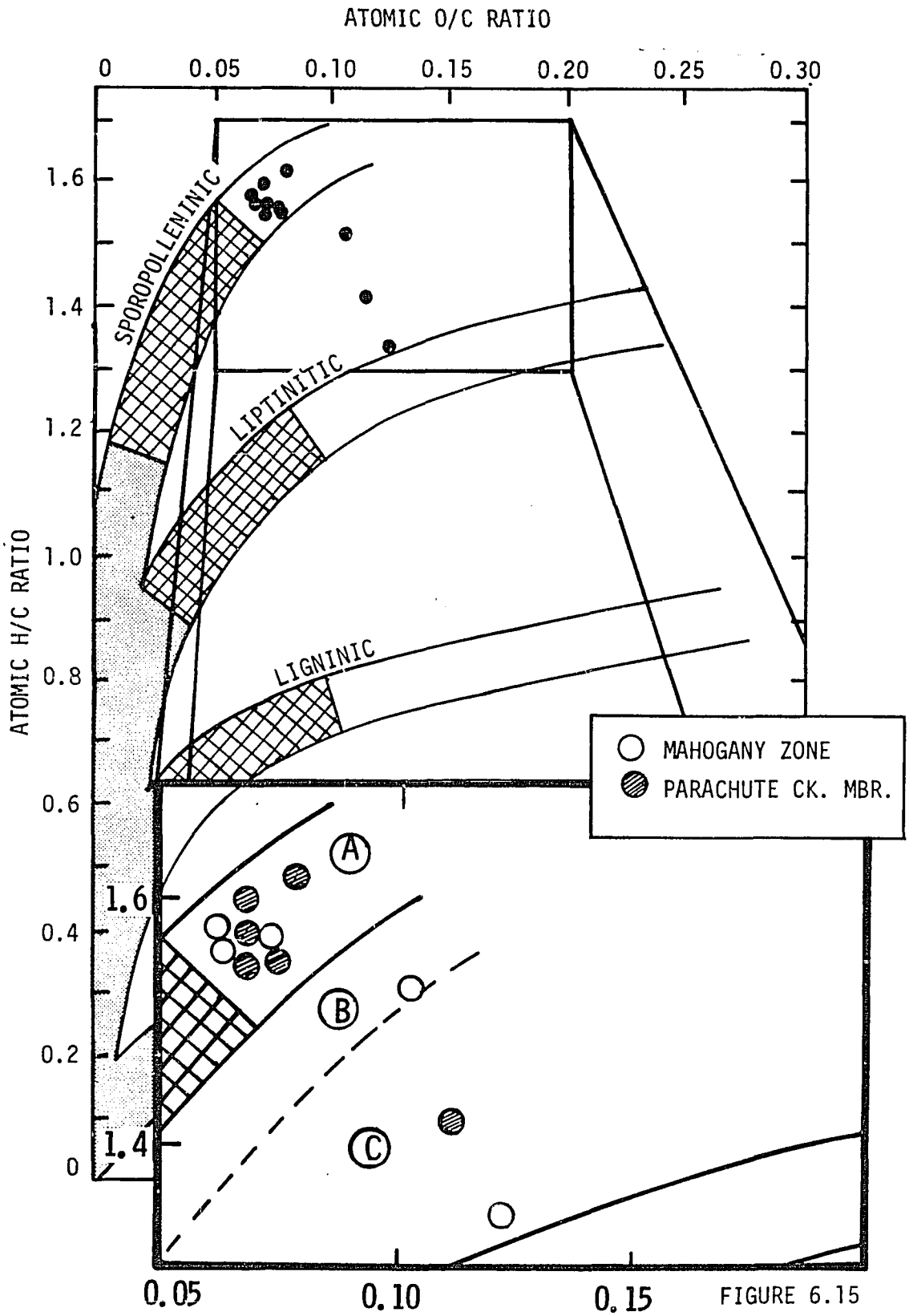

FIGURE 6.15

Figure 6.16: Ternary diagrams showing mineralogy of the Mahogany zone and Parachute Creek Member of the Green River Formation. Plots are based on data given in Appendix VII.

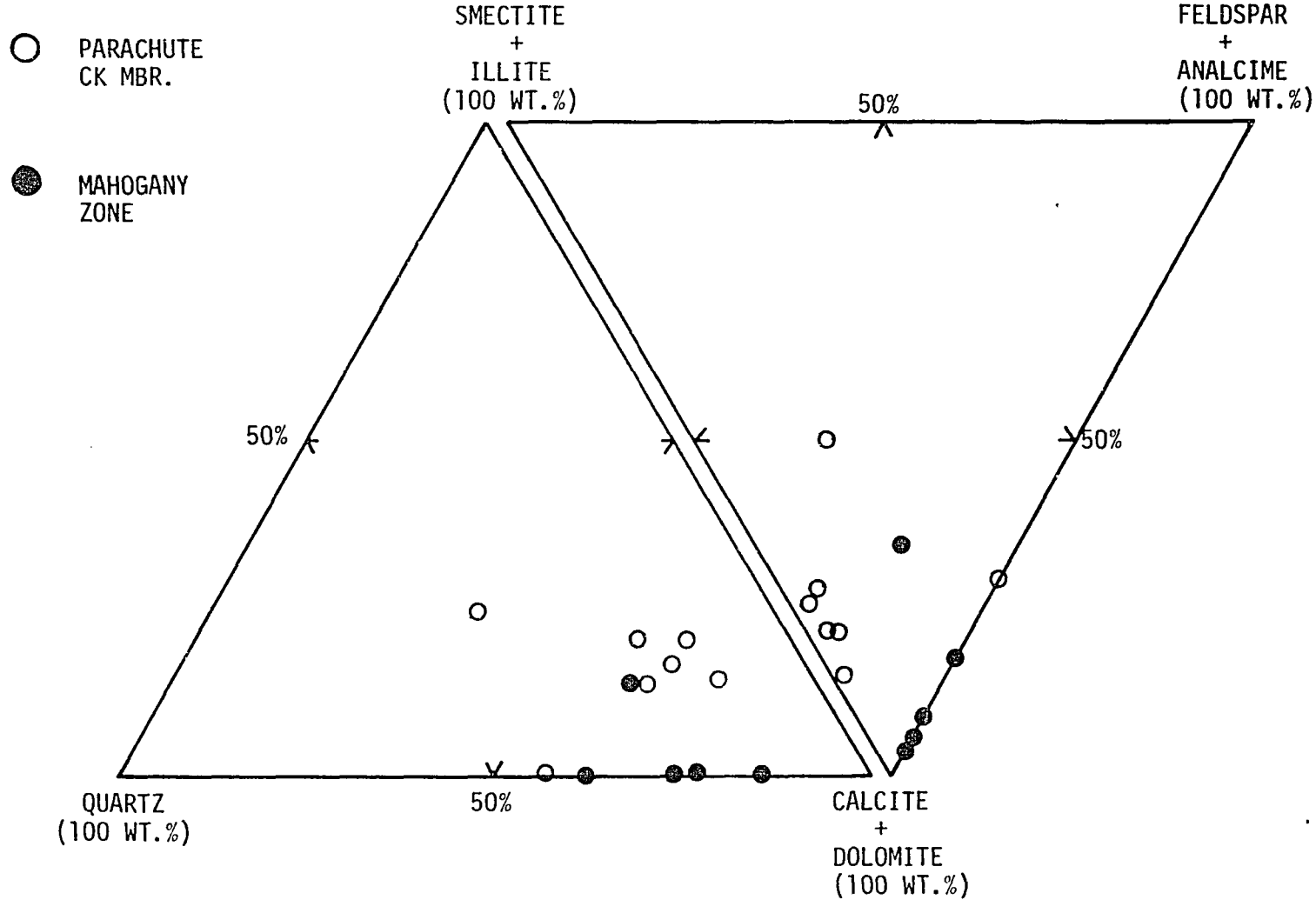

FIGURE 6.16

Table 6.10: Classification of rock types in the Mahogany Zone and Parachute Creek Member of the Green River Formation.

Rock Name*	Classified Samples	Number of Mahogany	Number of Parachute Ck.
Calcitic Micstone	GR-30, GR-31	2	0
Calcitic Marlstone	GR-25, GR-35, GR-37, GR-39	1	3
Dolomitic Marlstone	GR-26, GR-32, GR-34, GR-38	2	2
Quartzose Marlstone	GR-27, GR-39	0	2

*Nomenclature in accordance with Lewan (1978).

Table 6.11: Description of lacustrine facies sequence in the Parachute Creek Member and corresponding carbon isotope values of their kerogens and vanadium-nickel fractions of their bitumens.

Alkalinity	Facies	Description of Facies	*Kerogen δC_{13}	V/(Ni+V)
High	1	Feldspathic calcareous marlstone (diagnostic mineral=feldsar; N=2)	-30.9 $\pm$ 0.0	0.09 $\pm\pm$ 0.02
Increasing Na^+/H^+	2	Calcitic micstone (diagnostic mineral = minor feldspar and no clay minerals nor zeolites; N=2)	-30.4 $\pm$ 0.7	0.08 $\pm$ 0.01
	3	Feldspathic quartzose marlstone (diagnostic mineral = feldspar; N=2)	-29.9 $\pm$ 0.4	0.13 $\pm$ 0.01
	4	Analcimic dolomitic marlstone (diagnostic mineral = analcime; N=1)	-28.0 $\pm$ 0.0	0.28 $\pm$ 0.01
Low	5	Smectitic calcareous marlstone (diagnostic mineral = smectite; N=5)	-27.4 $\pm$ 0.7	0.08 $\pm$ 0.04

*Relative to PDB in per mil.
N = number of samples

on the basis of diagnostic authigenic silicates and are categorized on the basis of kerogen carbon isotopes.

The vanadium-nickel fractions of the bitumens from this facies sequence also suggest an increasing alkalinity as proposed in Figure 6.17. The smectite bearing shales of facies 5 are common in the western part of the Uinta Basin (Dyni, 1976), which represents a more normal lacustrine regime (Ryder et al., 1976). This facies is interpreted as being deposited under a condition of low alkalinity at low pH values in Eh-pH Field I. Under these conditions vanadium will occur as a quinquivalent anion and will not be competitive with available nickelous cations for tetrapyrrole bonding sites. This will result in bitumens with low vanadium-nickel fractions, which are observed in facies 5 as shown in Table 6.11. During periods of high evaporation the alkalinity of the lake and its pH would increase. The initial phases of this increasing alkalinity would be represented by facies 3 and 4 and are interpreted to have occurred in Eh-pH Field II. Under these conditions vanadyl cations will be competitive with nickelous cations for tetrapyrrole bonding sites, but increasing hydroxylation of vanadyl cations with increasing pH will reduce the competitiveness of the vanadyl cations. This results in the bitumens of facies 4 having a higher vanadium-nickel fraction than facies 3 and 5 (Table 6.11). As alkalinity and pH increase into facies 1 and 2, vanadium is oxidized to quinquivalent anions and will not be competitive with the available nickelous cations in Eh-pH Field I. Under these conditions the bitumens of these two facies will have low vanadium-nickel fractions as observed (Table 6.11).

Figure 6.17: Interpreted trend of the lacustrine facies sequence of the Parachute Creek Member on the Eh-pH diagram from Figure 6.6. Numbers on shaded trend correspond to facies given in Table 6.11.

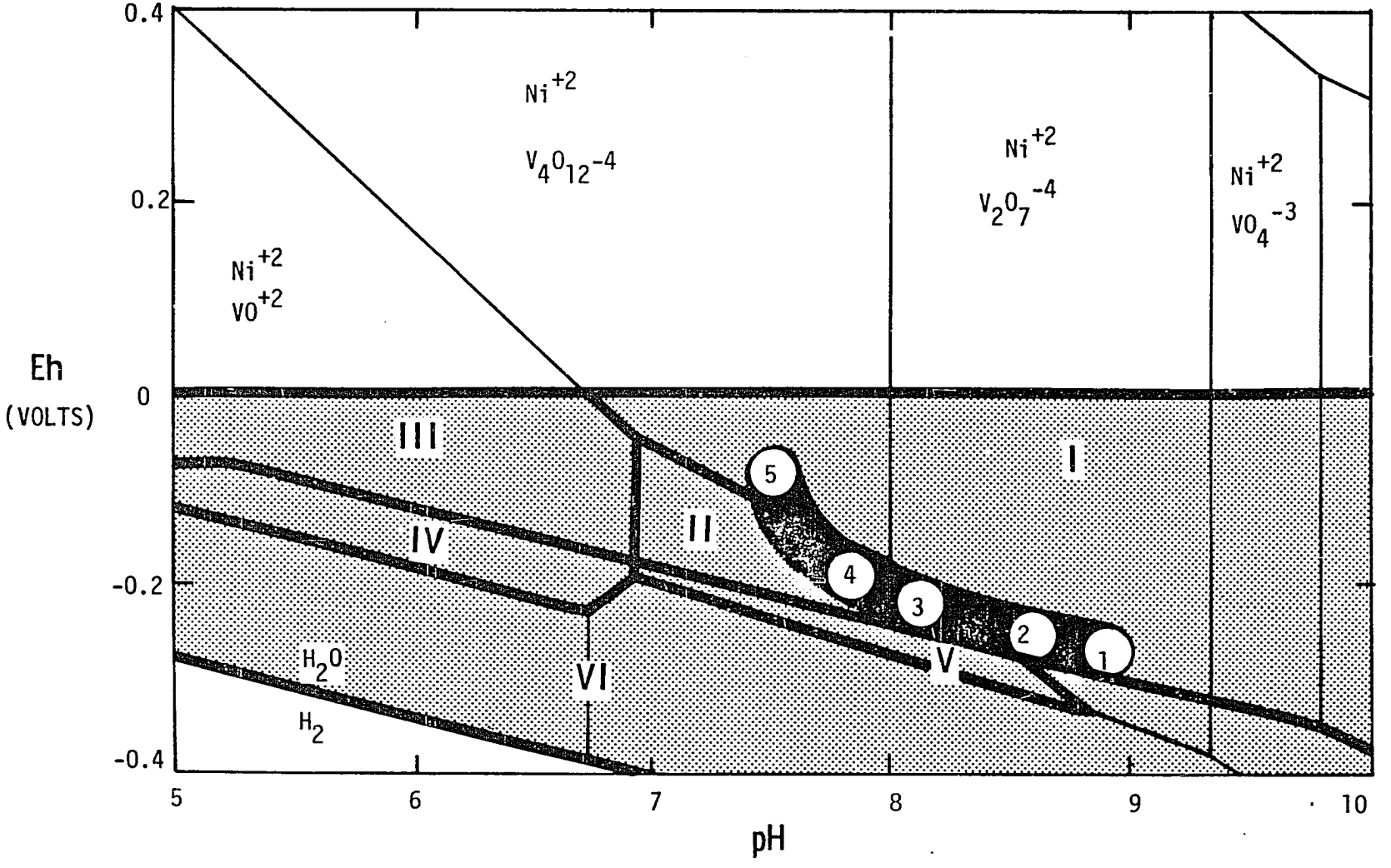

FIGURE 6.17

6.5 MOWRY SHALE

The Mowry Shale and equivalent Late Albian shales (i.e., Aspen Shale and Bootlegger Shale) were deposited in a large epicontinental sea that transgressed from a boreal sea over the northern portions of the western United States and western Canada (Figure 6.18; Davis, 1963; Williams and Stelck, 1975). This Cretaceous sea appears to have been in communication with the warmer waters of the Gulf of Mexico prior to and after Late Albian time, but apparently was only in communication with the cooler waters of a boreal sea during the deposition of the Mowry Shale (Reeside, 1957). In the open marine facies of the Mowry Shale, the abundance of radiolaria and fish remains (Reeside and Cobban, 1960) indicate an aerobic water column existed in the Mowry Sea, but the scarcity of benthonic organisms, lack of bioturbation, and preservation of organic matter indicate an anaerobic condition probably developed in the lower portions of the water column (Byers, 1973 and 1977). The lower anaerobic portion apparently did not extend into the marginal facies of the Mowry Shale as indicated by bioturbation (Byers and Larson, 1979) and lower concentrations of organic matter (Schrayer and Zarrella, 1963; Davis, 1970; Nixon, 1973). Volcanic activity appears to have been profuse during the deposition of the Mowry Shale (Reeside, 1957) and is reflected in the stratigraphic section by numerous bentonite beds (Slaughter and Earley, 1965). Westward the Mowry Shale becomes more sandy in character and eastward it thins as siliceous shale (Davis, 1970).

Figure 6.18: Map showing extent of Mowry Sea in the western interior of the United States, and the locations of successor basins around which the Mowry Shale is exposed and the outcrop near Steinaker Reservoir (modified after Figure 17 from Cobban, 1972). Insert map shows regional extent of Mowry Sea over North America and its relation to the Cretaceous Gulf of Mexico and boreal sea (modified after Figure 4 from Stelck, 1975).

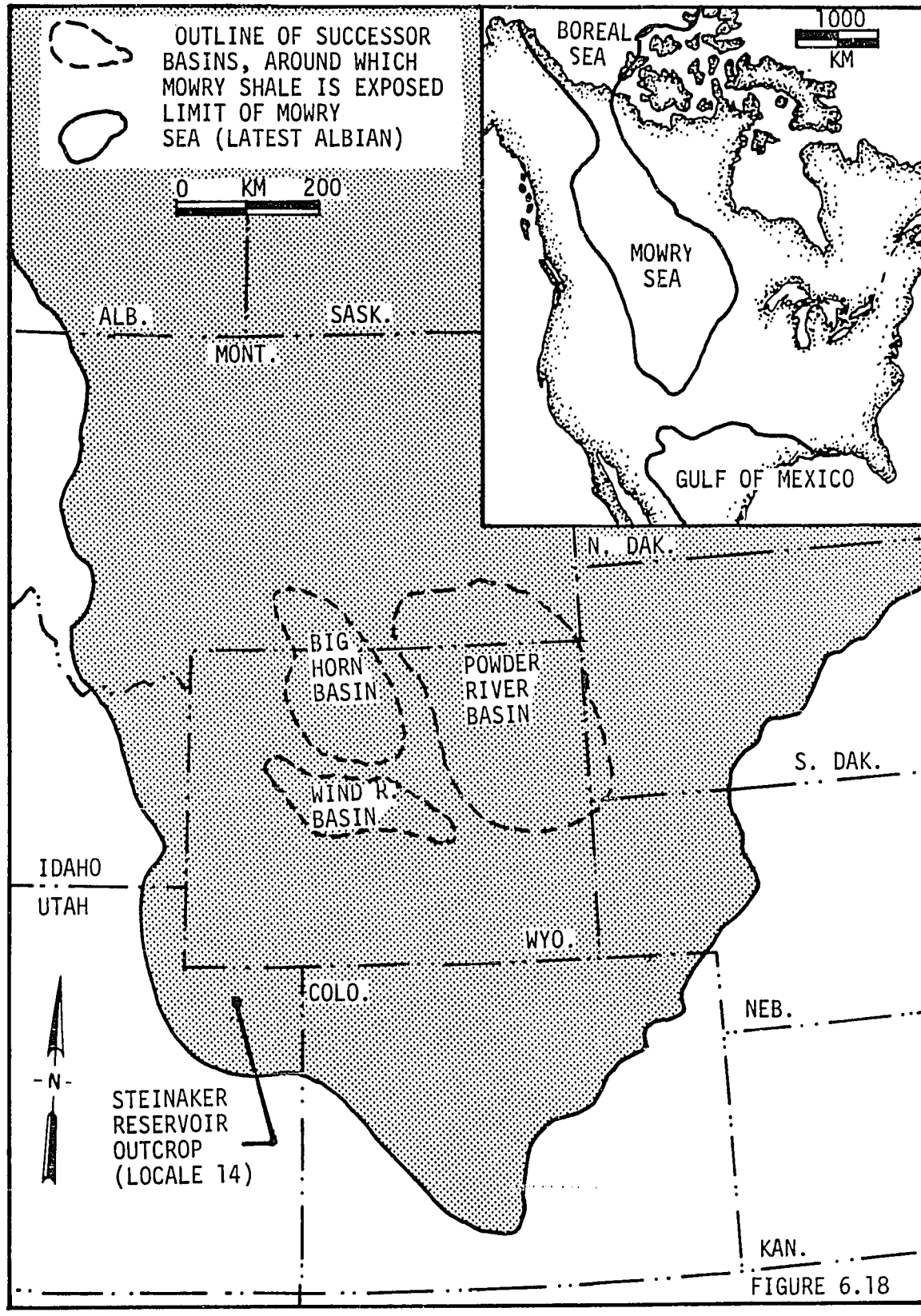

FIGURE 6.18

In this study, sampling of the Mowry Shale was concentrated in and around the Powder River Basin (Figure 6.19) with the exception of the sampling at the Steinaker Reservoir outcrop (Figure 6.18). Although good exposures of the Mowry Shale also occur around the Big Horn Basin and Wind River Basin, the study concentrated on the Powder River Basin because in this area the Mowry Shale has the highest organic carbon contents (Schrayer and Zarrella, 1963; Davis, 1970; Nixon, 1973) and the most uniform lithology (Davis, 1970). It should be emphasized that the Powder River Basin is a successor basin with respect to the Cretaceous rocks (Schwab, 1976), and its configuration had no apparent influence on the deposition of the Mowry Shale as noted by the distribution of organic carbon in Figure 6.19.

The siliceous shale facies as described by Davis (1970) predominates in the Mowry Shale particularly in the area of the Powder River Basin. The mineralogy of Mowry Shale samples collected for this study is given in Figures 6.20 and 6.21. These samples are predominantly quartzose claystones with smectite and illite being the primary clay minerals. Table 6.12 shows that radiolarian tests, fish remains, and silt-sand laminae are common in the Mowry Shale. Only five of the samples showed definite signs of bioturbation and these samples are predominantly quartzose mudstones (M-32, M-33, M-34, M-35) with relatively low organic carbon contents ($\leq$1.2 weight percent). As shown in Figure 6.22, most of the samples are organic, with the quartzose claystones predominating in the organic samples.

Figure 6.19: Map showing sampling localities, structure, and organic-rich portions of the Mowry Shale in the Powder River Basin of Wyoming. Sampling locality numbers correspond to those given in Appendix I. Structure contours are relative to sea level and are modified after Figure 6 from McGregor (1972). The high organic carbon area is modified after Figure 13 from Nixon (1973). General stratigraphic section of Mowry Shale is modified after Figure 1 from Davis (1970).

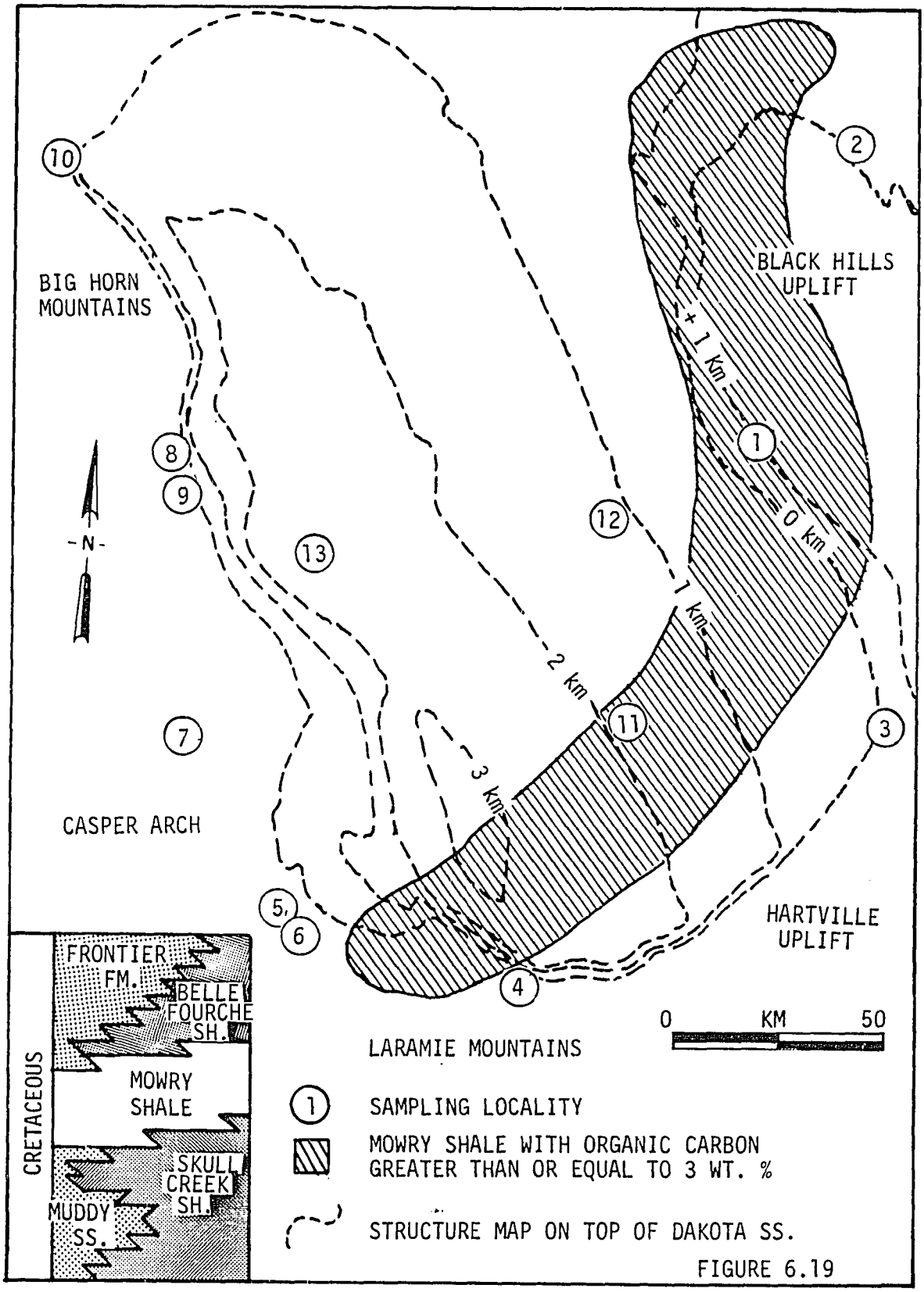

FIGURE 6.19

Figure 6.20: Ternary diagram showing mineralogy and rock types of the Mowry Shale samples. Plots are based on data given in Apendix VII.

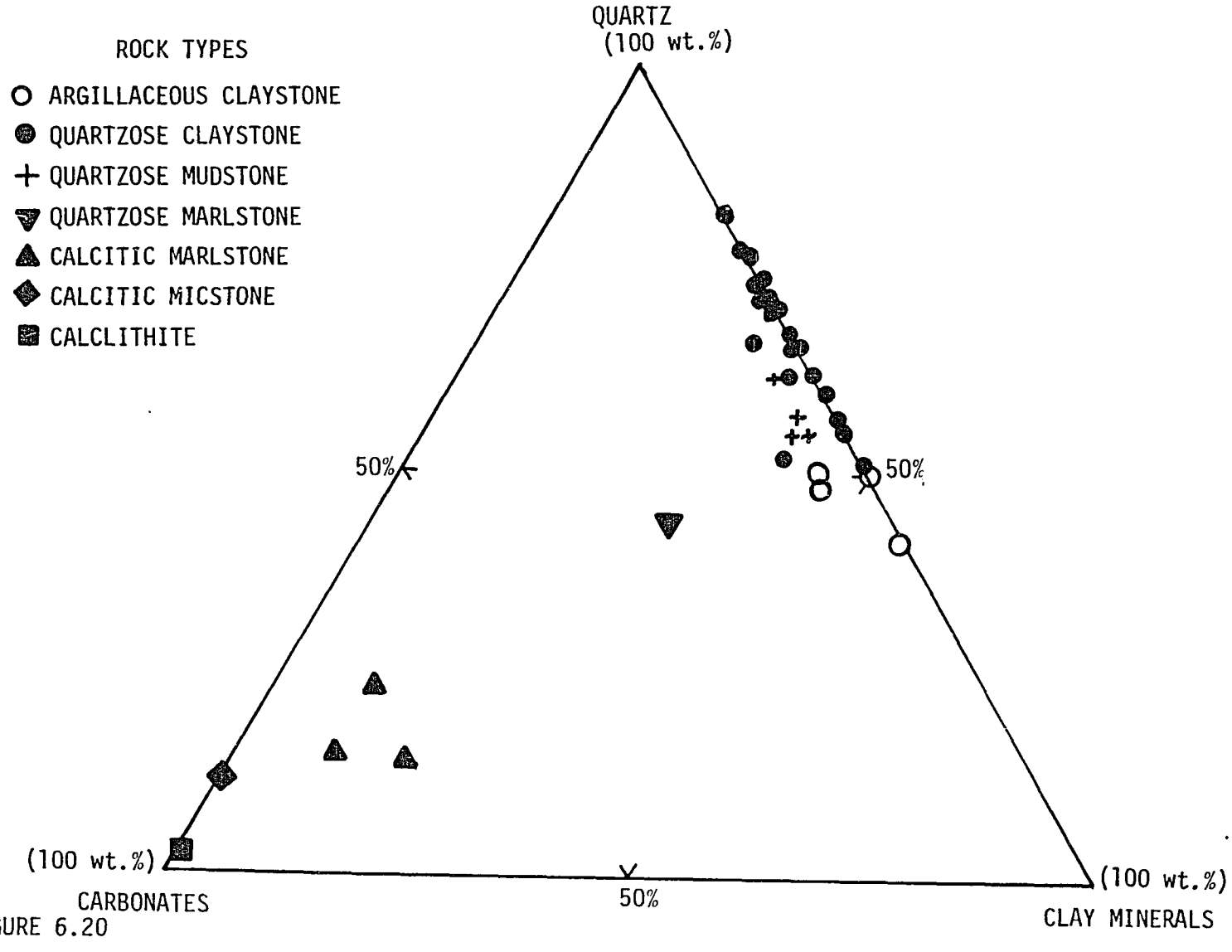

FIGURE 6.20

Figure 6.21: Ternary diagrams showing variations in the clay mineralogy and sample depth of the collected Mowry Shale samples. Plots are based on data given in Appendix VII.

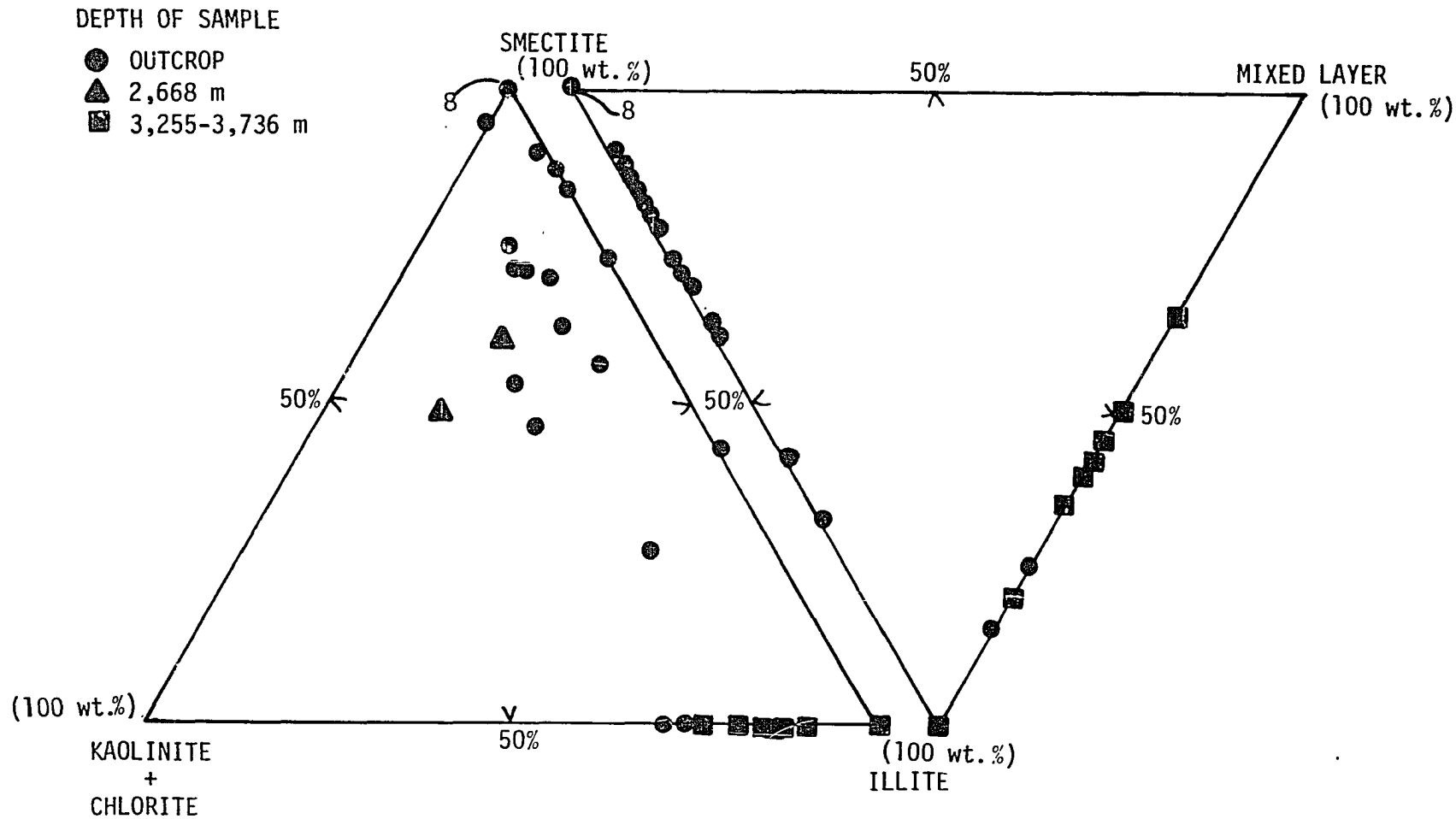

FIGURE 6.21

Table 6.12: Basic petrologic data on Mowry Shale samples used in this study.

Sample Number	Radiolaria Tests	Fish Remains	Inoceramus Fragmented Shells	Coal Layers	Silt-Sand Laminae
M-1	+	+	-	-	-
M-2	+	+	-	-	-
M-3	-	+	-	-	+
M-7	-	-	-	-	-
M-9	-	-	-	-	-
M-10	+	+	-	-	+
M-11	n.d.	+	-	-	+
M-12	-	+	-	-	-
M-13	-	+	+	-	-
M-15	-	-	-	-	+
M-16	-	-	-	-	-
M-17	+	+	-	-	+
M-18	+	+	-	-	-
M-19	+	+	-	-	+
M-20	-	+	-	-	+
M-21	+	+	-	-	+
M-22	+	+	-	-	-
M-23	n.d.	+	-	-	+
M-25	+	+	-	-	+
M-26	n.d.	-	-	-	B
M-27	+	+	-	-	+
M-28	+	+	+	-	+
M-29	+	-	+	-	-
M-30	n.d.	-	-	+	-
M-31	-	-	-	+	+
M-32	-	-	-	-	B
M-33	-	-	-	-	B
M-34	-	-	-	-	B
M-35	-	-	-	-	B
M-37	-	+	-	-	-
M-38	+	-	-	-	-
M-39	-	+	-	+	-
M-40	+	+	-	-	-
M-43	-	+	-	-	+
Percent of Occurrence	47	62	9	9	53

+ = present - = absent
B = Bioturbated Silt Laminae
n.d. = not determined

Figure 6.22: Histogram showing organic carbon content of samples used in this study and classification of their organic richness. Samples are from the Mowry Shale in the Powder River Basin and Steinaker reservoir outcrop.

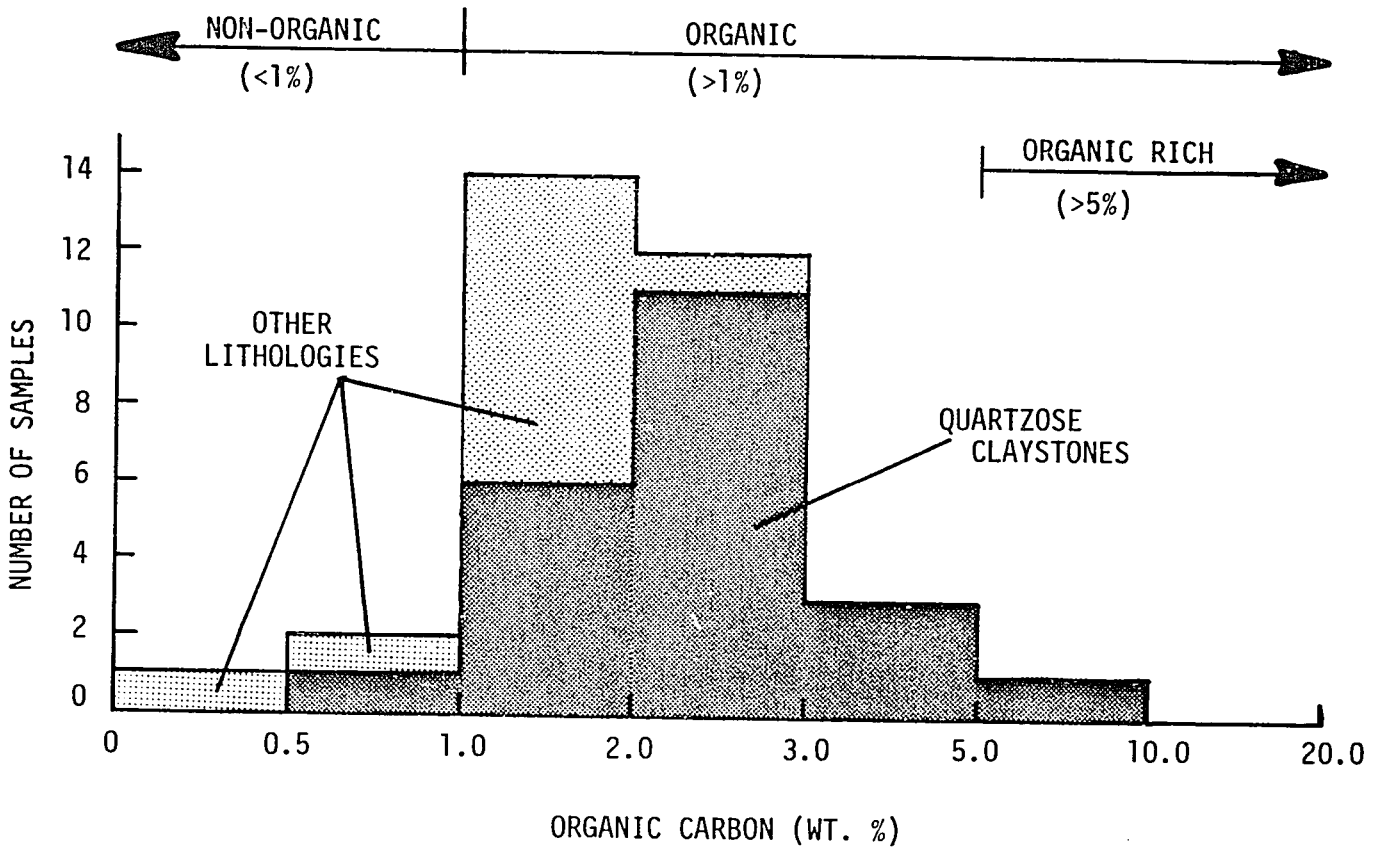

FIGURE 6.22

Visual analysis shows that the kerogens consist of varying mixtures of liptinitic and ligninic kerogens (Figure 6.23a). Although visual analysis indicates that liptinitic kerogen is predominant in most of the samples, the carbon isotope values of the kerogens indicate that the β+liptinitic kerogen may be mixed with more ligninic kerogen than indicated by visual analysis. This discrepancy may be explained by the observation that ligninic kerogen may be camouflaged by encompassing liptinitic kerogen and may be resolved by reflected light microscopy (Littlejohn, 1979, personal communique). In order to obtain a more accurate estimate of the amount of liptinitic kerogen present in the samples, two kerogen samples representing the extremes in visual analysis (M-31 and M-10) and their carbon isotope values were used to formulate a linear function from which percent of liptinitic kerogen in the intermediate samples could be determined (i.e., percent liptinitic kerogen = $-23.4\delta C^{13}-533.2$). It should be emphasized that this is only an approximation and similar approaches to evaluating mixtures of organic matter in recent sediments have been employed (e.g. Hedges and Parker, 1976; Hedges and Mann, 1979). The resulting estimates have been grouped into four broad compositional categories, which are shown in conjunction with their elemental analyses in Figure 6.24.

The elemental analyses plotted in Figure 6.24 show that most of the samples are at a low level of thermal maturation with the exception of the core samples from depths greater than 2.5 km, which are at moderate levels of thermal maturation. The isopleths constructed between the liptinitic and ligninic pathways represent physical mixtures of these

Figure 6.23: Characterization of kerogens from the Mowry Shale samples by a) visual analysis and b) carbon isotope values.

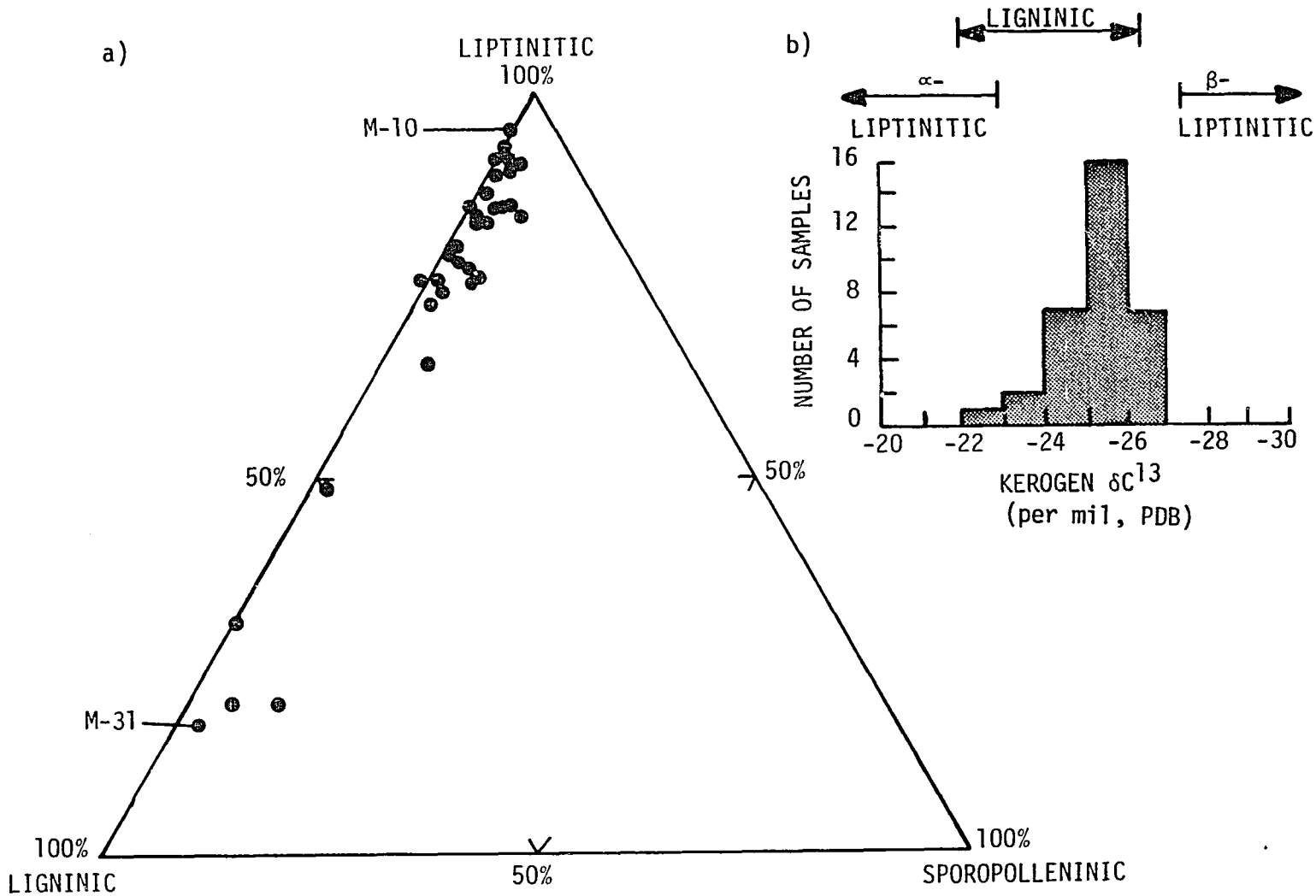

FIGURE 6.23

Figure 6.24: Atomic H/C ratio versus atomic O/C ratio plot of kerogens from the Mowry Shale samples. Thermal maturation pathways for the three kerogen types are the same as those presented in Figure 2.3.

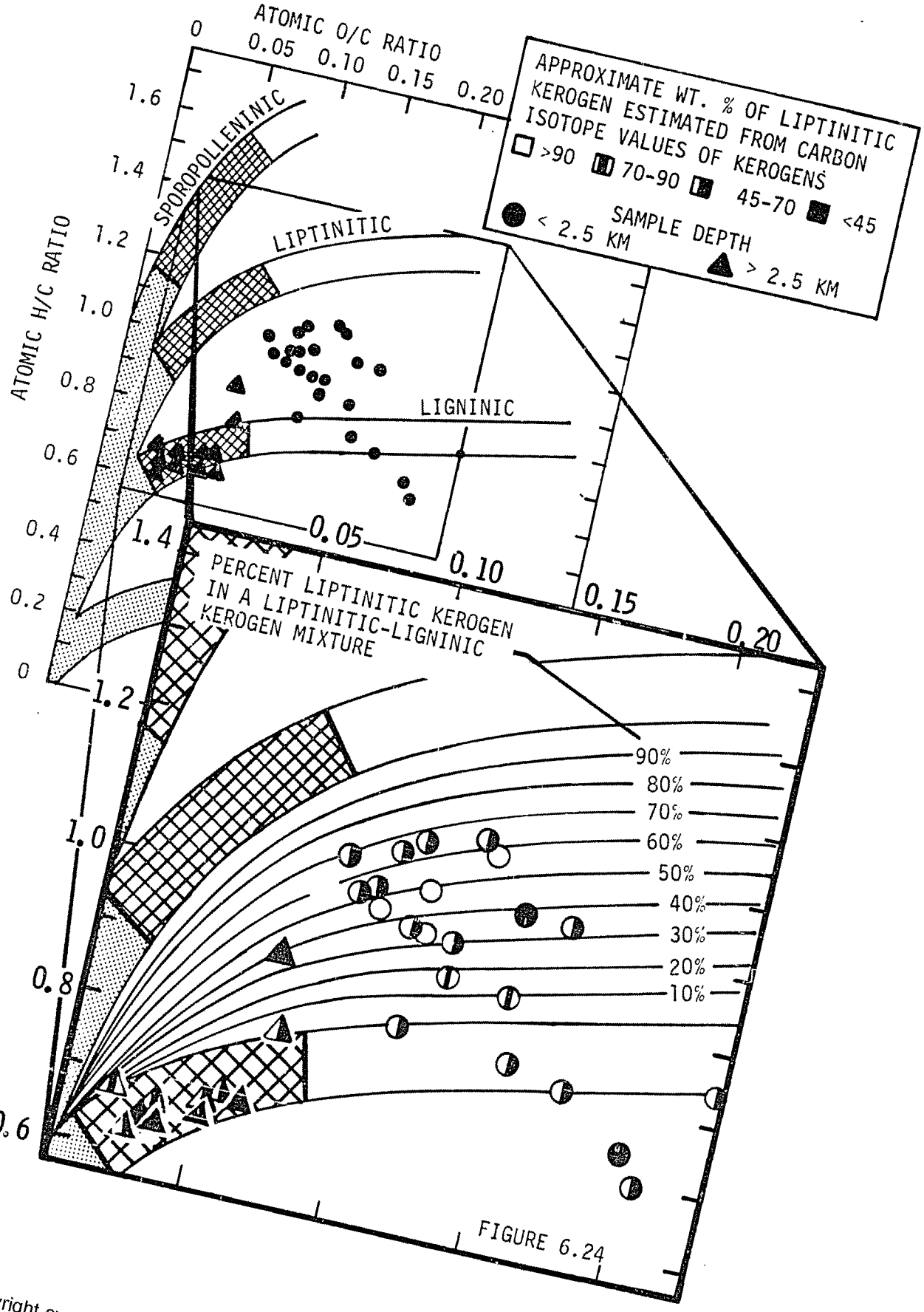

FIGURE 6.24

two kerogen types. The lack of agreement between the isopleth values and the estimates made from the carbon isotope values indicates that these kerogens from unweathered rocks have undergone varying degrees of oxidation in their depositional environments. It becomes apparent from this data that although the inorganic fraction of these rocks is rather uniform, the organic fraction is complex and consists of varying mixtures of liptinitic and ligninic kerogens at varying degrees of oxidation. This suggests that the source of organic matter fluctuated in the Mowry Sea as well as its exposure time to aerobic conditions.

Vanadium and nickel determinations were only made on 16 of the samples, because of insufficient bitumen (<1.5°/oo) in the remaining 17 samples (Figure 6.25). Ligninic kerogen predominated in the one analyzed sample that was not a quartzose claystone (M-31), and its nickel concentration was below the detection limit and thus its vanadium-nickel fraction could not be evaluated. Based solely on the vanadium-nickel fractions of the bitumens, five facies have been recognized and are described in Table 6.13. The uniform character of the inorganic fraction of these samples revealed no diagnostic mineralogical or petrological features.

The facies have been interpreted as a decreasing pH sequence with an accompanying decrease in Eh as suggested in Figure 6.26. This suggested trend may be attributed to the amount, type, and degree of oxidation of the organic matter that is incorporated into the sediment column and the redox potential of the water column above the sediment-water interface. Studies by several investigators indicate that organic matter and its

Figure 6.25: Histogram showing bitumen contents and limits of acceptability for vanadium and nickel analyses of bitumens from the Mowry Shale samples.

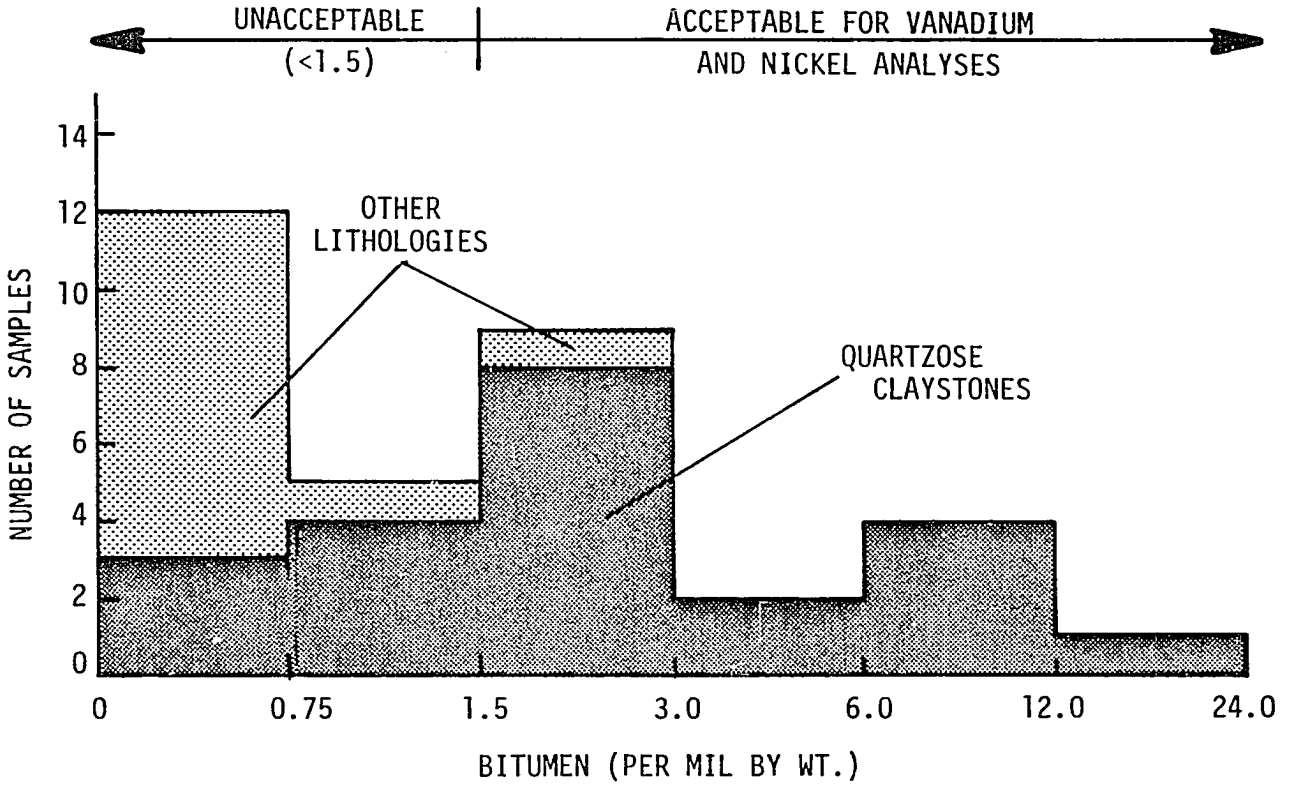

FIGURE 6.25

Table 6.13: Description of Mowry Shale facies, based on the vanadium-nickel fractions of their bitumen (V/(Ni+V)).

Eh-pH	Facies	V/(Ni+V)	Description	Sample Numbers
Moderate	1	0.01 + 0.00	Quartzose Claystones	M-28, M-29, M-30
Decreasing Eh and pH	2	0.09 + 0.02	Quartzose Claystones	M-15, M-17, M-18 M-38, M-39, M-43
	3	0.25 + 0.03	Quartzose Claystones	M-3, M-10, M-11, M-20, M-37
	4	0.37 + 0.02	Quartzose Claystones	M-12, M-21, M-22, M-25
Low	5	0.53 + 0.11	Quartzose Claystones	M-1, M-9

Figure 6.26: Interpreted trend of the Mowry Shale facies sequence on the Eh-pH diagram from Figure 6.6 Numbers on shaded trend correspond to facies given in Table 6.13.

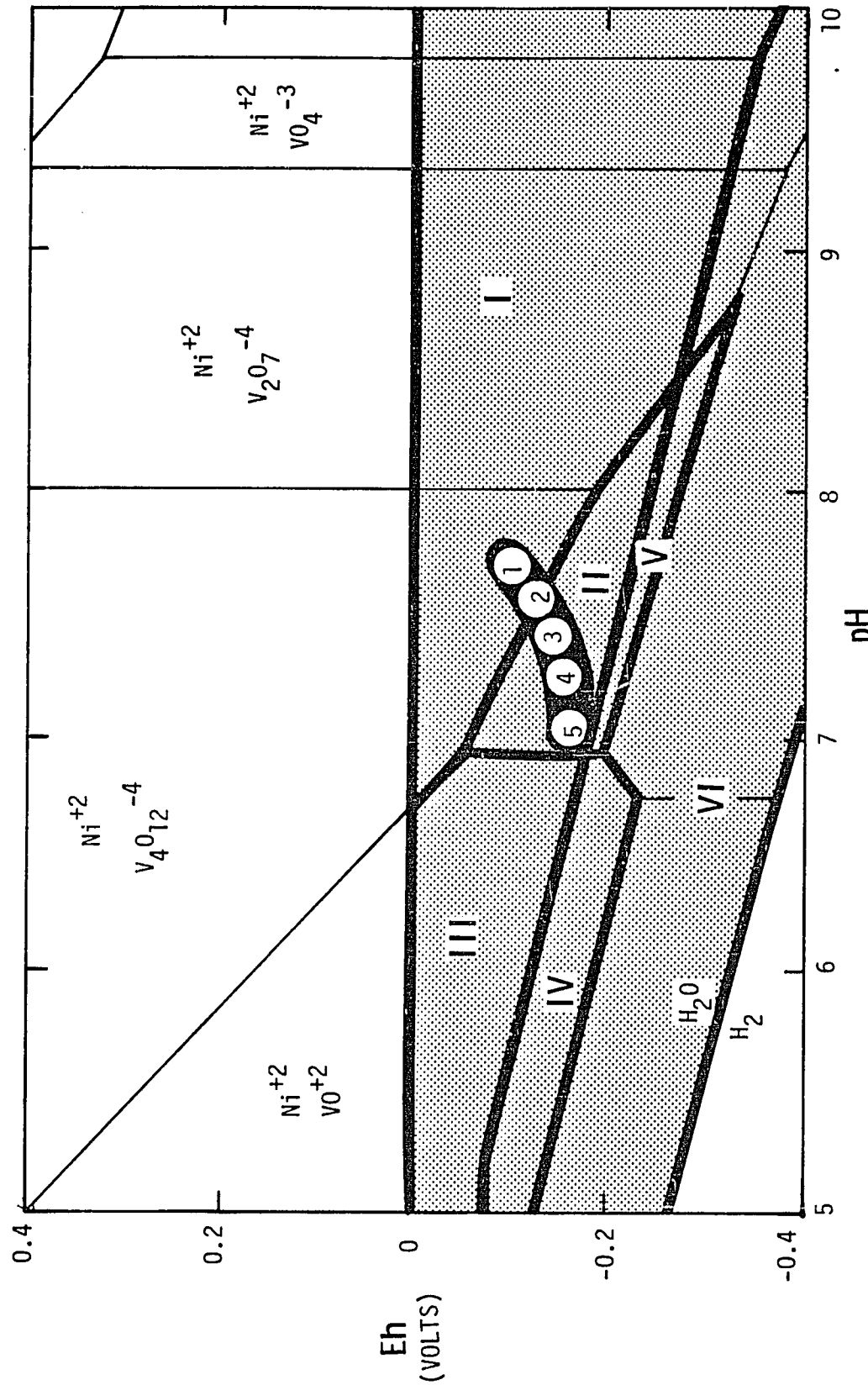

FIGURE 6.26

decomposition are the primary controls on the redox potential of marine sediments (Zobell, 1946) and soils (Burrows and Cordon, 1936). The general concept is that the greater the amount of organic matter incorporated into a sediment and the higher its susceptibility to bacterial degradation, the lower the redox potential of the system. The actual Eh value that will result in the interstitial waters will then be determined by the redox potential of the overlying water column and the degree of exchange between them. In addition to lowering the Eh of a sediment system, the bacterial generation of carbon dioxide and hydrogen sulfide during the degradation of the organic matter will cause a decrease in the pH (Berner, 1963; Siever et al., 1965; Thorstenson and Mackenzie, 1971 and 1974; Goldhaber and Kaplan, 1974). The resulting Eh-pH trend would be similar to the one suggested in Figure 6.26, and similar trends have been observed in nature (Lindblom and Lupton, 1961; Kemp, 1971). This trend is particularly applicable to sediments that are devoid of carbonate minerals, which may tend to buffer their interstitial waters at a higher pH. In the Mowry Shale samples carbonate was appreciable in only two of the samples in facies 1 and detectable in only two of the samples in facies 2. As shown in Figure 6.26, these two facies have been interpreted to have deviated the least from the pH range of 7.4 to 7.6 for normal marine waters near the sediment-water interface (Emery and Rittenberg, 1952; Siever et al., 1965; Murray et al., 1978; Sayles, 1979).

Although the amount and type of organic matter have been evaluated for the Mowry Shale samples, the susceptibility of the organic matter to

bacterial degradation in the sediment is difficult to assess. The amount of oxidized organic matter may be estimated (Figure 6.24), but distinguishing between oxidation that occurred in the sediment from that which occurred in the water column or during transport is not possible. Thus only the net effect of these variables has been interpreted on the Eh-pH diagram in Figure 6.26. Facies 1 is interpreted to represent conditions in Eh-pH Field I. Under these conditions vanadium will occur as a quinquivalent anion that will not be competitive with nickelous cations for tetrapyrrole bonding sites. This results in low vanadium-nickel fractions, which are characteristic of facies 1. Facies 2 through 5 are interpreted as a sequence of conditions from the boundary between Eh-pH Fields I and II to the low pH end in Eh-pH Field II. As the conditions of the facies approach the low pH values in Eh-pH Field II, the hydroxylation of vanadyl cations decreases and vanadyl cations become more competitive. This would result in the observed increase in the vanadium-nickel fractions of the bitumens from facies 2 through 5.

6.6 MONTEREY SHALE

During Middle and Late Miocene time, an inland extension of the Pacific Ocean over the presently existing Coast Ranges and San Joaquin Valley of southern California was the site for the deposition of the Monterey Shale (Figure 6.27; Reed, 1933; Kleinpell, 1938). The formation or entrapment of voluminous quantities of biogenic silica appears to have predominated within this extended ocean, as evident by the enormously thick sections (greater than 1000 meters) of rhythmically bedded

Figure 6.27: Map of southern California showing the limit of the Pacific Ocean during Late Miocene time and the major submarine basins. Map is based on work by Reed (1933), Reed and Hollister (1936), and Simonson (1958).

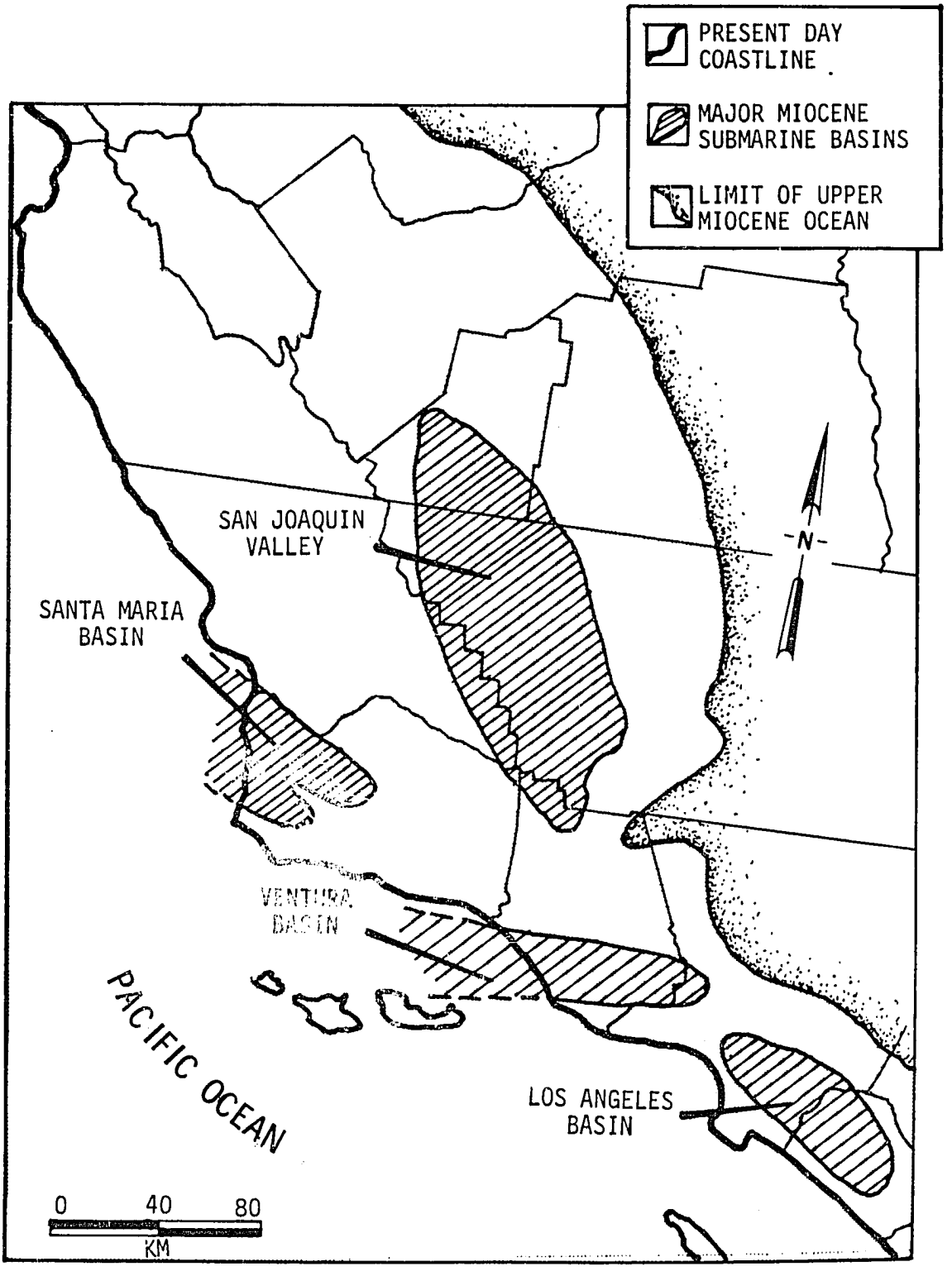

FIGURE 6.27

diatomaceous and siliceous rock sequences (Bramlette, 1946). In addition to this prominant siliceous rock sequence, the Monterey Shale also contains calcareous and to a lesser extent phosphatic rock sequences near its base (Smith, 1968; Pisciotto, 1978), and clastic rock sequences occur within it in some areas (eg. Modelo Canyon; Bramlette, 1946). The topography of the ocean floor during this time appears to have been irregular with deep submarine basins developing as a result of strike-slip faulting (Crowell, 1974). These pull-apart and tipped-wedge basins were apparently the sites for major sediment accumulations and are reflected on isopach maps as anomalously thick sections (Reed and Hollister, 1933; Simonson, 1958). The abundance of silica tests from planktonic organisms and the common occurrence of fish remains in the Monterey Shale (Bramlette, 1946) suggest that the water column was predominantly aerobic. The preservation of organic matter in some portions of the Monterey Shale suggest that dysaerobic and anaerobic conditions may have periodically developed in the lower parts of the water column. The common occurrence of bentonites (Kerr, 1931) and tuffs (Reed, 1933) in the Monterey Shale indicate that volcanism was active during this period of time.

The samples used in this study were collected from the outcrops shown in Figure 6.28. Sampling was restricted to the dark organic rocks within the sections at each locality. Since the collection of these samples, the author has examined three other outcrops where organic shales occur. Sufficient time was not available to include samples from these outcrops in this study, but their locations are noted in Figure 6.28 for

Figure 6.28: Geological map showing sampling localities of the Monterey Shale and the marine sedimentary rocks of Middle and Late Miocene age in southern California (modified from Jenkins, 1938). Localities referenced for future studies include Shell Beach (A, Sec. 4, T.32S., R.12E., San Luis Obispo Co.), Point Dume (B, Sec. 8, T.2S., R.18W., Los Angeles Co.), and Newport Bay (C, Sec. 26, T.6S., R.10W., Orange Co.). Insert showing types of rock sequences in the Monterey Shale is based on work by Pisciotto (1978) and a personal communique with Surdam (1979).

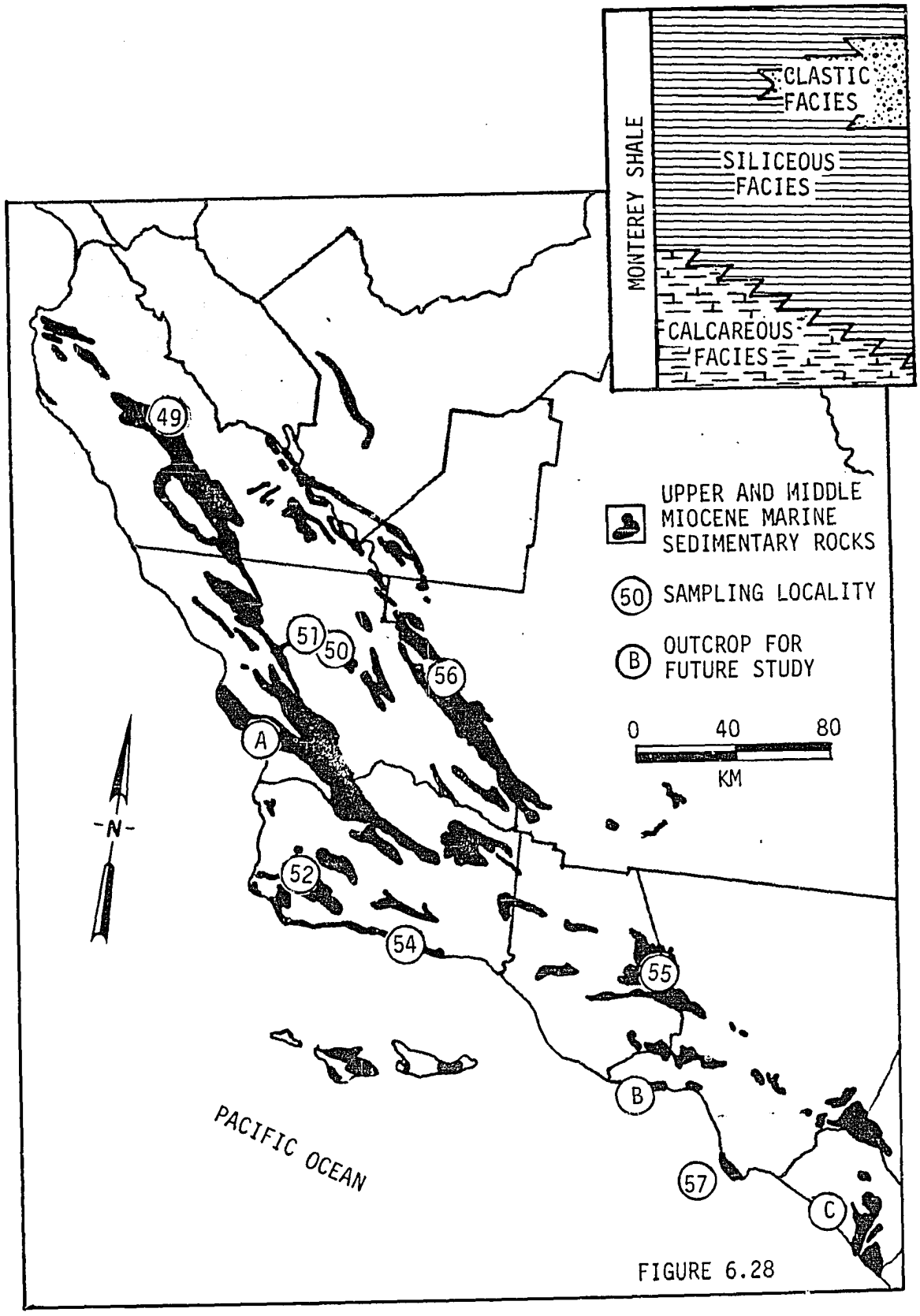

FIGURE 6.28

consideration in future studies. The mineralogy and rock types included in this study are given in Figure 6.29. Initially the primary silica component in the Monterey Shale appears to have been biogenic opal-A (Bramlette, 1946). As this amorphous material is subjected to increasing levels of diagenesis, it progressively develops order and dehydrates into opal-CT and eventually into quartz (Bramlette, 1946; Mizutani, 1970; Murata and Larson, 1975). This complete conversion of opal-A to quartz occurs within the low level of kerogen thermal maturation (Surdam, 1979, personal communique). The samples collected for this study occur intermediate on this silica diagenetic trend, and consist of mixtures of opal-CT and quartz.

The organic carbon analyses are shown in Figure 6.30. Generally, it was observed in the field that organic shales were more prevalent in calcareous rock sequences than in siliceous rock sequences. The author has noted that the organic richness of the siliceous rock sequences is usually overestimated. The siliceous rock sequence of the Monterey Shale at Chico Martinez Creek has been assumed by Friedman and Murata (1979) to be rich in organic matter, based on organic carbon analyses made by Phillippi (1965) on the Monterey Shale in the Los Angeles Basin area. Examination of the Chico Martinez Creek section, as well as the Reliz Canyon, Indian Creek, Rhodes Gulch, and Lompoc Mine sections, indicate that these siliceous rock sequences consist of non-organic rocks, and therefore extrapolation of organic richness over considerable distances is not advisable. The misconception that organic matter is prevalent in the Monterey Shale is in part the result of investigators using the word

Figure 6.29: Ternary diagrams showing mineralogy of rock types collected from the Monterey Shale for this study. Plots based on data given in Appendix VII.

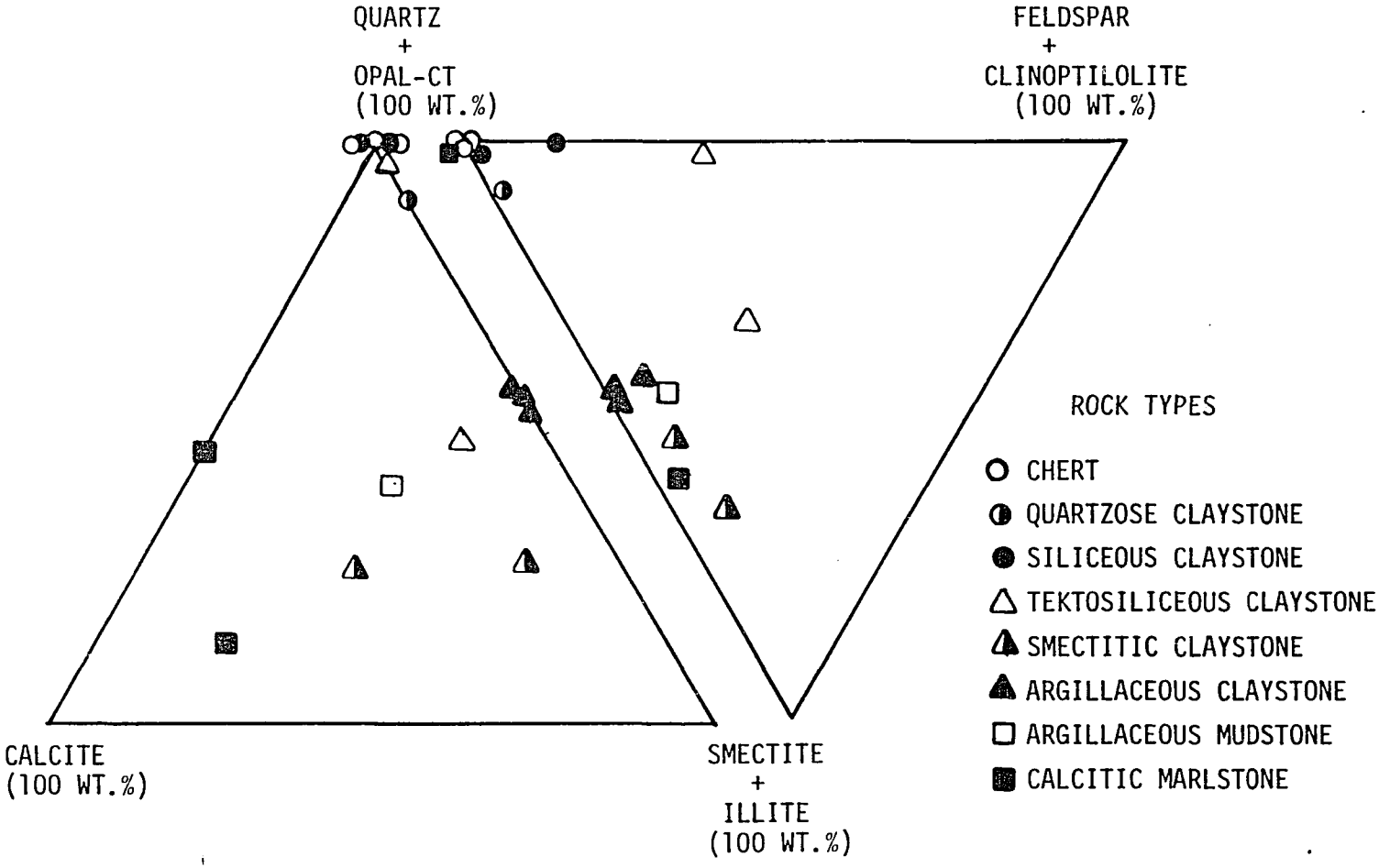

FIGURE 6.29

Figure 6.30: Histogram showing distribution of organic carbon in different rock sequences of the Monterey Shale, and classification of their organic richness.

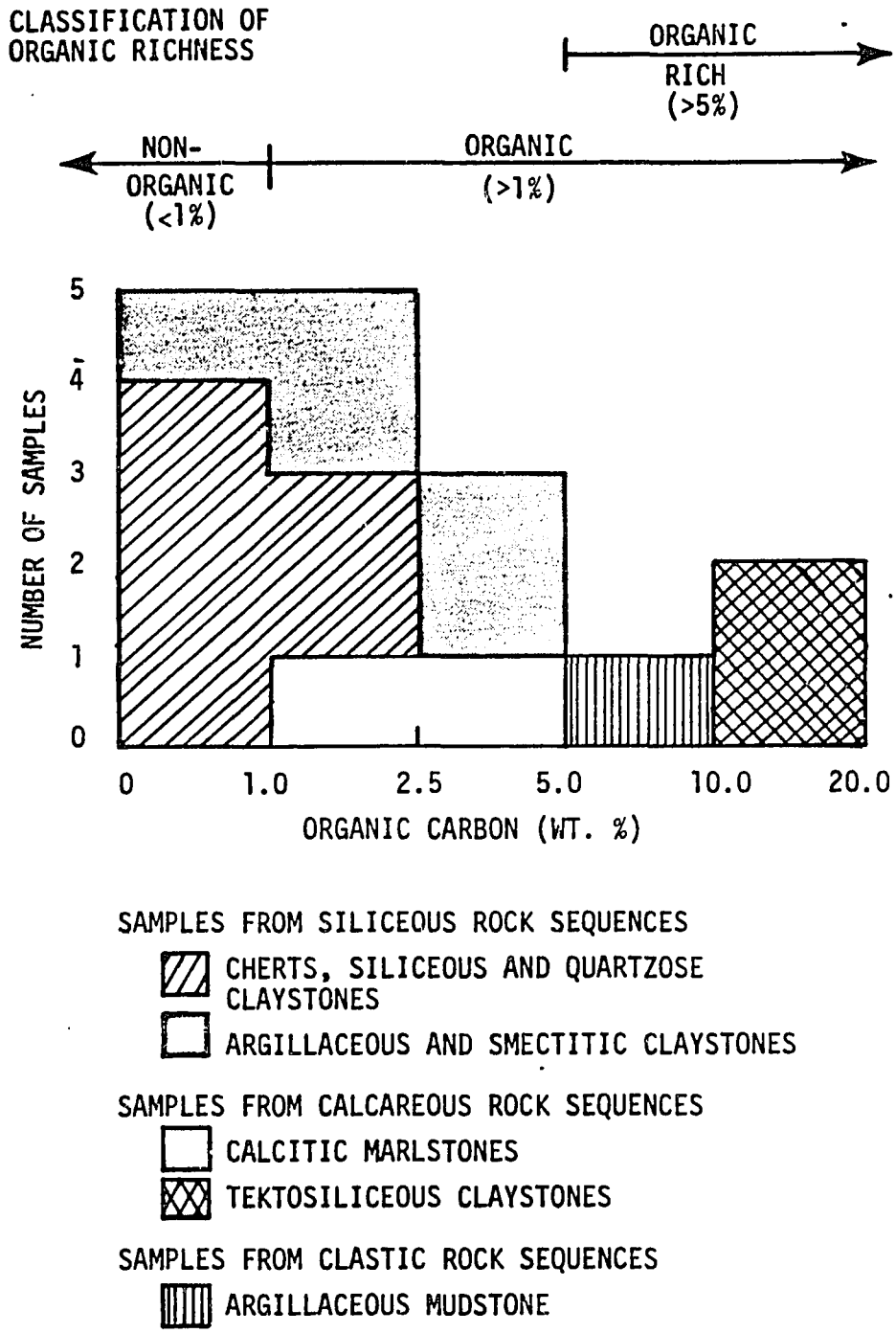

FIGURE 6.30

organic to describe rocks containing an abundance of tests or frustules (eg. Kleinpell, 1948; Bramlette, 1946; Dibblee, 1973). Fossiliferous or biogenic would be more appropriate adjectives for these rock types and would reduce confusion of these rocks with those that contain appreciable amounts of organic matter.

Carbon isotope values and visual analysis of the kerogens from these samples indicate that α-liptinitic kerogen comprises at least 90 percent of the kerogen (Figure 6.31). The only exception is sample MR-2 which contains greater than 90% β-sporopolleninic kerogen as indicated by its elemental analyses (Figure 6.32), as well as by its carbon isotope value (Figure 6.31). The elemental analyses plotted in Figure 6.32 show that these unweathered samples have experienced varying degrees of oxidation in their environment of deposition, all of the kerogens are at a low level of thermal maturation. The oxidation of the organic rocks from Agua Amarga outcrop (MR-15, MR-16, MR-17) may have been enhanced by the igneous intrusives that were emplaced in the Monterey Shale in this area during the Miocene (Woodring et al., 1946). Future research in this area may reveal some interesting relationships between organic sediments and igneous activity.

Vanadium and nickel analyses were only run on eight of the collected samples because of low bitumen contents and high elemental sulfur contamination in the remaining samples (Figure 6.33). Although this data is limited and reconnoiter in character, six facies have been proposed (Table 6.14) and their interpretation is given in Figure 6.34.

Figure 6.31: Histogram showing the distribution of kerogen δC^{13} values of Monterey Shale samples and their relationship to visual kerogen analyses.

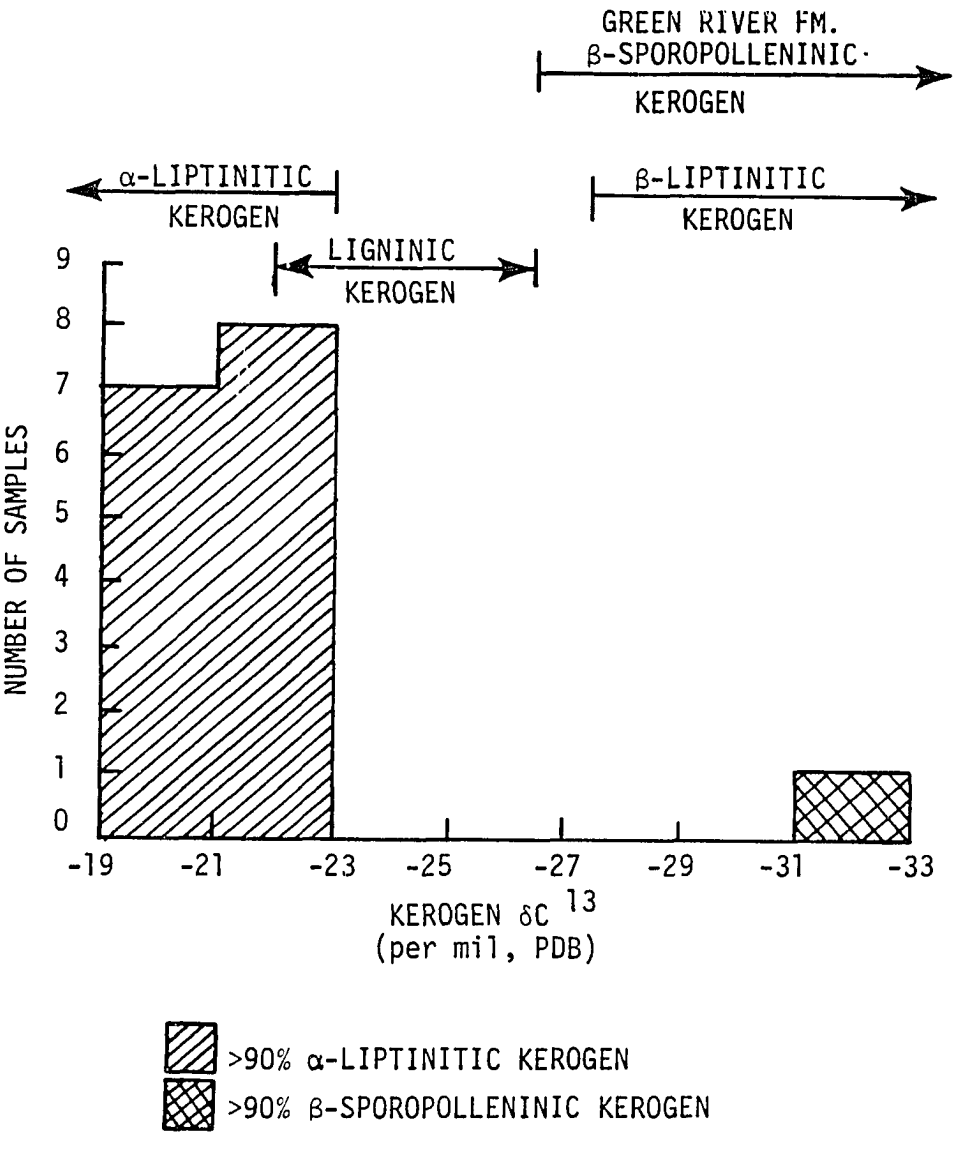

FIGURE 6.31

Figure 6.32: Atomic H/C ratios versus atomic O/C ratio plot of kerogens from the Monterey Shale samples. Thermal maturation pathways for the different kerogen types are the same as those presented in Figure 2.3.

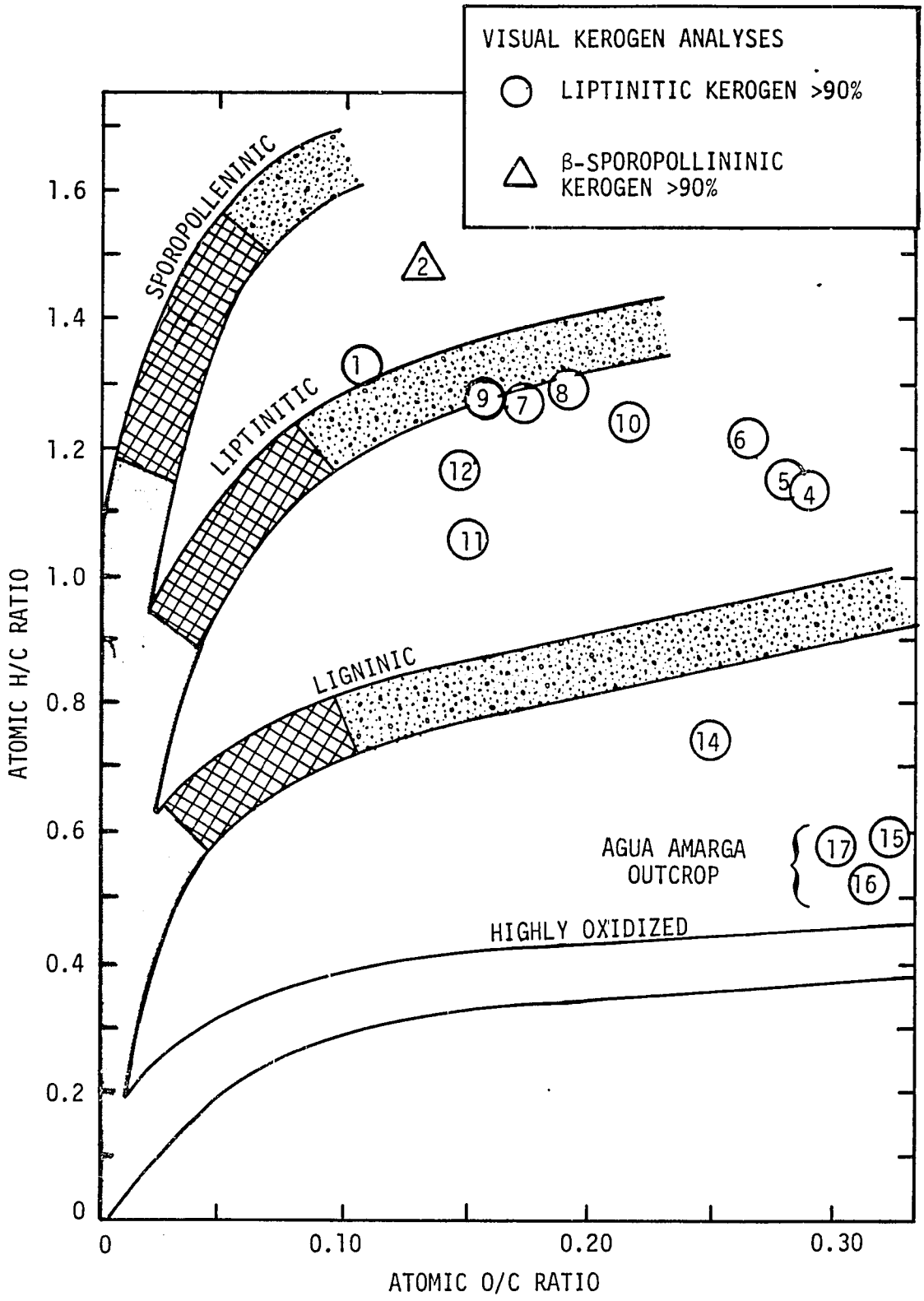

FIGURE 6.32

Figure 6.33: Histogram showing bitumen contents and limits of acceptability for vanadium and nickel analyses of bitumens from the Monterey Shale samples.

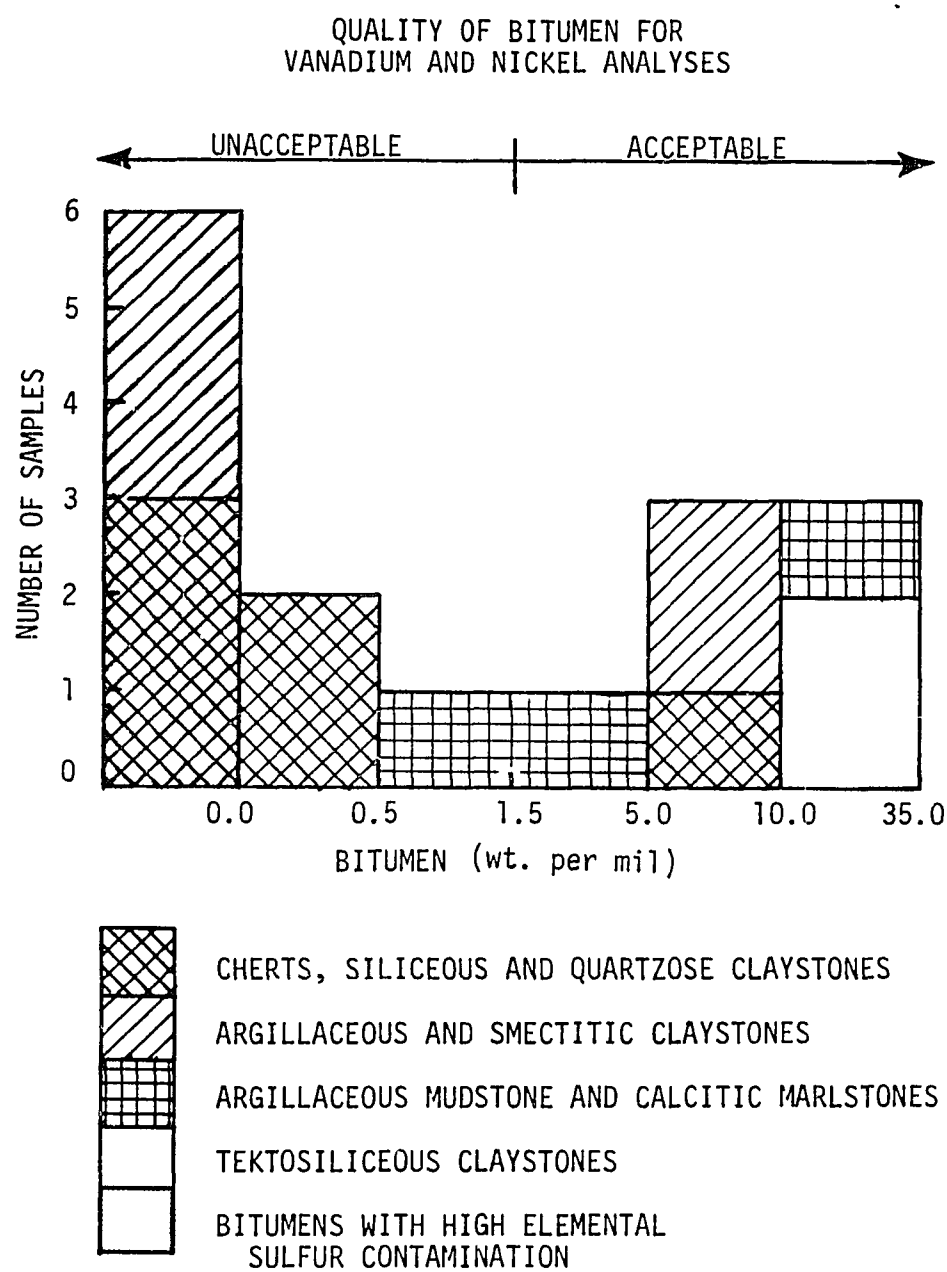

FIGURE 6.33

Figure 6.34: Interpreted trends for the proposed facies of the Monterey Shale samples on the Eh-pH diagram from Figure 6.6. Numbers on shaded trends correspond to facies given in Table 6.14.

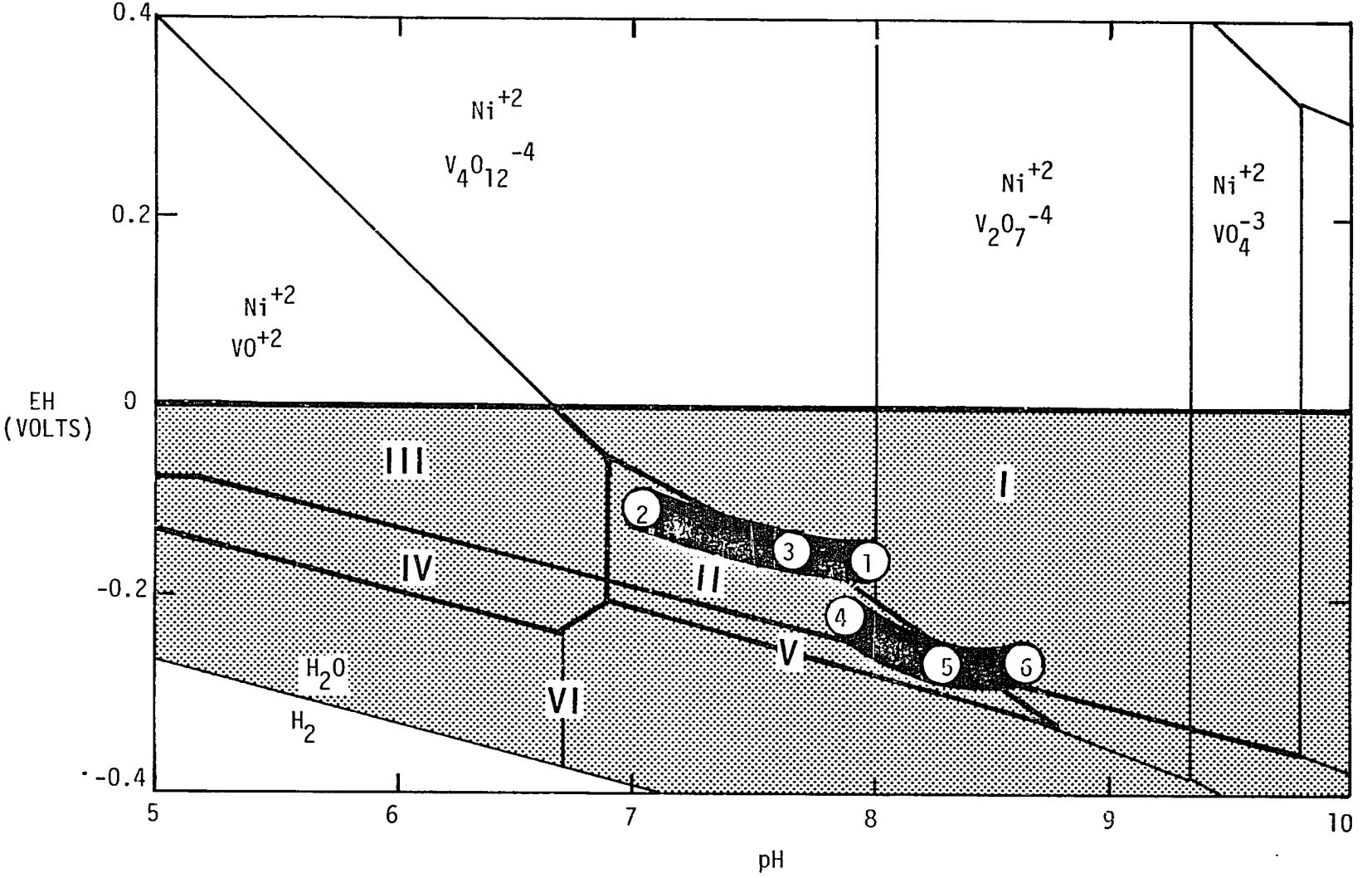

FIGURE 6.34

Table 6.14: Description of Monterey Shale facies and the vanadium-nickel fractions of their bitumens (V/(Ni+V)).

Facies	V/(Ni+V)	Description	Sample Numbers
1	0.03	Foraminiferal argillaceous mudstone containing illite and smectite. Rock unit occurs in a predominantly clastic sequence.	MR-12
2	0.62 + 0.02	Argillaceous and quartzose claystones containing smectite. Rock unit occurs in a predominantly siliceous shale and diatomite sequence.	MR-5, MR-6
3	0.16	Argillaceous claystone containing smectite. Rock unit occurs in a predominantly siliceous shale and diatomite sequence.	MR-7
4	0.30 + 0.02	Foraminiferal argillaceous mudstone containing illite and smectite. Rock unit occurs in a predominantly clastic sequence.	MR-12
5	0.46	Organic rich tektosiliceous claystone containing illite and clinoptilolite. Rock unit occurs in a predominantly calcareous shale sequence.	MR-10
6	<0.02	Organic rich tektosiliceous claystone containing clinoptilolite and no clay minerals. Rock unit occurs in a predominantly calcareous shale sequence.	MR-11

Facies 1 has a low vanadium-nickel fraction and is associated with a clastic rock sequence. This facies has been interpreted to represent conditions in Eh-pH Field I where quinquivalent vanadium anions will not be competitive with the nickelous cations for tetrapyrrole bonding sites. Facies 2 and 3 are associated with siliceous rock sequences and are interpreted to represent conditions in Eh-pH Field II and on the boundary between Eh-pH Field I and II, respectively. Under these conditions vanadyl cations will become less competitive with nickelous cations due to increasing hydroxylation with increasing pH.

Facies 4, 5, and 6 are associated with calcareous rock sequences and are interpreted to represent a much lower Eh trend than facies 1, 2, and 3 (Figure 6.34). The presence of the zeolite clinoptilolite and the absence of smectite in facies 5 and 6 suggests a high alkalinity in the sediment system (Mariner and Surdam, 1970; Cosgrove and Papavassiliou, 1979). In facies 5, illite coexists with clinoptilolite and the 0.46 vanadium-nickel fraction suggests that this facies may occur on the boundary between Eh-pH Fields II and V. At high pH values along this boundary, vanadyl cations will be hindered by hydroxyls and nickelous cations will be hindered by sulfides. This situation would result in both cations having a reduced but equal competitiveness for tetrapyrrole bonding sites.

In facies 6 the higher clinoptilolite content and complete absence of illite suggests that the alkalinity was higher than in facies 5. The low vanadium-nickel fraction of this facies suggests that vanadium

cations were not competitive with nickelous cations for bonding sites and the conditions probably represent those of Eh-pH Field I. The presence of smectite and the absence of zeolites in facies 4 suggests that its alkalinity was lower than that of facies 5 and 6. As shown in Figure 6.34, this facies has been interpreted to represent the conditions of Eh-pH Field II.

The Eh and pH conditions suggested for facies 1, 2, 3, and 4 could have developed readily under normal marine salinities and temperatures. As noted in the discussion on the Mowry Shale (Section 6.5), the Eh and pH of marine sediments is controlled by the oxygen content of the overlying water column, and the amount, type, and degree of degradation of the organic matter incorporated into the sediments. In addition, the presence of calcite in facies 1 and 4 suggests that higher pH values may be obtained due to carbonate buffering within the interstitial waters. The smectite to zeolite conversion that appears to have occurred in facies 5 and 6 suggest a high alkalinity in the interstitial waters of their sediments. The high alkalinity that induced a similar mineralogical conversion in the Green River Formation is attributed to excessive evaporation of Lake Gosiute (Section 6.4.1), but this type of mechanism does not appear to be feasible in the open marine setting of the Monterey Shale. An alternate mechanism would be that the rocks from facies 5 and 6 represent the periodical development of stratified hypersaline water or brine layers within the submarine basins. Recent examples of this type of setting include the Orca Basin in the Gulf of Mexico (Tompkins and Shephard, 1979) and the Atlantis II Deep in the Red Sea (Miller,

1969). It should also be noted that the samples from facies 5 and 6 contain the highest organic carbon concentrations (>10 weight percent) of the collected Monterey Shale samples, and therefore their sediment systems were likely to have achieved very low Eh conditions as indicated in Figure 6.34.

6.7 KREYENHAGEN SHALE

The Kreyenhagen Shale of California was deposited in an inland sea during Late Eocene and Early Oligocene times (Figure 6.35; von Estorff, 1930; Woodring et al., 1940; Cushman and Siegfus, 1942). This sea appears to have occupied a fore-arc basin and was restricted in part from the Pacific Ocean by an outer-arc ridge (Salina and Coast Ranges Uplands, Figure 6.36) which resulted from the development of a subduction complex to the west (Dickinson, 1976; Ingersoll, 1979). The Kreyenhagen Shale is best exposed in outcrop along the southwestern flank of the San Joaquin Valley in Merced, Fresno, King, and Kern Counties (Figure 6.36). Distinct lateral variations in the lithology of the Kreyenhagen Shale occur as shown in the insert of Figure 6.36, and these lithological variations have caused some confusion in defining this rock unit in the past (Woodring et al., 1940).

The organic calcareous rock sequence consists primarily of quartzose claystones and its calcareous character is due to its inclusion of foraminifera tests. The preservation of organic matter and the presence of benthonic forams (eg., Planularia cf. markleyana, Plectofrondicularia

Figure 6.35: Map of central California showing the Late Eocene and Early Oligocene inland sea, in which the Kreyenhagen Shale was deposited. Map is based on work by Reed (1933) and Reed and Hollister (1936).

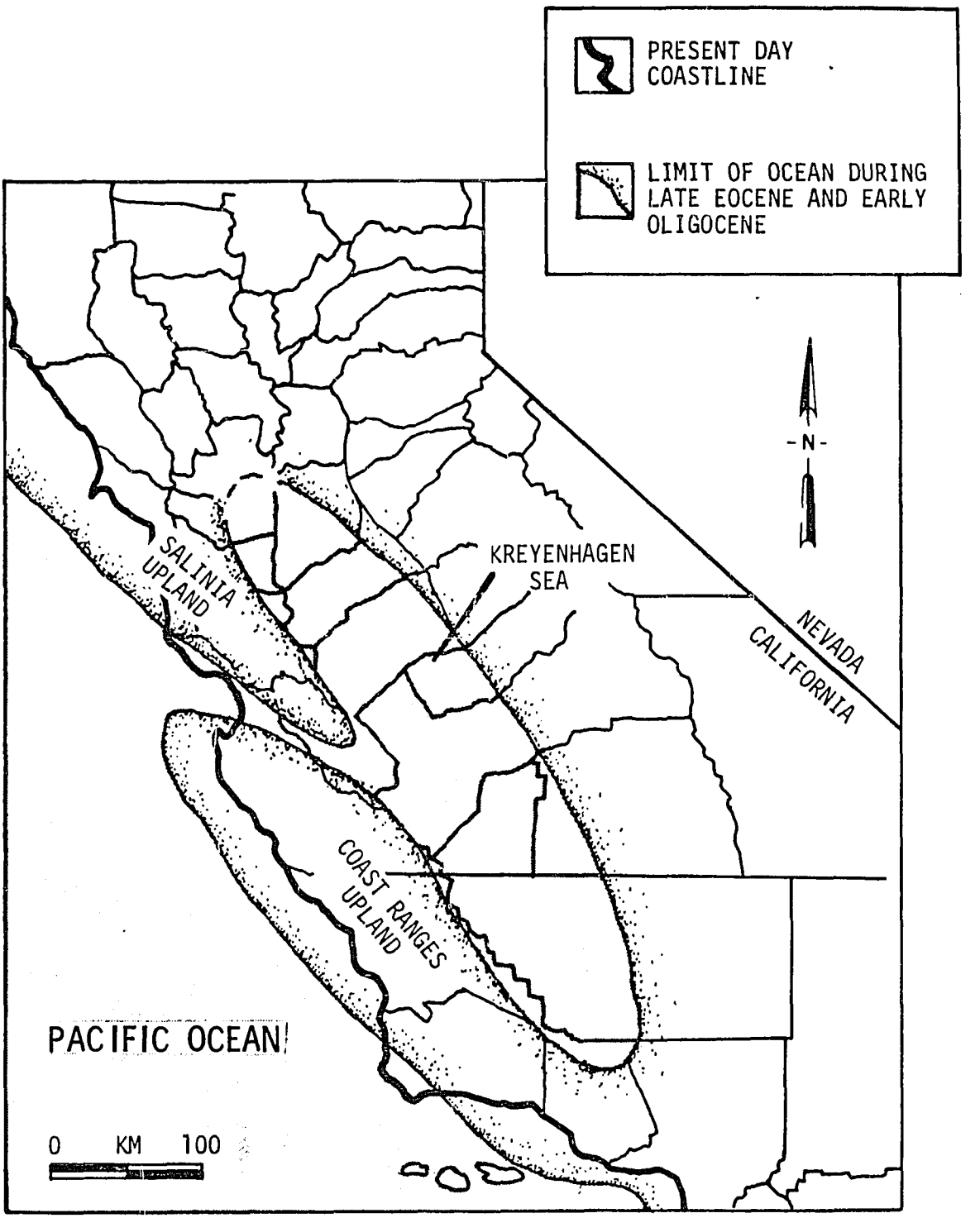

FIGURE 6.35

Figure 6.36: Geological map showing sampling localities of the Kreyenhagen Shale and the Late Eocene and Early Oligocene sedimentary rocks in central California (modified from Jenkins, 1938). Unsampled localities include Woo Ranch Canyon (A, Secs. 1 and 12, T.12S., R.10E., Merced Co.), Arroyo Ciervo (B, Secs. 22, and 23, T.16S, R.13E., Fresno Co.), Oil Canyon (C, Sec. 20, T.19S., R.15E., Fresno Co.), and Devils Den (D, T.25S, R.18E., Kern Co.). Insert showing type of rock sequences in the Kreyenhagen Shale is base of field work by the author and described sections by von Etorff (1930), Woodring and others (1940), Cushman and Siegfus (1942), Kidson (1965), and Watkins (1974).

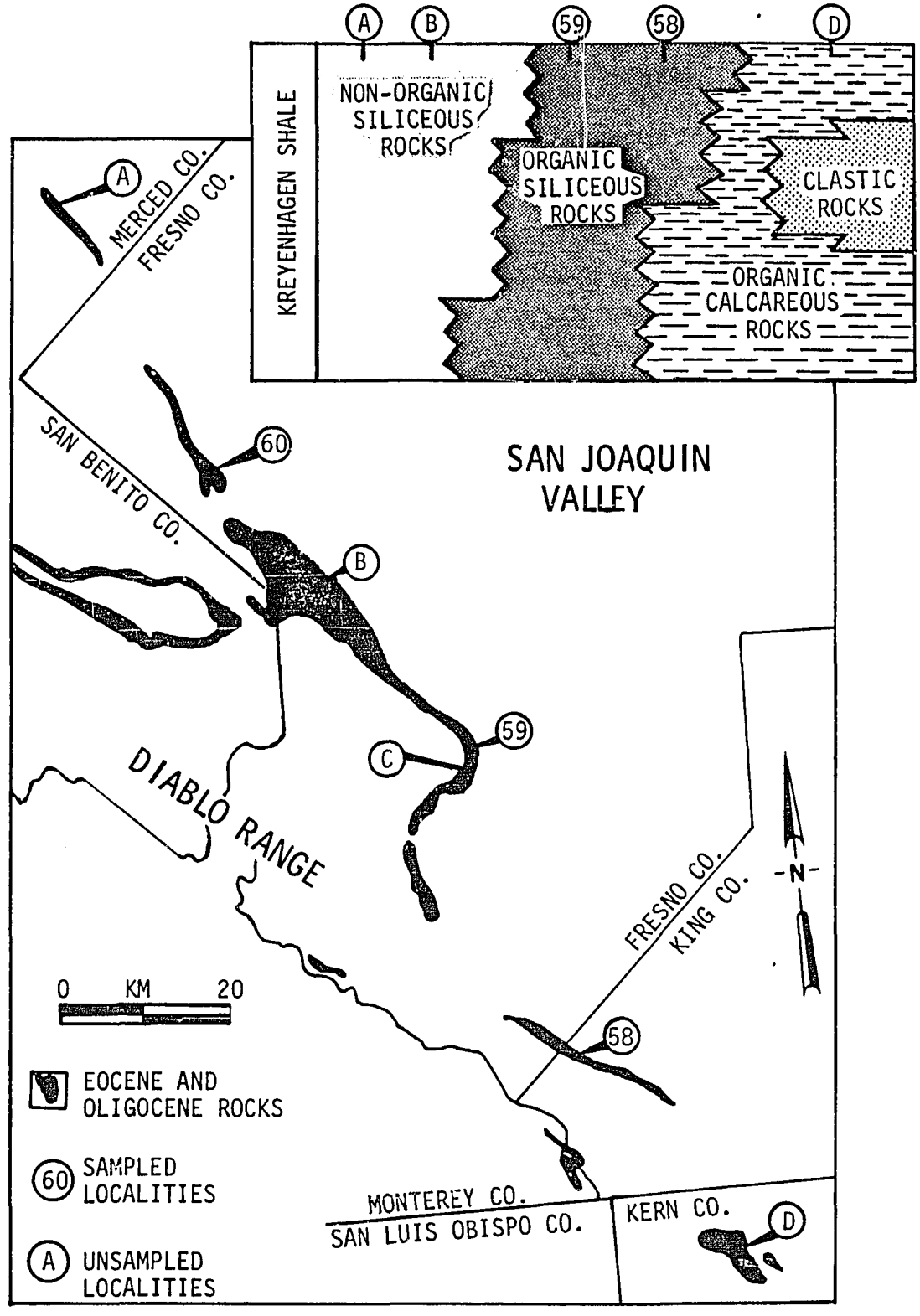

FIGURE 6.36

garzaensis, and Univerina garzaensis; Masters, 1975, personal communique) suggests that anaerobic conditions prevailed in the sediment column and dysaerobic conditions prevailed in the lower portion of the water column. The existence of benthonic forams under these conditions has been observed in recent marine environments (Phleger and Soutar, 1973). In the Devils Den area the calcareous rock sequence is divided by a clastic rock sequence (Woodring et al., 1940), which is referred to as the Point of Rock Sandstone. The organic siliceous rock sequence consists primarily of radiolarian siallitic claystones. This lithology overlies the organic calcareous rock sequence in the Garza Creek section and is exclusive in the exposed section at Skunk Hollow. The preservation of organic matter and the absence of benthonic life forms in this rock sequence suggests that anaerobic conditions prevailed in the lower portion of the water column, as well as within the sediment column. The non-organic siliceous rock sequence consists primarily of diatomaceous and siliceous shales that are similar in character to the siliceous rock sequence of the Monterey Shale (Woodring et al., 1940). The lack of organic matter and the presence of benthonic mega-invertebrates (eg. Delectopecten, Thysasira, Macrocallista, and Nuculana; Watkins, 1974) in this rock sequence suggests that aerobic condition prevailed in the bottom waters of the water column and in the upper portion of the sediment column.

Sampling for this study was restricted to the organic calcareous and organic siliceous rock sequences. One sample of argillaceous claystone was collected from the non-organic siliceous rock sequence, but its low

organic carbon content (0.2 weight percent) was insufficient for further analyses. The organic carbon content and mineralogy of the rock types sampled are shown in Figure 6.37. As shown in Figure 6.38, visual analyses and carbon isotopes indicate that the kerogen type is primarily α-liptinitic kerogen with minor amounts of ligninic kerogen. The elemental analyses of these kerogens indicate that they are at a low level of thermal maturation and have been subjected to some oxidation (Figure 6.38). In general, it is worth noting that the character of these kerogens and the mineralogy of their rocks is uniform, with the presence or absence of foraminifera tests being the most notable variable.

The vanadium-nickel fractions of the bitumens from these samples also are uniform, with a narrow range between 0.17 and 0.23. The two facies proposed in Table 6.15 are based solely on the presence or absence of foraminifera tests and the vanadium-nickel fractions of their bitumens do not appear to be significantly different. As shown in Figure 6.39, these two facies are interpreted to represent conditions within Eh-pH Field II. The slightly higher vanadium-nickel fraction of the bitumen in facies 1 suggests that it may have had a slightly lower pH than facies 2. At a slightly lower pH, less hydroxylation of vanadyl cations would occur and vanadium would become slightly more competitive with available nickelous cations for tetrapyrrole bonding sites.

Figure 6.37: Ternary diagrams showing mineralogy and organic carbon content of rock types collected from the Kreyenhagen Shale. Plots based on data given in Appendix VII.

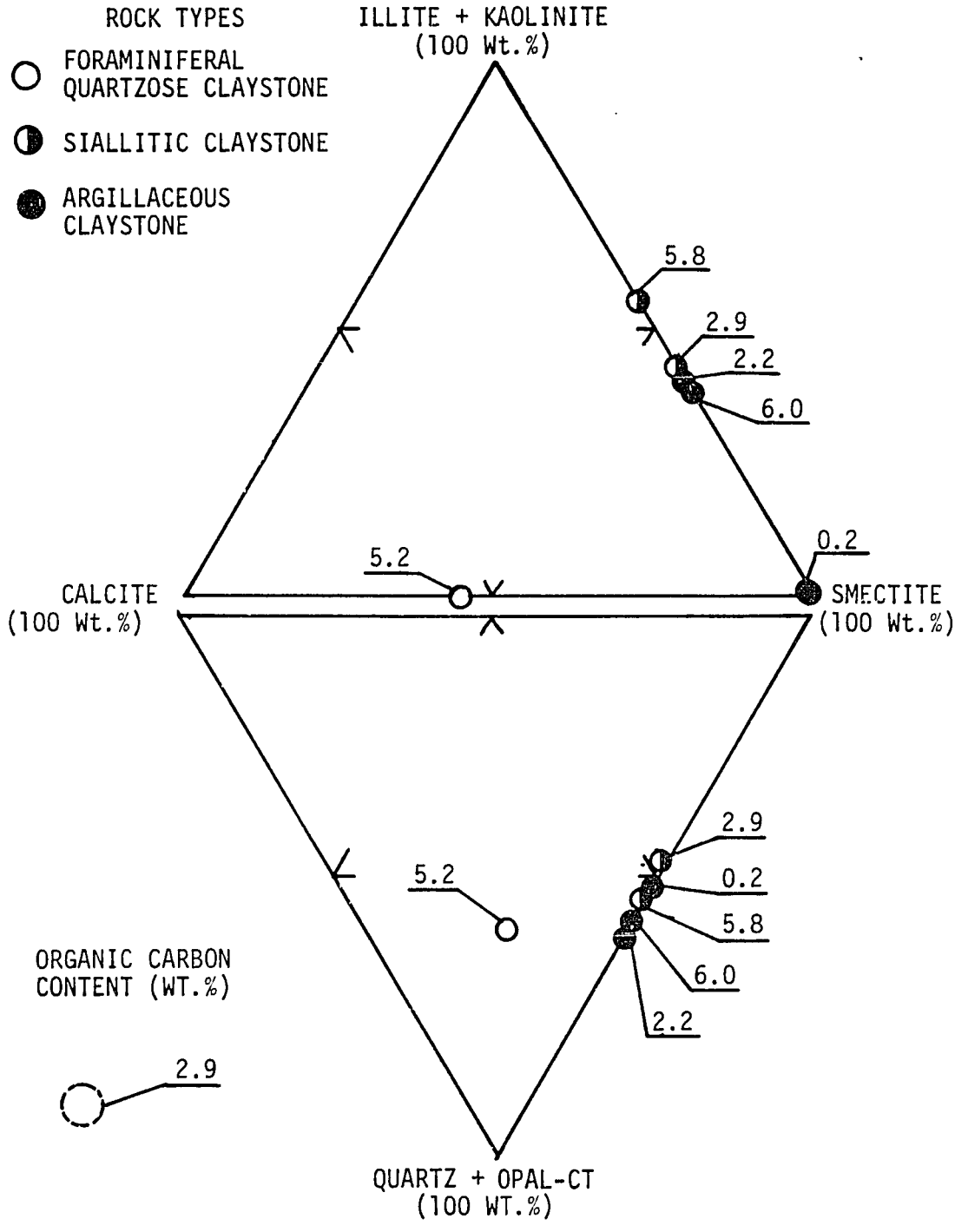

FIGURE 6.37

Figure 6.38: Atomic H/C ratio versus atomic O/C ratio plot of kerogens from the Kreyenhagen Shale samples. Kerogen carbon isotope values are relative to PDB and given in per mil units. Thermal maturation pathways for the different kerogen types are the same as those presented in Figure 2.3.

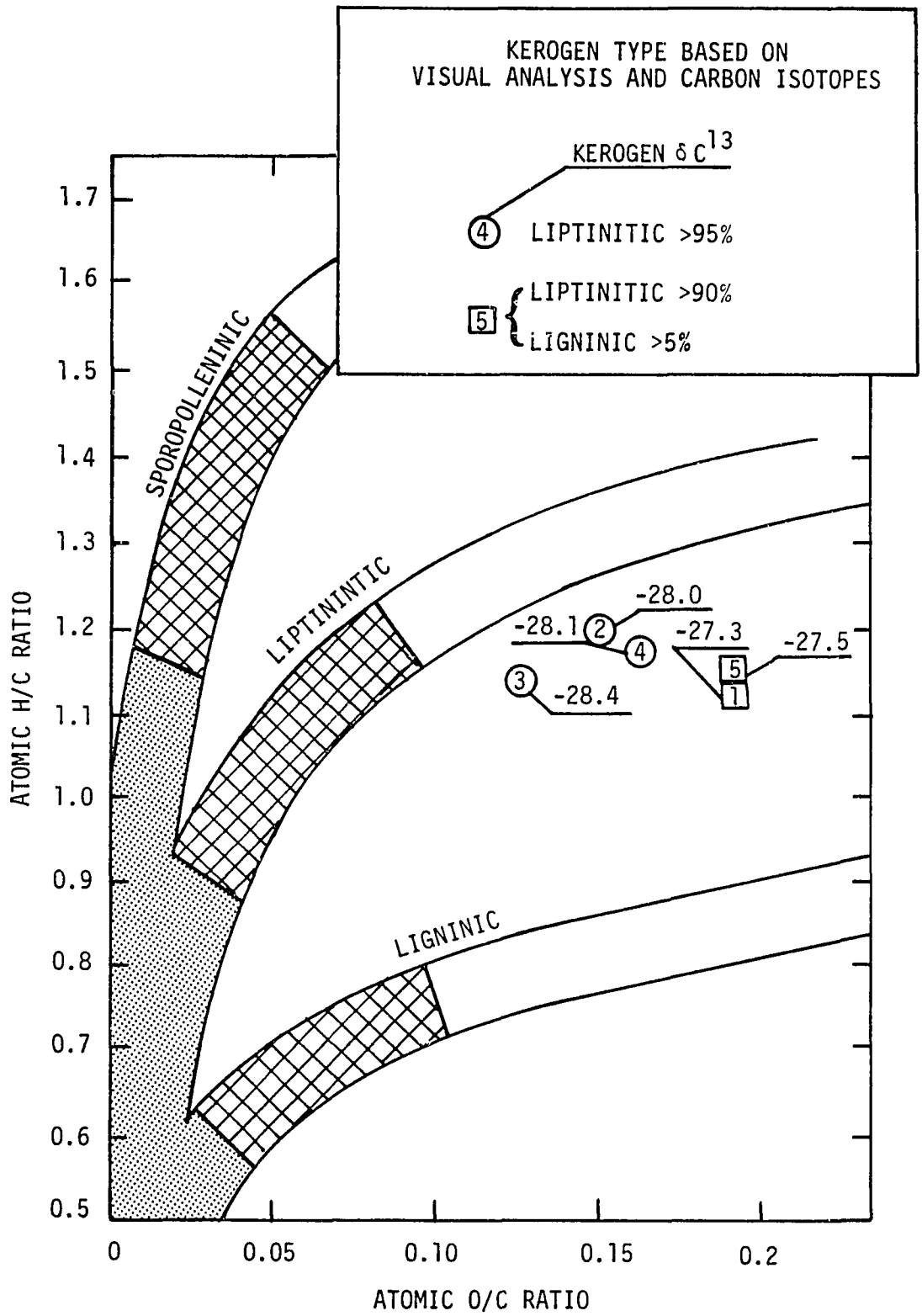

FIGURE 6.38

Table 6.15: Description of Kreyenhagen Shale facies and the vanadium-nickel fractions of their bitumens (V/(Ni+V)).

Facies	Description	V/(Ni+V)
1	Foraminiferal quartzose claystone from a calcareous rock sequence (N=1)	0.23
2	Argillaceous and siallitic claystones from organic siliceous rock sequences (N=4)	0.19 $\pm$ 0.02

N = number of samples

Figure 6.39: Interpretation of proposed Kreyenhagen Shale facies on the Eh-pH diagram presented in Figure 6.6. Circled numbers correspond to facies given in Table 6.15.

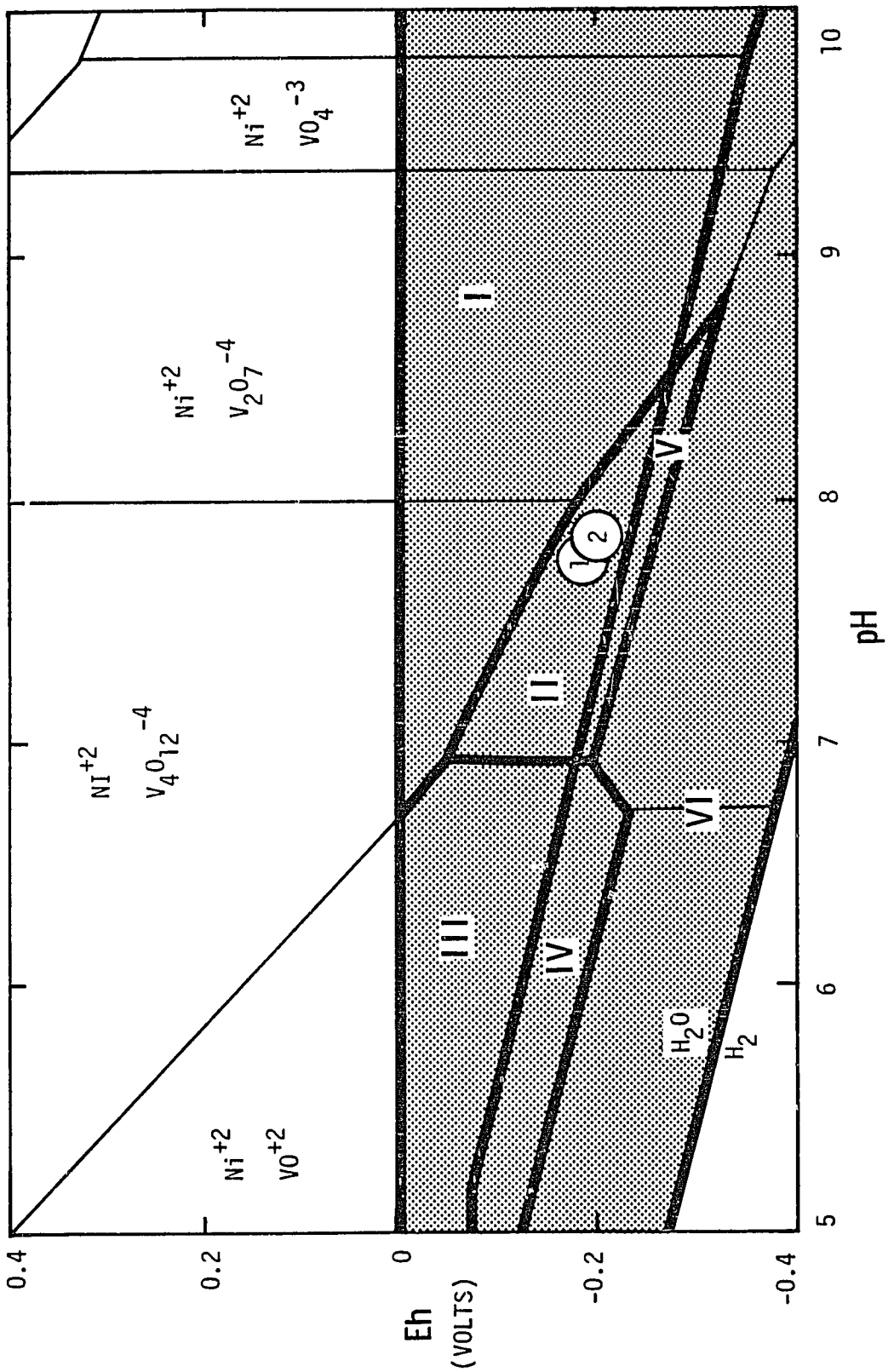

FIGURE 6.39

6.8 DEVONIAN-MISSISSIPPIAN BLACK SHALES

A vast epicontinental sea extended over a large portion of the eastern half of the United States during Late Devonian and Early Mississippian times (Figure 6.40; Conant and Swanson, 1961). Deltaic and prodeltaic sedimentation predominated along the eastern margin of this sea where the subsiding Appalachian Basin acted as a depocenter for large accumulations of sand, silt, and non-organic muds. Westward and southward, the prodeltaic sedimentation grades into open marine sedimentation, where fine-grained organic sediments accumulated over the midwestern states (Walker and Harms, 1971; Schwietering, 1978). The predominantly black and dark gray fine-grained rocks that resulted from this open marine environment are collectively referred to in this study as Devonian-Mississippian black shales, which consist of a number of formations; Grassy Creek Shale of Missouri, Woodford Shale of Oklahoma, Sheffield Formation of Iowa, Chattanooga Shale of Tennessee, New Albany Shale of Indiana, Antrim Shale of Michigan, Kettle Point Formation of Ontario, and Ohio Shale of Ohio. The tectonic setting of this epicontinental sea appears to have been the foreland basin of a subduction complex that was active along its eastern margin (Dineley, 1975; Schwietering, 1978).

Although organic matter and Tasmanites are abundant in the Devonian-Mississippian black shales, the occurrence of discernible fossils is not common. Some fossils that are encountered include Lingula, Foerstia, conodonts, and discernible plant debris (Hoskins and Cross, 1953; Conant and Swanson, 1961; Provo, 1977; Jordan, 1979). None of these fossils

Figure 6.40: Map showing extent of Devonian-Mississippian sea in the eastern half of the United States and basins around which outcrops of the Devonian-Mississippian black shales occur (modified after Conant and Swanson, 1961).

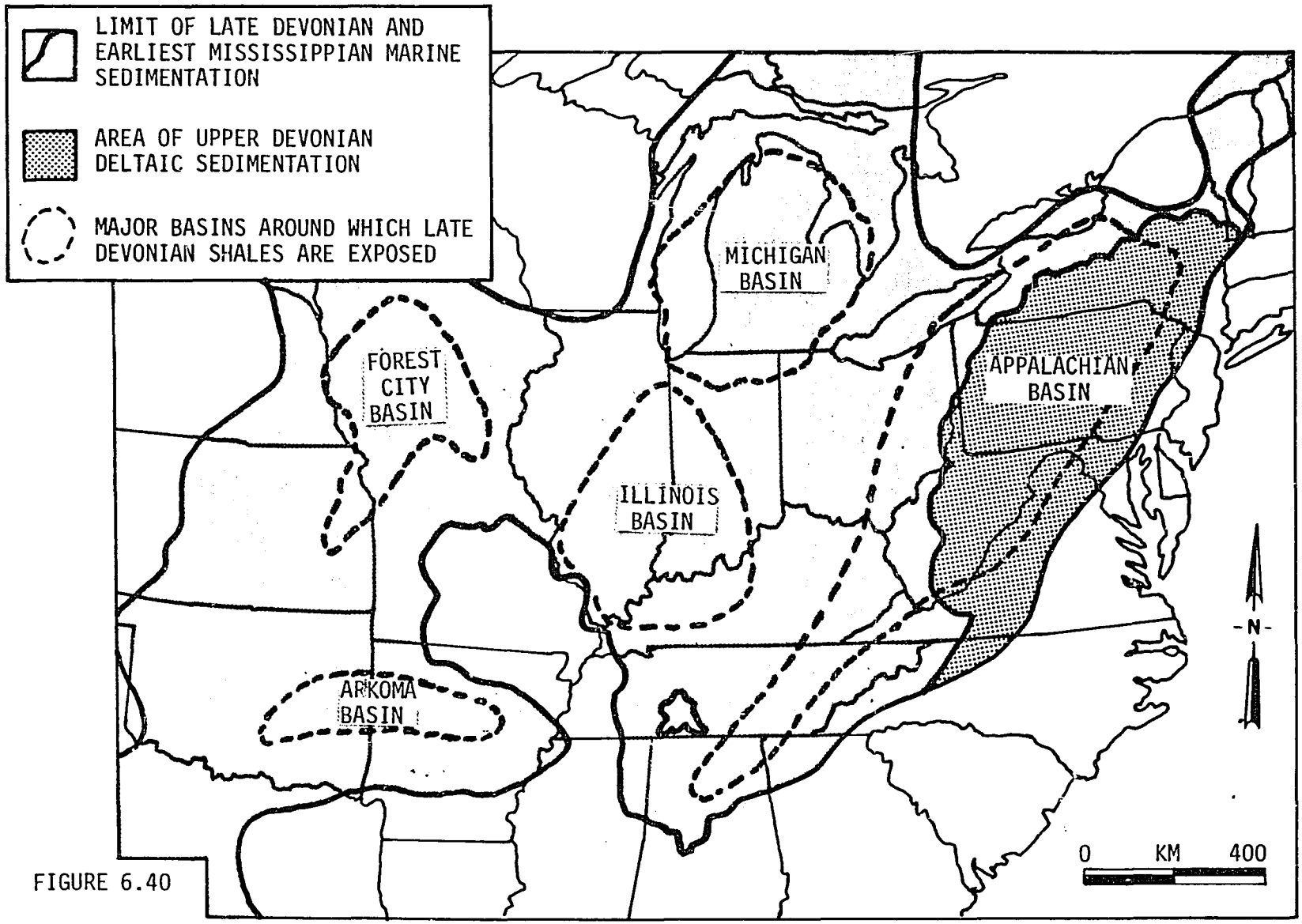

FIGURE 6.40

occur in abundance and are usually restricted to specific beds or zones within a stratigraphic section. The preservation of organic matter (Breger and Brown, 1962) and the dearth of planktonic and nektonic fossils as well as benthonic fossils in these rocks suggests that the water column of the Devonian-Mississippian Sea was predominantly anaerobic. The occurrence of interbeds of non-organic greenish and light gray shales and bioturbated intervals in some stratigraphic sections suggests that the prevalent anaerobic conditions were occasionally disrupted by aerobic conditions (Griffith, 1977; Jordan, 1979).

In this study samples were primarily collected from the New Albany Shale and Chattanooga Shale outcrops around the Cincinnati Arch, Nashville Dome, and Illinois Basin (Figure 6.41). Sampling was restricted to the black and dark gray fine-grained rocks in the sections and Figure 6.42 shows their distribution in four generalized sections in the study area. As shown in Figure 6.43, the mineralogy of the samples is quite uniform, with quartzose claystones being the most common rock type. Illite usually comprises more than 80 weight percent of the clay minerals with chlorite or kaolinite making up the difference (Appendix VII). Sand and silt are commonly disseminated in the rocks as well as concentrated in laminae (Table 6.16). The sand and silt grains usually consist of subangular to angular quartz, but dolomite grains are common in some samples (Table 6.16). In addition to sand and silt laminae, variations in the amount of organic matter diluted with the inorganic fractions of some rocks results in laminae with varying intensities of darkness. These are referred to as organic laminae and their identification

Figure 6.41: Geological map showing Devonian and Lower Mississippian rocks of the central lowland states (modified from King and Beikman, 1974), and localities where Devonian-Mississippian black shales were sampled for this study.

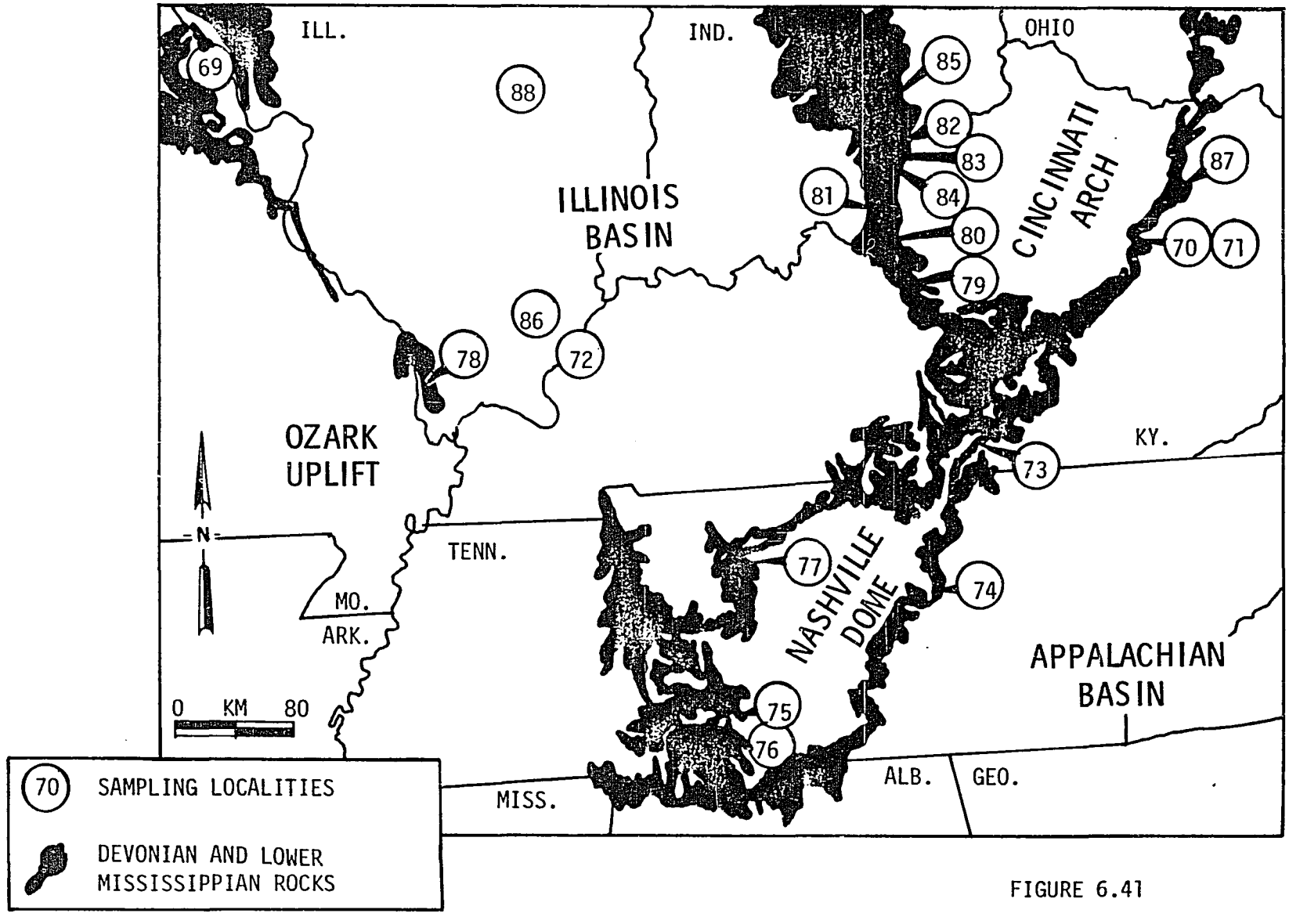

FIGURE 6.41

Figure 6.42: Generalized stratigraphic sections showing the occurrence and distribution of greenish and light gray fine grained rocks in the Devonian-Mississippian black shales.

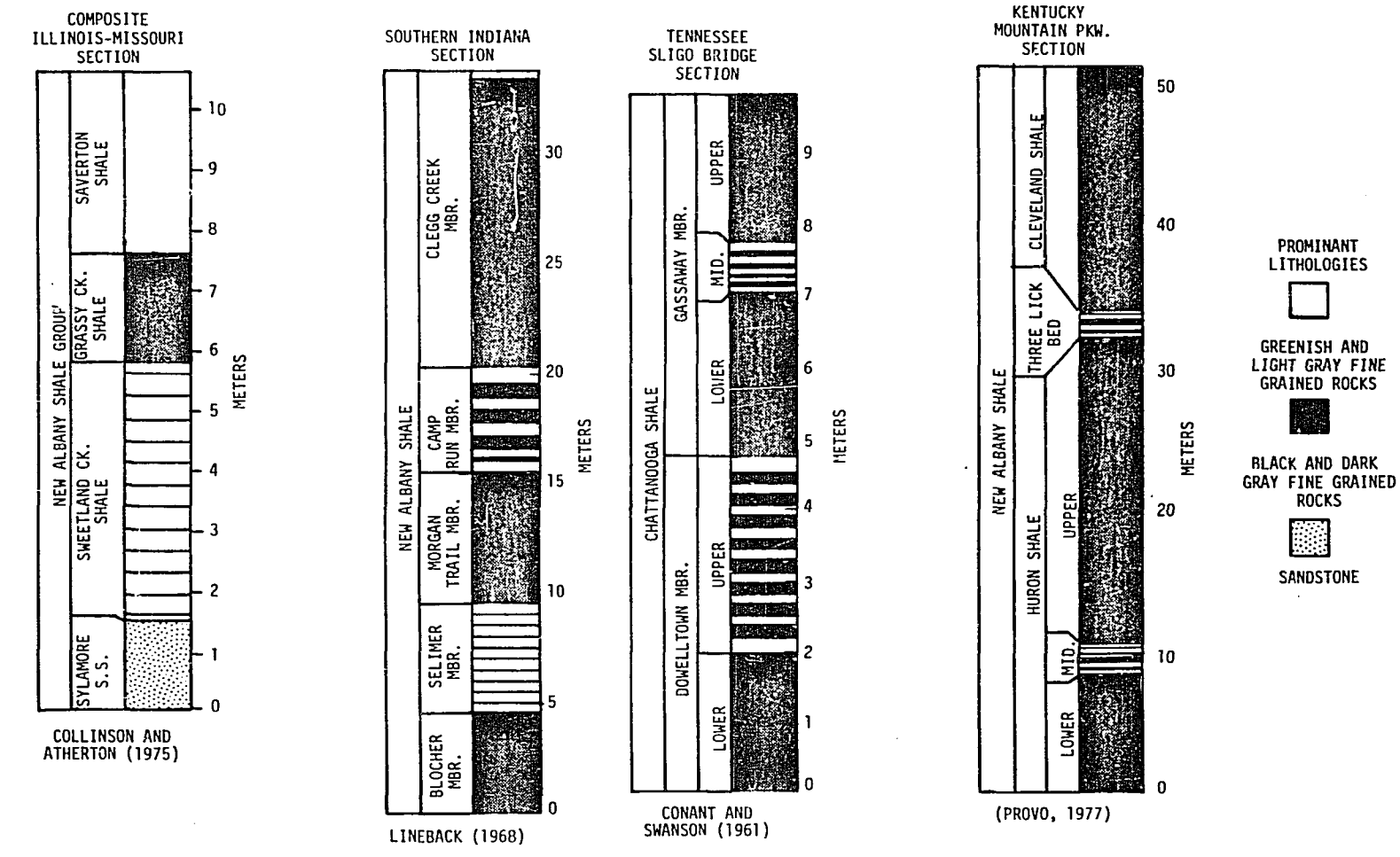

FIGURE 6.42

Figure 6.43: Ternary diagram showing mineralogy of rock types collected from the Devonian-Mississippian black shales. Plots based on data given in Appendix VII.

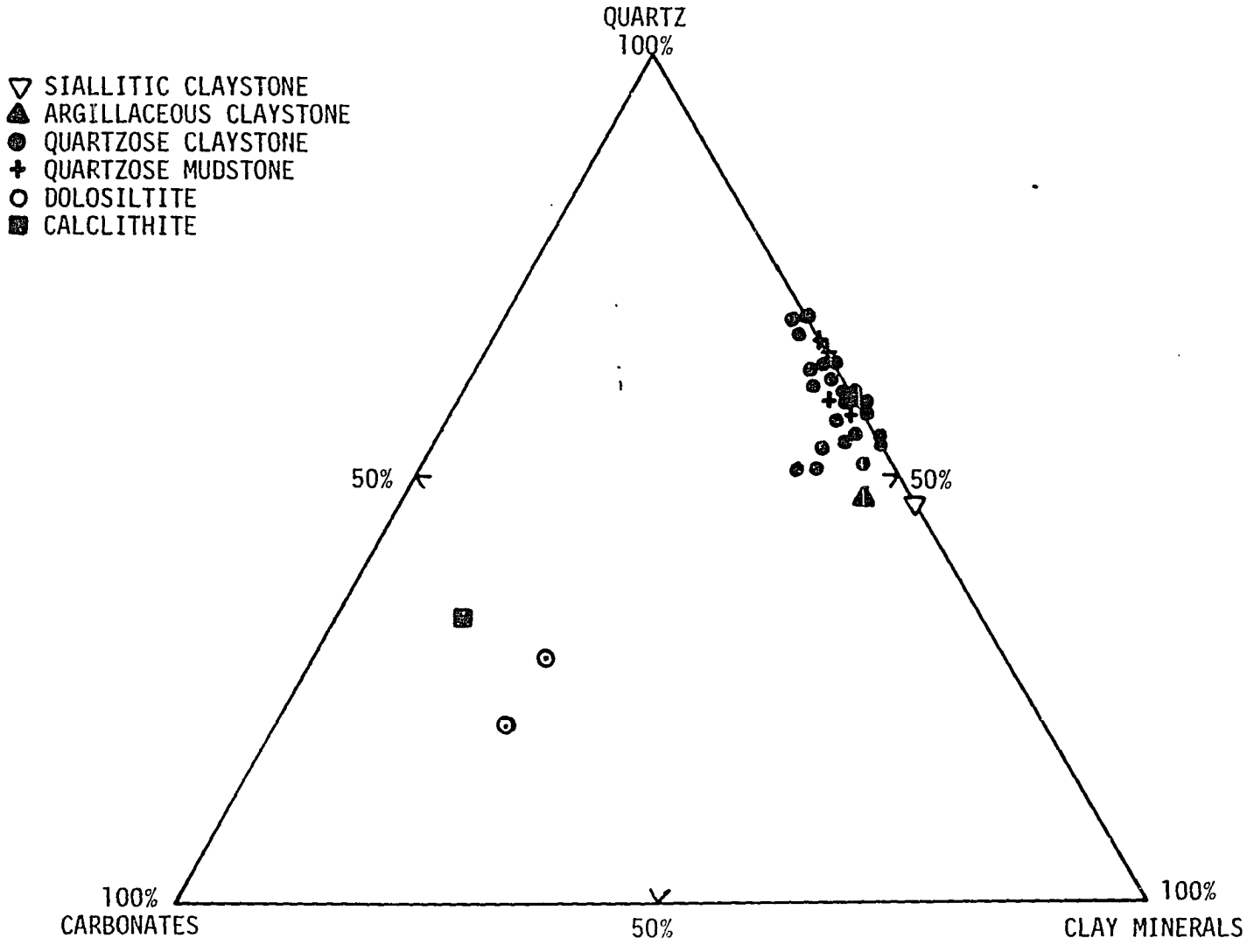

FIGURE 6.43

Table 6.16: Some petrographic observations made on the Devonian-Mississippian black shales collected for this study.

Sample Number	Sand and Silt Content Area (%)[1]	Composition of Sand and Silt Grains	Bedding Features[2]	Fossils[3]
NA-1	30	Quarts + Dolomite	SSS	-
NA-2	25	Dolomite	SSL, OL	L, T
NA-3	25	Quartz	Massive	T
NA-4	5	Quartz	SSL, OL	T
NA-5	20	Quartz	SSL, OL	T
NA-6	15	Quartz + Dolomite	SSS, OL	L, T
NA-7	10	Quartz	OL	T
NA-8	10	Quartz	OL	T
NA-9	10	Quartz	SSS, OL	T
NA-10	15	Quartz + Dolomite	SSB	T
NA-11	15	Quartz + Dolomite	SSB	T
NA-12	5	Quartz + Dolomite	SSL, OL	T
NA-13	30	Quartz	SSB	T
NA-14	10	Quartz	SSB, OL	T
NA-15	10	Quartz	SSS	T
NA-16	10	Quartz	SSL, OL	T
NA-17	35	Quartz	SSS	T
NA-18	80	Dolomite	Mottled	T
NA-19	30	Quartz + Dolomite	OL	T
NA-20	90	Quartz + Dolomite	Massive	-
NA-21	20	Quartz	SSL	T
NA-22	10	Quartz	SSL	T
NA-23	n.d.	n.d.	n.d.	n.d.
NA-24	n.d.	n.d.	n.d.	F
NA-25	5	Quartz	SSB	T
CH-1	10	Quartz	OL	L, T
CH-2	5	Quartz	SSB	T

Table 6.16 (continued): Some petrographic observations made on the Devonian-Mississippian black shales collected for this study.

Sample Number	Sand and Silt Content Area (%)[1]	Composition of Sand and Silt Grains	Bedding Features[2]	Fossils[3]
CH-3	15	Quartz	SSL, OL	T
CH-4	10	Quartz	Massive	T
CH-5	20	Quartz + Dolomite	SSS	T
CH-6	10	Quartz	SSL	T
CH-7	5	Quartz	SSS, OL	T
CH-8	25	Quartz	SSB	T
CH-9	15	Quartz	SSL, OL	T
CH-10	20	Quartz	SSL, OL	T
CH-11	15	Quartz	SSL, OL	T
CH-12	55	Quartz + Dolomite	Massive	T

n.d. = not determined

[1] Values are rounded to nearest 5 percent by area and do not include sand-silt laminae, streaks, or blebs.

[2] Bedding features are in accordance with Lewan (1978, Table 3): SSL = Sand-Silt Laminae, SSS = Sand-Silt Streaks, SSB = Sand-Silt Blebs, and OL = Organic Laminae.

[3] Fossil abbreviations include T = Tasmanites L = Lingula, and F = Foerstia.

usually requires petrographic examination of the rock in thin section. Flattened Tasmanites are usually observed in the samples, but Lingula and Foerstia are rare (Table 6.16).

One mineralogical aspect of the Devonian-Mississippian black shales that is unique in comparison to the other formations discussed in this chapter is its high concentration of iron sulfides in the form of pyrite and marcasite (Table 6.17). Large iron sulfide nodules, measuring several centimeters in diameter are quite common in the Devonian-Mississippian black shales. In addition to these obvious concentrations, sand and silt sized cubic iron sulfide is commonly observed petrographically in thin section. This type of iron sulfide may occur disseminated in the shale matrix or concentrated in sand and silt laminae. Based on the stable sulfur isotopes of the iron sulfides in the Devonian-Mississippian black shales and modern-day analogues, sulfate-reducing bacteria at the sediment-water interface and within the sediment column appear to be the most likely source of the sulfide (Maynard, 1980). The abundance of nodular and silt sized iron sulfide with light sulfur isotope values, suggests that the sediment and water conditions of the Devonian-Mississippian Sea were frequently favorable for the production of biogenic sulfide and that an adequate source of iron was available.

As shown in Figure 6.44, all of the samples are organic and the majority of them may be classified as organic rich. Visual analyses and carbon isotopes of the kerogens indicate that β-liptinitic kerogen predominates in all of the samples (Figure 6.45). The lesser amounts of

Table 6.17: Comparison of iron sulfide concentrations in Devonian-Mississippian black shales with those in the other formations discussed. Iron sulfides include pyrite and marcasite.

Formation	Mean Iron Sulfide Content (wt. %)*	Range of Iron Sulfide Standard Deviation (wt. %)*	Maximum Iron Sulfide Content (wt. %)*	Percentage of Samples with Iron Sulfides Equal to or Greater than 1 wt. %
Dev.-Miss. Black Shales (N=37)	5.0	1-9	23	95
Kreyenhagen Shale (N=6)	1.3	0-3	3	50
Mowry Shale (N=43)	0.9	0-2	4	42
Green River Formation (N=39)	0.9	0-3	10	26
Monterey Shale (N=17)	0.8	0-3	9	18

N - Number of samples
*Values obtained from Appendix VII

Figure 6.44: Histogram showing the distribution of organic carbon in different rock types collected from the Devonian-Mississippian black shales, and classification of their organic richness.

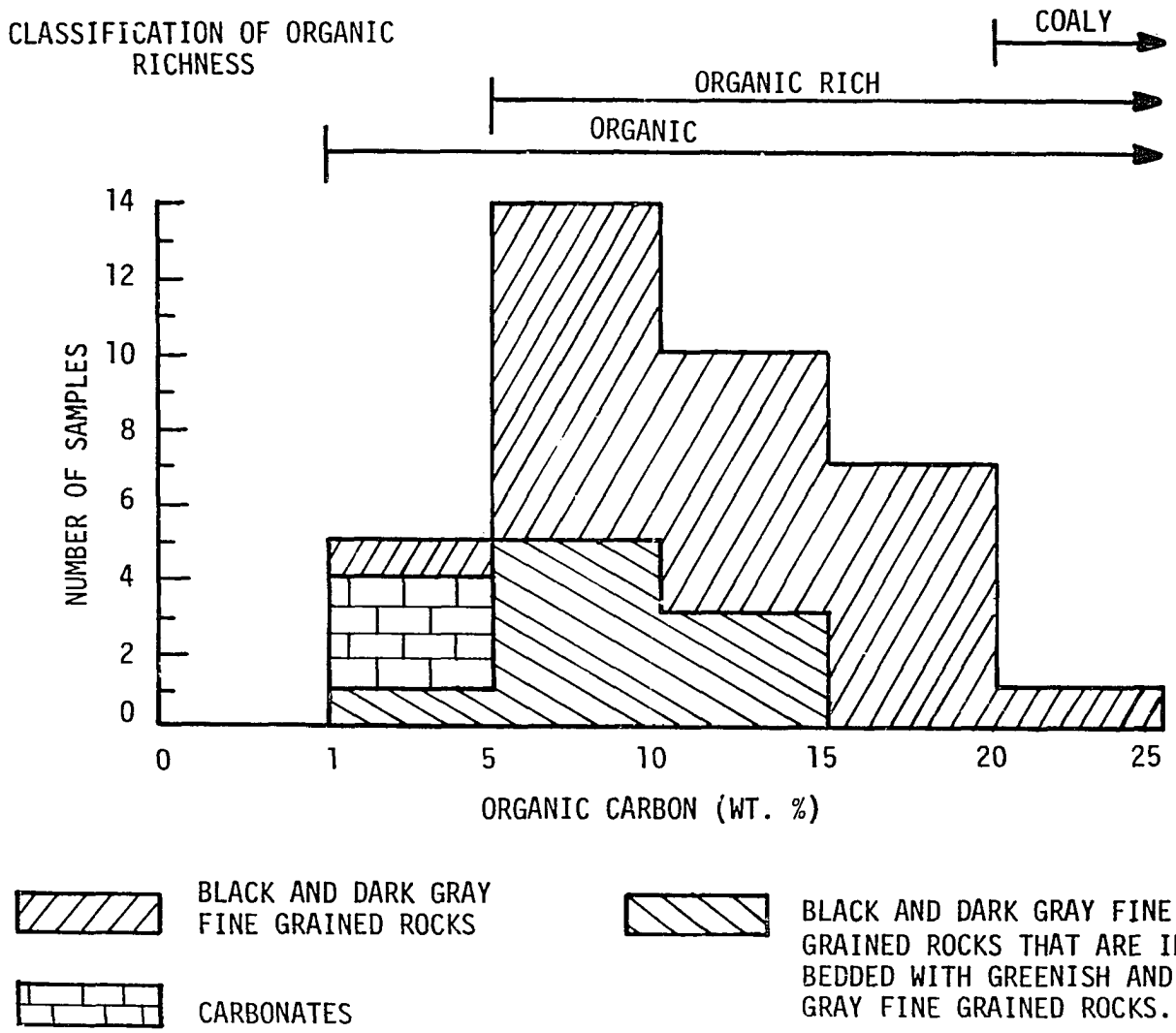

FIGURE 6.44

α-sporopolleninic kerogen in many of the samples are derived from Tasmanites. Elemental analyses plotted in Figure 6.46 show that the kerogens have a uniform composition and are at a moderate level of thermal maturation. It is interesting that only three of the kerogens (CH-10, NA-1, and NA-23) show definite signs of oxidation, and suggests that most of the organic matter was not subjected to aerobic conditions for prolonged durations. This is in good agreement with the interpretation, based on the lack of fossils, that the water column of the Devonian-Mississippian Sea was predominantly anaerobic.

The two samples showing the anomalously high degree of oxidation (Figure 6.46., NA-1 and NA-23), are from the Illinois-Kentucky mining district, which is the most complexly faulted area in the central craton of the United States (Heyland Brock, 1961). Hydrothermal activity appears to have been profuse in this area as indicated by the abundance of fluorite, sphalerite, galena, and barite veins along faults (Heyl and Brock, 1961, Figure 294.2). The area also contains highly radioactive zones (Trace, 1960), peridotite dikes, and explosion breccias (Clegg and Bradbury, 1956). These anomalous features and the domal structure of the area have lead investigator to interpret it as a cryptoexplosion structure (Brown et al., 1954; Bucher, 1963). The oxidation of organic matter in rocks by oxygenated hydrothermal solutions was postulated in Chapter 2 (Figure 2.3) and samples NA-1 and NA-23 may be examples of this type of oxidation.

Figure 6.45: Kerogen types in Devonian-Mississippian black shales as indicated by a) kerogen carbon isotopes and b) visual analysis.

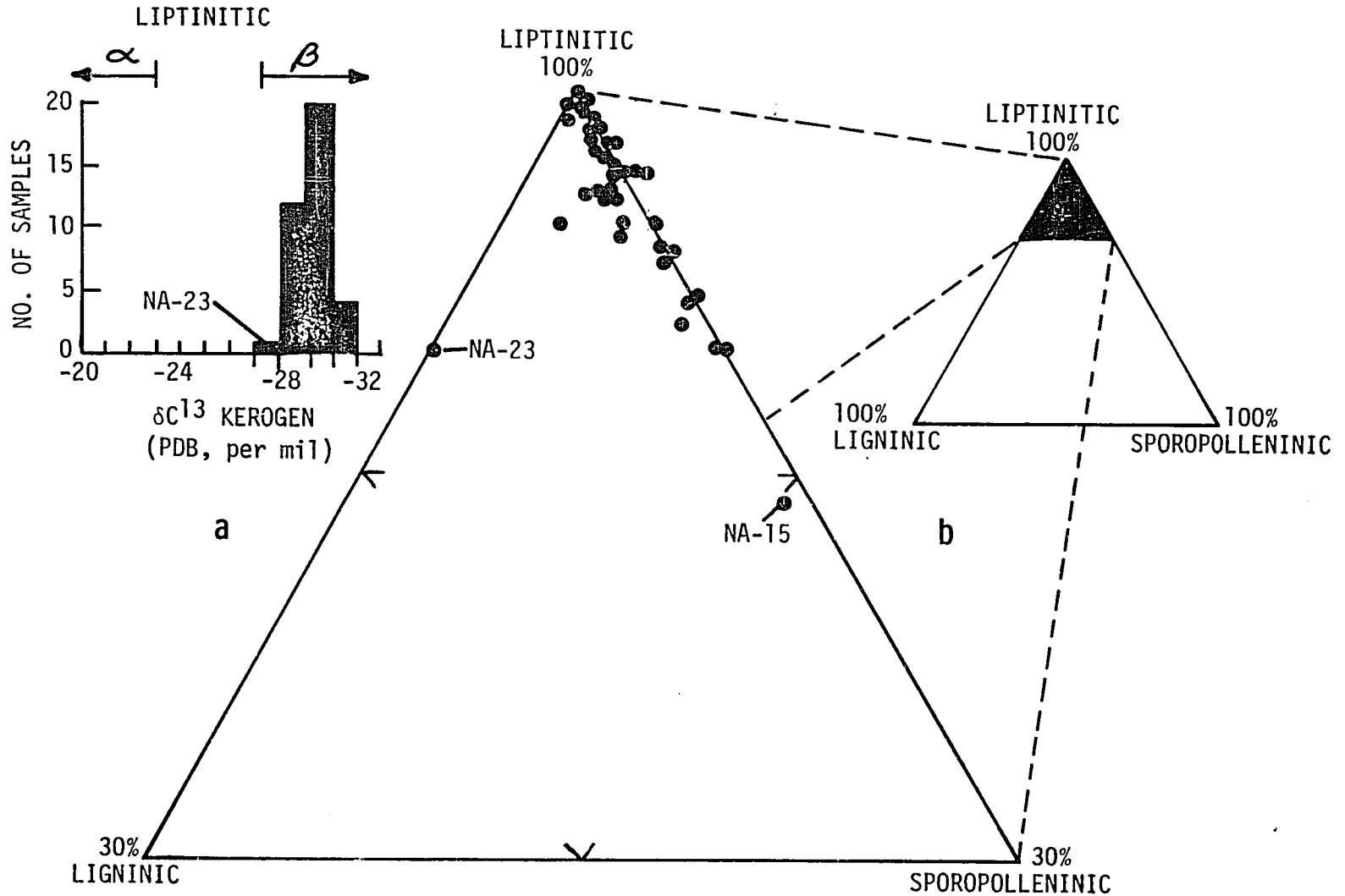

FIGURE 6.45

Figure 6.46: Atomic H/C ratio versus atomic O/C ratio plot of kerogens from the Devonian-Mississippian black shales. Thermal maturation pathways for the different kerogen types are the same as those presented in Figure 2.3

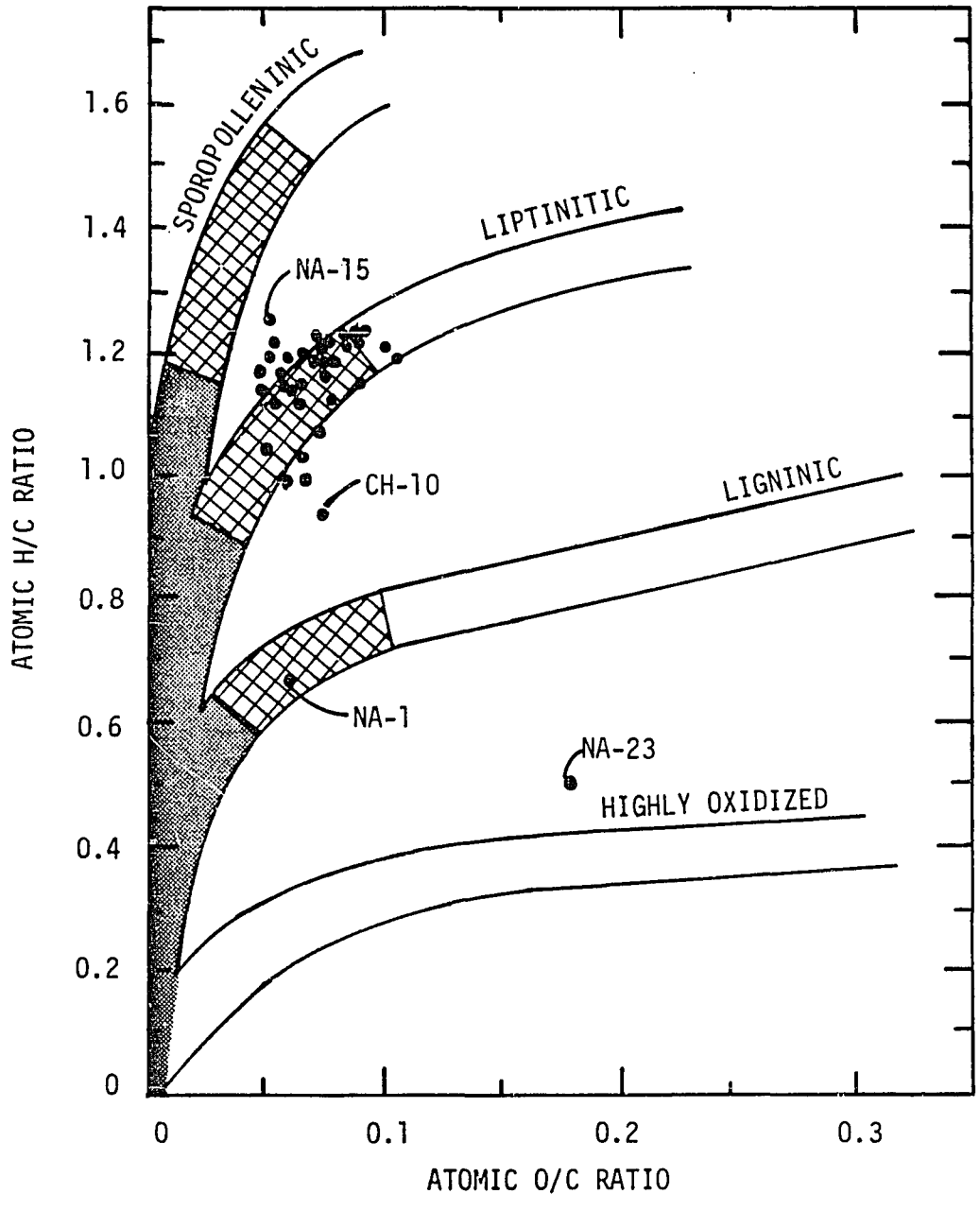

FIGURE 6.46

With the exception of samples NA-1 and NA-23, all of the samples contained sufficient bitumen for vanadium and nickel analyses. The vanadium-nickel fractions of the bitumens show a wide range of values that may be grouped into 8 distinct facies (Table 6.18). These facies are based solely on the vanadium-nickel fractions and cannot be correlated with the organic matter composition, mineralogy, or petrographic features. The primary factor controlling the interpretation of these facies in Figure 6.47 is considered to be the amount of biogenic sulfide generated in a system during the metallation of tetrapyrrole complexes. Berner (1963) has shown experimentally that the Eh and pH of a system decreases as the amount of biogenic sulfide increases. In facies 1, the amount of biogenic sulfide in the system is interpreted to be negligible, and the unhindered nickelous cations are more competitive for tetrapyrrole bonding sites than the vanadyl cations which will be hindered by complexing hydroxls in Eh-pH Field II. Conversely, in facies 8 the amount of biogenic sulfide in the system is interpreted to be large, and the stability of nickel-sulfides in Eh-pH Field IV suggests that nickelous cations will not be competitive with the unhindered vanadyl cations. The other facies (2 through 7) are interpreted to represent intermediate conditions between these two extreme conditions (Figure 6.47). The variable concentrations of biogenic sulfide proposed for this facies sequence is reflected in the Devonian-Mississippian black shales by the variable concentrations (i.e., <1 to 23 weight percent, Table 6.17), morphologies (i.e., very finely disseminated, silt and sand sized cubes, and nodules), mineralogy (i.e., marcasite and pyrite), and sulfur isotopes (i.e., +29.8 to -10.1 per mil, Maynard, 1980) of their iron sulfides.

CHAPTER 7

VANADIUM-NICKEL FRACTION IN OIL-TO-SOURCE ROCK CORRELATIONS

Correlation of an oil with the bitumen of the source rock from which it was expelled is one of the most difficult types of organic geochemical correlations (Brenneman and Smith, 1958; Tissot and Welte, 1978, p. 474; Hunt, 1979, p. 497), and Table 7.1 lists some of the parameters that have been used for this type of correlation. Two of the major difficulties encountered in this type of correlation are 1) oil accumulations may be a composite of oils expelled from several thermally mature portions of a source rock, and 2) the composition of oil usually deviates from its bitumen as a result of alteration during expulsion, migration, and entrapment. The first difficulty may be dealt with by setting up a thorough sampling program, while the second difficulty requires the use of a correlation parameter that will not be influenced by such alterations. The vanadium-nickel fraction appears to satisfy this requirement and is primarily controlled by the environment of deposition. As discussed in Chapter 4, the tenaceous bonding of vanadium and nickel to tetrapyrrole complexes suggests that their proportionality in oil will not be significantly altered during expulsion, migration, or entrapment. Although the concentrations of these two metals may change with the addition or subtraction of more volatile or alterable components, their proportionality should remain the same as that in the bitumen of the source rock from which they were expelled.

Table 7.1: Geochemical parameters used in oil-to-source rock correlations.

Correlation Parameter	Reference
Stable Carbon Isotopes ($\delta C13$)	Williams (1974), Welte and others (1975), Fuex (1977), and Stahl (1978)
Carbon Preference Index (CPI)	Taguchi (1975) and Tissot and Welte (1978, p. 485)
Isoprenoid Ratios (Pri/Phy, Norp/Pri)	Welte and others (1975), Tissot and Welte (1978, p. 485), and Ross and Harwood (1979)
Light Hydrocarbon Distribution (C_4-C_7)	Williams (1974), Swetland and Clayton (1976), and Cardwell (1977)
Heavy Normal Paraffin Distribution (n-C_{15+})	Williams (1974), Welte and others (1975), and Cardwell (1977)
Heavy Cyclic Hydrocarbon Distribution (C_{27+}-Cyclics)	Welte and others (1975), Seifert (1977 and 1978), and Seifert and Moldowan (1978 and 1979)
Proportionality of Paraffinic, Naphthenic and Aromatic Hydrocarbons (P/N, P+N/Ar, N/Ar)	Young and McIver (1977)
Proportionality of Vanadium and Nickel (Ni/V)	Taguchi (1975)

7.1 ALTERATION EFFECTS DURING ENTRAPMENT

During the entrapment of crude oil in a reservoir, a number of subsurface processes may alter its chemical composition and physical character. Several of the common alteration processes that are operative in this setting include thermal degradation, deasphalting, microbial degradation, and water washing (Connan et al., 1975; Milner et al., 1977). Determination of the effect of these types of alteration on the vanadium-nickel fraction of an entrapped crude oil is critical to evaluating its usefulness as an oil-to-source rock correlation parameter.

Thermal degradation of a crude oil may occur when its reservoir is subjected to a high thermal regime for a prolonged duration (Landes, 1967; Evans et al., 1971). This type of alteration causes thermal cracking and condensation of the crude oil constituents (Connan et al., 1975) which ultimately results in the complete conversion of the crude oil to graphite and methane. Investigations by Hodgson and Baker (1957) and Rosscup and Bowman (1967) have shown that vanadyl and nickelous tetrapyrrole complexes have a high thermal stability and their demetallation is unlikely within the thermal regime of diagenesis and low grade metamorphism (<400°C). Constantinides and others (1959) have experimentally demonstrated this thermal stability by subjecting a Kuwait crude oil residue to 390°C under a purging atmosphere for varying lengths of time. The results of this experiment showed that the vanadium and nickel concentrations decreased as thermal degradation

increased, but the vanadium-nickel fraction remained unchanged (Table 7.2).

Deasphalting is the precipitation of the asphaltene fraction from a crude oil as a result of the introduction of gaseous hydrocarbons into an oil reservoir (Evans et al., 1971; Milner et al., 1977). The source of the gaseous hydrocarbons may be internal (thermal degradation) or external to the reservoir, and the resulting crude oil has a lower specific gravity (Evans et al., 1971). As shown in Table 7.3, the loss of the asphaltene fraction of a crude oil would greatly reduce its vanadium and nickel concentrations, but the vanadium-nickel fraction of the remaining crude oil would be unchanged.

Microbial degradation usually occurs in shallow reservoirs when oxygenated waters are in contact with trapped crude oil (Winters and Williams, 1969). During this degradation, straight chain paraffins and low molecular weight constituents in a crude oil are preferentially consumed by aerobic bacteria (Jobson et al., 1972 and 1979; Bailey et al., 1973a and 1973b). Highly conjugated and high molecular weight constituents like tetrapyrroles and asphaltenes are not preferred in microbial degradation, and as a result they become concentrated in a crude oil as the degree of degradation increases (Bailey et al., 1973b). Although the concentrations of vanadium and nickel are likely to increase with increasing microbial degradation, the vanadium-nickel fraction of a degraded crude oil should remain unchanged.

Table 7.2: Influence of thermal degradation on the vanadium-nickel fraction of a Kuwait crude oil residue. Data is from Costantinides and others (1959, p. 140).

Duration (hrs.) at 390°C	Vanadium (ppm)	Nickel (ppm)	V/(Ni+V)
0	86.6	26.2	0.77
1	83.0	24.7	0.77
2	79.0	23.0	0.77
4	61.1	19.8	0.76
8	49.9	15.0	0.77

Table 7.3: Comparison of the vanadium-nickel fractions in the asphaltene and non-asphaltene fractions of two crude oils.

Crude Oil and Fraction	Vanadium (ppm)	Nickel (ppm)	V/(Ni+V)
Venezuelan Oil Residue[1]			
Asphaltene Fraction	1750	265	0.87
Non-Asphaltene Fraction	87	16	0.84
California Crude Oil[2]			
Asphaltene Fraction	62	852	0.07
Non-Asphaltene Fraction	5	59	0.08

[1]Data from Corbett (1967, Figure 4)

[2]Data from Filby (1975, Table 2.5)

The removal of soluble constituents from a crude oil by a dynamic water system in contact with a reservoir is referred to as water washing (Evans et al., 1971). Similar to microbial degradation of crude oils, the highly conjugated and high molecular weight constituents become concentrated in a water washed crude oil as the more soluble low molecular weight constituents are preferentially removed (Price, 1980). Data distinguishing between the effects of water washing and microbial degradation on the vanadium-nickel fraction of crude oils are not available, but studies on their combined effects, along with oxidation and inspissation have provided some data. Collectively, these four alteration processes may be referred to as weathering, and the results of two studies in Tables 7.4 and 7.5 show that the vanadium-nickel fraction of weathered crude oils remains unchanged.

7.2 ALTERATION EFFECTS DURING MIGRATION

A variety of mechanisms for oil migration have been proposed, and a good review of them is given by Hunt (1979, pp. 186-258). Based on geological considerations (Momper, 1978), along with natural and experimental observations (Lewan et al., 1979), the most feasible mechanism appears to be the migration of oil as a separate phase that is not miscible with formation waters. A crude oil migrating by this mechanism is susceptible to two types of alteration; 1) water washing, and 2) adsorption.

Solubility studies by McAuliffe (1964) suggest that water washed crude

Table 7.4: Comparison of vanadium-nickel fractions of Kuwait crude oil and Kuwait oil residue with naturally degraded crude oils that are suspected of being derived from Kuwait crude oil (Brunnock et al., 1958)

Type of Crude Oil	Vanadium (ppm)	Nickel (ppm)	V/(Ni+V)
Kuwait Crude Oil (sp.gr.=0.869)	27	9	0.75
Kuwait Oil Residue (sp.gr.=0.9295)	35	12	0.74
Degraded oils on rocky shores, beaches, and sea water, that are suspected of being derived from Kuwait crude oils (N=11, sp.gr.=0.9495+0.0174)	40±7	17±2	0.70±0.02

Table 7.5: Experimental results showing the influence of weathering on the vanadium-nickel fraction of a Kuwait crude oil residue in open tank experiments (Davis and Gibbs, 1975).

Exposure Time in Open Tanks (Weeks)	Specific Gravity (30°C/30°C)	V/(Ni+V)
0	0.9565	0.73
16	0.9595	0.77
36	0.9660	0.73
100	0.9825	0.75

oils will become enriched in paraffinic and high molecular weigh constituents as the more soluble low molecular weight napthenic and aromatic constituents are preferentially removed. This type of alteration is likely to cause an apparent increase in the vanadium and nickel concentrations of a crude oil as its migration distance increases, but as discussed in the previous section the vanadium-nickel fraction should remain unchanged.

The high molecular weight constituents of crude oils may be selectively removed by their adsorption on mineral surfaces in the rocks through which they migrate. This selective adsorption may be attributed to the common occurrence of hetero atoms (e.g. sulfur, nitrogen, and oxygen) in the high molecular weight constituents of crude oils, which gives them a more polar character. The result of this chromatographic effect is that a crude oil will become more depleted in high molecular weight constituents as its migration distance increases (Bonham, 1956; Hodgson and Baker, 1959; Riecker, 1962; Baker, 1962; Safronova et al., 1972). Dunning and others (1953) have shown that tetrapyrroles in crude oils have high interfacial activities and film-forming tendencies, which suggests that their chromatographic removal is likely during migration. A decrease in the concentrations of vanadium and nickel in a crude oil with increasing migration distance is therefore expected, but the vanadium-nickel fraction should remain unchanged. This has been verified by Al-Shahristani and Al-Atyia (1972) in Iraqi oil fields where vertical migration between reservoirs has been established. The results and

geological setting of one of the examples cited in their study is given in Figure 7.1.

7.3 ALTERATION EFFECTS DURING EXPULSION

In this discussion, the processes involved in the generation of oil and its migration out of a source rock will be collectively referred to as expulsion. As thermal maturation of a source rock increases, its expelled oil becomes progressively enriched in lower molecular weight constituents (Tissot et al., 1971; Tissot and Welte, 1978, pp. 400-408). In addition to this, experimental work by Espitalie and others (1980) indicates that high molecular weight constituents of a crude oil may be preferentially retained by the inorganic matrix of a source rock. It is expected that thermal maturation and rock matrix retention may alter the concentrations of vanadium and nickel in a crude oil, but the vanadium-nickel fraction should remain unchanged.

This was verified experimentally by the hydrous pyrolysis technique described by Lewan and others (1979), which generates pyrolysates that are compositionally similar to natural crude oils. The pyrolysis experiments consisted of subjecting aliquots of the same Woodford Shale sample to different temperatures between 330° and 370°C in the presence of liquid water for 72 hours. In Table 7.6, the results of these experiments show that the metal concentrations do decrease with expulsion and thermal maturation, but the vanadium-nickel fraction of the expelled

Figure 7.1: Cross-section showing vertical migration of crude oil from the lower reservoir into the upper reservoir along a structural fracture system in the Ain Zalah Field of Iraqi (modified after Dunnington, 1958, Figure 15). The vanadium and nickel analyses of the crude oils from this field are presented in the insert and were determined by Al-Shahristani and Al-Atyia (1972).

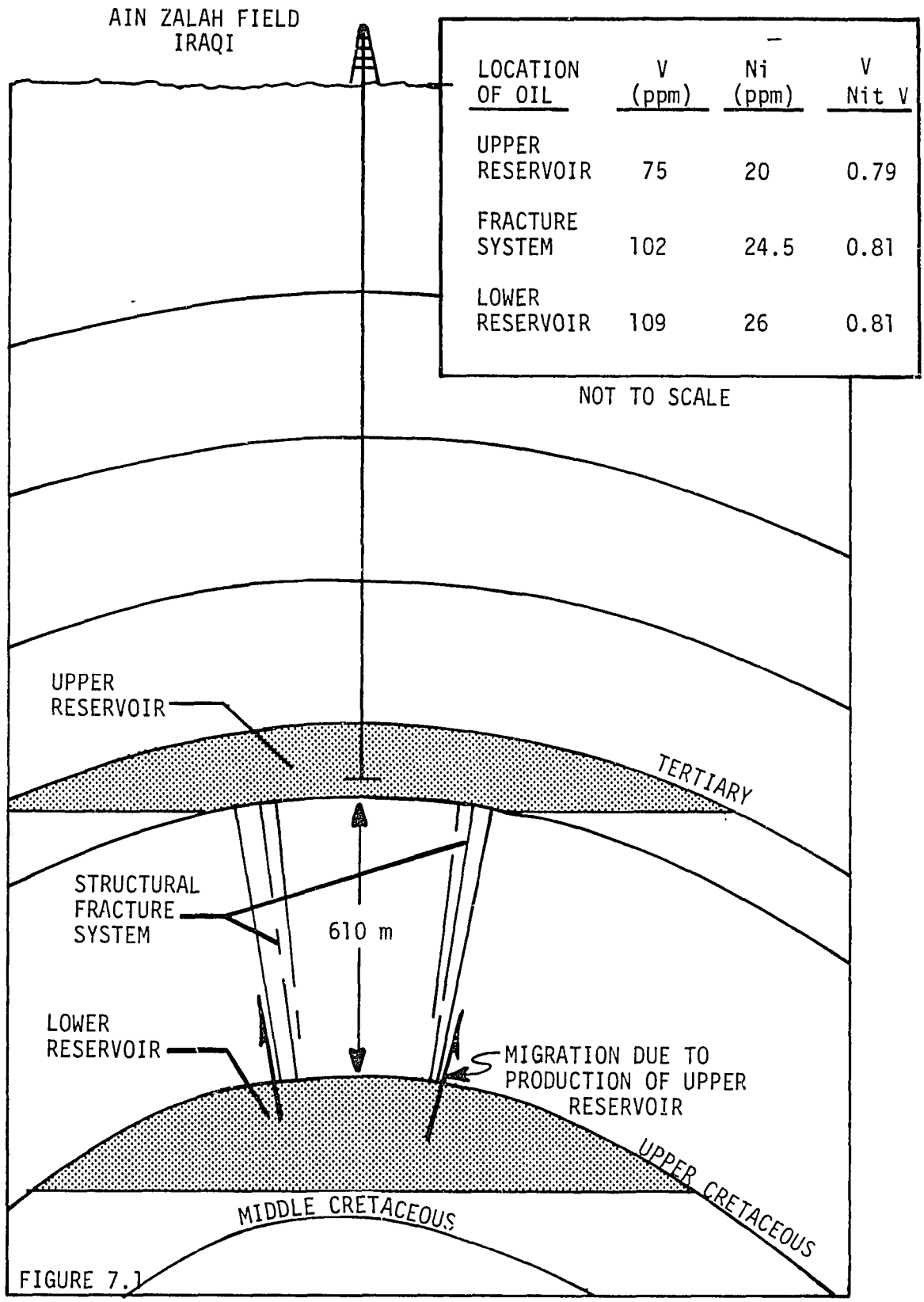

FIGURE 7.1

Table 7.6: Vanadium and nickel concentrations and vanadium-nickel fractions of pyrolysates expelled from Woodford Shale (WD-5) by hydrous pyrolysis at different temperatures for durations of 72 hours.

Nature of Pyrolysates	Temperature (°C) for 72 Hours 330	355	370
Pyrolysate Gases Expelled (wt. % of rock)	0.62	1.18	1.47
Pyrolysate Liquid Expelled (wt. % of rock)	0.92	2.50	2.25
Vanadium in Liquid Pyrolysate* (ppm)	170	145	90 89
Nickel in Liquid Pyrolysate* (ppm)	9	6	3 3
V/(Ni+V)	0.95	0.96	0.97 0.97

*Pyrolysates were diluted in benzene, filtered through 0.5μm filters, and then isolated by evaporation of the benzene in a rotary vacuum evaporator

pyrolysates remain unchanged. Table 7.7 shows that for the Woodford Shale and the Green River Shale, the vanadium-nickel fraction of their bitumens is essentially the same as that of their expelled pyrolysates. This suggests that the vanadium-nickel fraction of an expelled crude oil should be similar to the vanadium-nickel fraction of the bitumen of the source rock from which the crude oil was expelled.

7.4 DISCUSSION

The advantage of using the vanadium-nickel fraction in oil-to-source rock correlations is its ability to resist alteration during expulsion, migration and entrapment. This stability suggests that it may also be useful in oil-to-oil and oil-to-asphalt correlations. The two disadvantages of this correlation parameter include 1) sufficient uncontaminated bitumen must be present in a source rock and 2) stratigraphic and regional variations of the parameter in a source rock may be significant and must be evaluated.

As stated in Section 2.3, vanadium and nickel analyses were only determined on bitumens that comprised more than 1.5 weight per mil of a rock. This minimum requirement insures that the vanadium-nickel fraction will not be biased by vanadium and nickel concentrations in extractable inorganic contaminants. Source rocks that have undergone high levels of thermal maturation or high degrees of oxidation seldom satisfy this minimum bitumen requirement, and as a result, correlation by the

Table 7.7: Vanadium and nickel concentrations and vanadium-nickel fractions of bitumens and pyrolysates from the same rocks. Pyrolysates were generated by hydrous pyrolysis.

Rock Type and Organic Fraction	Vanadium (ppm)	Nickel (ppm)	V/(Ni+V)
Woodford Shale (WD-5)			
Bitumen	1910	79	0.96
(Benzene-Methanol)	1930	77	0.96
Pyrolysate* (330°-370°C/72 Hrs.)	89-170	3-9	0.95-0.97
Green River Shale (GR-37)			
Bitumen (Benzene-Methanol)	6	132	0.05
Pyrolysate* (310°C/120 Hrs.)	2.3	59.4	0.04

*Pyrolysates were diluted in benzene, filtered through 0.5μm filters, and then isolated by evaporation of the benzene in a rotary vacuum evaporator.

vanadium-nickel fraction of their bitumen is not applicable. Figure 7.2 shows a number of samples collected for this study that did not satisfy the minimum bitumen requirement due to their high level of thermal maturation or high degree of oxidation.

Proper implementation of the vanadium-nickel fraction in oil-to-source rock correlations requires an evaluation of its stratigraphic and regional variations in the source rocks of an area. The vanadium-nickel fraction of an oil accumulation represents a composite of oils expelled from thermally mature portions of a source rock that may have had vanadium-nickel fractions over a wide range of values. It is therefore important that a thorough and representative sampling of the source rocks of an area be done on a stratigraphic and regional basis. The resulting oil-to-source rock correlations may in some cases depend on a statistical approach as exemplified by Taguchi (1975) with Tertiary oils and source rocks in Japan.

It appears possible that the thermally mature portions of two different source rocks in a basin could expel crude oils with similar vanadium-nickel fractions. This would be particularly likely if both source rocks were deposited under the broad conditions of Eh-pH Field I. Within this extensive field only nickelous cations would be available and would result in distinctly low vanadium-nickel fractions (>0.10). The possibility of this situation indicates that the vanadium-nickel fraction should not be used alone, but rather, it should be used with other correlation parameters, such as those listed in Table 7.1.

Figure 7.2: Atomic H/C ratio versus atomic O/C ratio of samples that did not satisfy the minimum bitumen requirement for vanadium and nickel analyses.

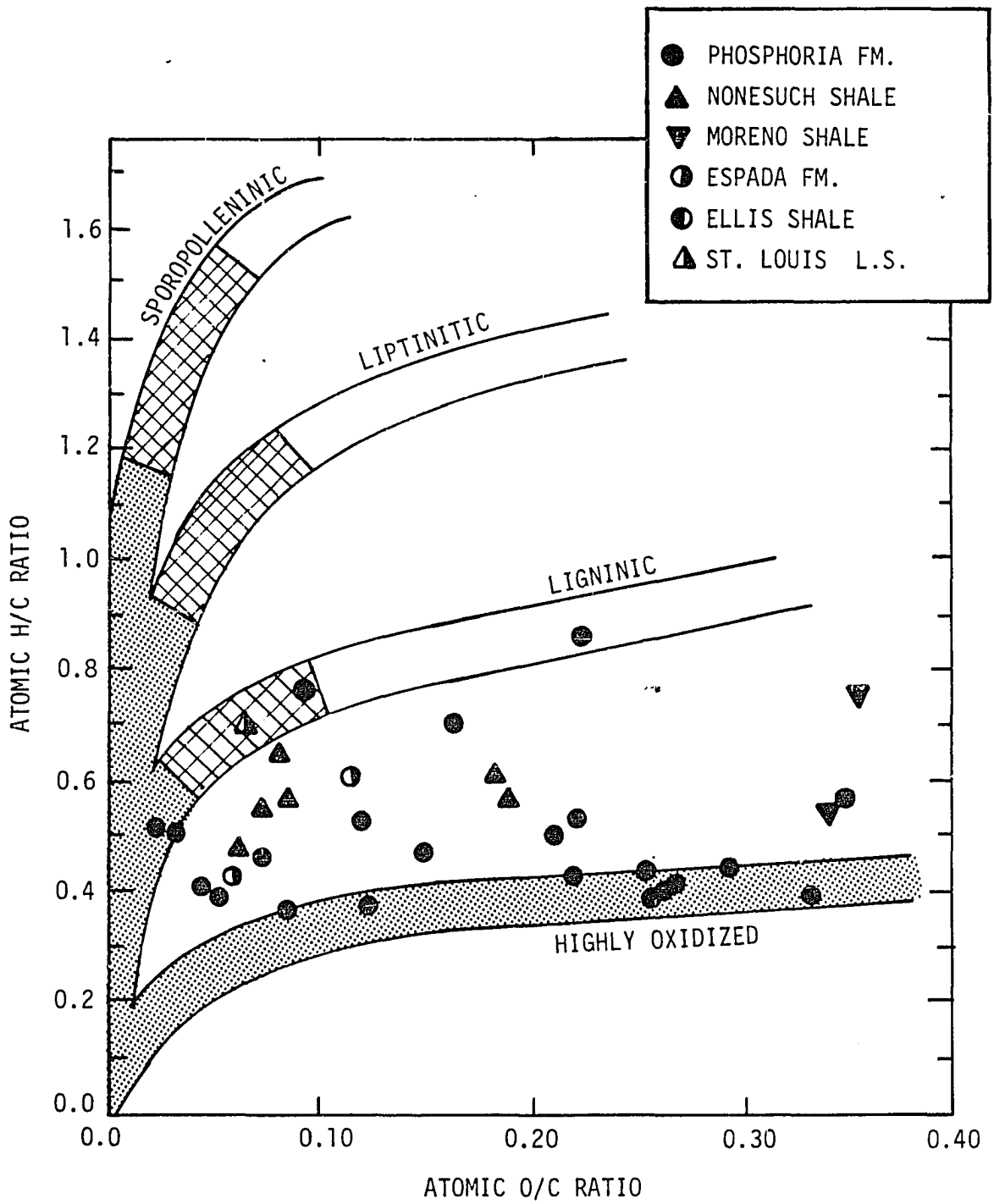

FIGURE 7.2

CHAPTER 8

SUMMARY OF CONCLUSIONS

Conclusions to the objectives stated in the form of questions in Chapter 1 have been discussed in detail within the text. A summary of these conclusions is given as follows:

8.1 PREFERENCE

The preferential concentration of vanadium and nickel appears to be dependent on the concentration of tetrapyrrole complexes in an organic substance. Tetrapyrrole complexes preferentially bond with these two metals because of their small atomic radii, favorable electron configurations, and availability as bivalent cations. Thus, organic accumulations containing tetrapyrrole complexes have the potential of being enriched in vanadium and nickel, while those deficient in tetrapyrrole complexes do not have the potential of being enriched in the two metals. The amount of tetrapyrrole complexes within an organic accumulation is dependent on the amount of chlorophyll in the source of the organic matter and the preservation of chlorophyll derivatives in the environment of deposition. Chlorophyll concentrations are high in algae and higher plants, but the subaerial habitat of the latter makes the preservation of its chlorophyll or derivatives less likely. Appreciable quantities of chlorophyll are not likely in sporopollenin derived from spores or pollen, but minor

quantities are likely in sporopollenin derived from the ultrastructure of some algae.

8.2 SOURCE

Although some vanadium and nickel in an organic accumulation may be endemic to its living organic sources, the source of enriched vanadium and nickel concentrations appears to be the aqueous metal cations in the interstitial waters of a sediment. This source of metals is dependent on the diffusion of metal cations from the overlying water body, and is only effective as long as the sediment system remains open.

8.3 PROPORTIONALITY

The proportionality of enriched vanadium and nickel in an organic accumulation is dependent on the hydrogen ion activity, redox potential, and biogenic sulfide activity of a sediment system. Hydrogen ion activity and redox potential determine whether or not the proper metal species will be available for bonding, while biogenic sulfide activity tends to reduce the bonding potential of available nickelous cations. Deciphering the effects of these variables on the metal proportionality of a particular rock unit is best accomplished with the use of Eh-pH diagrams in conjunction with geochemical and geological data.

8.4 OIL-TO-SOURCE ROCK CORRELATIONS

The ability of the vanadium-nickel fractions of a bitumen and an expelled crude oil to withstand alteration during thermal maturation, expulsion, migration, and entrapment, makes this a good parameter for oil-to-source rock correlations, as well as for oil-to-oil and oil-to-asphalt correlations. Proper use of this parameter for oil-to-source rock correlations requires a thorough sampling of source rocks in a basin in order to develop an understanding of the stratigraphic and regional variations of the vanadium-nickel fractions.

REFERENCES CITED

Abernethy, R. F., Peterson, M. J., and Gibson, F. H., 1969, Spectrochemical Analyses of Coal Ash for Trace Elements; U.S. Bur. Mines, Rept. Inv. 7281, 30p.

Adler, H. H., 1964, The Conceptual Uranium Ore Roll and its Significance in Uranium Exploration; Econ. Geol., v. 59, pp. 46-53.

Ahrens, L. H., 1952, The Use of Ionization Potentials Part 1. Ionic Radii of the Elements; Geochim. Cosmochim. Acta, v. 2, pp. 155-169.

Aizenshtat, Z., Dinur, D., and Nissenbaum, A., 1979, Tetrapyrroles and Associated Compounds in Dead Sea Asphalts; Chem. Geol., v. 24, pp. 161-174.

Al-Shahristani, H., and Al-Atyia, M. J., 1972, Vertical Migration of Oil in Iraqi Oil Fields: Evidence Based on Vanadium and Nickel Concentrations; Geochim. Cosmochim. Acta, v. 36, pp. 929-938.

Andelman, J. B., 1973, Incidence, Variability, and Controlling Factors for Trace Elements in Natural, Fresh Waters; in Trace Metals and Metal-Organic Interactions in Natural Waters, ed. Singer, Ann Arbor Science Publishers Inc., Ann Arbor, pp. 57-88.

Angino, E. E., 1964, Trace Elements and Cyclic Deposition; in Symposium on Cyclic Sedimentation, ed. Merriam, State of Kansas, Bull. No. 169, v. 1, pp. 21-30.

Atkinson, A. W., Jr., Gunning, B.E.S., and John, P.C.L., 1972, Sporopollenin in the Cell Wall of Chlorella and Other Algae: Ultrastructure, Chemistry, and Incorporation of ^{14}C-Acetate, Studied in Synchronous Cultures; Planta, v. 107, pp. 1-32.

Baas Becking, L.G.M., Kaplan, I.R., and Moore, D., 1960, Limits of the Natural Environment in Terms of pH and Oxidation-Reduction Potential; Jour. Geol., v. 68, pp. 243-284.

Baes, C. F., Jr., and Mesmer, R. E., 1976, The Hydrolysis of Cations; John Wiley & Sons, New York, 489p.

Bailey, N.J.L., Jobson, A. M., and Rogers, M. A., 1973a, Bacterial Degradation of Crude Oil: Comparison of Field and Experimental Data; Chem. Geol., v. 11, pp. 203-221.

Bailey, N.J.L., Krouse, H. R., Evans, C. R., and Rogers, M. A., 1973b, Alteration of Crude Oil by Waters and Bacteria -- Evidence from Geochemical and Isotope Studies; Amer. Assoc. Petrol. Geologists Bull., v. 57, pp. 1276-1290.

Baker, B. L., and Hodgson, G. W., 1961, Rate of Formation of the Nickel Complex of Pheophytin a; J. Phys. Chem., v. 65, pp. 1078-1079.

Baker, B. L., and Hodgson, G. W., 1968, Chlorins in Recent Marine Sediments on the North Atlantic Continental Shelf off Nova Scotia, Canada; Chem. Geol., v. 3, pp. 119-133.

Baker, D. R., 1962, Organic Geochemistry of Cherokee Group in Southeastern Kansas and Northeastern Oklahoma; Amer. Assoc. Petrol. Geologists Bull., v. 46, pp. 1621-1642.

Baker, D. R., and Claypool, G. E., 1970, Effects of Incipient Metamorphism on Organic Matter in Mudrock; Amer. Assoc. Petrol. Geologists Bull., v. 54, pp. 456-468.

Baker, E. W., 1966, Mass Spectrometric Characterization of Petroporphyrins; J. Amer. Chem. Soc., v. 88, pp. 2311-2315.

Baker, E. W., Huang, W. Y., Palmer, S. E., and Rankin, J. G., 1977, Mass and Electron Paramagnetic Resonance Spectrometric Analyses of Selected Organic Components of Cretaceous Shales of Marine Origin; Preprints, Div. Petrol. Chem., Amer. Chem. Soc. v. 22, pp. 739-752.

Baker, E. W., and Smith, G. D., 1973, Pleistocene Changes in Chlorophyll Pigments; in Advances in Organic Geochemistry, ed. Tissot and Bienner, Editions Technip, Paris, pp. 649-660.

Baker, E. W., and Smith, G. D., 1974, Fossil Porphyrins and Chlorins in Deep Ocean Sediments, II; Preprints, Div. Petrol. Chem., Amer. Chem. Soc., v. 19, pp. 744-768.

Baker, E. W., Yen, T. F., Dickie, J. P., Rhodes, R. E., and Clavi, L. F., 1967, Mass Spectrometry of Porphyrins: II. Characterization of Petroporphyrins; J. Amer. Chem. Soc., v. 89, pp. 3631-3639.

Ball, J. S., and Wenger, W. J., 1960, Metal Content of Twenty-four Petroleums; Jour. Chem. Eng. Data, v. 5, pp. 553-557.

Barghoorn, E. S., Knoll, A. H., Dembicki, H., Jr., and Meinschein, W. G., 1977, Variation in Stable Carbon Isotopes in Organic Matter from the Gunflint Iron Formation; Geochim. Cosmochim. Acta, v. 41, pp. 425-430.

Barnes, J. W., and Dorough, G. D., 1950, Exchange and Replacement Reactions of α, β, γ, δ-Tetraphenyl- Metalloporphins; J. Amer. Chem. Soc., v. 72 pp. 4045-4050.

Beach, L. K., and Shewmaker, J. E., 1957, The Nature of Vanadium in Petroleum; Indust. and Eng. Chem., v. 49, pp. 1157-1164.

Berner, R. A., 1963, Electrode Studies of Hydrogen Sulfide in Marine Sediments; Geochim. Cosmochim. Acta, v. 27, pp. 563-575.

Berner, R. A., 1964a, Iron Sulfides Formed from Aqueous Solution at Low Temperatures and Atmospheric Pressure; Jour. Geol., v. 72, pp. 293-306.

Berner, R. A., 1964b, Stability Fields of Iron Minerals in Anaerobic Marine Sediments; Jour. Geol., v. 72, pp. 826-834.

Berner, R. A., 1967, Thermodynamic Stability of Sedimentary Iron Sulfides; Amer. J. Sci., v. 265, pp. 773-785.

Berner, R. A., 1969, Migration of Iron and Sulfur within Anaerobic Sediments during Early Diagenesis; Amer. J. Sci., v. 267, pp. 19-42.

Berner, R. A., 1970, Sedimentary Pyrite Formation; Amer. J. Sci., v. 268, pp. 1-23.

Berner, R. A., 1971, Principles of Chemical Sedimentology; McGraw-Hill Book Co., New York, 240p.

Berner, R. A., 1972, Sulfate Reduction, Pyrite Formation, and the Oceanic Sulfur Budget; in The Changing Chemistry of the Oceans, eds. Dyrssen and Jagner, John Wiley & Sons, Inc., New York, pp. 347-362.

Berrill, N. J., 1950, The Tunicata, with an Account of the British Species; Printed for the Ray Society, Bernard Quaritch, Ltd., London, 346p.

Bertrand, D., 1950, The Biochemistry of Vanadium; Amer. Mus. Nat. Hist., v. 94, Art. 7, pp. 409-455.

Bidwell, R.G.S., 1974, Plant Physiology, Macmillan Publishing Co., Inc., New York, 643p.

Black, W.A.P., and Mitchell, R.L., 1952, Trade Elements in the Common Brown Algae and in Sea Water; J. Mar. Biol. Assoc. U.K., v. 30, pp. 575-584.

Bloomfield, C., and Kelso, W. I., 1973, The Mobilization and Fixation of Molybdenum, Vanadium, and Uranium by Decomposing Plant Matter; J. Soil Sci., v. 24, pp. 368-379.

Blotcky, A. J., Flacone, C., Medina, V. A., Rack, E. P., and Hobson, D. W., 1979, Determination of Trace-Level Vanadium in Marine Biological Samples by Chemical Neutron Activation Analysis; Anal. Chem., v. 51, pp. 178-182.

Blumer, M., Ehrhard, M., and Jones, J. H., 1973, The Environmental Fate of Standard Crude Oil; Deep-Sea Res., v. 20, pp. 239-259.

Blumer, M., and Rudrum, M., 1970, High Molecular Weight Fossil Porphyrins: Evidence for Monomeric and Dimeric Tetrapyrroles about 1100 Molecular Weight; J. Inst. Petrol., v. 56, pp. 99-106.

Blumer, M., and Snyder, W. D., 1967, Porphyrins of High Molecular Weight in a Triassic Oil Shale: Evidence by Gel Permeation Chromatography; Chem. Geol., v. 2, pp. 35-45.

Boles, J. R., and Surdam, R. C., 1979, Diagenesis of Volcanogenic Sediments in a Tertiary Saline Lake, Wagon Bed Formation, Wyoming; Amer. J. Sci., v. 279, pp. 832-853.

Bollingberg, H. J., 1975, Geochemical Prospecting Using Seaweed, Shellfish, and Fish; Geochim. Cosmochim. Acta, v. 39, pp. 1567-1570.

Bonatti, E., Kraemer, T., and Rydell, H., 1972, Classification and Genesis of Submarine Iron-Manganese Deposits; in Ferromanganese Deposits on the Ocean Floor, ed. Horn, Arden House, New York, pp. 149-166.

Bonham, L. D., 1956, Geochemical Investigation of Crude Oils; Amer. Assoc. Petrol. Geologists Bull., v. 40, pp. 897-908.

Bordovskiy, O.K., 1965, Sources of Organic Matter in Mar. Basins; Mar. Geol., v. 3, pp. 5-31.

Boucher, L. J., Tynan, E. C., and Yen, T. F., 1968, Spectral Properties of Oxovanadium (IV) Complexes I. β-Ketimines; Inorg. Chem. v. 7, pp. 731-736.

Boucher, L. J., and Yen, T. F., 1968, Spectral Properties of Oxovanadium (IV) Complexes II. Bistrifluoroacetylacetone-ethylenediimine; Inorg. Chem., v. 7, pp. 2665-2667.

Boucher, L. J., and Yen, T. F., 1969, Spectral Properties of Oxovanadium(IV) Complexes III. Salicyaldimines; Inorg. Chem., v. 8, pp. 689-692.

Boyle, R. W., 1977, Cupriferous Bogs in the Sackville Area, New Brunswick, Canada; J. Geochem. Explor., v. 8, pp. 495-527.

Bradley, W. H., 1931, Origin and Microfossils of the Oil Shale of the Green River Formation of Colorado and Utah; U.S.G.S. Prof. Paper, 168, 58p.

Bradley, W. H., 1964, Geology of Green River Formation and Associated Eocene Rocks in Southwestern Wyoming and Adjacent Parts of Colorado and Utah; U.S.G.S. Prof. Paper, 496A, 86p.

Bradley, W. H., and Eugster, H. P., 1969, Geochemistry and Paleolimnology of the Trona Deposits and Associated Authigenic Minerals of the Green River Formation of Wyoming; U.S.G.S. Prof. Paper, 496-B, 71p.

Bramlette, M.N., 1946, The Monterey Formation of California and the Origin of its Siliceous Rocks; U.S.G.S. Prof. Paper, 212, 57p.

Branthaver, J. F., and Dorrence, S. M., 1978, Organometallic Complexes in Domestic Tar Sands; in Analytical Chemistry of Liquid Fuel Sources, ed. Uden, Siggia, and Jensen, Advances in Chemistry Series 170, Amer. Chem. Soc., pp. 143-149.

Breger, I. A., and Brown, A., 1962, Kerogen in the Chattanooga Shale; Science, v. 137, pp. 221-224.

Brenneman, M. C., and Smith, P. V., Jr., 1958, The Chemical Relationships Between Crude Oils and Their Source Rocks; in Habitat of Oil, Ed. Weeks, Amer. Assoc. Petrol. Geologists, Tulsa, pp. 818-849.

Brewer, P. G., and Spencer, D. W., 1974, Distribution of Some Trace Elements in Black Sea and their Flux Between Dissolved and Particulate Phases; in The Black Sea - Geology, Chemistry, and Biology, eds. Degens and Ross, Amer. Assoc. Petrol. Geologists Memoir 20, pp. 137-143.

Brongersma-Sanders, M., 1951, On Conditions Favoring the Preservation of Chlorophyll in Marine Sediments; Proc. 3rd World Petrol. Cong., Hague, Sec. I, pp. 401-411.

Brooks, J., 1971, Some Chemical and Geochemical Studies on Sporopollenin; in Sporopollenin, Academic Press, London, pp. 351-407.

Brooks, J., 1978, Personal Communique; The British National Oil Corp., 150 St. Vincent St., Glasgow, G2 5LJ, Scotland.

Brooks, J., Grant, P. R., Muir, M., Gijzel, P. Van, and Shaw, G., 1971, Sporopollenin Academic Press, London, 718p.

Brooks, J., and Shaw, G., 1968, Identity of Sporopollenin with Older Kerogen and New Evidence for the Possible Biological Source of Chemicals in Sedimentary Rocks; Nature, v. 220, pp. 678-679.

Brooks, J., and Shaw, G., 1970, Relationship of Kerogen and Sporopollenin; Nature, v. 227, pp. 195-196.

Brooks, J., and Shaw, G., 1972, Geochemistry of Sporopollenin; Chem. Geol., v. 10, pp. 69-87.

Brooks, R. R., Presley, B. J., and Kaplan, I. R., 1968, Trace Elements in the Interstitial Waters of Marine Sediments; Geochim. Cosmochim. Acta, v. 32, pp. 397-414.

Brooks, R. R., Lee, J., Reeves, R. D., and Jaffre, T., 1977, Detection of Nickeliferous Rocks by Analysis of Herbarium Specimens of Indicator Plants; J. Geochem. Explor., v. 7, pp. 49-57.

Brown, J. S., Emery, J. A., and Meyer, P. A., Jr., 1954, Explosion Pipe in Test Well on Hicks Dome, Hardin County, Illinois; Econ. Geol., v. 49, pp. 891-902.

Brown, S. R., 1969, Paleolimnological Evidence from Fossile Pigments; Mitt. Internat. Verein. Limnol., v. 17, pp. 95-103.

Brown, S. R., 1979, Personal Communique; Department of Biology, Queen's University, Kingston, Ontario, Canada.

Brown, S. R., Daley, R. J., and McNeely, R. N., 1977, Composition and Stratigraphy of the Fossil Phorbin Derivatives of Little Round Lake, Ontario; Limnol. Oceanog., v. 22, pp. 336-348.

Brunnock, J. V., Duckworth, D. F., and Stephens, G. G., 1968, Analysis of Beach Pollutants; J. Inst. Petrol., v. 54, pp. 310-325.

Buchheim, H. P., and Surdam, R. C., 1977, Fossil Catfish and the Depositional Environment of the Green River Formation, Wyoming; Geology, v. 5, pp. 196-198.

Bucher, W. H., 1963, Cryptoexplosion Structures Caused from Without or from Within the Earth? ("Astroblemes" or "Geoblemes"); Amer. J. Sci., v. 261, pp. 597-649.

Burgess, J. D., 1974, Microscopic Examination of Kerogen (Dispersed Organic Matter) in Petroleum Exploration; in Carbonaceous Materials as Indicators of Metamorphism, eds. Dutcher, Hacquebard, Schopf, and Simon, G.S.A. Spec. Paper 153, pp. 19-29.

Burns, R. G., 1970, Mineralogical Applications of Crystal Field Theory; University Press; Cambridge, 224p.

Burrows, W., and Cordon, T. C., 1936, The Influence of the Decomposition of Organic Matter on the Oxidation-Reduction Potential of Soils; Soil Sci., v. 42, pp. 1-10.

Byers, C. W., 1973, Biogenic Structures of Black Shale Paleoenvironments; Ph.D. Dissertation, Yale University, 134p.

Byers, C. W., 1977, Biofacies Patterns in Euxinic Basins; in Deep Water Carbonate Environments, SEPM Spec. Publ. 25, pp. 5-17.

Byers, C. W., and Larson, D. W., 1979, Paleoenvironments of Mowry Shale (Lower Cretaceous), Western and Central Wyoming; Amer. Assoc. Petrol. Geologists Bull., v. 63, pp. 354-361.

Calder, J. A., and Parker, P. L., 1973, Geochemical Implications of Induced Changes in C^{13} Fractionation by Blue-Green Algae; Geochim. Cosmochim. Acta., v. 37, pp. 133-140.

Cameron, C. C., and Wright, N. A., 1977, Some Peat Bogs in Washington County, Maine: Their Formation and Trace Element Content; Interdisciplinary Studies of Peat and Coal Origins, eds. Given and Cohen, G.S.A. Microform Publication No. 7, pp. 50-71.

Cannon, H. L., 1952, The Effect of Uranium-Vanadium on the Vegetation of the Colorado Plateau; Amer. J. Sci., v. 250, pp. 735-770.

Cannon, H. L., 1960, Botanical Prospecting for Ore Deposits; Science, v. 132, pp. 591-598.

Cannon, H. L., 1963, The Biochemistry of Vanadium; Soil Sci., v. 96, pp. 196-204.

Cardwell, A. L., 1977, Petroleum Source-Rock Potential of Arbuckle and Ellenburger Groups, Southern Mid-Continent, United States; Quart. Colo. School Mines, v. 72, pp. 1-134.

Casagrande, D. J., and Erchull, L. D., 1977, Metals in Plants and Waters in the Okefenokee Swamp and their Relationship to Constituents Found in Coal; Geochim. Cosmochim. Acta, v. 41, pp. 1391-1394.

Casagrande, D. J., and Hodgson, G. W., 1974, Generation of Homologous Porphyrins Under Simulated Geochemical Conditions; Geochim. Cosmochim. Acta, v. 38, pp. 1745-1758.

Cashion, W. B., 1967, Geology and Fuel Resources of the Green River Formation Southeastern Uinta Basin, Utah and Colorado; U.S.G.S. Prof. Paper, 548, 48p.

Caughey, W. S., and Corwin, A. H., 1955, The Stability of Metalloetioporphyrins Toward Acids; J. Amer. Chem. Soc., v. 77, pp. 1509-1513.

Cheshire, M. V., Berrow, M. L., Goodman, B. A., and Mundie, C. M., 1977, Metal Distribution and Nature of Some Cu, Mn, and V Complexes in Humic and Fulvic Acid Fractions of Soil Organic Matter; Geochim. Cosmochim. Acta, v. 41, pp. 1131-1138.

Clayton, J. L., and Swetland, P. J., 1978, Subaerial Weathering of Sedimentry Organic Matter; Geochim. Cosmochim. Acta., v. 42, pp. 305-312.

Clegg, K. E., and Bradbury, J. C., 1956, Igneous Intrusive Rocks in Illinois and Their Economic Significance; Illinois Geological Survey, Rept. Invest. 197, 19p.

Cobban, W. A., 1972, Cretaceous Stages; Cretaceous System, in Geological Atlas of the Rocky Mountain Region, Rocky Mountain Assoc. Geologists, Denver, pp. 190-206.

Collins, A. G., 1975, Geochemistry of Oilfield Water; Elsevier Scientific Publ. Co., Amsterdam, 496p.

Collinson, C., and Atherton, E., 1975, Devonian System; in Handbook of Illinois Stratigraphy, Illinois State Geological Survey, Bull. 95, pp. 104-123.

Comer, J. B., and Littlejohn, R., 1977, Content, Composition, and Thermal History of Organic Matter in Mesozoc Sediments, Falkland Plateau; in Initial Reports of the Deep Sea Drilling Project, v. 36, U.S. Government Printing Office, pp. 941-944.

Compston, W., 1960, The Carbon Isotopic Composition of Certain Marine Invertebrates and Coals from Australian Permian; Geochim. Cosmochim. Acta, v. 18, pp. 1-22.

Conant, J. B., Hyde, J. F., Moyer, W. W., and Dietz, E. M., 1931, Studies in the Chlorophyll Series IV. The Degradation of Chlorophyll and Allomerized Chlorophyll to Simple Chlorins; J. Amer. Chem. Soc., v. 53, pp. 359-373.

Conant, L. C., and Swanson, V. E., 1961, Chattanooga Shale and Related Rocks of Central Tennessee and Nearby Areas; U.S.G.S. Prof. Paper, 357, 91p.

Connan, J., LeTran, K., and Der Wdie, B. Van, 1975, Alteration of Petroleum Reservoirs; 9th World Petroleum Congress Proceedings, v. 2, pp. 171-178.

Corbett, L. W., 1967, Distribution of Heavy Metals in Asphalt Residua; Preprints, Div. Petrol. Chem. Amer. Chem. Soc., v. 12, pp. A83-A87.

Corcoran, E. F., 1957, Quantitative Studies on Organic Matter and Associated Biochromes in Marine Sediments; Unpublished Ph.D. Dissertation, University of California, Los Angeles.

Corwin, A. H., 1959, Petroporphyrins; Proc. 5th World Petroleum Congress, Sec. V, pp. 120-129.

Cosgrove, M. E., and Papavassiliou, C. Th., 1979, Clinoptilolite in DSDP Sediments of the Indian Ocean (Site 223, LEG 23): Its Stability Conditions and Estimation of its Free Energy; Mar. Geol., v. 33, pp. M77-M84.

Constantinides, G., Arich, G., and Lomi, C., 1959; Detection and Behaviour of Porphyrin Aggregates in Petroleum Residues and Bitumens; 5th World Petrol. Cong., Sec. V, pp. 131-142.

Cotton, F. A., 1964, Ligand Field Theory; J. Chem. Educ., v. 41, pp. 466-476.

Craig, H., 1953, The Geochemistry of the Stable Carbon Isotopes; Geochim. Cosmochim. Acta, v. 3, pp. 53-92.

Craig, H., 1957, Isotopic Standards for Carbon and Oxygen and Correction Factors for Mass Spectrometer Analysis of Carbon Dioxide; Geochim. Cosmochim. Acta, v. 12, pp. 133-149.

Crowell, J. C., 1974, Origin of Late Cenozoic Basins in Southern California; in Tectonics and Sedimentation, ed. Dickinson, Society of Econ. Paleo. and Miner. Spec. Publ. 22, pp. 190-204.

Culbertson, W. C., 1971, Stratigraph of the Trona Deposits in the Green River Formation, Southwest Wyoming; Contr. Geol., Trona Issue, v. 10, pp. 15-23.

Currie, R. I., 1962, Pigments in Zooplankton Faeces; Nature, v. 193, pp. 956-957.

Crute, M. B., 1959, The Crystal Structure of Nickel Etioporphyrin II; Acta Cryst., v. 12, pp. 24-28.

Cushman, J. A., and Siegfus, S. S., 1942, Foraminifera from the Type Area of the Kreyenhagen Shale of California; Trans. San Diego Soc. Nat. Hist., v. 9, pp. 385-426.

Daley, R. J., 1973, Experimental Characterization of Lacustrine Chlorophyll Diagensis: II. Bacterial, Viral, and Herbivore Grazing Effects; Arch. Hydrobiol. v. 72, pp. 409-439.

Daley, R. J., and Brown, S. R., 1973, Experimental Characterization of Lacustrine Chlorophyll Diagenesis: I. Physiological and Environmental Effects; Arch. Hydrobiol., v. 72, pp. 277-304.

Daley, R. J., Brown, S. R., and McNeely, R. N., 1977, Chromatographic and SCDP Measurements of Fossil Phorbins and the Postglacial History of Little Round Lake, Ontario; Limnol. Oceanog., v. 22, pp. 349-360.

Davis, J. C., 1963, Origin of the Mowry Shale; Wyoming Univ. Contr. Geology, v. 2, p. 135-146.

Davis, J. C., 1970, Petrology of Cretaceous Mowry Shale of Wyoming; Amer. Assoc. Petrol. Geologists Bull., v. 54, pp. 487-502.

Davis, S. J., and Gibbs, C. F., 1975, The Effect of Weathering on a Crude Oil Residue Exposed at Sea; Water Res., v. 9, pp. 275-285.

Dean, R. A., and Girdler, R. B., 1960, Reaction of Metal Etioporphyrins on Dissolution in Sulfuric Acid; Chem. Indust., January 23, pp. 100-101.

Dean, R. A., and Whitehead, E. V., 1963, The Composition of High Boiling Distillates and Residues; Proc. Sixth World Petroleum Congress, Sec. 5, pp. 261-280.

Deardorff, D. L., and Mannion, L. E., 1971, Wyoming Trona Deposits; Wyoming Univ. Contr. Geol., Trona Issue, v. 10, pp. 25-37.

Degens, E. T., Behrenot, M., Gotthard, B., and Reppmann, E., 1968b, Metabolic Fractionation of Carbon Isotopes in Marine Plankton-II. Data on Samples Collected off the Coasts of Peru and Ecuador; Deep-Sea Res., v. 15, pp. 11-20.

Degens, E. T., Guillard, R. R. L., Sackett, W. M., and Hellebust, J. A., 1968a, Metabolic Fractionation of Carbon Isotopes in Marine Plankton-I. Temperature and Respiration experiments; Deep-Sea Res., v. 15, pp. 1-9.

Degens, E. T., Williams, E. G., and Keith, M. L., 1957, Environmental Studies of Carboniferous Sediments Part I: Geochemical Criteria for Differentiating Marine from Fresh-Water Shales; Amer. Assoc. Petrol. Geologists Bull., v. 42, pp. 2427-2455.

DeNiro, M. J., and Epstein, S., 1978, Influence of Diet on the Distribution of Carbon Isotopes in Animals; Geochim. Cosmochim. Acta, v. 42, pp. 495-506.

Denson, N. M., and Gill, J. R., 1965, Uranium-Bearing Lignite and Carbonaceous Shale in the Southwestern Part of the Williston Basin - A Regional Study; U.S.G.S. Prof. Paper, 463, 62p.

Devine, S. B., Ferrell, R. E., Jr., and Billings, G. K., 1972, A Quantitative X-Ray Diffraction Technique Applied to Fine-Grained Sediments of the Deep Gulf of Mexico; Jour. Sed. Pet., v. 42, pp. 468-475.

Dibblee, T. W., Jr., 1973, Stratigraphy of the Southern Coast Ranges Near the San Andreas Fault from Cholame to Maricopa, California; U.S.G.S. Prof. Paper, 764, 45p.

Dickinson, W. R., 1976, Sedimentary Basins Developed During Evolution of Mesozoic-Cenozoic Arc-Trench System in Western North America; Can. J. Earth Sci., v. 13, pp. 1268-1287.

Didyk, B. M., Alturki, Y. I. A., Pillinger, C. T., and Eglinton, G., 1975, Petroporphyrins as Indicators of Geothermal Maturation; Nature, v. 256, pp. 563-565.

Didyk, B. M., Simoneit, B. R. T., Brassell, S. C., and Eglinton, G., 1978, Organic Geochemical Indicators of Palaeoenvironmental Conditions of Sedimentation; Nature, v. 272, pp. 216-222.

Dineley, D. L., 1975, North Atlantic Old Red Sandstone - Some Implications for Devonian Paleogeography; in Canada's Continental Margins and Offshore Petroleum Exploration, eds. Yorath, Parker, and Glass, Canadian Society of Petroleum Geologists, Memoir 4, pp. 773-790.

Dow, W. G., 1977, Kerogen Studies and Geological Interpretations; J. Geochem. Explor., v. 7, pp. 79-99.

Drozdova, T. V., 1975, Geochemical Conditions for the Preservation of Amino Acids and Porphyrin Structures in Sediments; in Recent Contributions to Geochemistry and Analytical Chemistry, ed. Tugarinov, John Wiley & Sons, Inc., New York, pp. 523-529.

Drozdova, T. V., and Gorskiy, Yu. N., 1972, Conditions of Preservation of Chlorophyll, Pheophytin and Humic Matter in Black Sea Sediments; Geochem. Internat. v. 9, pp. 208-218.

Dunning, H. N., Moore, J. W., and Denekas, M. O., 1953, Interfacial Activities and Porphyrin Contents of Petroleum Extracts; Ind. Eng. Chem., v. 45, pp. 1759-1765.

Dunnington, H. V., 1958, Generation, Migration, Accumulation, and Dissipation of Oil in Northern Iraq; in Habitat of Oil, ed., Weeks, Amer. Assoc. Petrol. Geologists, Tulsa, pp. 1194-1251.

Duschatko, R. W., and Nash, A. J., 1973, Quantitative Mineralogy from X-Ray Diffraction; Amoco Production Company Research Department, Report No. F73-G-4, 14p.

Dwiggins, C. W., Jr., Willcox, K. W., Doughty, D. A., and Heemstra, R. J., 1969, Separation and Characterization of Metalo-Organic Materials in Petrol.; U. S. Bur. of Mines Rept. of Inv. 7273, 41p.

Dyni, J. R., 1976, Trioctahedral Smectite in the Green River Formation, Duschesne County, Utah; U.S.G.S. Prof. Paper, 967, 14p.

Eglinton, G., 1969, Organic Geochemistry: The Organic Chemist's Approach; in Organic Geochemistry, ed. Eglinton and Murphy, Springer-Verlag, New York, pp. 20-73.

Emery, K. O., 1960, The Sea Off Southern California; John Wiley & Sons, Inc., New York, 366p.

Emery, K. O., and Rittenberg, S. C., 1952, Early Diagenesis of California Basin Sediments in Relation to Origin of Oil; Amer. Assoc. Petrol. Geologists Bull., v. 36, pp. 735-806.

Erdman, J. G., Ramsey, V. G., and Hanson, W. E., 1956a, Volatility of Metallo-Porphyrin Complexes; Science, v. 123, p 502.

Erdman, J. G., Ramsey, V. G., Kalenda, N. W., and Hanson, W. E., 1956b, Synthesis and Properties of Porphyrin Vanadium Complexes; Jour. Amer. Chem. Soc., v. 78, pp. 5844-5847.

Erdman, J. G., Walter, J. W., and Hanson, W. E., 1957, The Stability of the Porphyrin Metallo Complexes; Amer. Chem. Soc. Div., Petrol. Chem., Preprints, v. 2, pp. 259-267.

Erickson, M. P., 1952, New Locality of Shortite; Amer. Mineral., v. 37, pp. 332-334.

Erickson, R. L., Myers, A. T., and Horr, C. A., 1954, Association of Uranium and Other Metals with Crude Oil, Asphalt, and Petroliferous Rocks; Amer. Assoc. Petrol. Geologists Bull., v. 38, pp. 2200-2218.

Espitalié, J., Madec, M., and Tissot, B., 1980, Role of Mineral Matrix in Kerogen Pyrolysis: Influence on Petroleum Generation and Migration; Amer. Assoc. Petrol. Geologists Bull., v. 64, pp. 59-66.

Eugster, H. P., and Hardie, L. A., 1975, Sedimentation in an Ancient Playa-Lake Complex: The Wilkins Peak Member of the Green River Formation of Wyoming; Geol. Soc. Amer. Bull., v. 86, pp. 319-334.

Eugster, H. P., and Surdam, R. C., 1973; Depositional Environment of the Green River Formation of Wyoming: A Preliminary Report; Geol. Soc. Amer. Bull., v. 84, pp. 1115-1120.

Evans, C. R., Rogers, M. A., and Bailey, N.J.L., 1971, Evolution and Alteration of Petroleum in Western Canada; Chem. Geol., v. 8, pp. 147-170.

Evans, H. T., Jr., 1970, Vanadium-Section A. Crystal Chemistry; in Handbook of Geochemistry, ed. K. H. Wedepohl, Springer-Verlag, Berlin, pp. 23A1-23A7.

Evans, H. T., Jr., and Garrels, R. M., 1958, Thermodynamic Equilibria of Vanadium in Aqueous Systems as Applied to the Interpretation of the Colorado Plateau Ore Deposits; Geochim. Cosmochim. Acta, v. 15, pp. 131-149.

Fahey, J. J., 1962, Saline Minerals of the Green River Formation; U.S.G.S. Prof. Paper, 405, 50p.

Fallon, R. D. and Brock, T. D., 1979, Decomposition of Blue-Green Algal (Cyanobacterial) Blooms in Lake Mendota, Wisconsin; App. Environ. Microbiol., v. 37, pp. 820-830.

Fawcett, P., Green, D., and Shaw, G., 1971, The Determination of Trace Elements in Pollen and Sporopollenin Using Neutron Activation Analysis; Radiochem. Radioanal. Letters, v. 8, p. 37-40.

Fawcett, P., Green, D., and Shaw, G., 1973, The Application of Neutron Activation Analysis to the Determination of Trace Elements in Pollen and Sporopollenins; J. Radioanal. Chem., v. 13, pp. 313-318.

Fawcett, P., Green, D., and Shaw, G., 1974, The Determination of Phosphorous in Pollen Grain Wall Materials Using Neutron Activation Analysis Radiochem. Radioanal. Letters, v. 17, pp. 121-127.

Filby, R. H., 1975, The Nature of Metals in Petroleum; in The Role of Trace Elements in Petroleum; ed. Yen, Ann Arbor Science Publishers, Inc., Ann Arbor, pp. 31-58.

Filby, R. H., and Shah, K. R., 1975, Neutron Activation Methods for Trace Elements in Crude Oils; in The Role of Trace Metals in Petroleum, ed. Yen, Ann Arbor Science Publishers, Ann Arbor, pp. 89-110.

Fleischer, E. G., 1963, The Structure of Nickel Etioporphyrin I.; J. Amer. Chem. Soc., v. 85, pp. 146-148.

Fontugne, M., and Duplessy, J. C., 1978, Carbon Isotope Ratio of Marine Plankton Related to Surface Water Masses; Earth Planet. Sci. Lett., v. 41, pp. 365-371.

Forsman, J. P., 1963, Geochemistry of Kerogen; in Organic Geochemistry, ed. Breger, Pergamon Press, New York, pp. 148-182.

Fowler, S. W., 1977, Trace Elements in Zooplankton Particulate Products; Nature, v. 269, pp. 51-53.

Friedman, I., and Murata, K. J., 1979, Origin of Dolomite in Miocene Monterey Shale and Related Formations in the Temblor Range, California; Geochim. Cosmochim. Acta, v. 43, pp. 1357-1365.

Fry, B., and Parker, P. L., 1979, Animal Diet in Texas Seagrass Meadows: δC^{13} Evidence for the Importance of Benthic Plants; Estuarine Coast. Mar. Sci., v. 8, pp. 499-509.

Fuex, A. N., 1977, The Use of Stable Carbon Isotopes in Hydrocarbon Exploration; Jour. Geochem. Explor., v. 7, pp. 155-188.

Galehouse, J. S., 1971, Point Counting; in Procedures in Sedimentary Petrology, ed. Carver, Wiley-Interscience, New York, pp. 385-408.

Gamble, D. S., and Schnitzer, M., 1973, The Chemistry of Fulvic Acid and its Reactions with Metal Ions; in Trace Metals and Metal-Organic Interactions in Natural Waters, ed. Singer, Ann Arbor Science Publishers Inc., Ann Arbor, pp. 265-302.

Garrels, R. M., and Christ, C. L., 1965, Solutions, Minerals, and Equilibria; Freeman, Cooper, and Company, San Francisco, 450p.

Gasin, C. L., 1959, Paleontological Exploration and Dating of the Early Tertiary Deposits in Basins Adjacent to the Uinta Mountains; in Guidebook to the Geology of the Wasatch and Unta Mountains Transition Area, Intermountain Assoc. Petrol. Geologists, 10th Ann. Field Conf., pp. 131-138.

Gazin, C. L., 1965; Early Eocene Mammalian Faunas and their Environment in the Vicinity of the Rock Springs Uplift, Wyoming; in Sedimentation of

Late Cretaceous and Early Tertiary Outcrops, Rock Springs Uplift, Wyoming Geol. Assoc. Guidebook, 19th Field Conf., pp. 171-180.

Gehman, H. M., 1962, Organic Matter in Limestones; Geochim. Cosmochim. Acta, v. 26, pp. 885-897.

Glasby, G. P., 1975, Limitations of Crystal Field Theory Applied to Sedimentary Systems: Discussion; Geoderma, v. 13, pp. 363-367.

Goldberg, E. D., 1961, Marine Geochemistry; Ann. Rev. Phys. Chem., v. 12, pp. 29-48.

Goldberg, E. D., 1965, Minor Elements in Sea Water; in Chemical Oceanography, v. 1, eds. Riley and Skirrow, Academic Press, London, pp. 163-196.

Goldhaber, M. B., and Kaplan, I. R., 1974, The sulfur Cycle; in The Sea, v. 5, ed. Goldberg, John Wiley & Sons, New York, pp. 569-655.

Goldhaber, M. B., and Kaplan, I. R., 1975, Controls and Consequences of Sulfate Reduction Rates in Recent Marine Sediments; Soil Sci., v. 119, pp. 42-55.

Goldschmidt, V. M., 1954, Geochemistry; ed. Muir, Oxford University Press, Lond, 730p.

Good, B. H., and Chapman, R. L., 1978, The Ultrastructure of Phycopeltis (Chroolepidaceae:Chlorophyta). I. Sporopollenin in the Cell Walls; Amer. J. Bot., v. 65, pp. 27-33.

Gorhan, E., and Sanger, J., 1967, Plant Pigments in Woodland Soils; Ecology, v. 48, pp. 306-308.

Gormly, J. R., and Sackett, W. M., 1977, Carbon Isotope Evidence for the Maturation of Marine Lipids; in Advances in Organic Geochemistry 1975, eds. Campos and Goni, Empressa Nacional Adaro de Investigaciones Mineras, Madrid, pp. 321-339.

Griffith, C., 1977, Stratigrahy and Paleoenvironment of the New Albany Shale (Upper Devonian) of North-Central Kentucky; Unpublished M.S. Thesis, University of Wisconsin-Madison, Dept. of Geology, 214p.

Gulyayeva, L. A., and Lositskaya, I. F., 1967, Interaction Between Petrol. and Vanadium in Aqueous Solutions; Geochem. International, v. 4, pp. 699-709.

Haines, E. B., and Montague, C. L., 1979, Food Sources of Estuarine Invertebrates Analyzed Using $^{13}C/^{12}C$ Ratios; Ecology, v. 60, pp. 48-56.

Haji-Vassiliou, A., and Kerr, P. F., 1973, Analytic Data on Nature of Urano-Organic Deposits; Amer. Assoc. Petrol. Geologists Bull., v. 57, pp. 1291-1296.

Harrison, A. G., and Thode, H. G., 1958, Mechanism of the Bacterial Reduction of Sulfate from Isotope Fractionation Studies; Trans. Farad. Soc, v. 54, pp. 84-92.

Harwood, R. J., 1977, Oil and Gas Generation by Laboratory Pyrolysis of Kerogen; Amer. Assoc. Petrol. Geologists Bull., v. 61, pp. 2082-2102.

Hatcher, P. G., Simoneit, B. R., and Gerchakov, S. M., 1977, The Organic Geochemistry of a Recent Sapropelic Environment: Mangrove Lake, Bermuda; in Advances in Organic Geochemistry 1975, eds. Campos and Goni, Empressa Nacional Adaro De Investigaciones Mineras, Madrid, p. 469-484.

Heath, G. R., Moore, T. C., Jr.,and Dauphin, J. P., 1978, Organic Carbon in Deep-Sea Sediments; in The Fate of Fossil Fuel CO_2 in the Oceans, eds. Andersen and Malahoff, Plenum Publishing Corp., New York, pp. 605-625.

Hedges, J. I., and Mann, D. C., 1979, The Lignin Geochemistry of Marine Sediments from the Southern Washington Coast; Geochim. Cosmochim. Acta, v. 43, pp. 1809-1818.

Hedges, J. I., and Parker, P. L., 1976, Land-Derived Organic Matter in Surface Sediments from the Gulf of Mexico; Geochim. Cosmochim. Acta, v. 40, pp. 1019-1029.

Henry, R. P., Mitchell, P.C.H., and Prue, J. E., 1973, Hydrolysis of the Oxovanadium (IV) Ion and the Stability of its Complexes with the 1,2-Dihydroxybenzenato (2^-) Ion; J. Chem. Soc., Dalton Trans., 1973, pp. 1156-1159.

Heyl, A. V., and Brock, M. R., 1961, Structural Framework of the Illinois-Kentucky Mining District and its Relation to Mineral Deposits; U.S.G.S. Prof. Paper, 424-D, pp. 3-6.

Hodgson, G. W., 1954, Vanadium, Nickel, and Iron Trace Metals in Crude Oils of Western Canada; Amer. Assoc. Petroleum Geologists Bull., v. 38, pp. 2537-2554.

Hodgson, G. W., and Baker, B. L., 1957, Vanadium, Nickel,and Porphyrins in Thermal Geochemistry of Petroleum; Amer. Assoc. Petrol. Geologists Bull., v. 41, p. 2413-2426.

Hodgson, G. W., and Baker, B. L., 1959, Geochemical Aspects of Petroleum Migration in Pembina, Redwater, Joffee, and Lloydminster Oil Fields of Alberta and Saskatchewan, Canada; Amer. Assoc. Petrol. Geologists Bull., v. 43, pp. 311-328.

Hodgson, G. W., Baker, B. L., and Peake, E., 1967, Geochemistry of Porphyrins; in Fundamental Aspects of Petroleum Geochemistry, eds., Nagy and Colombo, Elsevier, Amsterdam, pp. 177-259.

Hodgson, G. W., and Hitchon, B., 1959, Primary Degradation of Chlorophyll Under Simulated Petroleum Source Rock Sedimentation Conditions; Amer. Assoc. Petroleum Geologists Bull., v. 43, pp. 2481-2492.

Hodgson, G. W., Hitchon, B., Elofson, R. M., Baker, B. L., and Peake, E., 1960, Petroleum Pigments from Recent Fresh-Water Sediments; Geochim. Cosmochim. Acta, v. 19, pp. 272-288.

Hodgson, G. W., Hitchon, B., Taguchi, K., Baker, B. L.,and Peake, E., 1968, Geochemistry of Porphyrins, Chlorins, and Polycyclic Aromatics in Soils, Sediments, and Sedimentary Rocks; Geochim. Cosmochim. Acta, v. 32, pp. 737-772.

Hodgson, G. W., Strosher, M., and Casagrande, D. J., 1972, Geochemistry of Porphyrins: Analytical Oxidation to Maleimides; in Advances in Organic Geochemistry 1971, ed. Braunschweig, Pergamon Press, Oxford, pp. 151-161.

Hoefs, J., 1973, Stable Isotope Geochemistry; Springer-Verlag, New York, 140p.

Hoff, R. E., 1964, Vanadyl Porphyrins in Boscan Crude Oil; Ph.D. Dissertation, University of Utah, Dept. of Chemistry, 112p.

Holland, H. D., 1972, The Geologic History of Seawater-An Attempt to Solve the Problem; Geochim. Cosmochim. Acta, v. 35, pp. 637-653.

Holm-Hansen, O., 1969, Determination of Microbial Biomass in Ocean Profiles; Limno. Oceanog., v. 14, pp. 740-747.

Hoskins, J. H., and Cross, A. T., 1953, The Petrification Flora of the Devonian-Mississippian Black Shale; Paleobot., v. 1, pp. 215-238.

Hunt, J. M., 1961, Distribution of Hydrocarbons in Sedimentary Rocks; Geochim. Cosmochim. Acta, v. 22, pp. 37-49.

J. M., 1979, Petroleum Geochemistry and Geology; W. H. Freeman and Co., San Francisco, 617p.

Hunt, M., and Jamieson, G. W., 1958, Oil and Organic Matter in Source Rocks of Petroleum; in Habitat of Oil, ed. Weeks, Amer. Assoc. Petrol. Geologists, Tulsa, pp. 735-746.

Hunt, J. M., 1973, Organic Geochemistry of the Marine Environment; in Advances in Organic Geochemistry 1972, eds. Tissot and Bienner, Editions Technip, Paris, pp. 593-605.

Hyden, H. J., 1956, Uranium and Other Trace Metals in Crude Oils of the Western United States; USGS Prof. Paper, 300, pp. 511-519.

Iannuzzi, M. M., and Rieger, P. H., 1975, Nature of Vanadium (IV) in Basic Aqueous Solution; Inorg. Chem., v. 14, pp. 2895-2899.

Ingersoll, R. V., 1979, Evolution of the Late Cretceous Forearc Basin, Northern and Central California; Geol. Soc. Amer. Bull., v. 90, pp. 813-826.

Jackson, T. A., Fritz, P., and Drimmie, R., 1978, Stable Carbon Isotope Ratios and Chemical Properties of Kerogen and Extractable Organic Matter in Pre-Phanerozoic and Phanerozoic Sediments - Their Interpretation and Possible Paleobiological Significance; Chem. Geol., v. 21, pp. 335-350.

Jannasch, H. W., and Jones, G. E., 1959, Bacterial Populations in Sea Water as Determined by Different Methods of Enumeration; Limno. Oceanog., v. 4, pp. 128-139.

Jenkins, O. P., 1938, Geological Map of California; State of California, Department of Natural Resources, Division of Mines, 6 Sheets.

Jobson, A., Cook, F. D., and Westlake, D.W.S., 1972, Microbial Utilization of Crude Oil; App. Microbiol., v. 23, pp. 1082-1089.

Jobson, A. M., Cook, F. D., and Westlake, D.W.S., 1979, Interaction of Aerobic and Anaerobic Bacteria in Petroleum Biodegradation; Chem. Geol., v. 24, pp. 355-365.

Jordan, D. W., 1979, Trace Fossils and Stratigraphy of the Devonian Black Shale in East-Central Kentucky; unpublished M.S. Thesis, University of Cincinnati, Dept. of Geology, 194p.

Joslyn, M. A., and Mackinney, G., 1938, The Rate Conversion of Chlorophyll to Pheophytin; J. Amer. Chem. Soc., v. 60, pp. 1132-1136.

Kallio, R. E., 1979, Personal Communique; Department of Microbiology, University of Illinois, Urbana, Ill. 61801.

Kaplan, I. R., and Rittenberg, S. C., 1964, Microbiological Fractionation of Sulfur Isotopes; J. Gen. Microbiol., v. 34, pp. 195-212.

Keith, M. L., and Weber, J. M., 1964, Carbon and Oxygen Isotopic Composition of Selected Limestones and Fossils; Geochim. Cosmochim. Acta, v. 28, pp. 1787-1816.

Kemp, A.L.W., 1971, Organic Carbon and Nitrogen in the Surface Sediments of Lakes Ontario, Erie, and Huron; J. Sed. Pet., v. 41, pp. 537-548.

Kemp, A.L.W., and Thode, H.G., 1968, The Mechanism of the Bacterial Reduction of Sulfate and of Sulfite From Isotope Fractionation Studies; Geochim. Cosmochim. Acta, v. 32, pp. 71-91.

Kerr, P. F., 1931, Bentonite from Ventura, California; Econ. Geol., v. 26, pp. 153-168.

Kidson, E. J., 1965, A Biostratigraphic study of Fossil Silicofalgellates (Cretaceous-Recent) from California with Observations on Their Evolution; unpublished M.S. Thesis, Dept. of Geology, Wichita State Univ., 178p.

King, P. B., and Beikman, H. M., 1974, Geological Map of the United States; Scale 1:2,500,000, U.S. Geol. Surv.

Kleinpell, R. M., 1938, Miocene Stratigraphy of California; Amer. Assoc. Petrol. Geologists, Tulsa, 450p.

Knezevic, M. Z., and Chen, K. Y., 1977, Organometallic Interactions in Recent Marine Sediments; in Chemistry of Marine Sediments, ed. Yen, Ann Arbor Science Publishers Inc., Ann Arbor, pp. 223-241.

Kochenov, A. V., and Kreshtapova, V. N., 1967, Rare and Dispersed Elements in the Peats of the Northern Part of the Russian Platform; Geochem. Int., v. 4, pp. 286-294.

Konovalov, G. S., 1973, The Dynamics of Rare and Trace Element (Micro Elements) Content and Their Drainage from the USSR Territory into the Sea Basins; Proc. Symp.Hydrogeochem. and Biogeochem., v. 1, pp. 606-612.

Kovdi, V. A., Yakushevskaya, I. V., Tyoryokanov, A. N., 1959, Trace Elements in the Soils of the Soviet Union; publ. MGU.

Koyama, T., Nikaido, M., Tomino, T., and Hayakawa, H., 1973, Decomposition of Organic Matter in Lake Sediments; Proc. Int. IAGC et al. Hydrogeochem. Biogeochem. Symp., Tokyo, v. 2, pp. 512-535.

Koyama, T., Shimomura, O., and Yanagi, K., 1968, Vertical Distribution of Pigments in Lake Sediments as Determined by Paper Chromatograhy; Geochem. J., v. 2, pp. 87-103.

Koyama, T., and Tomino, T., 1967, Decomposition Process of Organic Carbon and Nitrogen in Lake Water; Geochem. J., v. 1, pp. 109-124.

Krauskopf, K. B., 1955, Sedimentary Deposits of Rare Metals; Econ. Geol., 50th Ann. Vol. 1905-1955, pp. 411-463.

Krauskopf, K. B., 1967, Introduction to Geochemistry, McGraw-Hill Book Co., New York, 721p.

Kribek, B., Kaigl, J., and Oruzinsky, V., 1977, Characteristics of Di- and Trivalent Metal-Humic Acid Complexes on the Basis of Their Molecular-Weight Distribution; Chem. Geol., v. 19, pp. 73-81.

Krishnamurthy, R., and Schaap, W. B., 1969, Computing Ligand Field Potentials and Relative Energies of d Orbitals; J. Chem. Educ., v. 46, pp. 799-810.

Krumbein, W. C., and Garrels, R. M., 1952, Origin and Classification of Chemical Sediments in Terms of pH and Oxidation - Reduction Potentials; Jour. Geol., v. 60, pp. 1-33.

Kullerud, G., and Yund, R. A., 1962, The Ni-S System and Related Minerals; J. Petrol., v. 3, pp. 126-175.

Lamort, C., 1956, Etude Spectrophotometrique des Modifications des Chlorophylles a et b sous l'Influence de Divers Agents Physiques et Chimiques; Rev. Ferment. Ind. Aliment., v. 11, pp. 34-45.

Landes, K. K., 1967, Eometamorphism, and Oil and Gas in Time and Space; Amer. Assoc. Petrol. Geologists Bull., v. 51, pp. 828-841.

Lemberg, R., and Legge, J. W., 1949, Hematin Compounds and Bile Pigments; Interscience, New York, 755p.

Lewan, M. D. 1975, Geochemistry and Geology of the Kreyenhagen Shale, California; Amoco Production Co. Technical Service, Report No. 9359CQ, 53p.

Lewan, M. D., 1978, Laboratory Classification of Very Fine-Grained Sedimentary Rocks; Geology, v. 6, pp. 745-748.

Lewan, M. D., Winters, J. C., and McDonald, J. H., 1979, Generation of Oil-Like Pyrolysates from Organic-Rich Shales; Science, v. 6, pp. 745-748.

Leythaeuser, D., 1973, Effects of Weathering on Organic Matter in Shales; Geochim. Cosmochim. Acta., v. 37, pp. 113-120.

Li, Y. H., and Gregory, S., 1974, Diffusion of Ions in Sea Water and in Deep-Sea Sediments; Geochim. Cosmochim. Acta, v. 38, pp. 703-714.

Lindblom, G. P., and Lupton, M. D., 1961, Microbiological Aspects of Organic Geochemistry; Developments in Industrial Microbiology Proceedings, 17th Meeting, v. 2, ed. Rich, Plenum Press, New York, pp. 9-21.

Lineback, J. A., 1968, Subdivisions and Depositional Environments of New Albany Shale (Devonian-Mississippian) in Indiana; Amer. Assoc. Petrol. Geologists Bull., v. 52, pp. 1291-1303.

Littljohn, R., 1979, Personal Communique; Amoco Production Co. Research Center, P. O. Box 591, Tulsa, Oklahoma 74102.

Livingstone, D. A., 1963, Data of Geochemistry: Chapter G. Chemical Composition of Rivers and Lakes; U.S.G.S. Prof. Paper, 440-G, 64p.

Lorenzen, C. J., 1967, Vertical Distribution of Chlorophyll and Phaeo-pigments: Baja California; Deep-Sea Res., v. 14, pp. 735-745.

Lundberg, J. G., and Case, G. R., 1970, A New Catfish from the Eocene Green River Formation, Wyoming; Jour. Paleontology, v. 44, pp. 451-457.

Lyons, W. B., and Gaudette, H. E., 1979, Sulfate Reduction and the Nature of Organic Matter in Estuarine Sediments; Org. Geochem., v. 1, pp. 151-155.

MacCarthy, P., and Mark, H. B., Jr., 1976, Perspectives in Humic Acid Research Part II: Principles of Humic Acid Chemistry; Graduate Research Journal, University of Cincinnati, v. 2, pp. 63-74.

Mackenzie, F. T., 1975, Sedimentary Cycling and the Evolution of Seawater; in Chemical Oceanography, ed. Riley, Academic Press, New York, pp. 309-364.

Manskaya, S. M., and Drozdova, T. V., 1968, Geochemistry of Organic Substances; Pergamon Press, Oxford, 345p.

Mariner, R. H., and Surdam, R. C., 1970, Alkalinity and Formation of Zeolites in Saline Alkaline Lakes; Science, v. 170, pp. 977-979.

Martin, D. F., and Ramaiah, K., 1965, Five-Co-Ordinate Compounds III. Kinetics of Some Reactions of Bisacetylacetonepropylenediimino oxovanadium (IV); J. Inorg. Nucl. Chem., v. 27, pp. 2027-2035.

Martin, J. H., and Knaver, G. A., 1973, The Elemental Composition of Plankton; Geochim. Cosmochim. Acta, v. 37, pp. 1639-1653.

Masters, B. A., 1975, Personal Communique; Amoco Production Co. Research Center, P. O. Box 591, Tulsa, Oklahoma 74102.

Maynard, J. B., 1979, Carbon Isotopes as Indicators of the Source of Organic Matter in Devonian Shales of the Appalachian Basin; in preparation.

Maynard, J. B., 1980,, Sulfur Isotopes of Iron Sulfides in Shales of the Appalachian Basin: Influence of Sedimentation Rate; Amer. J. Sci., in press.

McAuliffe, C., 1964, Solubility in Water of Paraffin, Cycloparaffin, Olefin, and Aromatic Hydrocarbons; Amer. Chem. Soc., Div. Petrol. Chem. Meeting, Chicago, Ill., August 30-September 4, pp. 275-285.

McBride, M. B., 1978 Transition Metal Bonding in Humic Acid: An ESR Study; Soil Sci., v. 126, pp. 200-209.

McCready, R.G.L., 1975, Sulfur Isotope Fractionation by Desulfovibrio and Desulfotomaculum Species; Geochim. Cosmochim. Acta, v. 39, pp. 1395-1401.

McCready, R.G.L., and Kaplan, I. R., 1974, Fractionation of Sulfur Isotopes by Yeast Saccharomyces cerevisiae; Geochim. Cosmochim. Acta, v. 38, pp. 1239-1253.

McGregor, A. A., 1972, The Powder River Basin; Petrol. and Natural Gas, in Geological Atlas of the Rocky Mountain Region; Rocky Mountain Assoc. Geologists, Denver, pp. 268-270.

McIver, R. D., 1959, Composition of Kerogen - Clue to its Role in the Origin of Petroleum; Proc. 7th World Petrol. Congress, Elsevier Publishing Company pp. 25-36.

McKenzie, R. M., 1975, Limitations of Crystal Field Theory Applied to Sedimentary Systems: A Reply; Geoderma, v. 13, pp. 369-372.

McKirdy, D. M., and Powell, T. G., 1974, Metamorphic Alteration of Carbon Isotopic Composition in Ancient Sedimentary Organic Matter: New Evidence from Australia and South Africa; Geology, v. 2, pp. 591-595.

Meade, R. H., 1966, Factors Influencing the Early Stages of the Compaction of Clays and Sands-Review; J. Sed. Petrol., v. 36, pp. 1085-1101.

Mechalas, B. J., and Rittenberg, S. C., 1960, Energy Coupling in Desulfovibrio Desulfuricans; J. Bact., v. 80, pp. 501-507.

Metzler, D. E., 1977, Biochemistry; Academic Press, New York, 1129p.

Miller, A. R., 1969, Atlantis II Account; in Hot Brines and Recent Heavy Metal Deposits in the Red Sea, eds. Degens and Ross, Springer-Verlag Inc., New York, pp. 15-17.

Milner, C.W.D., Rogers, M. A., and Evans, C. R., 1977, Petroleum Transformations in Reservoirs; J. Geochem. Explor., v. 7, pp. 101-153.

Mizutani, S., 1970, Silica Minerals in the Early Stage of Diagenesis; Sedimentology, v. 15, pp. 419-436.

Momper, J. A., 1978, Oil Migration Limitations Suggested by Geological and Geochemical Considerations; in Physical and Chemical Constraints on Petroleum Migration Amer. Assoc. Petrol. Geologists, Cont. Educ. Crs. Note Ser. No. 8, B1-B60.

Moore, C. A., 1968, Quantitative Analysis of Naturally Occurring Multicomponent Mineral Systems by X-Ray Diffraction; Clays and Clay Min., v. 16, pp. 325-336.

Morandi, J. R., and Jensen, H. B., 1964, Porphyrin Skeleton Survives Retorting; Chem. Eng. News, v. 42, p. 48.

Morandi, J. R., and Jensen, H. B., 1966, Comparison of Porphyrins from Shale Oil, Oil Shale, and Petroleim by Adsorption and Mass Spectrometry; J. Chem. Eng. Data, v. 11, pp. 81-88.

Morey, P. R., and Morey, E. D., 1969, Senckenberg Lignite: A Lignitized Wood with Apparently Original Cellulose and Lignin; Science, v. 164, pp. 836-838.

Murata, K.J.,and Larson, R. R., 1975, Diagenesis of Miocene Siliceous Shale, Temblor Range, California; Jour. Res. U.S.G.S., v. 3, pp. 553-566.

Murray, J. W., Grundmanis, V., and Smethie, W. M., Jr., 1978; Interstitial Water Chemistry in the Sediments of Saanich Inlet; Geochim. Cosmochim. Acta, v. 42, pp. 1011-1026.

Naboko, S. I., Pilipenko, G. F., and Glavatskikh, S. F., 1973, Chemical Differentiation of Metalliferous Hydrothermal Waters of Uzon Caldera in the Area of Their Discharge; Proc. Symp. Hydrogeochem. and Biogeochem., v. 1, pp. 182-195.

Nicholls, G. D., Curl, H., Jr., and Bowen, V. T., 1959, Spectrographic Analyses of Marine Plankton; Limnol. Oceanog., v. 4, pp. 472-478.

Nissenbaum, A., 1974, The Orgnanic Geochemistry of Marine and Terrestrial Humic Substances: Implications of Carbon and Hydrogen Isotope Studies; in Advances in Organic Geochemistry 1973, ed. Tissot and Bienner, Editions Technip, Paris, pp. 39-52.

Nissenbaum, A., Baedecker, M. J., and Kaplan, I. R., 1972, Organic Geochemistry of Dead Sea Sediments; Geochim. Cosmochim. Acta, v. 36, pp. 709-727.

Nissenbaum, A., and Swaine, D. J., 1976, Organic Matter - Metal Interactions in Recent Sediments: The Role of Humic Substances; Geochim. Cosmochim. Acta, v. 40, pp. 809-816.

Nixon, R. P., 1973, Oil Source Beds in Cretaceous Mowry Shale of Northwestern Interior United States; Amer. Assoc. Petrol. Geologists Bull., v. 57, pp. 136-161.

Noddack, I., and Noddack, W., 1939, Die Häufigkeiten der Schwermetalle in Meerestieron; Arkiv. För. Zoologi., v. 32A, pp. 1-35.

Oehler, J. H., Aizenshtat, Z., and Schopf, J. W., 1974, Thermal Alteration of Blue-Green Algae and Blue-Green Algal Chlorophyll; Amer. Assoc. Petrol. Geologists Bull., v. 58, p. 124-132.

Oppenheimer, C. H., 1960, Bacterial Activity in Sediments of Shallow Marine Bays; Geochim. Cosmochim. Acta, v. 19, pp. 244-260.

Orr, W. L., Emery, K. O., and Grady, J. R., 1958, Preservation of Chlorophyll Derivatives in Sediments off Southern California; Amer. Assoc. Petrol. Geologists Bull., v. 42, pp. 925-962.

Ostroumov, E. A., and Silina, O. M., 1952, Concerning Certain Regularities in the Distribution of Vanadium in Contemporary Marine Deposits; Dokl. AN USSR, v. 86, p. 365.

Pace, N., 1941, Pigments of the Marine Diatom Nitzchia Closterium; Jour. Biol. Chem., v. 140, pp. 483-489.

Park, R., and Epstein, S., 1960, Carbon Isotope Fractionation During Photosynthesis; Geochim. Cosmochim. Acta, v. 21, pp. 110-126.

Park, R., and Epstein, S., 1961, Metabolic Fractionation of C^{13} and C^{12} in Plants; Plant Physio., v. 36, pp. 133-138.

Parker, P. L., 1964, The Biochemistry of the Stable Isotopes of Carbon in a Marine Bay; Geochim. Cosmochim. Acta, v. 28, pp. 1155-1164.

Parkinson, T. F., 1977, Personal Communique, Nuclear Research Laboratory, Virginia Polytechnic Institute and State University, Blacksburg, Virginia, 24061.

Pauli, F. W., 1975, Heavy Metal Humates and Their Behavior Against Hydrogen Sulfide; Soil Sci., v. 119, pp. 98-105.

Pillippi, G. T., 1965, On the Depth, Time and Mechanism of Petroleum Generation; Geochim. Cosmochim. Acta, v. 29, pp. 1021-1049.

Phleger, F. B., and Soutar, A., 1973, Production of Benthic Foraminifera in Three East Pacific Oxygen Minima; Micropaleo., v. 19, pp. 110-115.

Pisciotta, K. A., 1978, Basinal Sedimentary Facies and Diagenetic Aspects of the Monterey Shale, California; Ph.D. Dissertation, University of California, Santa Cruz, 450p.

Potter, P. E., Shimp, N. F., and Witters, J., 1963, Trace Elements in Marine and Fresh-Water Argillaceous Sediments; Geochim. Cosmochim. Acta, v. 27, pp. 669-694.

Pommer, A. M., 1958, Reduction of Quinquevalent Vanadium Solutions by Wood and Lignite; Geochim. Cosmochim. Acta, v. 13, pp. 20-27.

Presley, B. J., Kolodny, Y., Nissenbaum, A., and Kaplan, I. R., 1972, Early Diagenesis in a Reducing Fjord, Saanich Inlet, British Columbia-II. Trace Element Distribution in Interstitial Water and Sediment; Geochim. Cosmochim. Acta, v. 36, pp. 1073-1090.

Price, L. C., 1980, Crude Oil Degradation as an Explanation of the Depth Rule; Chem. Geol., v. 28, pp. 1-30.

Provo, L. J., 1977, Stratigraphy and Sedimentology of Radioactive Devonian-Mississippian Shales of the Central Appalachian Basin; Ph.D. Dissertation, University of Cincinnati, Dept. of Geology, 177p.

Rabinowitch, E. I., 1945, Photochemistry of Pigments in Vivo; Chapter 19, in Photosynthesis and Related Processes, Interscience Publishers, Inc., New York, pp. 537-560.

Rackley, R. I., 1972, Environment of Wyoming Tertiary Uranium Deposits; Amer. Assoc. Petrol. Geologists Bull., v. 56, pp. 755-774.

Ramm, A. E., and Bella, D. A., 1974, Sulfide Production in Anaerobic Microcosms; Limnol. Oceanog., v. 19, pp. 110-118.

Rashid, M. A., 1971, Role of Humic Acids of Marine Origin and Their Different Molecular Weight Fractions in Complexing Di- and Tri-valent Metals; Soil Sci., v. 111, pp. 298-306.

Rashid, M. A., and Reinson, G. E., 1979, Organic Matter in Surficial Sediments of the Miramichi Estuary, New Brunswick, Canada; Estuarine Coast. Mar. Sci., v. 8, pp. 23-36.

Raymont, J.E.G., 1963, Plankton and Productivity in the Oceans; Pergamon Press, New York, 660p.

Reed, R. D., 1933, Geology of California; Amer. Assoc. Petrol. Geologists, Tulsa, 355p.

Reed, R. D., and Hollister, J. S., 1936, Structural Evolution of Southern California; Amer. Assoc. Petrol. Geologists, Tulsa,157p.

Reeside, J. B., Jr., 1957, Paleoecology of the Cretaceous Seas of the Western Interior of the United States; in Treatise on Marine Ecology and Paleoecology, ed. Ladd, G.S.A. Mem. 67, pp. 505-541.

Reeside, J. B., Jr., and Cobban, W. A., 1960, Studies of the Mowry Shale (Cretaceous) and Contemporary Formations in the United States and Canada; U.S.G.S. Prof. Paper, 355, 121p.

Rho, J. H., Bauman, A. J., Boettger, H. G., 1973, A Search for Porphyrin Biomarkers in Nonesuch Shale and Extraterrestrial Samples; Space Life Sci., v. 4, pp. 69-77.

Rhoads, D. C., and Morse, J. W., 1971, Evolutionary and Ecologic Significance of Oxygen-Deficient Marine Basins; Lethaia, v. 4, pp. 413-428.

Richards, F. A., 1970, The Enhanced Preservation of Organic Matter in Anoxic Marine Environments; in Symposium on Organic Matter in Natural Waters, ed. Hood, Inst. Mar. Sci. Ocass. Publ. No. 1, pp. 399-411.

Riecker, R. E., 1962, Hydrocarbon Fluorescence and Migration of Petroleum; Amer. Assoc. Petrol. Geologists Bull., v. 46, pp. 60-75.

Riley, J. P., 1965, Analytical Chemistry of Sea Water; in Chemical Oceanography, v. 2, eds. Riley and Skirrow, Academic Press, London, pp. 295-424.

Riley, J. P., and Roth, I., 1971, The Distribution of Trace Elements in Some Species of Phytoplankton Grown in Culture; J. Mar. Biol. Ass. U.K., v. 51, pp. 63-72.

Roberts, R. M., Gilbert, J. C., Rodewald, L. B., and Wingrove, A. S., 1974, An Introduction to Modern Experimental Organic Chemistry Holt, Rinehart and Winston, Inc., New York, 528p.

Robertson, J. M., 1936, An X-Ray Study of the Phthalocyanines, 2. Structure Determination of the Metal Free Compound; Jour. Chem. Soc., v. 1936, pp. 1195-1209.

Robertson, J. M., and Woodward, I., 1937, An X-Ray Study of Phthalocyanines, 3. Quantitative Structure Determination of Nickel Phthalocyanines; Jour. Chem. Soc., v. 1937, pp. 219-230.

Robie, R. A. Hemingway, B. S., and Fisher, J. R., 1978, Thermodynamic Properties of Minerals and Related Substances at 298.15K and 1 Bar (10^5 Pascals) Pressure and at Higher Temperatures; Geol. Surv. Bull., No. 1452, 456p.

Roehler, H. W., 1965, Early Tertiary Deposits in the Rock Springs Uplift Area; in Sedimentation of Late Cretaceous and Early Tertiary Outcrops, Rock Springs Uplift, Wyoming Geol. Assoc. Guidebook, 19th Field Conf., pp. 140-150.

Roehler, H. W., 1968, Redefinition of the Tipton Shale Member of the Green River Formation of Wyoming; Amer. Assoc. Petroleum Geologists Bull., v. 52, pp. 2249-2256.

Ronov, A. D., 1958, Organic Carbon in Sedimentary Rocks; Geochemistry, v. 5, p. 510-536.

Ross, L. M., and Harwood, R. J., 1979, Organic Geochemical Correlation of San Juan Basin Oils and Oil Source Sequences; Abstracts of 1979 Annual Meeting of the Geological Society of America, San Diego, p. 506.

Rosscup, R. J., and Bowman, D. H., 1967, Thermal Stabilities of Vanadium and Nickel Petroporphyrins; Amer. Chem. Soc., Div. Petrol. Chem., Preprints, v. 12, pp. A-77 to A-81.

Ruch, R. R., Gluskoter, H. J., and Shimp, N. F., 1974, Occurrence and Distribution of Potentially Volatile Trace Elements in Coal; Illinois State Geol. Survey, Env. Geol. Notes, No. 72, 96p.

Ryder, R. T., Fouch, T. D., and Elison, J. H., 1976, Early Tertiary Sedimentation in the Western Uinta Basin, Utah; Geol. Soc. Amer. Bull., v. 87, pp. 496-512.

Sackett, W. M., Eadie, B. J., and Exner, M. E., 1974, Stable Isotope Composition of Organic Carbon in Recent Antarctic Sediments; in Advances in Organic Geochemistry 1973, eds. Tissot and Bienner, editions Technip, Paris, pp. 661-671.

Sackett, R. M., and Thompson, R. R., 1963, Isotopic Organic Carbon Composition of Recent Continental Derived Clastic Sediments of Eastern Gulf Coast, Gulf of Mexico; Amer. Assoc. Petrol. Geologists Bull., v. 47, pp. 525-531.

Safronova, T. P., Zhuze, T. P., and Sushilin, A. V., 1972, Chromatographic Separation of a Gseous Mixture of Petroleum Hydrocarbons During its Migration Through Rocks; Doklady Akad. Nauk SSSR, v. 207, pp. 193-196.

Sanger, J. E., 1968, A Quantitative Study of Leaf Pigments from Initiation in Buds to Decomposition in Soils; Ph.D. Dissertation, University of Minnesota, 252p.

Sanger, J. E., 1971a, Quantitative Investigations of Leaf Pigments from Their Inception in Buds Through Autumn Coloration to Decomposition in Falling Leaves; Ecology, v. 52, pp. 1075-1089.

Sanger, J. E., 1971b, Identification and Quantitative Measurement of Plant Pigments in Soil Humus Layers; Ecology, v. 52,, pp. 959-963.

Sanger, J. E., and Gorham, E., 1970, The Diversity of Pigments in Lake Sediments and its Ecological Significance; Limnol. Oceanog., v. 15, pp. 59-69.

Saraceno, A. J., Fanale, D. T., and Coggeshall, N. D., 1961, An Electron Paramagnetic Resonance Investigation of Vanadium in Petroleum Oils; Anal. Chem., v. 33, pp. 500-505.

Sayles, F. L., 1979, The Composition and Diagenesis of Interstitial Solutions: I. Fluxes Across the Sea Water - Sediment Interface in the Atlantic Ocean; Geochim. Cosmochim. Acta, v. 43, pp. 527-545.

Schiffman, R. A., and Miller, A. R., 1978, Knudsen Effusion of an Incongruent Subliming System: Thermodynamics of Nickel-Sulfur; High Temp. Sci., v. 10, pp. 17-26.

Schnitzer, M., and Hoffman, I., 1967, Thermogravimetric Analysis of the Salts and Metal Complexes of a Soil Fulvic Acid: Geochim. Cosmochim. Acta, v. 31, pp. 7-15.

Schnitzer, M., and Khan, S. U., 1972, Reactions of Humic Substances with Metal Ions and Hydrous Oxides; in Humic Substances in the Environment, Marcel Dekker, Inc., New York, pp. 203-251.

Schrayer, G. J., and Zarrella, W. M., 1963, Organic Geochemistry of Shales: I. Distribution of Organic Matter in the Siliceous Mowry Shale of Wyoming; Geochim. Cosmochim. Acta, v. 27, pp. 1033-1046.

Schwab, F. L., 1976, Modern and Ancient Sedimentary Basins: Comparative Accumulation Rates; Geology, v. 4, pp. 723-727.

Schwietering, J. F., 1978, Preliminary Model of Catskill Delta in West Virginia; in First Eastern Gas Shales Symposium , eds. Schott, Overbey, Hunt, and Komar, MERC/SP-77/5, pp. 195-205.

Sclater, F. R., Boyle, E., and Edmond, J. M., 1976, On the Marine Geochemistry of Nickel; Earth Planet. Sci. Lett., v. 31, pp. 119-128.

Seifert, W. K., 1977, Source Rock/Oil Correlations by C_{27}-C_{30} Biological Marker Hydrocarbons; in Advances in Organic Geochemistry 1975, eds. Campos and Goni, Madrid, pp. 21-43.

Seifert, W. K., 1978, Steranes and Terpanes in Kerogen Pyrolysis for Correlation of Oils and Source Rocks; Geochim. Cosmochim. Acta, v. 42, pp. 473-484.

Seifert, W. K., and Moldowan, J. M., 1978, Applications of Steranes, Terpanes, and Monoaromatics to the Maturation, Migration, and Source of Crude Oils; Geochim. Cosmochim. Acta, v. 42, pp. 77-95.

Seifert, W. K., and Moldowan, J. M., 1979, The Effect of Biodegradation on Steranes and Terpanes in Crude Oil; Geochim. Cosmochim. Acta, v. 43, pp. 111-126.

Sheppard, R. A., and Gude, A. J., 1968, Distribution and Genesis of Authigenic Silicate Minerals in Tuffs of Pleistocene Lake Tecopa, Inyo County, California; U.S.G.S. Prof. Paper, 597, 38p.

Sheppard, R. A., and Gude, A. J., 1969, Diagenesis of Tuffs in the Barstow Formation, Mud Hills, San Bernardino County, California; U.S.G.S. Prof. Paper, 634, 35p.

Shiobara, M., and Taguchi, K., 1977, Early Diagenetic Transformation of Porphyrin Compounds in Some Japanese Sediments; in Advances in Organic Geochemistry 1975, eds. Campos and Goni, Empresa Nacional Adaro de Investigaciones Mineras, S.A. Madrid, pp. 237-251.

Shishkina, O. V., 1964, Chemical Composition of Pore Solutions in Oceanic Sediments; Geochem. International, v. 1, pp. 522-528.

Sholkovitz, E., 1973, Interstitial Water Chemistry of the Santa Barbara Basin Sediments; Geochim. Cosmochim. Acta, v. 37, pp. 2043-2073.

Siever, R., Beck, K. D., and Berner, R. A., 1965, Composition of Interstitial Waters of Modern Sediments; Jour. Geol., v. 73, p. 39-73.

Simonson, R. R., 1958, Oil in the San Joaquin Valley, California; in Habitat of Oil, ed. Weeks, Amer. Assoc. Petrol. Geologists, Tulsa, p. 99-112.

Slaughter, M., and Earley, J. W., 1965, Mineralogy and Geological Significance of the Mowry Bentonites, Wyoming; Geol. Soc. Amer. Spec. Paper, 83, 116p.

Sleggs, G. F., 1927, Marine Phytoplankton in the Region of La Jolla, California, During the Summer of 1924; Bull. Scripps Inst. Oc., Tech. Ser., v. 1, pp. 93-117.

Smith, B. N., and Epstein, S., 1971, Two Categories of C^{13}/C^{12} Ratios for Higher Plants; Plant Physio. v. 47, pp 380-384.

Smith, P. B., 1968, Paleoenvironment of Phosphate-Bearing Monterey Shale in Salinas Valley, California; Amer. Assoc. Petrol. Geologists Bull., v. 52, pp. 1785-1791.

Smith, S. W., 1974, Geochemistry of Oil-Shale Genesis in Colorado's Piceance Creek Basin; in Energy Resources of the Piceance Creek Basin, Colorado, Rocky Mountain Assoc. Geologists, 1974 - Guidebook, pp. 71-79.

Stahl, W. J., 1978, Source Rock-Crude Oil Correlation by Isotopic Type-Curves; Geochim. Cosmochim. Acta, v. 42, pp. 1573-1577.

Stanier, R. Y., Adelberg, E. A., and Ingraham, J. L., 1976, The Microbial World; Prentice-Hall Inc., Englewood Cliffs, N.J., 871p.

Stanley, K. O., and Surdam, R. C., 1978, Sedimentation on the Front of Eocene Gilbert-Type Deltas, Washakie Basin, Wyoming; J. Sed. Pet., v. 48, lpp. 557-573.

Staplin, F. L., 1969, Sedimentary Organic Matter, Organic Metamorphism, and Oil and Gas Occurrences; Bull. Canadian Petrol. Geol., v. 17, pp. 47-66.

Stelck, C. R., 1975, The Upper Albian Milammina Manitobensis Zone in Northeastern British Columbia; in The Cretaceous System in the Western Interior of North America, ed. Caldwell, The Geol. Assoc. Canada Spec. Paper, 13, pp. 253-275.

Stewart, F. H., 1963, Marine Evaporites; Chapter Y, in Data of Geochemistry, Sixth Edition, ed. Fleischer, U.S.G.S. Prof. Paper, 440, pp. Y-1 to Y-52.

Stuermer, D. H., Peters, K. E., and Kaplan, I. R., 1978, Source Indicators of Humic Substances and Proto-Kerogen. Stable Isotope Ratios, Elemental Composition and Electron Spin Resonance Spectra; Geochim. Cosmochim. Acta, v. 42, pp. 989-997.

Sugawara, K., Naito, H., and Yamada, S., 1956, Geochemistry of Vanadium in Natural Waters; Jour. Earth Sci. (Nagoya Univ.), v. 4, pp. 44-61.

Sugihara, J. M., 1975, Personal Communique; Chemistry and Physics College, North Dakota State University.

Sugihara, J. M., Branthaver, J. F., and Wilcox, K. W., 1975, Oxidative Demetallation, in The Role of Trace Metals in Petroleum, ed. Yen, Ann Arbor Science Publishers Inc., Ann Arbor, pp. 183-193.

Surdam, R. C., 1979, Personal Communique, University of Wyoming, Dept. of Geology, Laramie, Wyoming, 82071.

Surdam, R. C., and Stanley, K. O., 1979, Lacustrine Sedimentation During the Culminating Phase of Eocene Lake Gosiute, Wyoming (Green River Formation); Geol Soc. Amer. Bull., v. 90, pp. 93-110.

Surdam, R. C., and Wolfbauer, C. A., 1975, Green River Formation, Wyoming: A Playa-Lake Complex; Geol. Soc. Amer. Bull. v. 86, pp. 335-345.

Swaine, D. J., 1975, Trace Elements in Coals; in Recent Contributions to Geochemistry and Analytical Chemistry, ed. Tugarinov, John Wiley & Sons, New York, pp. 539-550.

Swetland, P. J., and Clayton, J. L., 1976, Source Beds of Petroleum in the Denver Basin; U.S.G.S. Open-File Report 76-572, 23p.

Szabo, I., 1958, Kationok Adszorpcioja Humusz Preparatumon; Comm. Third Math.-Phys. Class Hung. Acad. Sci., v. 8, pp. 395-402.

Szalay, A., and Szilagyi, M., 1967, The Association of Vanadium with Humic Acids; Geochim. Cosmochim. Acta, v. 31, pp. 1-6.

Szalay, A., and Szilagyi, M., 1969, Accumulation of Microelements in Peat Humic Acids and Coal; in Advances in Organic Geochemistry 1968, Pergamon Press, Oxford, pp. 567-577.

Szilagyi, M., 1971, The Role of Organic Material in the Distribution of Mo, V, and Cr in Coal Fields; Econ. Geol., v. 66, pp. 1075-1078.

Szilagyi, M., 1972, The Geochemical Role of Standard Potential in Reactions Between Humic Substances and Metals; Geochem. International, v. 9, pp. 402-406.

Taguchi, K., 1975, Geochemical Relationships Between Japanese Tertiary Oils and Their Source Rocks; 9th World Petroleum Congress Proceedings, v. 2, pp. 193-194.

Thiede, J., and Van Andel, T. H., 1977, The Paleoenvironment of Anaerobic Sediments in the Late Mesozoic South Atlantic Ocean; Earth Plant. Sci. Letters, v. 33, pp. 301-309.

Thomas, D. W., and Blumer, M., 1964, Porphyrin Pigments of a Triassic Sediment; Geochim. Cosmochim. Acta, v. 28, pp. 1147-1154.

Thorstenson, D. C., and Mackenzie, F. T., 1971, Experimental Decomposition of Algae in Sea Water and Early Diagenesis; Nature, v. 234, pp. 543-545.

Thorstenson, D. C., and Mackenzie, F. T., 1974, Time Variability of Pore Water Chemistry in Recent Carbonate Sediments, Devil's Hole, Harrington Sound, Bermuda; Geochim. Cosmochim. Acta, v. 38, pp. 1-19.

Tissot, B., Califet-Debyser, Y., Deroo, G., and Oudin, J. L., 1971, Origin and Evolution of Hydrocarbons in Early Toarcian Shales, Paris Basin, France; Amer. Assoc. Petrol. Geologists Bull., v. 55, pp. 2177-2193.

Tissot, B., Deroo, G., and Hood, A., 1978, Geochemical Study of the Uinta Basin: Formation of Petroleum From the Green River Formation; Geochim. Cosmochim. Acta, v. 42, pp. 1469-1485.

Tissot, B., Durand, B., Espitalié, J., and Combaz, A., 1974, Influence of Nature and Diagenesis of Organic Matter in Formation of Petroleum; Amer. Assoc. Petrol. Geologists Bull., v. 58, pp. 499-506.

Tissot, B., and Welte, D. H., 1978, Petroleum Formation and Occurrence Springer-Verlag, New York, 538p.

Tompkins, R. E., and Shephard, L. E., 1979, Orca Basin: Depositional Processes, Geotechnical Properties and Clay Mineralogy of Holocene Sediments Within an Anoxic Hypersaline Basin, Northwest Gulf of Mexico; Mar. Geol., v. 33, pp. 221-238.

Toth, D. J., and Lerman, A., 1977, Organic Matter Reactivity and Sedimentation Rates in the Ocean; Amer. J. Science,, v. 277, pp. 465-485.

Trace, R. D., 1960, Significance of Unusual Mineral Occurrence at Hicks Dome, Hardin County, Illinois; U.S.G.S. Prof. Paper, 400-B, pp. 63-64.

Trask, P. D., and Patnode, H. W., 1942, Source Beds of Petroleum Amer. Assoc. Petroleum Geologists, Tulsa, 566p.

Vallentyne, J. R., 1960, Fossil Pigments; in Comparative Biochemistry of Photoreactive Systems, Academic Press, New York, pp. 83-105.

Van Dijk, H., 1971, Cation Binding of Humic Acids; Geoderma, v. 5, pp. 53-67.

Van West, F. P., 1972, Green River Oil Shale; in Geological Atlas of the Rocky Mountain Region, Rock Mountain Assoc. Geologists, Denver, pp. 287-292.

Vaughan, G. B., Tynan, E. C., and Yen, T. F., 1970, Vanadium Complexes and Porphyrins in Asphaltene, 2. The Nature of Highly Aromatic Substituted Porphins and Their Vanadyl Chelates; Chem. Geol., v. 6, pp. 203-219.

Vine, J. D., and Tourtelot, E. B., 1970, Geochemistry of Black Shale Deposits - A Summary Report; Econ. Geol., v. 65, pp. 253-272.

Vinkler, P., Lakatos, B., and Meisel, J., 1976, Infrared Spectroscopic Investigation of Humic Substances and Their Metal Complexes; Geoderma, v. 15, lpp. 231-242.

Vinogradov, A. P., 1936, Concerning the Origin of Vanadium in Petroleum and Solid Bitumens; Coll. of Akad. V. I. Vernadskii, 145.

Vinogradov, A. P., 1953, The Elemental Chemical Composition of Marine Organisms; Memoir No. II, Sears Foundtion for Marine Research, Yale University, New Haven, 647p.

Volkmann, C. M., and Oppenheimer, C. ., 1962, The Microbial Decomposition of Organic Carbon in Surface Sediments of Marine Bays of the Central Texas Gulf Coast; Publ. Inst. Mar. Sci, v. 8, pp. 80-96.

Von Estorff, F. E., 1930, Keyenhagen Shale at Type Locality, Fresno County, California; Amer. Assoc. Petrol. Geologists Bull., v. 14, pp. 1321-1336.

Waksman, S. A., and Carey, C. L., 1935, Decomposition of Organic Matter in Sea Water by Bacteria, I., Jour. Bact., v. 29, pp. 531-543.

Waksman, S. A., and Renn, C. E., 1936, Decomposition of Organic Matter in Sea Water by Bacteria, III. Factors Influencing the Rate of Decomposition; Biol. Bull., v. 70, pp. 472-483.

Walker, R. G., and Harms, J. C., 1971, The "Catskill Delta": A Prograding Muddy Shoreline in Central Pennsylvania; Jour. Geol., v. 79, pp. 381-399.

Waples, D. W., 1977, C/N Ratios in Source Rock Studies; Miner. Indust. Bull., v. 20, pp. 1-8.

Watkins, R., 1974, Paleobiology of an Offshore Molluscan Fauna from the California Oligocene; Palaeogeogr., Palaeoclimatol., Palaeoecol., v. 15, pp. 245-266.

Welte, D. H., 1974, Recent Advances in Organic Geochemistry of Humic Substances and Kerogen; in Advances in Organic Geochemistry 1973, eds. Tissot and Bienner, Editions Technip, Paris, pp. 3-31.

Welte, D. H., Hagemann, H. W., Hollerbach, A., Leythaeuser, D., and Stahl, W., 1975, Correlation Between Petroleum and Source Rock; in 9th World Petroleum Congress Proceedings, v. 2, pp. 179-191.

Wetzel, R. G., 1975, Limnology, W. B. Saunders Company, London, 743p.

Williams, G. D., and Stelck, C. R., 1975, Speculations on the Cretaceous Plaeogeography of North America; in The Cretaceous System in the Western Interior of North America, ed. Caldwell, Geol. Assoc. Canada, Spec. Paper 13, pp. 1-20.

Williams, J. A., 1974, Characterization of Oil Types in Williston Basin; Amer. Assoc. Petrol. Geologists Bull., v. 58, pp. 1243-1252.

Wilson, S. A., and Weber, J. H., 1979, An EPR Study of the Reduction of Vanadium (V) to Vanadium (IV) by Fulvic Acid; Chem. Geol., v. 26, pp. 345-354.

Winters, J. C., and Williams, J. A., 1969, Microbiological Alteration of Crude Oil in the Reservoir; Symp. Petroleum Transformations in Geologic Environments, Amer. Chem. Soc., New York City Meeting, Sept. 7-12, pp. E22-E31.

Witherspoon, P. A., and Nagashima, K., 1957, Use of Trace Metals to Identify Illinois Crude Oils; Ill. State Geol. Surv., Circular 239, 15p.

Woodring, W. P., Bramlette, M. N., and Kew, W.S.W., 1946, Geology and Paleontology of Palos Verdes Hills, California; U.S.G.S. Prof. Paper, 207, 145p.

Woodring, W. P., Stewart, R., and Richards, R. W., 1940, Geology of the Kettleman Hills Oil Field, California; U.S.G.S. Prof. Paper, 195, 170p.

Wright, R. J., 1955, Ore Controls in Sandstone Uranium Deposits of the Colorado Plateau; Econ. Geol., v. 50, pp. 135-155.

Yen, T. F., 1975, Chemical Asects of Metals in Native Petroleum; in The Role of Trace Metals in Petroleum, ed. Yen, Ann Arbor Science Publishers Inc., Ann Arbor, pp. 1-30.

Yen, T. F., and Silverman, S. R., 1969, Geochemical Significance of the Changes in the Chemical Structures of the Complex Heterocyclic Components of Petroleum; Amer. Chem. Soc. Reprints, v. 14, pp. E32-E41.

Yentsch, C. S., 1965, Distribution of Chlorophyll and Pheophytin in the Open Ocean; Deep-Sea Res., v. 12, pp. 653-666.

Young, A., and McIver, R. D., 1977, Distribution of Hydrocarbons Between Oils and Associated Fine Grained Sedimentary Rocks, II: Physical Chemistry Applied to Petroleum Geochemistry; Amer. Assoc. Petrol. Geologists Bull., v. 61, pp. 1407-1436.

Young, E. G., and Langille, W. M., 1958, The Occurrence of Inorganic Elements in Marine Algae of the Atlantic Provinces of Canada; Can. J. Botany, v. 36, pp. 301-310.

Yudovich, Ya. E., Korycheva, A. A., Obruchnikov, A. S., and Stepanov, Yu. V., 1972, Mean Trace-Element Contents in Coals; Geochem. Internat., v. 9, pp. 712-720.

Zobell, C. E., 1942, Changes Produced by Microorganisms in Sediments After Deposition; J. Sed. Pet., v. 12, pp. 127-156.

Zobell, C. E., 1946a; Marine Microbiology Chronica Botanica Company, Waltham, Mass., 240p.

Zobell, C. E., 1946b, Studies on Redox Potential of Marine Sediments; Amer. Assoc. Petrol. Geologists Bull., v. 30, pp. 477-513.

Zsolnay, A., 1978, The Weathering of Tar on Bermuda; Deep-Sea Res., v. 25, pp. 1245-1252.

Zubovic, P., Stadnichenko, T., and Sheffey, N., 1960a., Comparative Abundance of the Minor Elements in Coals from Different Parts of the United States; U.S.G.S. Prof. Paper, 400-B, pp. B87-B89.

Zubovic, P., Stadnichenko, T., and Sheffey, N., 1960b., Relation of the Minor Element Content of Coal to Possible Source Rocks; U.S.G.S. Prof. Paper, 400-B, pp. B82-B84.

APPENDIX I: LOCALITY DESCRIPTIONS FOR ROCK SAMPLES

Local No.	Locality Name	State	County	Location	Type of Exposure
1	Thornton Dome	Wyo.	Crook	Sec.8,T.48N.,R.65W.	SC
2	Belle Fourche	Wyo.	Crook	Sec.20,T.57N.,R.62W.	RC
3	Mule Creek	Wyo.	Weston	Sec.11,T.39N.,R.61W.	SC
4	Wagon Hound Creek	Wyo.	Converse	Sec.23,T.31N.,R.72W.	SC
5	Goose Egg	Wyo.	Natrona	Sec.6,T.32N.,R.80W.	SC
6	State 220	Wyo.	Natrona	Sec.6,T.32N.,R.80W.	R
7	Cottonwood Creek	Wyo.	Natrona	Sec.32,T.39N.,R.85W.	SC
8	Horse Creek	Wyo.	Johnson	Sec.2,T.46N.,R.83W.	SC
9	Beaver Creek	Wyo.	Johnson	Sec.35,T.47N.,R.83W.	HS
10	Amsden Creek	Wyo.	Sheridan	Sec.36,T.57N.,R.87W.	Q
11	Inexco #10 Steinle Ranch	Wyo.	Converse	Sec.6,T.38N.,R.69W.	DH
12	YHS #3 Wheatly Federal D	Wyo.	Campbell	Sec.20,T.46N.,R.70W.	DH
13	Amerada Petr. #1 Unit Smith's Cut	Wyo.	Johnson	Sec.10,T.44N.,R.79W.	DH
14	Steinaker Reservoir	Utah	Uintah	Sec.35,T.3S.,R.21E.	R
15	Baldwin Creek	Wyo.	Fremont	Sec.18,T.33N.,R.100W.	SC
16	Negro Hollow	Mont.	Jefferson	Sec.4,T.2N,R.2W.	SC
17	Limekiln Creek	Mont.	Madison	Sec.10,T.1S.,R.3W.	SC
18	Warm Springs Mine	Mont.	Powell	Sec.11,T.10N.,R.10W.	M
19	North Central Mine	Mont.	Beaverhead	Sec.6,T.2S.,R.9W.	M
20	Taylor Mountain	Idaho	Clark	Sec.11,T.14N.,R.40E.	M
21	Teton Pass	Wyo.	Teton	Sec.23,T.41N.,R.118W.	R
22	Astoria	Wyo.	Lincoln	Sec.32,T.39N.,R116W.	R+RC
23	Simplot #16-127	Idaho	Caribou	Sec.24,T.8S.,R.42E.	DH
24	North Trail	Idaho	Caribou	Sec.24,T.8S.,R.42E.	M
25	Gay Mine	Idaho	Bingham	Sec.27,T.4S.,R.37E.	M
26	Taggart	Utah	Morgan	Sec.26,T.4N.,R.3E.	HS
27	Leefe Mine	Wyo.	Lincoln	Sec.2,T.21N.,R.120W.	M
28	Vernal Mine	Utah	Uintah	Sec.30,T.3N.,R.22E.	M
29	East Bear Lake	Idaho	Bear Lake	Sec.12,T.15S.,R.44E.	M
30	Anderson Mine	Mont.	Powell	Sec.10,T.10N.,R.10W.	M
31	White Mountain A	Wyo.	Sweetwater	Sec.30,T.19N.,R.105W.	HS
32	White Mountain B	Wyo.	Sweetwater	Sec.31,T.19N.,R.105W.	HS
33	Pilot Butte	Wyo.	Sweetwater	Sec.30,T.20N.,R.105W.	HS
34	Firehole Canyon	Wyo.	Sweetwater	Sec.20,T.16N.,R.106W.	HS
35	So. Chimney Rock	Wyo.	Sweetwater	Sec.24,T.16N.,R.106W.	HS
36	Tollgate Rock	Wyo.	Sweetwater	Sec.15,T.18N.,R.107W.	RC

Local No.	Locality Name	State	County	Location	Type of Exposure
37	Big Island Mine	Wyo.	Sweetwater	Sec.14,T.20N.,R.109W.	M
38	The Palisades	Wyo.	Sweetwater	Sec.9,T.18N.,R.107W.	RC
39	Three Mile Canyon	Utah	Uintah	Sec.4,T.12S.,R.25E.	HS
40	Hells Hole Canyon	Utah	Uintah	Sec.20,T.10S.,R.25E.	HS
41	Evacuation Creek	Utah	Uintah	Sec.27,T.11S.,R.25E.	HS
42	Santio Crossing	Utah	Uintah	Sec.29,T.12S.,R.21E.	HS
43	Willow Creek	Utah	Uintah	Sec.13,T.12S.,R.20E.	R
44	Gate Canyon	Utah	Duchesne	Sec.20,T.11S.,R.15E.	HS
45	Avintaquin Creek	Utah	Duchesne	Sec.27,T.6S.,R.8W.	HS
46	Whirlpool Canyon	Utah	Uintah	Sec.33,T.3S.,R.25E.	RC
47	Bush Creek	Utah	Uintah	Sec.17,T.3S.,R.22E.	M
48	Cole Creek	Nevada	Elko	Sec.34,T.32N.,R.52E.	T
49	Reliz Canyon	Calif.	Monterey	Sec.35,T.19S.,R.6E.	HS
50	Indian Creek	Calif.	San Luis Obispo	Sec.20,T.28S.,R.15E.	SC
51	Rhodes Gulch	Calif.	San Luis Obispo	Sec.21,T.28S.,R.14E.	SC
52	Lompoc Mine	Calif.	Santa Barbra	2500 Miguelito Rd., Lompoc	M
53	Refugio Pass	Calif.	Santa Barbra	Sec.1,T.5N.,R.31W.	R
54	Ellwood Beach	Calif.	Santa Barbra	Sec.23,T.4N.,R.29W.	S
55	Modelo Canyon	Calif.	Ventura	Sec.17,T.4N.,R.18E.	HS
56	Chico Martinez	Calif.	Kern	Secs.2,9,10 and 11,T.29S.,R.20E.	HS
57	Agua Amarga	Calif.	Los Angeles	Sec.2,T.5S.,R.15W.	SC
58	Garza Creek	Calif.	Kings	Sec.3,T.23S.,R.16E.	HS
59	Skunk Hollow	Calif.	Fresno	Sec.9,T.19S.,R.15E.	LE
60	Panoche Creek	Calif.	Fresno	Sec.16,T.15S.,R.12E.	R
61	Escarpado Creek	Calif.	Fresno	Sec.8,T.15S.,R.12E.	SC
62	Nojoqui Canyon	Calif.	Santa Barbra	Sec.24,T.6N.,R.32W.	R
63	No.1 Birdbear	N.Dakota	Dunn	Sec.22,T.149N.,R.91W.	DH
64	No. 1 Donahue	North Dakota	Williams	Sec.23,T.154N.,R.100W	DH
65	White Pine Mine	Mich.	Ontonagon	N-1/2,T.50N.,R.41W.	M
66	Big Iron River	Mich.	Ontonagon	Sec.13,T.51N.,R.42W.	RC
67	McGuire Creek	Mich.	Ontonagon	Sec.28,T.51N.,R.38W.	SC
68	Newton Co. Quarry	Ind.	Newton	Sec.25,T.27N.,R.9W.	Q
69	Champ Clark Bridge	Mo.	Pike	Sec.18,T.54N.,R.1W.	RC
70	No. Clay City	Ky.	Powell	0.7 mi. no. of Clay City on east side of Mountain Parkway	R

Local No.	Locality Name	State	County	Location	Type of Exposure
71	So. Clay City	Ky.	Powell	S.E. corner of Mountain Parkway and Route 1057 intersection.	R
72	Hicks Branch	Ill.	Hardin	Sec.25,T.11S.,R.7E.	SC
73	Bow	Ky.	Cumberland	2.9 mi. east of courthouse in Burkesville on no. side of Route 90.	R
74	Sligo Bridge	Tenn.	DeKalb	0.3 mi. east of Sligo Bridge on Route 70.	R
75	Leatherwood Creek	Tenn.	Giles	N.W. side of Route 31A, 2.8 mi. N.E. of its intersection with Route 31.	R
76	McAfee Hill	Tenn.	Giles	So. side of Route 64, 9.2 mi. east of its intersection with Route 31.	HS
77	Pegram	Tenn.	Cheatham	2.2 mi. west of Pegram on north side of Route 70.	R
78	Cany Creek	Ill.	Union	Sec.10,T.12S.,R.2W.	SC
79	Rolling fork	Ky.	Nelson	4.9 mi. on Route 84 from its intersection with Route 247.	R+SC
80	Lebanon Junction	Ky	Bullitt	Along no. entrance ramp onto I-65 from Route 61.	R
81	Keyhole Knob Quarry	Ky.	Jefferson	West side of I-65, 6 mi. no. of its intersection with Route 44.	Q 82
82	Silver Creek	Ind.	Clark	Lot 240, Clark's Grant	R
83	Speed	Ind.	Clark	Lot 167, Clark's Grant	R
84	Sellersburg	Ind.	Clark	Lot 110, Clark's Grant	R
85	Vernon	Ind.	Jennings	Sec.14,T.6N.,R.8E.	R
86	Horseshoe	Ill.	Saline	Sec.36,T.9S.,R.7E.	HS
87	Morehead	Ky.	Rowan	On I-65, 1.35 mi east of Bath-Rowan County Line.	R
88	Effingham Well	Ill.	Effingham	Not available (I.G.S.)	DH

Local No.	Locality Name	State	County	Location	Type of Exposure
89	Big Creek	Ill.	Hardin	Sec.8,T.12S.,R.8E.	R
90	Olga	W. Va.	McDowell	Not available (I.G.S.)	UK
91	Hillsboro	Ill.	Montgomery	Not available (I.G.S.)	UK
92	Seminoe	Wyo.	Carbon	Not available (I.G.S.)	UK
93	Harold	Ky.	Floyd	4.6 mi. no. of Harold on Route 460.	R
94	Allen	Ky.	Floyd	10.5 mi. no. of Allen on Route 460.	R
95	Paris	Tenn.	Henry	0.2 mi. so. of Paris on Route 79.	R
96	Bexar	Ala.	Marion	Just east of Ala.-Miss. border on no. side of Route 78.	R
97	Long Key	Fl.	Keys	Sec.4,T.65S.,R.35E.	RS
98	Sugar Loaf Key	Fl.	Keys	Sec.26,T.66S.,R.27E.	RS
99	Ohio Key	Fl.	Keys	Sec.24,T.66S.,R.30E.	RS
100	Dauphin Is. School	Al.	Mobile	T.9S.,R.1W.	RS
101	Coden Beach	Al.	Mobile	Sec.6,T.7S.,R.2W.	RS
102	Bayou Aloe	Al.	Mobile	Sec.8,T.9S.,R.1W.	RS
103	St. Josephs Bay	Fl.	Gulf	Sec.14,T.9S.,R.11W.	RS
104	Keystone Pk. Cove	Ok.	Tulsa	Sec.8,T.19N.,R.10E.	RS
105	Big Pine Key	Fl.	Keys	T.66S.,R.19E.	RS
106	Springer	Ok.	Carter	Sec.1,T.3S.,R.1E.	R

*Type of exposusure includes hill sides (HS), stream cuts (SC), river cuts (RC), road cuts (R), mine (MS), quarry (Q), drill hole (DH), recent setting (RS), and unknown(UK).

APPENDIX II: INVENTORY OF COLLECTED SAMPLES

Sample No.	Geologic Age	Formation	Member	Bed or Stratigraphic Position	Type of Sample*	Local No.
NS 1	Precambrian	Nonesuch	Upper Shale	Bed #43	MS	65
NS 2	Precambrian	Nonesuch	Parting Shale	Bed #23	MS	65
NS 3	Precambrian	Nonesuch	Upper Shale	Bed #43	OIC	66
NS 4	Precambrian	Nonesuch	Parting Shale	Bed #23	OIC	67
NS 5	Precambrian	Nonesuch	Parting Shale	Junior	OIC	67
NS 6	Precambrian	Nonesuch	Upper Shale	Bed #43	OIC	67
MQ 1	Ordovician	Maquoketa		8m above base	MS	68
MQ 2	Ordovician	Maquoksta		7.5m above base	MS	68
NA 1	Dev.-Miss.	New Albany	Grassy Creek	5m below Saverton	OIC	72
NA 2	Dev.-Miss.	New Albany	Lower Huron	3m below Mid. Huron	OIC	70
NA 3	Dev.-Miss.	New Albany	Mid. Huron		OIC	70
NA 4	Dev.-Miss.	New Albany	Upper Huron	11m below 3 Lick Bed	OIC	70
NA 5	Dev.-Miss.	New Albany	Mid. Huron		OIC	70
NA 6	Dev.-Miss.	New Albany	Lower Huron	2.5m below Mid. Huron	OIC	70
NA 7	Dev.-Miss.	New Albany	Three Lick	Below upper gray shale	OIC	71
NA 8	Dev.-Miss.	New Albany	Cleveland	3.5m above base	OIC	71
NA 9	Dev.-Miss.	New Albany	Grassy Creek	0.1m below top	OIC	69
NA 10	Dev.-Miss.	New Albany	Grassy Creek	5.0m below top	OIC	78
NA 11	Dev.-Miss.	New Albany	Grassy Creek	8.0m below top	OIC	78
NA 12	Dev.-Miss.	New Albany	Lower Huron	1.6m above base	OIC	79
NA 13	Dev.-Miss.	New Albany	Mid. Huron		OIC	79
NA 14	Dev.-Miss.	New Albany	Upper Huron	2.0m above base	OIC	80
NA 15	Dev.-Miss.	New Albany	Mid. Huron		OIC	80
NA 16	Dev.-Miss.	New Albany	Cleveland	3.2m below top	OIC	81
NA 17	Dev.-Miss.	New Albany	Cleveland	4.2m below top	OIC	81
NA 18	Dev.-Miss.	New Albany	Clegg Creek	Near base	OIC	82
NA 19	Dev.-Miss.	New Albany	Camp Run	2.4m below top	OIC	83
NA 20	Dev.-Miss.	New Albany	Clegg Creek	2.0m above base	OIC	84
NA 21	Dev.-Miss.	New Albany	Clegg Creek	1.0m above base	OIC	84
NA 22	Dev.-Miss.	New Albany	Morgan Trail		OIC	85
NA 23	Dev.-Miss.	New Albany	Grassy Creek		OIC	86
NA 24	Dev.-Miss.	New Albany	Mid. Huron		OIC	87
NA 25	Dev.-Miss.	New Albany	Grassy Creek(?)	933m	CR	88
CH 1	Dev.-Miss.	Chattanooga	Upper Gassaway	0.25m below top	OIC	73
CH 2	Dev.-Miss.	Chattanooga		4.0m below top	OIC	73
CH 3	Dev.-Miss.	Chattanooga		0.3m above base	OIC	73

Sample No.	Geologic Age	Formation	Member	Bed or Stratigraphic Position	Type of Sample*	Local No.
CH 4	Dev.-Miss.	Chattanooga	L. Dowellton	1.0m above base	OIC	74
CH 5	Dev.-Miss.	Chattanooga	U. Dowellton	0.4m below top	OIC	74
CH 6	Dev.-Miss.	Chattanooga	L. Gassaway	0.3m above base	OIC	74
CH 7	Dev.-Miss.	Chattanooga	M. Gassaway		OIC	74
CH 8	Dev.-Miss.	Chattanooga	U. Gassaway	0.7m above base	OIC	74
CH 9	Dev.-Miss.	Chattanooga	L. Dowellton	0.25m above base	OIC	75
CH 10	Dev.-Miss.	Chattanooga	L. Dowellton	1.2m above base	OIC	76
CH 11	Dev.-Miss.	Chattanooga	Gassaway	2.25m below top	OIC	77
CH 12	Dev.-Miss.	Chattanooga	Dowellton	1.5m above base	OIC	77
WD 5	Dev.-Miss.	Woodford		12.5m below top	OIC	106
WD 7	Dev.-Miss.	Woodford		12.6m below top	OIC	106
W 1	Devonian	Woodruff			OIC	48
W 1	Devonian	Woodruff			OIC	48
W 3	Devonian	Woodruff			OIC	48
B 1	Dev.-Miss.	Bakken		3064-3072m	CR	63
B 2	Dev.-Miss.	Bakken		3356-3360m	CR	64
SL 1	Miss.	St. Louis			OIC	89
MC 1	Penn.	Manning Canyon			OIC	46
MC 2	Penn.	Manning Canyon			OIC	46
MC 3	Penn.	Manning Canyon			OIC	46
HA 9	Penn.	Breathitt	Upper Elkhorn	No. 1 Coal	OIC	93
HA 22	Penn.	Breathitt	Upper Elkhorn	No. 3 Coal	OIC	94
PO 1	Penn.	Pocahontas		#4 seam	MS	90
I 1	Penn.	Carbondale		Herrin #6 seam	MS	91
P 1	Permian	Phosphoria	Retort	Lowest Phosphorite Bed	OIC	15
P 2	Permian	Phosphoria	Retort	4.3m below top	OIC	15
P 3	Permian	Phosphoria	Retort	3.5m below top	OIC	16
P 4	Permian	Phosphoria	Retort	4.0m below top	OIC	16
P 5	Permian	Phosphoria	Retort		OIC	17
P 6	Permian	Phosphoria	Retort		MS	18
P 7	Permian	Phosphoria	Retort		MS	19
P 8	Permian	Phosphoria	Retort	2.9m above mine floor	MS	20

Sample No.	Geologic Age	Formation	Member	Bed or Stratigraphic Position	Type of Sample*	Local No.
P 9	Permian	Phosphoria	Retort	2.0m above mine floor	MS	20
P 10	Permian	Phosphoria	Retort	0.3m below top	OIC	21
P 11	Permian	Phosphoria	Meade Peak		OIC	21
P 12	Permian	Phosphoria	Meade Peak	Lower part of unit	OIC	21
P 13	Permian	Phosphoria	Retort	Bed Rt-71	OIC	22
P 14	Permian	Phosphoria	Retort	Uppermost phosphorite	OIC	22
P 15	Permian	Phosphoria	Meade Peak		OIC	22
P 16	Permian	Phosphoria	Meade Peak		OIC	22
P 17	Permian	Phosphoria	Meade Peak	3m below top	CI	23
P 18	Permian	Phosphoria	Meade Peak	5.8m below top	CI	23
P 19	Permian	Phosphoria	Meade Peak	3m below top	MS	24
P 20	Permian	Phosphoria	Meade Peak	Lowermost phosphorite	MS	24
P 21	Permian	Phosphoria	Meade Peak	5.8m below top	MS	24
P 22	Permian	Phosphoria	Meade Peak	Main bed	MS	25
P 23	Permian	Phosphoria	Meade Peak	29m below top	MS	25
P 24	Permian	Phosphoria	Meade Peak	Middle siltstone	MS	25
P 25	Permian	Phosphoria	Meade Peak	17.9m below top	OIC	26
P 26	Permian	Phosphoria	Meade Peak	16.5m below top	OIC	26
P 27	Permian	Phosphoria	Meade Peak	Lower ore section	MS	27
P 28	Permian	Phosphoria	Meade Peak	Base of unit	MS	28
P 29	Permian	Phosphoria	Meade Peak	Lowermost phosphorite	MS	28
P 30	Permian	Phosphoria	Meade Peak		MS	29
P 31	Permian	Phosphoria	Meade Peak		MS	29
E 1	Jurassic	Ellis			MS	30
M 1	Cretaceous	Mowry		14.3m below top	OIC	1
M 2	Cretaceous	Mowry		15.8m below top	OIC	1
M 3	Cretaceous	Mowry		37.5m below top	OIC	1
M 4	Cretaceous	Mowry		52.4m below top	OIC	1
M 5	Cretaceous	Mowry		52.4m below top	OIC	1
M 6	Cretaceous	Mowry		52.4m below top	OIC	1
M 7	Cretaceous	Mowry		29.7m below top	OIC	2
M 8	Cretaceous	Mowry		29.7m below top	OIC	2
M 9	Cretaceous	Mowry		39.6m below top	OIC	2
M 10	Cretaceous	Mowry		31.5m below top	OIC	2
M 11	Cretaceous	Mowry		4.6m below top	OIC	3
M 12	Cretaceous	Mowry		13.4m below top	OIC	3
M 13	Cretaceous	Mowry		11.5m below top	OIC	3
M 14	Cretaceous	Mowry		11.5m below top	OIC	3
M 15	Cretaceous	Mowry		20.7m below top	OIC	4

Sample No.	Geologic Age	Formation	Member	Bed or Stratigraphic Position	Type of Sample*	Local No.
M 16	Cretaceous	Mowry		22.9m below top	OIC	4
M 17	Cretaceous	Mowry		52.7m below top	OIC	5
M 18	Cretaceous	Mowry		7.3m below top	OIC	5
M 19	Cretaceous	Mowry		14.0m below top	OIC	6
M 20	Cretaceous	Mowry		29.0m below top	OIC	7
M 21	Cretaceous	Mowry		10.4m below top	OIC	7
M 22	Cretaceous	Mowry		24.1m below top	OIC	8
M 23	Cretaceous	Mowry		Base of section	OIC	9
M 24	Cretaceous	Mowry		Base of section	OIC	9
M 25	Cretaceous	Mowry		29.6m below top (?)	OIC	10
M 26	Cretaceous	Mowry		3258-3260m	CR	11
M 27	Cretaceous	Mowry		3260-3261m	CR	11
M 28	Cretaceous	Mowry		3256-3257m	CR	11
M 29	Cretaceous	Mowry		3257-3258m	CR	11
M 30	Cretaceous	Mowry		2669-2670m	CR	12
M 31	Cretaceous	Mowry		2668-2669m	CR	12
M 32	Cretaceous	Mowry		3732.6-3733.4m	CR	13
M 33	Cretaceous	Mowry		3734-3736m	CR	13
M 34	Cretaceous	Mowry		3736-3737m	CR	13
M 35	Cretaceous	Mowry		3738-3738.4m	CR	13
M 37	Cretaceous	Mowry		8.5m below top	OIC	14
M 38	Cretaceous	Mowry		8.45m below top	OIC	14
M 39	Cretaceous	Mowry		17.1m above base	OIC	14
M 40	Cretaceous	Mowry		17.7m above base	OIC	14
M 41	Cretaceous	Mowry		14.7m above base	OIC	14
M 42	Cretaceous	Mowry		14.7m above base	OIC	14
M 43	Cretaceous	Mowry		14.7m above base	OIC	14
F 1	Cretaceous	Frontier		Coal seam	MS	47
F 2	Cretaceous	Frontier		Coal seam	MS	47
ES 1	Cretaceous	Espada		Uppermost 20m of unit	OIC	62
MO 1	Cretaceous	Moreno	Terra Loma	51m below top	OIC	61
MO 2	Cretaceous	Moreno	Dos Palos	152m below top	OIC	61
H 1	Cret.-Paleo	Ferris		Hanna #24 seam	MS	92
GR 1	Eocene	Green River	Wilkins Peak	63m above White Band	OIC	31
GR 2	Eocene	Green River	Wilkins Peak	63.05m above White Band	OIC	31
GR 3	Eocene	Green River	Wilkins Peak	62.9m above White Band	OIC	31

Sample No.	Geologic Age	Formation	Member	Bed or Stratigraphic Position	Type of Sample*	Local No.
GR 4	Eocene	Green River	Wilkins Peak	4m below White Band	OIC	31
GR 5	Eocene	Green River	Tipton	38m below top	OIC	32
GR 6	Eocene	Green River	Tipton	37.96m below top	OIC	32
GR 7	Eocene	Green River	Tipton	15m below top	OIC	32
GR 8	Eocene	Green River	Tipton	15m below top	OIC	32
GR 9	Eocene	Green River	Wilkins Peak	16.5m above White Band	OIC	33
GR 10	Eocene	Green River	Wilkins Peak	16.46m above White Band	OIC	33
GR 11	Eocene	Green River	Tipton	4.5m below top	OIC	33
GR 12	Eocene	Green River	Tipton	1.8m above Unit B	OIC	34
GR 13	Eocene	Green River	Wilkins Peak	8.5m above Unit B	OIC	35
GR 14	Eocene	Green River	Tipton	1.8m above Unit B	OIC	34
GR 15	Eocene	Green River	Wilkins Peak	61.5m below Tower Ss.	OIC	36
GR 16	Eocene	Green River	Wilkins Peak	0.4m below No.25 Trona	MS	37
GR 17	Eocene	Green River	Wilkins Peak	0.42m below No.25 Trona	MS	37
GR 18	Eocene	Green River	Wilkins Peak	0.5m below No.25 Trona(?)	MS	37
GR 19	Eocene	Green River	Wilkins Peak	5m above L. Big Is. Trona	MS	37
GR 20	Eocene	Green River	Wilkins Peak		MS	37
GR 21	Eocene	Green River	Wilkins Peak		MS	37
GR 22	Eocene	Green River	Wilkins Peak	Trona No. 25 bed	MS	37
GR 23	Eocene	Green River	Wilkins Peak	11.5m below Tower Ss.	OIC	38
GR 24	Eocene	Green River	Wilkins Peak	13.0m below Tower Ss.	OIC	38
GR 25	Eocene	Green River	Parachute Creek	Mahogany Bed	OIC	39
GR 26	Eocene	Green River	Parachute Creek	Mahogany Bed	OIC	39
GR 27	Eocene	Green River	Parachute Creek		OIC	40
GR 28	Eocene	Green River	Douglas Creek	8m below Mahogany	OIC	41
GR 29	Eocene	Green River	Parachute Creek	1.2m below Mahogany	OIC	41
GR 30	Eocene	Green River	Parachute Creek	Mahogany Bed	OIC	42
GR 31	Eocene	Green River	Parachute Creek	Mahogany Bed	OIC	42
GR 32	Eocene	Green River	Parachute Creek	Mahogany Bed	OIC	42
GR 33	Eocene	Green River	Evacuation Creek		OIC	43
GR 34	Eocene	Green River	Parachute Creek	Mahogany Bed	OIC	44
GR 35	Eocene	Green River	Parachute Creek	Mahogany Bed	OIC	44
GR 36	Eocene	Green River	Parachute Creek	Mahogany Bed	OIC	44
GR 37	Eocene	Green River	Parachute Creek	Mahogany Unit 68	OIC	45
GR 38	Eocene	Green River	Parachute Creek	Mahogany Unit 68	OIC	45
GR 39	Eocene	Green River	Parachute Creek	Mahogany Unit 80	OIC	45
K 1	Eocene	Kreyenhagen		Unit D	OIC	58
K 2	Eocene	Kreyenhagen		Unit E	OIC	58
K 3	Eocene	Kreyenhagen		Unit G	OIC	58
K 4	Eocene	Kreyenhagen		Unit F	OIC	59

Sample No.	Geologic Age	Formation	Member	Bed or Stratigraphic Position	Type of Sample*	Local No.
K 5	Eocene	Kreyenhagen		Unit E	OIC	59
K 6	Eocene	Kreyenhagen			OIC	60
CD 1	Eocene	Cozy Dell		Uppermost 7m of unit	OIC	53
MR 1	Miocene	Monterey	Lower Member		OIC	49
MR 2	Miocene	Monterey	Middle Member		OIC	50
MR 3	Miocene	Monterey	Middle Member		OIC	51
MR 4	Miocene	Monterey	Middle Member		OIC	51
MR 5	Miocene	Monterey	Middle Member	G2A Crude Bed	MS	52
MR 6	Miocene	Monterey	Middle Member	G2A Crude Bed	MS	52
MR 7	Miocene	Monterey	Middle Member	F Crude Bed	MS	52
MR 8	Miocene	Monterey	Middle Member		OIC	54
MR 9	Miocene	Monterey	Middle Member		OIC	54
MR 10	Miocene	Monterey	Lower Member		OIC	54
MR 11	Miocene	Monterey	Middle Member		OIC	54
MR 12	Miocene	Monterey	Upper Member		OIC	55
MR 13	Miocene	Monterey	Upper Member		OIC	55
MR 14	Miocene	Monterey	Upper Member (?)		OIC	56
MR 15	Miocene	Monterey	Altimira Shale	14.3m below top	OIC	57
MR 16	Miocene	Monterey	Altimira Shale	17.9m below top	OIC	57
MR 17	Miocene	Monterey	Altimira Shale	28.4m below top	OIC	57
RE 1	Recent			Calcareous Ooze	SS	97
RE 2	Recent			Algal Mat	SS	98
RE 3	Recent			Under Clay	SS	99
RE 4	Recent			Peat	SS	99
RE 5	Recent (?)			Lagoon	SS	100
RE 6	Recent			Lagoon	SS	101
RE 7	Recent			Marsh	SS	102
RE 8	Recent			Fecal Pellets	SS	103
RE 9	Recent			Wood Debris	SS	104
IM 1	Recent	Phaeophyta	Laminaria			105
IM 2	Recent	Chlorophyta	Codiaceae			106

*Types of samples collected include outcrops (OIC), mines and quarries (MS), drill hole cores (CR) and sediment (SS).

APPENDIX III: LOCALITY DESCRIPTIONS FOR PETROLEUM SAMPLES

SPL. No.	State	County	Location	Depth(m)	Field Name	Well No.	Operator
Utah-1	Utah	Uintah	Sec.24,T.11S.,R.24E.	0.0	Rainbow Vein	---	---
Utah-2	Utah	Uintah	Sec.24,T.24S.,R.11E.	0.0	Rainbow Vein	---	---
Utah-3	Utah	Uintah	Sec.30,T.14S.,R.20E.	1155.2	Flat Rock	2	Hiko Bell
Utah-4	Utah	Uintah	T.9S.,R.24E.	0.0	Independent Vein	---	---
Utah-5	Utah	Uintah	Sec.23,T.5S,R.23E.	1286.6	Ashly	T.E.H.1	R. Lacy
Utah-6	Utah	Uintah	Sec.23,T.5S,R.23E.	548.6	Ashly	T.E.H.5S	R. Lacy
Utah-7	Utah	Uintah	Sec.23,T.7S,R.23E.	1706.9	Red Wash	12-23B	Chevron
Utah-8	Utah	Uintah	Sec.4,T.12S.,R.25E.	0.0	Dragon Vein	-----	-----
Utah-9	Utah	Uintah	Sec.34,T.9S,R.24E.	0.0	Little Emma Vein	-----	-----
Utah-10	Utah	Uintah	Sec.9,T.12S.,R.25E.	0.0	-----	-----	-----
Utah-11	Utah	Uintah	Sec.23,T.5S.,R.21E.	0.0	County Pit	---	Uintah Co.
Utah-12	Utah	Uintah	Sec.23,T.9S.,R.21E.	2743.2	Bitter Creek	N.B.4	Gas Prod.Intp.
Utah-13	Utah	Uintah	Sec.22,T.9S.,R.22E.	1706.9	Bitter Creek	Chap.30-22	Belco Petrol.
Utah-14	Utah	Uintah	Sec.18,T.2N.,R.1W.	0.0	-----	-----	-----
Utah-15	Utah	Uintah	Sec.20,T.1S.,R.18E.	2834.6	Roosevelt	1	D&J
Utah-16	Utah	Duchesne	Sec.16,T.4S.,R.4W.	914.4	Ute Tribal	5&8	Intermt.Oil
Utah-17	Utah	Duchesne	Sec.31,T.1S.,R.4W.	3989.5	Altamont	1-31-A4	Shell
Utah-18	Utah	Duchesne	Sec.34,T.1S.,R.4W.	3863.6	Altamont	1-34-A4	Shell
Colo-1	Colorado	Rio Blanco	Sec.33,T.2N.,R.102W.	975.4	Rangely	M2	Twin Arrow
Colo-2	Colorado	Rio Blanco	Sec.33,T.2N.,R.102W.	594.4	Rangely	M21	Twin Arrow
Colo-3	Colorado	Rio Blanco	Sec.20,T.2N.,R.102W.	1889.8	Rangely	UP101x20	Chevron
Mich-1	Michigan	Ontonagon	Sec.4,T.50N.,R.42W.	304.8		---	White Pine
Wyo-1	Wyoming	Campbell	Sec.5,T.56N.,R.74W.	1478.3	Recluse	Fed.Tank Batt.	Beard
Wyo-2	Wyoming	Crook	Sec.14,T.57N.,R.74W.	2133.6	W. Sandbar	1 Greenough	Monsanto
Wyo-3	Wyoming	Campbell	Sec.28,T.57N.,R.72W.	1935.8	Hunter Ranch	4 Hunter	Davis
Ken-1	Kentucky	Estill	S.side of Route 52, W. of Irvine	0.0	-----	---	-----
*Ken-2	Kentucky	Metcalfe	K.G.S.	-----	-----	-----	-----
*Ken-3	Kentucky	Lee	K.G.S.	-----	-----	-----	-----
*Ken-4	Kentucky	Warren	K.G.S.	-----	-----	-----	-----
*Ken-5	Kentucky	Lawrence	K.G.S.	-----	-----	-----	-----
Calif-1	California	Santa Barbra	Sec.15,T.4N.R.19W	1036.3	Ellwood	2	Burmah
Calif-2	California	Santa Barbra	Offshore	2676.4	S. Ellwood	-----	Atl. Richfield
Calif-3	California	Santa Barbra	Offshore	1219.2	S. Ellwood	-----	Atl. Richfield

*Samples supplied by J. Ponsetto of the Kentucky Geological Survey (K.G.S.)

Calif-4	California	Kern	Sec.35,T.12N.,R.24W.	223.4	Midway So.	337	Mobil
Calif-5	California	Kern	Sec.35,T.12N.,R.24W.	588.6	Midway So.	243	Mobil
Calif-6	California	Kern	Sec.13,T.28S.,R.20E.	371.9	Beldridge So.	81A-13	Belridge
Calif-7	California	Fresno	T.20S.,R.16E.	2362.2	Coalinga Nose	Composite	Union
Calif-8	California	Fresno	T.20S.,R.16E.	563.9	E. Coalinga	Composite	Shell
Calif-9	California	Fresno	Sec.28,T.24S.,R.18E.	304.8	Pyramid Hills	N.D.1-10	Mobil

APPENDIX IV: Organic Carbon and Bitumen Analyses

Sample No.	Organic Carbon (Wt. %)	Bitumen (Wt. °/oo)	Sample No.	Organic Carbon (Wt. %)	Bitumen (Wt. °/oo)
NA 1	5.9	0.6	MR 1	0.9	0.1
NA 2	16.2	10.8	MR 2	0.5	0.3
NA 3	12.4	4.7	MR 3	0.4	6.9
NA 4	8.8	3.8	MR 4	1.3	2.1
NA 5	10.9	5.9	MR 5	1.9	9.3
NA 6	15.2	10.9	MR 6	1.9	5.5
NA 7	7.5	3.6	MR 7	4.0	5.7
NA 8	7.7	3.7	MR 8	4.0	20.5
NA 9	7.1	3.9	MR 9	1.4	0.8
NA 10	7.8	3.3	MR 10	15.2	32.0
NA 11	8.4	2.6	MR 11	11.1	22.2
NA 12	16.9	13.3	MR 12	5.1	4.6
NA 13	5.1	4.2	MR 13	3.8	4.3
NA 14	17.0	6.0	MR 14	0.2	5.2
NA 15	10.1	4.7	MR 15	1.3	13.5
NA 16	13.6	5.1	MR 16	0.7	23.5
NA 17	10.8	4.1	MR 17	2.2	8.6
NA 18	4.7	1.9	MO 1	0.6	0.7
NA 19	3.4	2.2	MO 2	0.6	0.5
NA 20	3.4	1.2	ES 1	0.8	0.1
NA 21	10.5	3.8	M 1	2.9	7.3
NA 22	6.2	3.7	M 2	1.2	0.4
NA 23	2.5	0.1	M 3	2.5	6.0
NA 24	5.1	4.1	M 7	1.3	0.7
NA 25	7.1	4.7	M 9	3.1	11.7
CH 1	20.6	10.1	M 10	3.2	6.8
CH 2	11.3	3.2	M 11	2.7	3.5
CH 3	8.2	1.7	M 12	2.2	2.2
CH 4	18.3	5.3	M 13	2.6	0.04
CH 5	9.8	6.8	M 15	2.2	1.2

Sample No.	Organic Carbon (Wt. %)	Bitumen (Wt. °/oo)	Sample No.	Organic Carbon (Wt. %)	Bitumen (Wt. °/oo)
CH 6	16.8	5.6	M 16	0.3	0.04
CH 7	9.8	5.6	M 17	5.0	2.3
CH 8	12.9	3.0	M 18	1.8	1.1
CH 9	13.1	6.0	M 19	2.4	2.2
CH 10	16.5	3.9	M 20	1.4	14.1
CH 11	11.1	4.4	M 21	2.8	2.6
CH 12	3.9	2.6	M 22	1.8	2.8
B 1	15.0	13.6	M 23	2.0	1.3
B 2	12.4	8.5	M 24	1.5	0.9
W 1	5.6	2.0	M 25	3.5	4.2
W 2	3.3	2.0	M 26	0.6	0.3
W 3	5.5	2.3	M 27	1.3	0.4
NS 1	0.5	0.03	M 28	2.5	2.8
NS 2	0.7	0.05	M 29	1.7	1.7
NS 3	0.6	0.03	M 30	2.1	0.7
NS 4	0.6	0.06	M 31	7.6	1.1
NS 5	0.6	0.06	M 32	1.2	0.6
NS 6	0.5	0.03	M 33	1.0	0.5
MQ 1	0.8	0.7	M 34	1.0	0.5
MQ 2	1.5	1.3	M 35	1.2	0.6
MC 1	9.5	5.4	M 37	1.5	1.4
MC 2	46.9	67.0	M 38	2.4	1.9
MC 3	7.0	4.3	M 39	2.9	1.7
GR 1	8.8	20.6	M 40	0.9	0.4
GR 2	4.9	11.5	M 41	1.8	1.5
GR 3	9.9	23.0	M 42	1.6	1.2
GR 4	12.9	36.6	M 43	1.6	1.1
GR 5	11.1	12.9	P 1	0.6	1.7
GR 6	15.1	6.7	P 2	1.1	1.7
GR 7	10.9	14.4	P 3	0.3	0.03
GR 8	8.9	14.9	P 4	0.3	0.02
GR 9	13.0	27.7	P 5	0.4	0.04
GR 10	17.6	31.7	P 6	0.3	0.08

Sample No.	Organic Carbon (Wt. %)	Bitumen (Wt. °/oo)	Sample No.	Organic Carbon (Wt. %)	Bitumen (Wt. °/oo)
GR 11	19.4	6.8	P 7	4.8	0.01
GR 12	15.7	25.1	P 8	0.1	0.01
GR 13	14.0	23.3	P 9	0.1	0.02
GR 14	8.3	17.0	P 10	0.4	0.02
GR 15	15.1	18.3	P 11	0.6	0.02
GR 16	16.1	18.9	P 12	0.5	0.05
GR 17	19.5	22.2	P 13	4.9	0.1
GR 18	15.2	21.7	P 14	2.4	0.04
GR 20	4.5	18.9	P 15	1.5	0.05
GR 21	15.5	17.6	P 16	11.7	0.1
GR 22	0.01	nd	P 17	1.9	0.07
GR 23	11.5	33.7	P 18	3.0	0.06
GR 24	10.8	24.5	P 19	1.2	0.02
GR 25	23.6	32.2	P 20	1.5	0.01
GR 26	22.8	58.0	P 21	9.1	0.03
GR 27	31.6	24.9	P 22	1.2	0.04
GR 28	3.6	13.1	P 23	12.6	2.1
GR 29	22.7	32.6	P 24	4.5	2.1
GR 30	8.6	19.6	P 25	1.1	0.02
GR 31	4.4	19.9	P 26	1.4	0.05
GR 32	28.2	23.3	P 27	2.2	0.04
GR 33	1.9	7.5	P 28	0.4	0.05
GR 34	4.1	11.5	P 29	0.2	0.1
GR 35	16.9	45.2	P 30	1.3	0.05
GR 36	11.4	29.9	P 31	5.2	0.1
GR 37	15.8	22.4	PC 1	0.8	2.6
GR 38	4.5	11.3	EU 1	2.5	1.5
GR 39	12.4	12.9	SL 1	0.4	0.2
			E 1	0.5	0.02
CD 1	1.1	1.1			
K 1	2.2	5.7	RE 1	1.9	8.7
K 2	6.0	10.0	RE 2	0.2	0.3
K 3	5.2	4.6	RE 3	1.8	8.2

Sample No.	Organic Carbon (Wt. %)	Bitumen (Wt. °/oo)	Sample No.	Organic Carbon (Wt. %)	Bitumen (Wt. °/oo)
K 4	5.8	7.6	RE 4	19.9	54.8
K 5	2.9	5.8	RE 5	1.7	1.0
K 6	0.2	nd	RE 6	1.1	1.1
F 1	60.3	41.1	RE 7	1.8	6.6
F 2	58.8	32.1	RE 8	1.2	16.5
HA 9	77.1	49.1	RE 9	nd	20.7
HA 22	66.1	44.9	LM 1	nd	235.5
I 1	48.4	46.8	LM 2	nd	30.7
PO 1	41.5	1.5	H 1	59.3	16.5

nd = Not Determined

Appendix V: Kerogen Analyses

Spl. No.	Normalized Elemental Analysis				Amount Analyzed	δC13
	Wt. % N	Wt. % C	Wt. % H	Wt. % O	Wt. %	(°/oo, PDB)
NA 1	2.2	87.0	4.8	6.0	76.7	-29.1
NA 2	3.5	87.6	8.2	5.7	85.1	-28.9
NA 3	2.6	81.8	8.1	7.5	72.2	-29.3
NA 4	2.3	81.8	7.9	7.9	74.3	-28.7
NA 5	2.5	78.8	7.8	10.9	77.9	-29.1
NA 6	3.6	82.4	8.3	5.7	85.9	-29.1
NA 7	2.4	82.9	7.5	7.2	80.4	-29.1
NA 8	1.6	84.2	8.1	6.2	79.2	-28.0
NA 9	2.5	83.0	8.2	6.4	77.0	-29.1
NA 10	2.5	84.4	8.2	4.9	75.7	-29.1
NA 11	2.5	83.4	7.9	6.2	72.1	-29.7
NA 12	3.1	80.8	8.0	8.1	88.1	-29.8
NA 13	2.8	79.9	8.2	9.2	75.0	-29.7
NA 14	2.8	80.2	8.2	8.9	68.6	-28.7
NA 15	2.4	83.3	8.8	5.6	71.8	-29.3
NA 16	2.7	81.4	8.1	7.8	68.0	-28.9
NA 17	2.6	82.6	7.9	6.9	66.5	-30.0
NA 18	2.5	81.2	8.2	8.0	67.7	-29.7
NA 19	2.5	80.0	8.2	9.3	81.8	-29.5
NA 20	2.5	82.3	8.2	7.0	69.8	-30.0
NA 21	2.4	80.3	8.2	9.2	71.8	-28.9
NA 22	2.5	81.4	8.3	7.9	71.4	-29.1
NA 23	2.0	76.8	3.2	18.1	88.3	-27.1
NA 24	2.7	80.1	7.7	9.5	59.1	-28.7
NA 25	2.3	79.0	7.9	10.8	62.9	-29.5
CH 1	2.7	83.8	6.9	6.6	78.4	-28.8
CH 2	2.7	83.0	7.1	7.3	77.3	-28.5
CH 3	2.5	84.1	8.0	5.4	64.7	-29.1
CH 4	1.9	83.0	7.4	7.7	71.5	-29.9
CH 5	2.1	80.3	7.9	6.4	69.2	-30.6

Spl. No.	Normalized Elemental Analysis				Amount Analyzed	δC13
	Wt. % N	Wt. % C	Wt. % H	Wt. % O	Wt. %	(°/oo, PDB)
CH 6	1.6	82.3	7.7	8.4	73.5	-28.6
CH 7	1.9	84.3	7.9	6.0	71.9	-30.0
CH 8	2.1	85.0	7.4	5.5	72.5	-29.5
CH 9	2.4	81.1	8.0	8.5	67.1	-28.8
CH 10	2.3	83.1	6.5	8.1	64.4	-28.6
CH 11	2.1	83.1	7.7	7.2	72.8	-29.1
CH 12	2.2	83.7	8.1	6.0	75.5	-29.3
M 1	3.6	76.8	6.2	13.5	82.9	-26.8
M 2	3.1	75.0	6.8	15.1	89.0	-26.7
M 3	2.9	75.0	6.1	12.4	85.8	-25.5
M 7	3.2	73.1	6.2	17.5	79.6	-25.4
M 9	3.4	77.0	7.0	12.7	75.5	-25.2
M 10	3.3	76.8	6.6	13.3	82.0	-26.8
M 11	3.4	80.1	6.5	11.1	83.9	-25.4
M 12	1.9	72.5	4.2	21.3	89.1	-24.9
M 13	3.0	69.1	4.9	23.1	74.6	-24.8
M 15	2.5	74.9	6.4	16.2	96.2	-22.9
M 16	2.7	82.0	5.5	9.8	89.7	-25.2
M 17	2.1	75.5	5.8	16.6	92.3	-26.5
M 18	2.9	75.0	5.2	16.9	95.2	-25.4
M 19	2.9	73.6	4.9	18.6	90.2	-25.7
M 20	2.4	79.2	6.6	11.9	85.0	-26.9
M 21	2.3	75.1	6.0	16.6	93.4	nd
M 22	2.7	77.1	5.9	14.4	88.2	-25.5
M 23	2.5	72.5	4.5	20.5	93.1	-24.6
M 24	1.9	72.6	3.9	21.6	89.7	-24.1
M 25	2.5	75.8	7.0	14.7	83.7	-25.5
M 26	1.0	89.3	4.7	5.0	69.7	-25.0
M 27	1.5	88.4	4.7	5.4	91.6	-24.1
M 28	1.2	89.3	5.1	4.4	78.2	-26.2
M 29	1.6	87.3	4.9	6.1	58.8	-26.1
M 30	2.3	85.0	4.9	7.9	94.3	-23.7
M 31	0.4	88.8	4.7	6.1	94.0	-23.6

Spl. No.	Normalized Elemental Analysis				Amount Analyzed	δC13
	Wt. % N	Wt. % C	Wt. % H	Wt. % O	Wt. %	(^{o}/oo, PDB)
M 32	2.1	83.9	4.8	9.2	43.6	-24.5
M 33	1.2	83.6	6.3	9.0	77.1	-24.5
M 34	1.9	85.0	4.9	8.2	80.6	-24.6
M 35	1.1	86.0	5.0	8.0	82.8	-25.2
M 37	2.4	79.3	6.7	11.7	67.8	-25.4
M 38	2.0	79.9	6.7	11.4	71.9	-25.3
M 39	2.5	80.2	7.0	10.4	69.5	-25.2
M 40	2.3	78.5	7.0	12.1	74.3	-24.7
M 41	2.1	78.0	5.4	14.6	77.3	-25.4
M 42	2.0	75.9	4.6	17.5	90.1	-24.7
M 43	2.1	78.9	5.5	13.5	79.0	-25.2
P 1	2.4	81.9	8.2	7.4	79.3	nd
P 2	3.3	81.6	8.4	6.8	107.3	nd
P 5	2.5	73.7	3.2	20.6	81.9	-29.5
P 6	2.1	86.5	3.3	8.2	87.7	nd
P 8	4.4	48.5	6.2	41.0	14.9	nd
P 10	6.2	68.7	4.9	20.2	11.4	-29.9
P 11	2.2	79.2	3.1	15.6	79.7	-28.2
P 12	2.4	81.4	3.5	12.8	85.3	nd
P 13	2.9	81.1	2.6	13.4	82.9	nd
P 14	2.6	85.4	2.7	9.3	84.0	-28.4
P 15	3.2	87.8	2.9	6.2	82.9	nd
P 16	3.8	87.9	3.1	5.3	82.8	-28.9
P 17	2.4	64.6	3.0	30.0	21.3	nd
P 18	3.1	65.7	2.2	29.0	80.7	-27.9
P 19	3.3	70.2	2.6	23.8	84.8	-28.4
P 20	3.0	73.0	2.6	21.4	82.3	-28.6
P 21	2.6	68.2	2.6	26.6	83.6	nd
P 22	3.4	72.8	3.1	20.7	69.4	-28.9
P 23	4.1	86.4	4.6	5.0	86.2	-29.0
P 24	3.2	86.0	4.5	6.2	77.1	-29.2
P 25	2.9	69.9	2.4	24.9	75.2	nd
P 26	2.3	70.6	2.3	24.8	72.1	nd

Spl. No.	Normalized Elemental Analysis				Amount Analyzed	δC13
	Wt. % N	Wt. % C	Wt. % H	Wt. % O	Wt. %	(°/oo, PDB)
P 27	2.5	70.9	2.3	24.4	80.9	nd
P 28	6.4	73.4	4.3	15.9	61.6	nd
P 29	2.7	82.1	5.2	10.0	70.1	-28.4
P 30	1.8	91.4	3.9	2.8	67.0	nd
P 31	2.6	89.6	3.8	4.0	82.7	nd
NS 1	3.0	85.1	3.9	8.0	57.4	-33.4
NS 2	2.7	83.9	3.9	9.4	55.3	nd
NS 3	2.9	86.6	3.4	7.2	57.0	-31.3
NS 4	3.3	74.7	3.8	18.1	34.7	-32.5
NS 5	1.9	84.5	4.6	9.0	50.9	-33.5
NS 6	3.0	75.0	3.5	18.5	55.2	nd
MR 1	2.5	77.7	8.6	11.2	82.2	nd
MR 2	2.1	75.7	9.3	13.0	78.6	nd
MR 4	3.2	65.4	6.2	25.1	88.0	-21.6
MR 5	3.3	65.7	6.3	24.7	84.6	nd
MR 6	3.3	66.4	6.7	23.6	84.3	nd
MR 7	3.8	71.8	7.6	16.8	83.0	-20.6
MR 8	3.7	70.4	7.6	18.2	82.2	-20.2
MR 9	3.8	72.9	7.8	15.5	77.0	-20.2
MR 10	3.6	69.1	7.2	20.1	84.5	-20.3
MR 11	3.4	85.6	7.5	17.3	85.6	-21.3
MR 12	4.2	73.9	7.2	14.7	81.8	-22.8
MR 13	4.0	71.8	7.0	17.2	84.1	-22.6
MR 14	3.6	68.9	4.3	23.2	66.3	nd
MR 15	5.8	63.0	3.1	28.2	62.2	nd
MR 16	8.6	62.4	2.7	26.3	75.8	-19.2
MR 17	5.3	64.9	3.6	26.3	55.5	nd
K 1	3.5	71.2	6.6	18.7	90.0	-27.3
K 2	3.6	74.0	7.4	15.1	85.0	nd
K 3	3.6	76.4	7.2	12.8	77.9	-28.4
K 4	4.0	72.9	7.1	16.0	84.4	-28.1
K 5	3.3	71.3	6.8	18.6	74.8	-27.5
MO 1	1.8	65.4	2.9	29.9	77.5	-24.3

Spl. No.	Normalized Elemental Analysis				Amount Analyzed	δC13
	Wt. % N	Wt. % C	Wt. % H	Wt. % O	Wt. %	(°/oo, PDB)
MO 2	3.1	63.1	3.9	29.9	79.7	nd
W 1	2.6	72.7	5.5	19.2	89.1	-29.7
W 2	2.6	73.1	6.5	17.8	90.9	-29.8
W 3	2.7	83.3	7.2	6.6	82.9	nd
MC 1	0.8	75.0	3.5	20.8	89.3	-23.3
MC 2	0.6	73.2	3.5	22.7	90.4	nd
MC 3	0.9	78.4	3.0	17.7	90.4	-22.4
LM 1	0.9	59.1	4.8	35.2	89.7	-17.2
LM 2	5.0	70.4	8.0	16.7	88.8	-17.2
GR 1	2.5	79.0	9.6	8.9	88.6	-28.5
GR 2	2.6	74.8	9.3	13.4	91.9	-31.7
GR 3	2.6	78.2	9.9	9.3	87.2	-27.4
GR 4	3.0	76.9	9.4	10.8	90.2	-28.2
GR 5	2.6	77.7	10.1	9.6	92.4	-32.7
GR 6	2.6	77.2	9.9	10.4	87.9	-33.5
GR 7	3.0	78.5	9.8	8.7	92.2	-31.7
GR 8	2.9	76.2	9.2	11.8	90.2	-32.0
GR 9	3.0	78.8	9.0	9.2	91.0	-27.7
GR 10	3.0	77.9	9.5	9.6	90.4	-27.1
GR 11	2.6	77.8	10.6	9.0	85.6	-33.8
GR 12	2.9	79.1	10.0	8.0	92.2	-30.9
GR 13	3.1	78.4	9.6	9.0	90.8	-29.5
GR 14	2.5	73.5	8.6	15.4	91.7	-31.5
GR 15	2.6	76.6	10.5	10.2	79.2	-31.8
GR 16	2.9	77.9	10.6	8.7	85.6	-31.1
GR 17	2.9	78.1	10.6	8.5	86.3	-31.1
GR 18	2.7	79.0	10.8	7.6	88.0	-31.4
GR 20	2.6	77.5	10.3	9.6	93.7	-32.5
GR 21	2.7	79.4	10.6	7.3	86.6	-31.4
GR 23	2.7	74.1	9.3	14.0	84.4	-31.1
GR 24	2.6	73.8	9.3	14.2	94.8	-33.1
GR 25	2.8	78.7	10.1	8.4	90.9	-30.9
GR 26	2.9	80.6	10.5	6.0	91.9	-28.0

Spl. No.	Normalized Elemental Analysis				Amount Analyzed	δC13
	Wt. % N	Wt. % C	Wt. % H	Wt. % O	Wt. %	(°/oo, PDB)
GR 27	3.0	78.3	10.6	8.1	92.5	-29.5
GR 28	2.7	74.8	8.5	14.1	95.3	-31.5
GR 29	3.3	79.3	10.4	7.0	90.1	-30.2
GR 30	2.9	76.8	9.7	10.7	90.8	-31.1
GR 31	3.0	76.1	8.5	12.4	91.0	-29.7
GR 32	3.0	79.8	10.5	6.6	87.7	-30.9
GR 33	3.3	78.2	9.0	9.5	87.6	-29.4
GR 34	2.6	79.8	10.3	7.3	94.1	-26.6
GR 35	2.7	76.8	9.1	11.4	92.2	-27.4
GR 36	2.7	76.2	9.3	11.8	92.1	-27.7
GR 37	2.4	79.9	10.6	7.1	87.0	-27.7
GR 38	2.5	79.3	10.3	7.9	90.0	-28.4
GR 39	2.6	80.3	10.3	6.8	94.0	-26.9
HA 9	1.8	83.0	5.4	9.9	93.9	-23.0
HA 22	0.9	82.2	5.8	11.1	85.5	-22.9
H 1	0.8	72.1	4.3	22.8	91.9	-24.8
I 1	1.6	78.9	5.3	14.2	90.6	-24.0
PO 1	0.4	91.9	3.9	3.8	92.5	-22.7
F 1	1.6	76.8	5.5	16.1	92.3	-25.2
F 2	0.9	79.2	5.3	14.7	91.3	-25.3
RE 1	2.3	63.4	7.2	27.1	89.6	-19.7
RE 2	2.6	65.0	6.4	26.0	80.8	-21.2
RE 3	2.0	65.4	5.9	28.8	86.3	nd
RE 4	1.4	63.9	5.3	29.4	84.0	-26.4
RE 5	4.2	62.5	4.3	29.1	75.3	-24.6
RE 6	1.6	65.4	5.2	27.8	66.5	-23.4
RE 7	1.8	67.4	5.6	25.2	77.4	nd
RE 8	3.3	67.2	6.8	22.7	43.6	-17.6
RE 9	1.0	61.5	4.9	32.6	92.5	-28.8
PC 1	1.8	74.7	5.2	18.3	87.8	-25.5
EU 1	1.1	73.6	4.7	20.5	89.6	nd
E	0.8	89.1	3.2	6.9	68.1	nd
SL 1	1.2	86.8	5.0	7.1	71.9	-29.0

Spl. No.	Normalized Elemental Analysis				Amount Analyzed	δC13
	Wt. % N	Wt. % C	Wt. % H	Wt. % O	Wt. %	(^{o}/oo, PDB)
CD 1	1.8	77.9	5.7	14.7	91.4	-28.6
ES 1	2.2	81.3	4.1	12.4	84.8	nd
MQ 1	2.2	82.0	8.4	7.4	78.4	-29.0
MQ 2	2.2	81.2	8.5	8.1	68.8	-29.2
B 1	2.6	83.5	7.2	5.7	81.0	nd
B 2	3.5	85.5	5.5	5.5	79.7	nd

nd = Not Determined

APPENDIX VI: Vanadium and Nickel Concentrations in Bitumen

Sample No.	Vanadium (ppm)	Nickel (ppm)	V / Ni+V	Sample No.	Vanadium (ppm)	Nickel (ppm)	V / Ni+V
PC 1	86	218	0.28	MC 1	36	BDL	1.00
EU 1	91	65	0.58	MC 2	2	11	0.15
CD 1	7.2	74	0.09	MC 3	72	26	0.73
NA 2	578	245	0.70	GR 1	4.1	43	0.09
NA 3	427	280	0.60	GR 2	4.5	22	0.17
NA 4	123	103	0.54	GR 3	6.6	35	0.16
NA 5	330	495	0.40	GR 4	28.6	100	0.22
NA 6	537	523	0.51	GR 5	3.5	121	0.03
NA 7	508	628	0.45	GR 6	7.1	119	0.06
NA 8	234	370	0.39	GR 7	5.4	41	0.12
NA 9	343	183	0.65	GR 8	1.9	67	0.03
NA 10	123	18	0.87	GR 9	36.8	100	0.27
NA 11	274	63	0.81	GR 10	32.4	58	0.36
NA 12	1080	497	0.68	GR 11	2.7	144	0.02
NA 13	347	474	0.42	GR 12	5.2	75	0.07
NA 14	200	56	0.78	GR 13	9.7	21	0.31
NA 15	362	334	0.52	GR 14	1.0	48	0.02
NA 16	239	39	0.86	GR 15	1.5	110	0.01
NA 17	343	173	0.66	GR 16	8.6	230	0.04
NA 18	367	105	0.78	GR 17	6.9	196	0.03
NA 19	89	304	0.23	GR 18	1.8	105	0.02
NA 20	360	206	0.64	GR 20	0.8	93	0.01
NA 21	401	293	0.58	GR 21	0.6	111	0.01
NA 22	390	287	0.58	GR 23	2.4	21	0.10
NA 24	70	174	0.29	GR 24	1.7	21	0.08
NA 25	36	33	0.52	GR 25	6.7	63	0.10
CH 1	605	183	0.77	GR 26	17.8	46	0.28
CH 2	347	870	0.29	GR 27	29.8	194	0.13
CH 3	647	112	0.85	GR 28	5.8	58	0.09
CH 4	1760	126	0.93	GR 29	12.6	93	0.12
CH 5	523	71	0.88	GR 30	1.9	25	0.07
CH 6	455	226	0.67	GR 31	2.6	28	0.09
CH 7	479	1030	0.32	GR 32	4.7	60	0.07
CH 8	340	51	0.87	GR 33	2.7	80	0.03
CH 9	1040	474	0.69	GR 34	3.9	65	0.06
CH 10	779	660	0.54	GR 35	7.3	41	0.15
CH 11	292	640	0.31	GR 36	2.3	BDL	nd
CH 12	569	89	0.87	GR 37	6.3	132	0.05
B 1	949	688	0.58	GR 38	4.6	54	0.08
B 2	71	84	0.46	GR 39	7.2	132	0.05
W 1	423	120	0.78	K 1	62	215	0.22
W 2	483	97	0.83	K 2	78	388	0.17
W 3	1300	142	0.90	K 2	56	190	0.23
MQ 1	7	102	0.07	K 4	88	419	0.17
MQ 2	8	141	0.05	K 5	58	228	0.20

Sample No.	Vanadium (ppm)	Nickel (ppm)	$\frac{V}{Ni+V}$	Sample No.	Vanadium (ppm)	Nickel (ppm)	$\frac{V}{Ni+V}$
MR 5	320	215	0.60	M 1	55	67	0.45
MR 6	305	163	0.65	M 3	14	41	0.26
MR 7	245	1240	0.16	M 9	33	21	0.61
MR 8	11	23	0.32	M 10	26	67	0.28
MR 9	80	209	0.28	M 11	47	144	0.24
MR 10	261	304	0.46	M 12	11	19	0.36
MR 11	BDL	893	nd	M 15	7	114	0.06
MR 12	8	239	0.03	M 17	9	96	0.09
MR 13	3	162	0.02	M 18	7	111	0.06
MR 16	40	269	0.13	M 19	6	BDL	nd
RE 1	1.3	79	0.02	M 20	40	118	0.26
RE 2	3.9	BDL	nd	M 21	16	26	0.37
RE 3	2.7	56	0.05	M 22	17	27	0.39
RE 4	BDL	178	nd	M 25	32	63	0.34
RE 5	105	30	0.78	M 28	0.8	59	0.01
RE 6	7.0	150	0.04	M 29	0.2	37	0.01
RE 7	3.7	95	0.04	M 30	1.4	185	0.01
RE 8	BDL	14	nd	M 31	1.6	BDL	nd
RE 9	1.5	17	0.08	M 37	36	145	0.20
F 1	1.3	BDL	nd	M 38	27	252	0.10
F 2	1.8	BDL	nd	M 39	17	159	0.10
HA 9	0.5	7	0.06	M 41	10	133	0.07
HA 22	1.0	19	0.05	M 42	6	67	0.09
I 1	12.3	11	0.52	M 43	9	78	0.10
PO 1	5.1	81	0.06	P 1	47	66	0.42
H 1	0.8	BDL	nd	P 2	5	93	0.05
WD 5A	1910	78	0.96	P 23	29	28	0.51
WD 5B	1930	79	0.96	P 24	71	3900	0.02
WD 7A	4760	159	0.97	LM 1	BDL	18.8	nd
WD 7B	4490	177	0.96	LM 2	5.1	BDL	nd

BDL - Below Detection Limit
nd - Not Determined

APPENDIX VII: Mineralogy of Rock Samples (Wt. %)*

Spl. No.	Quartz	Feldspar	Analcite	Illite	Smectite	Kaolinite	Calcite	Dolomite	Apatite	Pyrite
P 1	11	-	-	-	-	-	15	25	45	4
P 2	38	2	-	20	-	-	9	17	14	-
P 3	52	-	-	-	-	3	2	-	43	-
P 4	53	-	-	-	-	-	-	-	47	-
P 5	99	-	-	-	-	-		1	-	-
P 6	13	-	-	-	-	-	-	-	87	-
P 7	2	-	-	-	-	-	-	-	98	-
P 8	17	-	-	-	-	-	-	-	83	-
P 9	23	-	-	-	-	-	-	-	77	-
P 10	1	-	-	-	-	-	-	-	99	-
P 11	31	-	-	-	-	-	4	-	64	-
P 12	100	-	-	-	-	-	-	-	-	-
P 13	35	-	10	44	-	-	-	-	11	-
P 14	35	-	-	-	-	-	-	-	65	-
P 15	4	-	-	-	-	-	10	86	-	-
P 16	12	-	-	9	-	3		60	16	-
P 17	17	1	-	-	-	-	-	-	82	-
P 18	14	1	-	14	-	-	-	-	71	-
P 19	4	-	-	-	-	-	-	-	95	-
P 20	8	-	-	-	-	-	-	-	92	-
P 21	15	1	-	14	-	-	3	-	67	-
P 22	3	-	-	-	-	-	-	-	97	-
P 23	9	2	-	14	-	-	17	-	58	-
P 24	66	9	-	10	-	-	-	9	9	6
P 25	23	-	-	-	-	-	-	-	77	-
P 26	49	1	-	11	4	4	-	-	31	-
P 27	16	1	-	-	-	tr	-	-	83	-
P 28	32	-	-	21	-	-	-	-	47	-
P 29	6	-	-	7	-	-	21	6	59	-
P 30	30	1	-	-	6	-	2	60	-	1
P 31	4	-	-	21	-	-	-	1	95	-

	Quartz	Feldspar	Illite	Smectite	Kaolinite	Smec/Ill	Chlorite	Calcite	Dolomite	Gypsum	Pyrite
M 1	73	1	-	23	1	-	-	-	-	-	2
M 2	15	2	-	11	-	-	-	72	-	-	-
M 3	68	1	5	22	4	-	-	-	-	-	-
M 4	3	-	-	88	-	-	-	-	-	9	-
M 5	2	-	-	74	-	-	-	24	-	-	-
M 6	1	-	-	-	-	-	-	99	-	-	-
M 7	22	2	-	11	-	-	-	63	-	-	2
M 8	5	-	-	-	-	-	-	95	-	-	-
M 9	68	-	-	29	-	-	-	-	-	-	3
M 10	63	tr	3	29	tr	-	-	-	-	-	4
M 11	61	2	21	10	7	-	-	-	-	-	-
M 12	56	1	5	32	5	-	-	-	-	-	-
M 13	2	-	-	tr	-	-	-	96	-	-	2
M 14	3	-	-	-	-	-	-	97	-	-	-

	Quartz	Feldspar	Illite	Smectite	Kaolinite	SMEC/ILL	Chlorite	Calcite	Dolomite	Gypsum	Pyrite
M 15	59	2	24	-	8	7	-	-	-	-	-
M 16	14	-	12	-	5	2	-	67	-	-	-
M 17	70	1	5	24	-	-	-	-	-	-	-
M 18	77	1	-	22	-	-	-	-	-	-	-
M 19	76	1	-	23	-	-	-	-	-	-	-
M 20	64	2	19	13	-	-	-	-	-	-	-
M 21	81	1	-	18	-	-	-	-	-	-	-
M 22	69	2	7	20	-	-	-	-	-	-	1
M 23	49	1	12	27	11	-	-	-	-	-	-
M 24	54	3	13	19	10	-	-	-	-	-	1
M 25	67	2	14	15	-	-	-	-	-	-	2
M 26	65	2	15	-	-	15	3	-	-	-	-
M 27	66	2	15	-	2	12	2	-	-	-	-
M 28	62	2	28	-	-	-	-	-	4	-	4
M 29	42	3	9	-	1	18	1	20	3	-	3
M 30	51	1	8	23	17	-	-	-	-	-	-
M 31	42	1	11	34	8	-	4	-	-	-	-
M 32	53	3	29	-	2	7	1	-	4	-	1
M 33	55	3	20	-	2	13	1	-	4	-	1
M 34	61	2	16	-	4	11	2	-	4	-	-
M 35	53	3	22	-	3	12	-	-	5	-	1
M 37	72	1	7	16	3	-	-	-	-	-	1
M 38	72	tr	-	26	-	-	-	-	-	-	2
M 39	60	tr	4	31	-	-	-	-	3	-	2
M 40	12	1	-	-	-	-	-	87	-	-	-
M 41	48	1	9	30	4	-	-	-	5	-	3
M 42	47	1	16	25	5	-	-	-	6	-	-
M 43	50	1	6	28	3	-	2	-	8	-	2
NS 1	32	8	43	-	-	-	17	-	-	-	-
NS 2	38	9	33	-	-	-	20	-	-	-	-
NS 3	33	6	49	-	-	-	12	-	-	-	-
NS 4	23	7	22	-	-	-	18	27	-	-	3
NS 4	13	13	13	-	-	-	10	60	-	-	1
NS 6	24	13	24	-	-	-	20	16	-	-	3

	Quartz	Smectite	Illite	Feldspar	Analcite	Aragonite	Calcite	Dolomite	Shortite	Trona	Gypsum	Pyrite
GR 1	16	tr	-	2	9	-	21	49	-	-	-	3
GR 2	19	7	3	1	3	-	24	39	-	-	-	4
GR 3	41	16	7	4	14	-	11	-	-	-	-	7
GR 4	18	12	5	2	4	-	4	50	-	-	-	5
GR 5	30	-	-	4	28	-	-	38	-	-	-	-
GR 6	18	-	15	2	46	-	-	20	-	-	-	-
GR 7	19	-	21	3	44	-	-	13	-	-	-	-
GR 8	19	-	21	3	46	-	-	11	-	-	-	-
GR 9	30	7	8	5	-	-	-	50	-	-	-	-
GR 10	24	13	11	6	-	-	5	41	-	-	-	-
GR 11	54	tr	tr	3	24	-	5	13	-	-	-	-
GR 12	12	-	tr	21	-	-	-	67	-	-	-	-
GR 13	31	-	tr	3	-	-	8	58	-	-	-	-

	Quartz	Smectite	Illite	Feldspar	Analcite	Aragonite	Calcite	Dolomite	Shortite	Trona	Gypsum	Pyrite
GR 14	10	-	21	25	-	-	-	44	-	-	-	-
GR 15	22	-	-	11	-	-	42	25	-	-	-	-
GR 16	25	-	-	5	-	-	-	44	26	-	-	-
GR 17	27	-	-	5	-	-	-	53	15	-	-	-
GR 18	34	-	-	3	-	-	-	47	12	4	-	-
GR 19	-	-	-	-	-	-	-	-	-	100	-	-
GR 20	45	-	-	3	-	-	-	44	8	-	-	-
GR 21	31	-	11	9	-	-	-	40	9	-	-	-
GR 22	-	-	-	-	-	-	-	-	-	100	-	-
GR 23	27	-	-	5	-	-	25	43	-	-	-	-
GR 24	48	-	-	2	-	-	28	21	-	-	1	-
GR 25	24	-	-	6	-	-	42	28	-	-	-	-
GR 26	21	-	12	4	11	-	22	29	-	-	-	1
GR 27	35	-	-	19	-	-	-	46	-	-	-	-
GR 28	30	-	-	3	4	-	34	29	-	-	-	-
GR 29	35	-	22	11	-	-	6	26	-	-	-	-
GR 30	16	-	-	3	-	-	42	39	-	-	-	-
GR 31	14	-	-	2	-	-	65	18	-	-	-	1
GR 32	30	-	-	10	-	7	13	29	-	-	-	10
GR 33	17	10	5	6	-	-	21	41	-	-	-	-
GR 34	22	14	-	2	-	-	26	36	-	-	-	-
GR 35	17	16	-	2	-	-	50	13	-	-	-	2
GR 36	11	12	12	7	-	-	45	12	-	-	-	1
GR 37	12	20	-	2	-	-	59	5	-	-	-	2
GR 38	19	16	4	3	-	-	22	36	-	-	-	-
GR 39	15	12	-	1	-	-	66	6	-	-	-	-

	Quartz	Feldspar	Kaolinite	Illite	Chlorite	Dolomite	Siderite	Marcasite	Pyrite
NA 1	55	2	-	28	-	9	-	2	4
NA 2	57	2	-	36	3	-	-	1	1
NA 3	55	3	-	33	5	-	-	2	2
NA 4	56	1	-	35	3	-	1	2	2
NA 5	56	3	3	31	3	-	2	1	1
NA 6	58	2	2	36	2	-	-	-	-
NA 7	51	2	-	36	4	2	2	-	3
NA 8	56	2	-	38	tr	-	1	2	1
NA 9	46	2	-	36	14	-	-	1	1
NA 10	44	2	-	37	8	5	-	2	2
NA 11	57	2	-	28	5	2	1	3	1
NA 12	50	2	-	35	5	8	-	-	-
NA 13	56	2	-	34	5	-	1	tr	2
NA 14	50	3	-	36	3	-	-	4	4
NA 15	55	3	-	32	4	-	2	-	4
NA 16	59	2	-	29	4	-	-	3	3
NA 17	60	2	-	27	5	-	-	4	2
NA 18	27	2	4	18	-	39	4	-	6
NA 19	49	2	tr	37	4	-	6	-	2
NA 20	20	1	2	21	-	51	2	-	3
NA 21	64	3	-	29	-	-	-	2	2
NA 22	61	1	-	33	tr	2	1	1	1

	Quartz	Feldspar	Kaolinite	Illite	Chlorite	Dolomite	Siderite	Marcasite	Pyrite
NA 23	68	2	-	28	-	-	1	1	-
NA 24	50	2	tr	42	-	-	-	2	4
NA 25	49	2	-	29	7	4	2	4	3
CH 1	57	2	-	38	-	-	1	1	1
CH 2	50	3	-	36	-	-	1	4	6
CH 3	57	2	-	29	5	-	1	2	4
CH 4	48	2	-	35	6	-	3	-	6
CH 5	51	2	-	35	5	2	-	2	3
CH 6	54	3	-	37	-	-	-	3	2
CH 7	65	2	-	28	-	-	1	2	2
CH 8	59	3	-	30	-	-	-	4	4
CH 9	48	2	-	27	-	-	-	9	14
CH 10	51	3	-	34	-	-	-	7	5
CH 11	57	3	-	24	2	-	2	4	8
CH 12	33	1	-	13	-	49	2	2	-

	Quartz	Cristobalite and/or Tridymite	Feldspar	Illite	Smectite	Chlorite	Clinoptil-olite	Calcite	Mg-Calcite	Gypsum	Pyrite
MR 1	100	-	-	-	-	-	-	-	-	-	-
MR 2	100	-	-	-	-	-	-	-	-	-	-
MR 3	19	6	7	-	55	-	-	13	-	-	-
MR 4	21	5	4	-	32	-	-	38	-	-	-
MR 5	47	5	7	-	41	-	-	-	-	-	-
MR 6	80	9	2	-	9	-	-	-	-	-	-
MR 7	42	8	1	-	43	-	-	-	-	6	-
MR 8	11	2	1	-	20	-	-	65	-	1	-
MR 9	9	38	-	-	-	-	-	53	-	-	-
MR 10	33	-	1	26	-	-	21	-	9	10	-
MR 11	33	27	1	tr	-	-	33	-	-	6	-
MR 12	37	-	8	18	10	-	-	25	-	-	2
MR 13	22	-	4	10	10	3	-	48	-	1	2
MR 14	-	100	-	-	-	-	-	-	-	-	-
MR 15	62	16	13	-	-	-	-	-	-	-	9
MR 16	42	42	tr	-	-	-	-	-	-	16	-
MR 17	36	9	tr	36	-	-	-	-	-	19	-

	Quartz	Cristobalite	Feldspar	Kaolinite	Illite	Smectite	Clinoptil-olite	Gypsum	Jarosite	Calcite	Dolomite	Pyrite
K 1	42	3	4	8	12	31	-	-	-	-	-	-
K 2	36	3	7	5	14	31	-	-	-	-	-	3
K 3	54	2	1	-	-	18	-	tr	-	23	-	2
K 4	20	8	5	4	26	25	8	-	-	-	-	3
K 5	26	5	9	8	16	35	-	-	-	-	-	-
K 6	12	-	-	-	-	13	-	75	-	-	-	-
PC 1	35	11	-	10	38	6	-	-	-	-	-	-

	Quartz	Feldspar	Illite	Chlorite	Chlo/Verm	Smectite	Kaolinite	Dolomite	Calcite	Siderite	Marcasite	Pyrite
CD 1	32	10	54	-	4	-	-	-	-	-	-	-
MQ 1	24	-	19	tr	-	-	-	53	-	2	-	2
MQ 2	36	2	36	4	-	-	-	16	-	3	-	3
EU 1	81	-	17	1	-	-	1	-	-	-	-	-
ES 1	28	11	24	9	-	21	7	-	-	-	-	-
W 1	35	1	19	-	-	-	tr	43	-	2	-	-
W 2	26	1	14	-	-	-	-	59	-	-	-	-
W 3	13	1	13	-	-	-	-	64	7	-	1	1
E 1	41	-	39	4	-	-	-	14	-	-	-	2
SL 1	5	-	-	-	-	-	-	1	94	-	-	-
I 1	30	-	-	-	-	-	11	36	-	-	-	23
F 1	37	-	-	-	-	-	35	-	-	-	-	28
F 2	43	-	-	-	-	-	31	-	-	-	-	26
H 1	70	-	-	-	-	-	-	-	-	-	-	30
PO 1	17	-	-	-	-	-	83	-	-	-	-	-
HA 9	-	-	-	-	-	-	49	-	-	-	-	51
HA 22	9	-	-	-	-	-	91	-	-	-	-	-
MO 1	37	7	4	-	-	42	11	-	-	-	-	-
MO 2	29	3	16	-	-	39	13	-	-	-	-	-

	Quartz	Feldspar	Kaolinite	Illite	Smec/Ill	Chlorite	Dolomite	Jarosite	Gypsum	Marcasite	Pyrite
MC 1	35	tr	7	-	45	7	2	5	-	-	-
MC 2	22	-	-	-	-	-	-	-	78	-	-
MC 3	79	-	16	-	-	-	-	-	-	-	5
WD 5	81	-	1	16	-	-	-	-	-	-	2
WD 7	81	-	tr	18	-	-	-	-	tr	-	1

	Quartz	Feldspar	Illite	Calcite	Mg-Calcite	Dolomite	Marcosite	Pyrite
B 1	62	2	24	2	2	4	2	2
B 2	54	2	32	-	4	4	2	2

*Weight percent of inorganic fraction of rock samples
Smec/Ill = Mixed Layer Smectite-Illite
Chlo/Verm = Mixed Layer Chlorite - Vermiculite

APPENDIX VIII: Physical, Isotopic, and Compositional Data on Petroleum Samples

Sample No.	Specific Gravity	δC^{13}-Whole Oil (^{o}/oo, PDB)	δC^{13}-Saturates (^{o}/oo, PDB)	Sulfur (Wt.%)	Vanadium (ppm)	Nickel (ppm)
Utah-1	nd	-29.7	nd	0.36	2.0	21.4
Utah-2	nd	-29.6	nd	0.31	2.3	2.30
Utah-3	0.813	-26.7	nd	0.04	0.003	BDL
Utah-4	nd	-30.4	nd	0.33	nd	nd
Utah-5	0.867	-27.8	nd	0.46	7.0	BDL
Utah-6	0.859	-27.0	nd	0.12	0.2	BDL
Utah-7	0.891	-31.0	nd	0.17	0.2	44.9
Utah-8	nd	-29.6	nd	0.42	2.5	286
Utah-9	nd	-29.7	-35.0	0.36	8.6	252
Utah-10	nd	-29.9	-32.2	nd	3.3	98.3
Utah-11	nd	-30.1	-32.1	nd	3.7	22.7
Utah-12	0.762	-25.2	nd	0.05	0.003	4.0
Utah-13	0.749	-24.9	nd	0.09	0.2	4.4
Utah-14	nd	-30.0	-31.9	n.d.	2.0	51.0
Utah-15	0.888	-30.7	nd	0.34	0.4	10.2
Utah-16	0.962	-30.8	nd	0.15	0.4	67.9
Utah-17	0.864	-30.9	nd	0.08	BDL	BDL
Utah-18	0.973	-31.2	nd	0.04	0.2	BDL
Colo-1	0.853	-28.1	-28.1	0.50	0.3	13.1
Colo-2	0.820	-28.0	-28.0	0.09	0.3	29.7
Colo-3	0.855	-28.4	-28.5	0.12	1.4	4.6
Wyo-1	nd	-27.6	nd	0.11	0.02	12.7
Wyo-2	0.818	-27.9	nd	0.07	0.02	5.8
Wyo-3	nd	-27.3	nd	0.10	0.1	BDL
Ken-1	nd	-28.1	-28.4	nd	2.8	41.7
Ken-2	nd	nd	nd	nd	0.3	7.5
Ken-3	nd	nd	nd	nd	2.9	BDL
Ken-4	nd	nd	nd	nd	11.6	35.1

Sample No.	Specific Gravity	δC^{13}-Whole Oil (^{o}/oo, PDB)	δC^{13}-Saturates (^{o}/oo, PDB)	Sulfur (Wt.%)	Vanadium (ppm)	Nickel (ppm)
Ken-5	nd	nd	nd	nd	0.04	8.0
Calif-1	0.849	-23.8	-24.7	0.35	1.7	30.4
Calif-2	0.865	-25.3	-25.3	0.22	5.4	55.2
Calif-3	0.912	-22.3	-23.0	0.24	243.5	86.9
Calif-4	0.966	-22.8	-23.5	3.33	24.2	125.0
Calif-5	0.947	-22.7	-23.3	1.24	24.8	64.7
Calif-6	0.934	-22.2	-22.9	1.34	2.7	5.1
Calif-7	0.862	-28.5	-29.1	1.05	78.2	55.8
Calif-8	0.929	-24.5	-25.0	0.37	4.1	49.2
Calif-9	0.945	-27.5	-27.5	0.40	3.8	8.9
Mich 1	0.814	-31.9	-31.7	0.05	0.4	BDL

BDL = Below Detection Limit
nd = Not Determined

APPENDIX IX: GIBBS FREE ENERGIES AT 298°K AND 1 ATM FOR THE FORMATION OF PHASES CONSIDERED IN TEXT

Phase	State	ΔG_f° (kcal)	Source*
V	s	0.0	1
V^{+2}	aq	-54.2	1
V^{+3}	aq	-60.1	1
VO^{+2}	aq	-109.0	1
VO_2^+	aq	-142.0	1
V_2O_2	s	-189.0	1
V_2O_3	s	-271.0	1
V_2O_4	s	-318.0	1
V_2O_5	s	-344.0	1
$V_2O_7^{-4}$	aq	-417.3	2
VO_4^{-3}	aq	-219.2	2
$V_4O_9^{-2}$	aq	-665.3	1
$V_4O_{12}^{-4}$	aq	-774.9	2
$V_{10}O_{28}^{-6}$	aq	-1862.4	1
$HV_{10}O_{28}^{-5}$	aq	-1870.3	1
$H_2V_{10}O_{28}^{-4}$	aq	-1875.2	1
$V(OH)^{+2}$	aq	-112.8	1
$(VO)_2(OH)_2^{+2}$	aq	-322.28	3
$VO(OH)^+$	aq	-157.96	3
$VO(OH)_2$	s	-213.5	1
$V(OH)_3$	s	-218.0	1
Ni	s(II)	0.0	4
Ni^{+2}	aq	-11.53	4

Phase	State	ΔG_f° (kcal)	Source*
$HNiO_2^{-1}$	aq	-83.46	4
$NiCO_3$	s	-147.0	4
$NiSO_4$	s	-184.9	4
$NiSO_4 \cdot 6H_2O$	s(retgersite)	-531.7	5
$NiSO_4 \cdot 7H_2O$	s(morenosite)	-588.4	5
α-NiS	s	-17.7	4
β-NiS	s(millerite)	-20.6	5
γ-NiS	s	-27.3	4
NiS_2	s(vaesite)	-34.0	6
NiO	s(bunsenite)	-51.3	4
$Ni(OH)_2$	s	-108.3	4
$Ni_3O_4 \cdot 2H_2O$	s	-283.53	4
$Ni(OH)_3$	s	-129.5	4
$Ni_2O_3 \cdot H_2O$	s	-169.96	4
NiO_2	s	-47.5	4
$NiO_2 \cdot 2H_2O$	s	-164.8	4
S (orthorhombic)	s	0.0	4
S^{-2}	aq	21.96	4
HS^-	aq	3.01	4
H_2S	aq	-6.54	4
HSO_4^-	aq	-179.94	4
SO_4^{-2}	aq	-177.34	4
Fe^{+2}	aq	-20.3	4
FeS	s (black precipitate)	-21.3	7

Phase	State	ΔG_f^o (kcal)	Source*
FeS	s (mackinawite)	-22.3	7
FeS	s (pyrrhotite)	-24.2	7
FeS	s (troilite)	-22.9	8
FeS_2	s (marcasite)	-37.9	5
FeS_2	s (pyrite)	-38.3	5
H_2O	l	-56.69	4
H_2CO_3	aq	-149.0	4
HCO_3^-	aq	-140.31	4
$CO_3^=$	aq	-126.22	4

*Sources: 1. Evans and Garrels (1958), 2. Calculated From Equilibrium Constants Presented by Evans and Garrels (1958), 3. Postulated Hydrolysed Species That Exist Within A pH Range Of 2.69 to 3.30 (Henry et al, 1973); 4. Garrels and Christ (1965), 5. Robie and Others (1978), 6. Calculated by Extrapolating Temperature Function Presented by Schiffman and Miller (1978), 7. Berner (1967), and 8. Krauskopf (1967).

APPENDIX X: REACTIONS CONSIDERED IN THE CONSTRUCTION OF THE Eh-pH DIAGRAMS USED IN CHAPTER 6*

Reaction (1)

$$4\ VO(OH)_2 \rightleftarrows 2H^+ + V_4O_9^{-2} + 3H_2O$$

$$\Delta G_r = 19.0 \text{ kcal}$$

$$K = A_{V_4O_9^{-2}} \cdot A_{H^+}^2 = 10^{-13.93}$$

Reaction (2)

$$2H_2O + VO^{+2} \rightleftarrows VO(OH)_2 + 2H^+$$

$$\Delta G_r = 8.8 \text{ kcal}$$

$$K = \frac{A_{H^+}^2}{A_{VO^{+2}}} = 10^{-6.45}$$

Reaction (3)

$$H_2O = V^{+3} \rightleftarrows V(OH)^{+2} + H^+$$

$$\Delta G_r = 4.0 \text{ kcal}$$

$$K = \frac{A_{V(OH)^{+2}} \cdot A_{H^+}}{A_{V^{+3}}} = 10^{-2.93}$$

Reaction (4)

$$2H_2O + V(OH)^{+2} \rightleftarrows V(OH)_3 + 2H^+$$

$$\Delta G_r = 8.2 \text{ kcal}$$

$$K = \frac{A_{H^+}^2}{A_{V(OH)^{+2}}} = 10^{-6.01}$$

Reaction (5)

$$8H_2O + 10\ VO_2^+ \rightleftarrows H_2V_{10}O_{28}^{-4} + 14H^+$$

$$\Delta G_r = 4.4 \text{ kcal}$$

$$K = \frac{A_{H}^{14+} \cdot A_{H_2V_{10}O_{28}}^{-4}}{A_{VO_2^+}^{10}} = 10^{-3.23}$$

Reaction (6)

$$4H_2O + 2V_{10}O_{28}^{-6} \rightleftarrows 5V_4O_{12}^{-4} + 8H^+$$

$$\Delta G_r = 77.0 \text{ kcal}$$

$$K = \frac{A_{H}^{8+} \cdot A_{V_4O_{12}}^{5-4}}{A_{V_{10}O_{28}}^{2-6}} = 10^{-56.45}$$

Reaction (7)

$$4H_2O + 4VO_2^+ \rightleftarrows V_4O_{12}^{-4} + 8H^+$$

$$\Delta G_r = 22.28 \text{ kcal}$$

$$K = \frac{A_{H}^{8+} \cdot A_{V_4O_{12}}^{-4}}{A_{VO_2^+}^{4}} = 10^{-16.33}$$

Reaction (8)

$$2H_2O + V_4O_{12}^{-4} \rightleftarrows 2V_2O_7^{-4} + 4H^+$$

$$\Delta G_r = 53.67 \text{ kcal}$$

$$K = \frac{A_{H}^{4+} \cdot A_{V_2O_7}^{2-4}}{A_{V_4O_{12}}^{-4}} = 10^{-39.35}$$

Reaction (9)

$$H_2V_{10}O_{28}^{-4} \rightleftarrows HV_{10}O_{28}^{-5} + H^+$$

$$\Delta G_r = 4.9 \text{ kcal}$$

$$K = \frac{A_{HV_{10}O_{28}^{-5}} \cdot A_{H^+}}{A_{H_2V_{10}O_{28}^{-4}}} = 10^{-3.59}$$

Reaction (10)

$$H_2O + V_2O_7^{-4} \rightleftarrows 2VO_4^{-3} + 2H^+$$

$$\Delta G_r = 35.67 \text{ kcal}$$

$$K = \frac{A_{H^+}^2 \cdot A_{VO_4^{-3}}^2}{A_{V_2O_7^{-4}}} = 10^{-26.15}$$

Reaction (11)

$$H_2O + VO^{+2} \rightleftarrows VO(OH)^+ + H^+$$

$$\Delta G_r = 10.04 \text{ kcal}$$

$$K = \frac{A_{H^+} \cdot A_{VO(OH)^+}}{A_{VO^{+2}}} = 10^{7.36}$$

Reaction (12)

$$H_2O + VO(OH)^+ \rightleftarrows VO(OH)_2 + H^+$$

$$\Delta G_r = -1.26$$

$$K = \frac{A_{H^+}}{A_{VO(OH)^+}} = 10^{0.92}$$

Reaction (13)

$$HV_{10}O_{28}^{-5} \rightleftarrows V_{10}O_{28}^{-6} + H^+$$

$$\Delta G_r = 7.9 \text{ kcal}$$

$$K = \frac{A_{H^+} \cdot A_{V_{10}O_{28}^{-6}}}{A_{H\,V_{10}O_{28}^{-5}}} = 10^{-5.79}$$

Reaction (14)

$$V^{+2} \rightleftarrows V^{+3} + e$$

ΔG_r = -5.9 kcal

E° = 0.255 volts

$$Eh = 0.255 + 0.059 \log \frac{A_{V^{+3}}}{A_{V^{+2}}}$$

Reaction (15)

$$H_2O + V^{+3} \rightleftarrows VO^{+2} + 2H^+ + e$$

ΔG_r = 7.79 kcal

E° = 0.339 volts

$$Eh = 0.339 + 0.059 \log \frac{A_{VO^{+2}} \cdot A^2_{H^+}}{A_{V^{+3}}}$$

Reaction (16)

$$H_2O + VO^{+2} \rightleftarrows VO^{+2} + 2H^+ + e$$

ΔG_r = 23.1 kcal

E° = 1.000 volts

$$Eh = 1.000 + 0.059 \log \frac{A_{VO_2^+} \cdot A^2_{H^+}}{A_{VO^{+2}}}$$

Reaction (17)

$$V(OH)^{+2} \rightleftarrows VO^{+2} + H^+ + e$$

ΔG_r = 3.8 kcal

E° = 0.165 volts

$$Eh = 0.165 + 0.059 \log \frac{A_{VO^{+2}} \cdot A_{H^+}}{A_{V(OH)^{+2}}}$$

Reaction (18)

$$H_2O + V^{+2} \rightleftarrows V(OH)^{+2} + H^+ + e$$

ΔG_r = 1.91 kcal

E° = 0.082 volts

$$Eh = 0.082 + 0.059 \log \frac{A_{V(OH)^{+2}} \cdot A_{H^+}}{A_{V^{+2}}}$$

Reaction (19)

$$V(OH)_3 \rightleftarrows VO(OH)_2 + H^+ + e$$

$$\Delta G_r = 4.4 \text{ kcal}$$

$$E^\circ = 0.191 \text{ volts}$$

$$Eh = 0.191 + 0.059 \log (A_{H^+})$$

Reaction (20)

$$3H_2O + V^{+2} \rightleftarrows V(OH)_3 + 3H^+ + e$$

$$\Delta G_r = 6.27 \text{ kcal}$$

$$E^\circ = 0.272 \text{ volts}$$

$$Eh = 0.272 + 0.059 \log \frac{A_{H^+}^3}{A_{V^{+2}}}$$

Reaction (21)

$$H_2O + V(OH)_3 \rightleftarrows VO_4^{-3} + 5H^+ + 2e$$

$$\Delta G_r = 55.49 \text{ kcal}$$

$$E^\circ = 1.203 \text{ volts}$$

$$Eh = 1.203 + 0.0259 \log (A_{VO_4^{-3}} \cdot A_{H^+}^5)$$

Reaction (22)

$$8H_2O + 4VO^{+2} \rightleftarrows V_4O_{12}^{-4} + 16H^+ + 4e$$

$$\Delta G_r = 114.62 \text{ kcal}$$

$$E^\circ = 1.243 \text{ volts}$$

$$Eh = 1.243 + 0.0148 \log \frac{A_{V_4O_{12}^{-4}} \cdot A_{H^+}^{16}}{A_{VO^{+2}}^4}$$

Reaction (23)

$$4VO(OH)_2 \rightleftarrows V_4O_{12}^{-4} + 8H^+ + 4e$$

$$\Delta G_r = 79.5 \text{ kcal}$$

$$E^\circ = 0.862 \text{ volts}$$

$$Eh = 0.862 + 0.0148 \log A_{V_4O_{12}^{-4}} \cdot A_{H^+}^{8}$$

Reaction (24)

$$H_2O + 2VO(OH)_2 \rightleftarrows V_2O_7^{-4} + 6H^+ + 2e$$

$$\Delta G_r = 66.59 \text{ kcal}$$

$$E^\circ = 1.444 \text{ volts}$$

$$Eh = 1.444 + 0.0295 \log A_{V\ O^{-4}} \cdot A_{H_{4\ 7}^{+}}^{6}$$

Reaction (25)

$$H_2O + 2V(OH)_3 \rightleftarrows V_2O_7^{-4} + 8H^+ + 4e$$

$$\Delta G_r = 75.39 \text{ kcal}$$

$$E^\circ = 0.817 \text{ volts}$$

$$Eh = 0.817 + 0.0148 \log A_{V_2O_7^{-4}} \cdot A_{H^+}^{8}$$

Reaction (26)

$$18H_2O + 10VO^2 \rightleftarrows HV_{10}O_{28}^{-5} + 35H^+ + 10e$$

$$\Delta G_r = 240.12 \text{ kcal}$$

$$E^\circ = 1.041 \text{ volts}$$

$$Eh = 1.041 + 0.0059 \log \frac{A_{HV_{10}O_{28}^{-5}} \cdot A_{H^+}^{35}}{A_{VO^{+2}}^{10}}$$

Reaction (27)

$$4V(OH)_3 \rightleftarrows V_4O_9^{-2} + 3H_2O + 6H^+ + 4e$$

$$\Delta G_r = 36.6 \text{ kcal}$$

$$E^\circ = 0.396 \text{ volts}$$

$$Eh = 0.396 + 0.0148 \log A_{V_4O_9^{-2}} \cdot A_{H^+}^{6}$$

Reaction (28)

$$4H_2O + Ni^{+2} \rightleftarrows NiO_3 \cdot 2H_2O + 4H^+ + 2e$$

$$\Delta G_r = 73.53 \text{ kcal}$$

$$E^\circ = 1.594 \text{ volts}$$

$$Eh = 1.594 + 0.0259 \log \frac{A_{H^+}^4}{A_{Ni^{+2}}}$$

Reaction (29)

$$2H_2O + Ni^{+2} \rightleftarrows NiO_2 + 4H^+ + 2e$$

$$\Delta G_r = 77.43 \text{ kcal}$$

$$E^\circ = 1.679 \text{ volts}$$

$$Eh = 1.679 + 0.0259 \log \frac{A_{H^+}^4}{A_{Ni^{+2}}}$$

Reaction (30)

$$4H_2O + Ni_2O_3 \cdot H_2O \rightleftarrows 2NiO_2 \cdot 2H2O + 2H^+ + 2e$$

$$\Delta G_r = 67.16 \text{ kcal}$$

$$E^\circ = 1.456 \text{ volts}$$

$$Eh = 1.456 + 0.0259 \log A_{H^+}^2$$

Reaction (31)

$$6H_2O + 3Ni^{+2} \rightleftarrows Ni_3O_4 \cdot 2H_2O + 84H^+ + 2e$$

$$\Delta G_r = 91.26 \text{ kcal}$$

$$E^\circ = 1.979 \text{ volts}$$

$$Eh = 1.979 + 0.0259 \log \frac{A_{H^+}^8}{A_{Ni^{+2}}^3}$$

Reaction (32)

$$2Ni_3O_4 \cdot 2H_2O \rightleftarrows 3Ni_2O_3 \cdot H_2O + 2H^+ + 2e$$

$$\Delta G_r = 57.18 \text{ kcal}$$

$E^\circ = 1.240$ volts

$Eh = 1.240 + 0.0259 \log A_{H^+}^2$

Reaction (33)

$4H_2O + 2Ni^{+2} \rightleftarrows Ni_2O_3 \cdot H_2O + 6H^+ + 2e$

$\Delta G_r = 79.9$ kcal

$E^\circ = 1.732$ volts

$$Eh = 1.732 + 0.0259 \log \frac{A_{H^+}^6}{A_{Ni^{+2}}^2}$$

Reaction (34)

$3Ni(OH)_2 \rightleftarrows Ni_2O_4 \cdot 2H_2O + 2H^+ + 2e$

$\Delta G_r = 41.37$ kcal

$E^\circ = 0.897$ volts

$Eh = 0.897 + 0.0259 \log A_{H^+}^2$

Reaction (35)

$3HNiO_2^- + H^+ \rightleftarrows Ni_3O_4 \cdot 2H_2O + 2e$

$\Delta G_r = -33.09$ kcal

$E^\circ = -0.717$ volts

$Eh = -0.717 + 0.0295 \log A_{H^+}^{-1} \cdot A_{HNiO_2}^{-3}$

Reaction (36)

$Ni \rightleftarrows Ni^{+2} + 2e$

$\Delta G_r = -11.53$ kcal

$E^\circ = -0.250$ volts

$Eh = -0.250 + 0.0295 \log A_{ni^{+2}}$

Reaction (37)

$2H_2O + Ni \rightleftarrows Ni(OH)_2 + 2H^+ + 2e$

$\Delta G_r = 5.1$ kcal

$E^\circ = 0.111$ volts

$Eh = 0.111 + 0.0259 \log A_H^{2+}$

Reaction (38)

$2H_2O + Ni \rightleftarrows HNiO_2^- + 3H^+ + 2e$

$\Delta G_r = 29.94$ kcal

$E^\circ = -0.649$ volts

$Eh = -0.649 + 0.0295 \log A_H^{3+} \cdot A_{HNiO_2^-}$

Reaction (39)

$2H_2O + Ni^{+2} \rightleftarrows Ni(OH)_2 + 2H^+$

$\Delta G_r = 16.69$ kcal

$$K = \frac{A_H^{2+}}{A_{Ni^{+2}}} = 10^{-12.19}$$

Reaction (40)

$Ni(OH)_2 \rightleftarrows HNiO_2^- + H^+$

$\Delta G_r = 24.84$ kcal

$K = A_{HNiO2^-} \cdot AH+ = 10^{-18.14}$

Reaction (41)

$2H_2O + NiO_2 \rightleftarrows NiO_2 \cdot 2H_2O$

$\Delta G_r = -3.9$ kcal

Reaction (42)

$2H_2O + Ni_2O_3 \cdot H_2O \rightleftarrows 2Ni(OH)_3$

$\Delta G_r = 24.36$ kcal

Reaction (43)

$Ni(OH)_2 \rightleftarrows NiO + H_2O$

$\Delta G_r = 0.3$ kcal

Reaction (44)

$$H_2CO_3 + Ni^{+2} \rightleftarrows NiCO_3 + 2H^+$$

$$\Delta G_r = 13.53 \text{ kcal}$$

$$K = \frac{A_{H^+}^2}{A_{Ni^{+2}}} = 10^{-9.92}$$

Reaction (45)

$$HCO_3^- + Ni^{+2} \rightleftarrows NiCO_3 + H^+$$

$$\Delta G_r = 4.84 \text{ kcal}$$

$$K = \frac{AH^+}{A_{Ni^{+2}}} = 10^{-3.55}$$

Reaction (46)

$$H_2S + Ni^{+2} \rightleftarrows NiS + 2H^+$$

$$\Delta G_r = 0.37 \text{ kcal}$$

$$K = \frac{A_{H^+}^2}{A_{H_2S} \cdot A_{Ni^{+2}}} = 10^{-0.27}$$

Reaction (47)

$$4H_2O + NiS \rightleftarrows Ni^{+2} + SO_4^{-2} + 8H^+ + 8e$$

$$\Delta G_r = 55.63 \text{ kcal}$$

$$E^\circ = 0.302 \text{ volts}$$

$$Eh = 0.302 + 0.0074 \log {}^{A}Ni^{+2} \cdot A\ SO_4^{-2} \cdot A_{H+}^8$$

Reaction (48)

$$NiS \rightleftarrows Ni^{+2} + S + 2e$$

$$\Delta G_r = 6.17 \text{ kcal}$$

$$E^\circ = 0.134 \text{ volts}$$

$$Eh = 0.134 + 0.0295 \log A_{Ni^{+2}}$$

Reaction (49)

$$H_2S + Ni \rightleftarrows NiS + 2H^+ + 2e$$

$$\Delta G_r = -11.16 \text{ kcal}$$

$$E^\circ = 0.242 \text{ volts}$$

$$Eh = -0.242 + 0.059 \log \frac{A_{H^+}^2}{A_{H_2S}}$$

Reaction (50)

$$HS^- + Ni \rightleftarrows NiS + H^+ + 2e$$

$$\Delta G_r = 20.71 \text{ kcal}$$

$$E^\circ = 0.449 \text{ volts}$$

$$Eh = 0.449 + 0.0259 \log \frac{A_{H^+}}{A_{HS^-}}$$

Reaction (51)

$$Ni \rightleftarrows Ni^{+2} + 2e$$

$$\Delta G_r = -11.53 \text{ kcal}$$

$$E^\circ = -0.250 \text{ volts}$$

$$Eh = -0.250 + 0.0295 \log A_{Ni^{+2}}$$

Reaction (52)

$$6H_2O + NiS \rightleftarrows Ni(OH)_2 + SO_4^{-2} + 10H^+ + 8e$$

$$\Delta G_r = 72.26 \text{ kcal}$$

$$E^\circ = 0.392 \text{ volts}$$

$$Eh = 0.392 + 0.0074 \log A_{SO_4^{-2}} \cdot A_{H^+}^{10}$$

Reaction (53)

$$6H_2O + NiS \rightleftarrows HNiO_2^- + SO4^{-2} + 11H^+ + 8e$$

$$\Delta G_r = 97.08 \text{ kcal}$$

$$E^\circ = 0.526 \text{ volts}$$

$$Eh = 0.526 + 0.0074 \log {}^{A}HNiO_2^{-} \cdot {}^{A}SO_4^{-2} \cdot A_H^{+1}$$

Reaction (54)

$$Ni^{+2} + SO_4^{-2} \rightleftarrows NiSO_4$$

$$\Delta G_r = 3.97 \text{ kcal}$$

Reaction (55)

$$Ni^{+2} + SO_4^{-2} + 6H_2O \rightleftarrows NiSO_4 \cdot 6H_2O$$

$$\Delta G_r = -2.69 \text{ kcal}$$

Reaction (56)

$$Ni^{+2} + SO_4^{-2} + 7H_2O \rightleftarrows NiSO_4 \cdot 7H_2O$$

$$\Delta G_r = -2.70 \text{ kcal}$$

*Values for Gibbs free energy of reaction (ΔG_r), equilibrium constant (K), standard electrode potential (E°), and Redox potential (Eh) are based on the Gibbs free energies (ΔG_f°) given in Appendix IX.